NOVEL REGULATION OF NEURONAL GENES IMPLICATED IN ALZHEIMER DISEASE BY MICRORNA

Justin M. Long

Submitted to the faculty of the University Graduate School
in partial fulfillment of the requirements
for the degree
Doctor of Philosophy
in the Program in Medical Neuroscience,
Indiana University

March 2013

Accepted by the Faculty of Indiana University, in partial
fulfillment of the requirements for the degree of Doctor of Philosophy.

Feng C. Zhou, PhD, Chair

Debomoy K. Lahiri, PhD

Doctoral Committee

Richard Nass, PhD

June 19, 2012

Yansheng Du, PhD

Martin R. Farlow, MD

ACKNOWLEDGEMENTS

I must first thank my research advisor, Dr. Debomoy Lahiri, who has provided invaluable advice, encouragement and mentorship during my tenure in his laboratory. I have learned much from him about the process of conducting vigorous science and the importance of communicating that science to the world. I appreciate the time and resources he has provided me during my development as a budding scientist. Without his professional support, my research training and the work described in this dissertation would not have been possible.

I must also thank the other members of my research committee: committee chair Dr. Feng Zhou, Dr. Richard Nass, Dr. Yansheng Du and Dr. Martin Farlow. They have been generous in providing their time and expertise throughout my training. Their mark is clearly evident in this dissertation, as their guidance has continually had a positive impact on the direction of my research. I truly appreciate their input.

Several collaborators provided key materials that were critical to the success of my research. I thank Dr. P Hemanchandra Reddy (Oregon Health and Science University, Beaverton, OR) and Dr. Peter Nelson (University of Kentucky, Lexington, KY) for providing brain specimens from their collections, Dr. Jack Rogers (Massachusetts General Hospital, Charlestown, MA) for providing plasmids, and Dr. Robert Vassar (Northwestern University, Chicago, IL) for providing anti-BACE1 antibody 3D5. I also thank Dr. Bob Niculescu for valuable feedback on my research and for providing open access to his real-time PCR instrument. Finally, I also wish to express my gratitude to the various funding sources that supported this work, including National Institutes of Aging and Alzheimer's Association grants to Dr. Lahiri and travel grants from the Alzheimer's Association and Dr. Joseph Hingtgen.

I would also like to thank all members of Dr. Lahiri's laboratory who have been instrumental in helping me survive the vagaries of biomedical research. I would like to

thank Dr. Jason Bailey who showed me the ropes as an early graduate student and taught me many valuable laboratory techniques. I also thank Dr. Balmiki Ray for establishing many research models and assays in the laboratory that contributed significantly to this work and for being willing to help with experiments whenever I was in a pinch. I thank Bryan Maloney for his valuable insight on molecular biology and statistical analysis. I also thank Nipun Chopra and Cindy Morgan for tolerating me as bench mates, helping with experiments when needed and general comedic relief. I finally thank all of these fellow lab members for their continued friendship and collegiality that has made time spent in the lab a pleasure.

I thank my family and friends for their ever present interest in my work and continual moral support. I thank my two young kids for never failing to bring a smile to my face and reminding me that life does not revolve around the laboratory. Most importantly, I thank my wife Melissa for her enduring patience during this long journey of a career path that I have chosen. Her unfailing love and support throughout this process has been the crutch on which I continue to lean.

ABSTRACT

Justin M. Long

NOVEL REGULATION OF NEURONAL GENES IMPLICATED IN ALZHEIMER DISEASE BY MICRORNA

Alzheimer disease (AD) results, in part, from the excess accumulation of the amyloid-β peptide (Aβ) as neuritic plaques in the brain. The short Aβ peptide is derived from a large transmembrane precursor protein, APP. Two different proteolytic enzymes, BACE1 and the gamma-secretase complex, are responsible for cleaving Aβ peptide from APP through an intricate processing pathway. Dysregulation of APP and BACE1 levels leading to excess Aβ deposition has been implicated in various forms of AD. Thus, a major goal in this dissertation was to discover novel regulatory pathways that control APP and BACE1 expression as a means to identify novel drug targets central to the Aβ-generating process. MicroRNAs (miRNA) are short, non-coding RNAs that act as post-transcriptional regulators of gene expression through specific interactions with target mRNAs. Global analyses predict that over sixty percent of human transcripts contain evolutionarily conserved miRNA target sites. Therefore, the specific hypothesis tested was that miRNA are relevant regulators of APP and BACE1 expression.

In this work, several specific miRNA were identified that regulate APP protein expression (miR-101, miR-153 and miR-346) or BACE1 expression (miR-339-5p). These miRNAs mediated their post-transcriptional effects via interactions with specific target sites in the *APP* and *BACE1* transcripts. Importantly, these miRNA also altered secretion of Aβ peptides in primary human fetal brain cultures. Surprisingly, miR-346 stimulated APP expression via target sites in the APP 5'-UTR. The mechanism of this effect appears to involve other RNA-binding proteins that bind to the APP 5'-UTR.

Expression analyses demonstrated that these miRNAs are expressed to varying degrees in the human brain. Notably, miR-101, miR-153 and miR-339-5p are dysregulated in the AD brain at various stages of the disease. The work in this dissertation supports the hypothesis that miRNAs are important regulators of APP and BACE1 expression and are capable of altering Aβ homeostasis. Therefore, these miRNA may possibly serve as novel therapeutic targets for AD.

Feng C. Zhou, PhD, Chair

TABLE OF CONTENTS

LIST OF TABLES

LIST OF FIGURES

LIST OF ABBREVIATIONS

A260	Absorbance at 260 nanometers wavelength
A280	Absorbance at 280 nanometers wavelength
A600	Absorbance at 600 nanometers wavelength
AD	Alzheimer disease
AD-LBV	Lewy body variant of Alzheimer disease
AGO	Argonaute subfamily protein
AICD	Amyloid-β precursor protein intracellular domain
ANOVA	Analysis of variance
APH	Anterior pharynx defective
APLP	Amyloid-β precursor protein-like protein ½
APP	Amyloid-β precursor protein
ARE	AU-rich element
ATXN1	Ataxin1
Aβ	Amyloid-β
BACE	β-site amyloid-β precursor protein-cleaving enzyme
BBB	Blood brain barrier
BCA	Bicinchoninic acid protein assay
bp	Base pairs
BSA	Bovine serum albumin
cDNA	Complementary DNA
CDS	Coding sequence
ceRNA	Competing endogenous RNA
CM	Conditioned media
CNS	Central nervous system
Ct	Crossing threshold
CTF	C-terminal fragment
DFO	Deferroxamine
DGCR8	DiGeorge critical region 8
DIV	Days *in vitro*
DMEM	Dulbecco's modified eagle's medium
DNA	Deoxyribonucleic acid
DS	Down syndrome
ds/ssRNA	Double stranded/single stranded RNA
E	PCR amplification efficiency
ECL	Enhanced chemiluminescence
ELISA	Enzyme-linked immunosorbent assay
EOAD	Early-onset Alzheimer disease
FAD	Familial Alzheimer disease
FBS	Fetal bovine serum
GFAP	Glial fibrillary acidic protein
GOI	Gene of interest
GRID1	Glutamate rec eptor delta 1 subunit
HCV	Hepatitis C virus
HRP	Horseradish peroxidase
HSD	Honest significant difference
HSP	Heat shock protein
HSV-TK	Herpes simplex virus thymidine kinase
IRE	Iron response element
IRP	Iron regulatory protein

IVIG	Intravenous immunoglobulins
kb	Kilobases
LB	Lysogeny broth
LNA	Locked nucleic acid
LOAD	Late-onset Alzheimer disease
Luc	Luciferase
MCI	Mild cognitive impairment
MCS	Multiple cloning site
MEM	Minimal essential medium
MHC	Major histocompatibility complex
miRNA	MicroRNA
miRNP	Microribonucleoprotein
MPAC	Metal protein attenuating compounds
M-PER	Mammalian protein extraction reagent
MRE	MicroRNA response element
mRNA	Messenger RNA
$Na_v\beta_2$	Voltage-gated sodium channel β_2 subunit
ncRNA	Non-coding RNA
NFT	Neurofibrillary tangles
NMDA	N-methyl-D-aspartate
NRG	Neuregulin
nt	Nucleotide
ORF	Open reading frame
PAP	Poly (A) polymerase
PARIS	Protein and RNA isolation system
PBMC	Peripheral blood mononuclear cells
PBS	Phosphate buffered saline
PCR	Polymerase chain reaction
P_{CT}	Probability of conserved targeting
PD	Parkinson disease
PMI	Post-mortem interval
Poly(Q)	Polyglutamine tract
pri-miRNA	Primary microRNA transcript
PSEN	Presenilin enhancer
PVDF	Polyvinyl difluoride
RA	Retinoic acid
RIN	RNA integrity number
RIP140	Receptor-interacting protein 140
RISC	RNA-induced silencing complex
RLC	RNA-induced silencing complex loading complex
RNA	Ribonucleic acid
ROS	Reactive oxygen species
RQ	Relative quantity
RRR	Relative response ratio
RT	Reverse transcription
RT-qPCR	Reverse transcription quantitative polymerase chain reaction
RVG	Rabies virus glycoprotein
SAD	Sporadic Alzheimer disease
SDS	Sodium dodecyl sulfate
SDS-PAGE	Sodium dodecyl sulfate-polyacrylamide gel electrophoresis
siRNA	Short interfering RNA

SNCA	α-synuclein
SNK	Student-Neuman-Keuls
Tg	Transgenic
TOP	Terminal oliogopyrimidine
TP	Target protector
TRBP	TAR-RNA binding protein
TTP	Tristetraprolin
uORF	Upstream open reading frame
UPR	Unfolded protein response
UTR	Untranslated region
YY1	Yin Yang 1
βME	β-mercaptoethanol

CHAPTER 1: INTRODUCTION

The anatomical and cytoarchitectural complexity of the central nervous system (CNS) is a function of an equally sophisticated molecular framework. Derangements in tightly regulated molecular pathways underlying this complexity are not surprisingly linked to many CNS disorders, including Alzheimer disease (AD), a debilitating neurodegenerative disorder of unknown etiology lacking effective therapeutics. Gene expression is a critical node at which regulatory influences on molecular pathways are exerted. As such, fleshing out the full complement of regulatory schemes responsible for control of CNS gene expression should be a priority in the search for novel points of intervention against CNS disorders. Elucidating these regulatory networks not only provides a reference for comparison to the diseased state but also expands the number of functionally validated drug targets that might be critical to developing effective therapeutics. In pursuit of this goal, this dissertation describes novel mechanisms utilized by human CNS cells to post-transcriptionally regulate expression of two gene products implicated in AD etiology and explores dysregulation of these mechanisms in the AD brain.

I. Alzheimer Disease (AD) Background

A. Clinical and neuropathological overview

Dementia is a devastating consequence of aging, and AD accounts for the largest proportion of dementia cases in the elderly. An estimated 5.4 million people will be afflicted with AD in the United States during 2012 [1,2]. With the expected increase in life expectancy and the aging of the baby boomer generation, that number is projected to rise to somewhere between 11 – 16 million people by 2050. The disease is

not only debilitating to the afflicted patient, but also results in a significant burden to caretakers and the national and global health care systems.

The earliest clinical manifestation of the disease is an anterograde amnesia characterized by loss in retention of newly formed memories [3]. Declarative memory (esp. episodic memory) is most profoundly affected in the early course of the disease. Deficits in language and visuospatial skills also occur early. Impairments in procedural memory, learned motor skills, and executive function only arise in more advanced stages of the disease. Depression and other mood disorders frequently manifest during the course of the disease [4], as do changes in personality [5]. The course of dementia is always progressive. Activities of daily living are profoundly affected and ultimately the patient becomes bed-ridden. This invariably leads to death, generally secondary to dehydration, malnutrition or infection [6]. The average life expectancy following diagnosis is generally between 3 to 8 years [7,8].

While clinical signs and symptoms often provide compelling, suggestive antemortem evidence of AD, definitive diagnosis still requires postmortem histochemical examination of the brain. The cardinal neuropathological findings of AD in the brain were originally described in 1907 in the first report of an early-onset form of AD by Alois Alzheimer [9]: extracellular neuritic plaques consisting primarily of fibrillar amyloid-β (Aβ) peptide [10] and intraneuronal neurofibrillary tangles (NFT) composed of paired helical filaments of hyperphosphorylated tau protein [11]. NFT and amyloid pathologies follow a stereotypic pattern of progression in the AD brain that somewhat correlates with clinical progression [12]. In fact, Braak staging of AD pathology is based upon the level of progression of NFT pathology [13]. NFT generally first affect the transentorhinal cortex in the earliest stages of disease, spreading next to the hippocampal formation, then the frontal, parietal and occipital cortices, finally affecting primary motor and sensory cortices only at the most advanced stage of the disease

[13]. Interestingly, the progression of anatomic regions affected by NFT somewhat tracks the clinical symptom progression. Areas first invested with NFT (i.e. transentorhinal cortex and hippocampal formation) play key roles in consolidating newly formed memories [14]. Areas last to be invested with NFT (i.e. primary motor and sensory cortices) are the areas to be last affected clinically (i.e. basic motor and sensory functions). Amyloid deposits follow a less predictable and correlative progression. Plaques generally first appear in the neocortex, spread in middle stages to the hippocampal formation, and move on to the primary motor and sensory cortices and subcortical structures in late stages of the disease [13,15]. Synaptic loss is another important feature of AD pathology and appears to occur early in disease progression and in numbers disproportionate to neuron loss. Synapse loss also appears to correlate with cognitive decline better than other pathological findings [16]. In end stages of AD, there is ultimately complete neuronal loss and frank neurodegeneration leading to generalized brain atrophy.

Cholinergic neurons are lost disproportionately to other transmitter systems in early stages of the disease, despite lack of significant pathology in the septal nuclei or nucleus basalis of Meynert [17,18]. Given the extensive cholinergic projections throughout the neo- and allocortex, this cholinergic loss likely contributes to early symptomatology. Intrahippocampal injections of Aβ peptide in animal models promotes a similar neurodegenerative phenotype in cholinergic centers, perhaps related to cholinergic axons that terminate in the hippocampus [19]. This suggests that early cholinergic loss in AD may be mediated by retrograde toxicity originating from axonal projections at sites of Aβ pathology. However, given the extent of neurodegeneration, it is likely that AD progresses to primarily a glutamatergic deficiency in late stages of the disease.

It is becoming increasingly clear that AD exists on a continuum, with the earliest pathological changes developing in the brain years before any clinical symptoms arise (i.e. preclinical AD). Recent efforts have focused on identifying biochemical and imaging biomarkers that might identify patients with preclinical findings that portend the eventual onset of clinically significant dementia [20–23]. Once the disease does become clinically apparent, changes in cognitive function are initially very subtle and do not meet the criteria for dementia. This intermediate state is classified as mild cognitive impairment (MCI) [24]. Among patients diagnosed with MCI, the rate of conversion to AD dementia is significantly higher as compared to age-matched populations that are cognitively normal [25].

B. Molecular mechanisms and genetics

Molecular mechanisms that underlie pathological findings and clinical symptoms in AD are still unclear. The amyloid cascade hypothesis posits that accumulation of Aβ either due to enhanced production or decreased clearance initiates a cascade of molecular events leading to neurodegeneration and dementia [26,27]. Inflammatory responses, mitochondrial dysfunction, oxidative stress, calcium dysregulation, impaired axonal transport, membrane damage and tau-based neurotoxicity, among others mechanisms, are likely participants in this cascade [28,29].

Aβ is derived from the parental amyloid-β precursor protein (APP). APP is a transmembrane protein that undergoes proteolytic processing by secretase enzymes to liberate soluble fragments (described in more detail below). Promiscuous C-terminal cleavage of the Aβ domain in APP by the γ-secretase complex is responsible for the generation of 40 and 42 amino acid forms of Aβ (Aβ40 and Aβ42). Aβ42 is much more hydrophobic than Aβ40 and has a much greater propensity to aggregate and form

oligomers [30]. The Aβ42 isoform accumulates to a greater extent than Aβ40 in all forms of AD and is the primary component of neuritic plaques [31].

AD is generally subdivided into two categories based upon age of onset: early-onset AD (EOAD) and late-onset AD (LOAD). EOAD, with age of onset prior to 60, constitutes less than 5% of all cases of AD. EOAD often results from inheritance of autosomal dominant single gene mutations in three different genes (*APP, PSEN1 and PSEN2*) [32]. This type of EOAD is also termed familial AD (FAD). Most mutations are located in *PSEN1* or *PSEN2* genes, with a smaller number localizing to the Aβ-encoding region of *APP. PSEN1* and *PSEN2* are components of the γ-secretase complex responsible for C-terminal cleavage of Aβ from APP. Mutations in these two genes appear to predominantly promote Aβ42 cleavage over Aβ40 [33,34]. Mutations in *APP* promote either enhanced Aβ aggregation or Aβ42 over Aβ40 production [35,36]. Therefore, the mechanism of elevated Aβ accumulation in FAD is related to mutations that promote elevated Aβ42 processing.

Most forms of LOAD are not inherited in Mendelian fashion and are termed sporadic AD (SAD). SAD is a complex disorder whose onset is influenced by multiple factors including genetics, the environment, and gene-environment interactions, with the greatest known risk factor being advanced age [37]. Heritability is still quite high for SAD, estimated somewhere between 50%-80%, but penetrance for single gene mutations is very low [38]. The cause of excess Aβ accumulation in the disease is still an enigma. Evidence suggests that both increased Aβ production and decreased Aβ clearance may play a role [39–41]. The *APOE* gene confers the greatest genetic risk for developing SAD, with the ε4 allele enhancing AD risk approximately 4-fold [42]. Interestingly, ApoE has been shown to promote Aβ proteolytic degradation [43]. The ε4 allele has diminished capacity to promote Aβ clearance, potentially explaining the risk conferred by inheriting this allele [41]. Several genome wide association studies have

identified multiple genes (*PICALM, CR1, CLU, BIN1)* that are associated with SAD at genome-wide significance [44–46]. However, the effect size for each of these genes in isolation is very small, highlighting the importance that gene-environment interactions likely play in SAD.

C. Support for centrality of amyloid-β to AD etiology

While valid criticisms exist, there is significant evidence supporting the Aβ-centric view put forward by the amyloid cascade hypothesis. Most prominently, the rare, early-onset forms of FAD that are inherited in autosomal dominant fashion are caused by single gene mutations that act to increase the ratio of the more amyloidogenic and toxic Aβ42 relative to the more benign Aβ40 [32]. The *APP* locus is contained on chromosome 21, and rare duplication events at this locus [47] or full trisomy of chromosome 21 in Down syndrome (DS) [30] result in FAD via a gene dosage effect. Genetic polymorphisms in the *APP* promoter that elevate APP expression have also been shown to be associated with AD [48,49].

Therefore, elevation of Aβ alone (or Aβ42, specifically) is sufficient to induce AD in these rare forms of AD and most likely in SAD cases. Given the similarity in clinical phenotype between FAD and SAD, the presumption is that similar molecular mechanisms may underlie both, though this is still an open question. It is important to point out that the contribution of various risk-modifying gene variants (e.g. *APOE, CLU, PICALM, CR1, BIN1*) to the elevated Aβ levels observed in SAD is unknown, perhaps with the exception of *APOE* [50]. Other evidence in support of the Aβ-centric position includes observations that Aβ has clearly neurotoxic and synaptotoxic effects both *in vitro* and *in vivo*, especially in its soluble oligomeric forms [51].

Other amyloid-independent mechanisms have been proposed to contribute to FAD and SAD pathogenesis and are reviewed elsewhere [52]. Interestingly, APP is

implicated in some of these amyloid-independent pathways. As an example, dysfunction of the endosomal system in Down syndrome and models of APP gene duplication has been attributed to a gene dosage effect of APP specifically mediated by increased levels of the β-cleaved C-terminal fragment of APP, not Aβ [53–55]. The evidence suggests that modulating levels of APP may represent an attractive therapeutic strategy for SAD and FAD, irrespective of the ultimate validity of the amyloid cascade hypothesis.

D. Current therapeutic strategies and limitations

Current FDA-approved therapeutic options for AD include use of cholinesterase inhibitors (donepezil, rivastigmine, and galantamiine) in mild-to-moderate AD and an uncompetitive N-methyl-D-aspartate (NMDA) receptor antagonist (memantine) in moderate-to-severe AD [56]. The goal of cholinesterase inhibition is to support cholinergic signaling early in the disease when cholinergic neurons are first lost. The mechanism of memantine activity may involve neuroprotection during episodes of glutamate neurotoxicity. Other neuroprotective and Aβ-modifying activities have been reported for cholinesterase inhibitors and memantine and may contribute to their clinical effect [57–59]. Unfortunately, these therapeutic options are only modestly effective at reducing symptoms and none modifies disease progression [60,61].

Newer strategies for treating AD span a wide spectrum, ranging from modifications of existing treatment modalities to entirely novel mechanisms. Many of these are still in early preclinical stages. For example, several inhibitors of the butyrylcholinesterase enzyme, which is increased in AD, decrease Aβ levels in both culture and animal models [62]. Alternatively, the potassium channel modulator diazoxide, which is currently approved for the treatment of hypoglycemia, has shown promise in animal models, perhaps by reversing brain hypometabolism as occurs in AD

[63]. Several compounds derived from natural sources are also showing promise in the preclinical setting, including S-allyl cysteine (SAC) and curcumin. SAC is a component of aged garlic and has been shown to protect cultured neuronal cells from oxidative stress and to increase synaptic markers in an animal model of AD [64,65]. Curcumin has been viewed as a potential therapeutic agent for AD since the discovery that it can dissociate amyloid plaque *in vitro* [66], although the extreme hydrophobicity of this molecule has impeded its development as an AD drug candidate. Recently developed nanotechnology has allowed the packaging of curcumin into highly soluble nanoparticles leading to greatly improved uptake in an animal model. In this model, nanocurcumin reduced oxidative stress and apoptotic markers [67].

The therapies furthest advanced along the clinical pipeline predominantly target Aβ production or Aβ clearance. The APP processing pathway is an obvious target for reducing Aβ production. Inhibition of β-secretase enzymatic activity has been actively pursued since the discovery of β-site APP cleaving enzyme 1 (BACE1), but the competing challenges of finding a candidate drug of sufficient size to target the BACE1 active site yet small enough to efficiently cross the blood brain barrier (BBB) have curtailed the identification of a suitable candidate [68,69]. Recent preclinical studies have demonstrated that a bi-specific anti-BACE1 neutralizing antibody inhibits Aβ production, thus providing an alternative mechanism for clinically inhibiting β-secretase activity [70,71]. The most advanced drugs targeting the APP processing pathway are γ-secretase inhibitors or modulators [72]. Unfortunately, two prominent candidates targeting γ-secretase were discontinued after disappointing phase III clinical trials. Tarenflurbil is a γ-secretase modulator that suppresses production of Aβ42 in favor of shorter Aβ peptides [73]. A promising phase II trial demonstrated a slower rate of cognitive decline in mild AD patients taking the drug as compared to placebo [74]. However, a follow-up phase III trial did not demonstrate any effect of the drug on

cognitive decline [75]. Similarly, semagacestat is a γ-secretase inhibitor that in a phase II trial reduced Aβ production in the human CNS [76]. A phase III follow-up trial was discontinued early when in-trail monitoring revealed a decrease in cognitive function among those patients receiving the inhibitor [77]. Therefore, targeting the γ-secretase complex may not represent a viable strategy for AD, especially given that important signaling molecules (e.g. Notch) are also γ-secretase substrates and that the complex may play a role in membrane turnover [78].

Other nascent therapeutics that have entered clinical trials target either Aβ aggregation or Aβ clearance. Tramiprosate is a glycosaminoglycan-mimetic that blocks Aβ aggregation [79]. A phase II trial showed that the drug reduced CNS Aβ42 levels [80]. However, a phase III trial did not show any effects of tramiprosate on cognitive decline [81]. Immune-based strategies for the treatment of AD hold great promise as an approach that may produce more potent disease-modifying effects than the current small molecule-based treatments. Both active immunization strategies and passive antibody formulations have been pursued. An initial vaccination clinical trial with Aβ42-adjuvant was halted, however, when a high incidence of meningoencephalitis was observed [82]. Passive immunotherapy with humanized monoclonal antibodies (bapineuzumab and solanezumab) is currently in phase III testing. Phase II clinical trials demonstrated that these antibodies reduce plasma and CSF Aβ but effects on cognition were fairly weak [83,84]. Another immunotherapy approach is the use of intravenous immunoglobulins (IVIG) [85,86]. Natural anti-Aβ antibodies are present in these preparations but not in high quantities [87]. Further clinical testing on the efficacy of IVIG for AD is in progress.

In summary, many preclinical studies have identified attractive new therapeutic targets and strategies. Unfortunately, as many of these treatment modalities have

moved into clinical trial testing, the results have been invariably disappointing. Therefore, the search for effective disease-modifying therapies continues.

II. Biology of amyloid-β precursor protein (APP)

A. Biochemical processing of APP

As briefly mentioned above, APP is a type I transmembrane protein that undergoes proteolytic processing by secretase enzymes to liberate soluble fragments (Figure 1) [88,89]. Amyloidogenic processing begins with proteolytic cleavage at the N-terminus of the Aβ domain in APP by β-secretase (BACE1). This cleavage event results in the release of the secreted beta-form of APP (sAPPβ) and the retention of the 99 amino acid C-terminal fragment (CTF) C99 in the membrane. Intramembranous cleavage of C99 at the C-terminus of the Aβ domain by the γ-secretase complex results in the release of both Aβ and the APP intracellular domain (AICD) [90].

The γ-secretase is a large complex composed of at least four different protein subunit substrates (Nicastrin, anterior pharynx defective 1 [APH1], presenilin enhancer [PSEN], and presenilin1 or presenilin 2). The proteolytic site appears to be located within the presenilin proteins [91]. Promiscuous C-terminal cleavage of the Aβ domain in APP by the γ-secretase complex is responsible for the generation of Aβ40 and Aβ42.

The non-amyloidogenic processing pathway involves initial cleavage by one of several α-secretases releasing sAPPα and leaving the C83 CTF [92]. By cleaving within the Aβ domain, α-secretase activity precludes Aβ production. Intramembranous cleavage of C83 by γ-secretase leads to the release of the non-amyloidogenic p3 peptide and AICD.

Both α- and β-secretases cleave APP on the luminal side of the membrane, resulting in release of sAPPα and sAPPβ into the extracellular or endosomal

compartments depending on holo-APP trafficking. Following intramembranous γ-secretase cleavage, Aβ or p3 are likewise released into extracellular or endosomal compartments, while AICD is released into the cytosol.

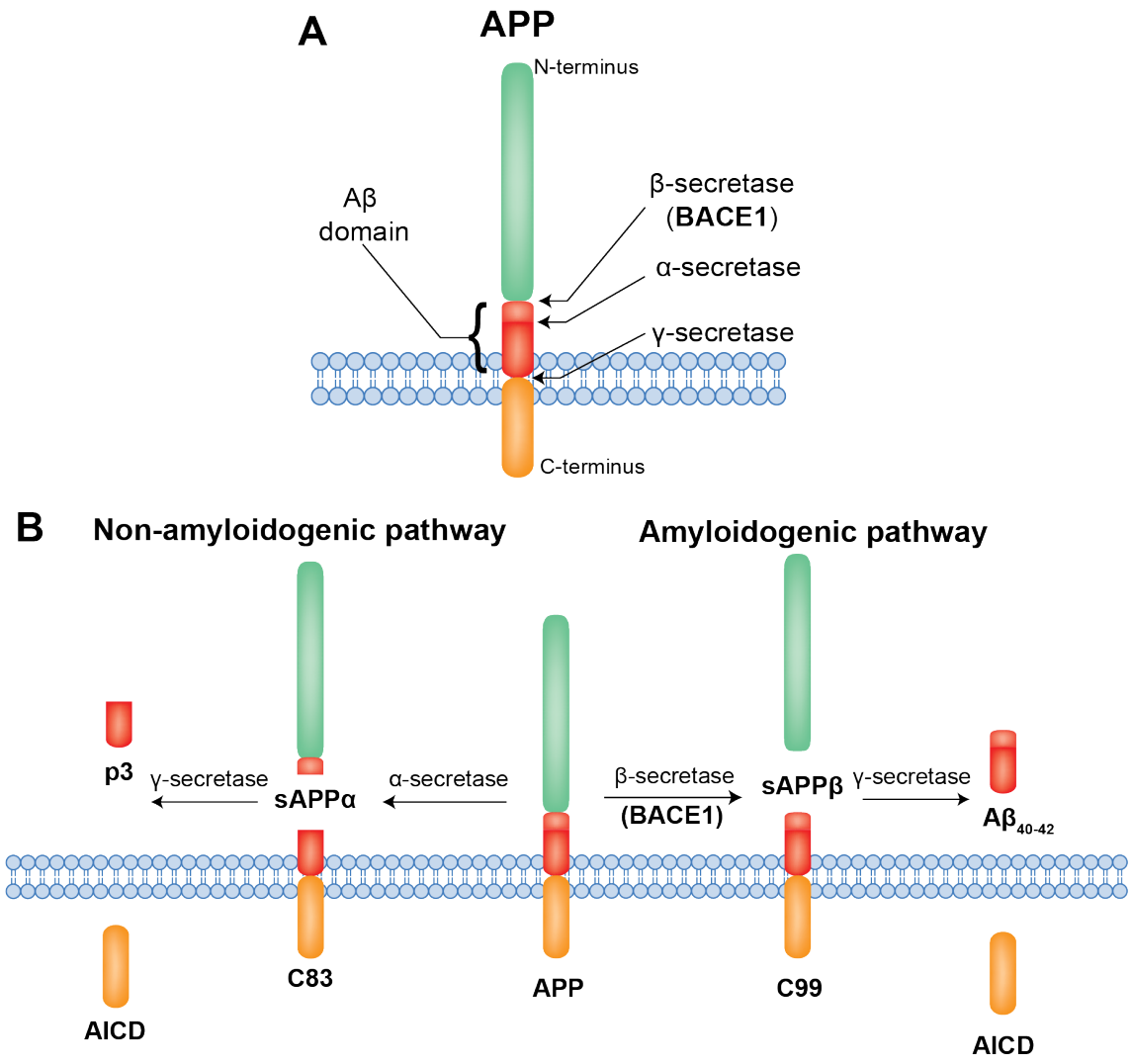

Figure 1: Biochemical processing of APP. (A) Schematic of the APP protein highlighting the Aβ domain and approximate locations of secretase target sites. The Aβ N-terminus is located on the luminal side of the protein and is defined by the presence of the β-secretase site. The C-terminus of the Aβ domain is located in the membrane and defined by the γ-secretase site. The α-secretase site is internally positioned within the Aβ domain. (B) Non-amyloidogenic processing requires sequential cleavage by α-secretase and the γ-secretase complex, releasing the non-amyloidogenic p3 peptide and AICD. Amyloidogenic processing requires sequential cleavage by β-secretase (BACE1) and the γ-secretase complex, releasing Aβ and AICD.

B. Physiological functions of APP

The primary physiological function of holo-APP is still unclear. However, biological activity of the secreted metabolite of APP is well-established. The first recognized biological effect of sAPP was its requirement for the normal proliferation of fibroblasts in culture [93] in addition to the promotion of neuronal PC12 cell adhesion to culture substratum [94]. Studies on cultured neurons and animals quickly followed and have since identified trophic effects that include: 1) the enhancement of neurite outgrowth [95–100], 2) stimulation of neural stem cell proliferation [101–103], differentiation and migration [104], 3) promotion of synaptogenesis [105–107], and 4) modulation of synaptic plasticity, learning and memory [108,109]. Additionally, sAPP has been demonstrated to protect neurons against a variety of insults that include glucose deprivation and excitotoxicity, Aβ and reactive oxygen species (ROS), and ischemic brain injury [110–112]. Following the discovery of multiple secretase activities [88,89], sAPPα was found to mediate the majority of neuronal-enhancing effects. Specifically, the neuroprotective action of sAPPα against glucose deprivation, excitotoxicity, and Aβ toxicity is 100-fold greater than that mediated by sAPPβ [113]. Interestingly, a pathological function for sAPPα has been recently suggested in autism, where elevated peripheral levels of sAPPα are present in severely autistic children [114–116].

A separate reported role for secreted APP is as a physiological signal for axonal degeneration and developmental pruning [117]. In cultured neurons under conditions of trophic withdrawal, BACE1 activity is stimulated leading to enhanced release of sAPPβ that is further degraded to an active 35 kDa N-terminal fragment (N-APP). This N-APP moiety serves to activate the DR6 death receptor. Axonal degeneration is then induced by activation of the caspase 6 apoptotic pathway. Therefore, sAPP may contribute to

normal neuronal development by both stimulating growth and neurite sprouting and by promoting pruning and maturation of newly formed synaptic connections.

Another APP metabolite with reported functional effects is AICD. This intracellular fragment, once released from APP, can act as a transcriptional co-activator with Fe65 and Tip60 [118,119]. AICD production may be induced by a Notch-like signal transduction system. In this system, APP acts as a receptor for TAG1, whereby binding of TAG1 ligand to APP induces γ-secretase cleavage of APP and subsequent release of AICD [120].

C. Transcriptional and post-transcriptional control of APP expression

The network of cis-acting elements and trans-acting factors that govern expression of APP is complex and still not fully elucidated. Studies of the APP promoter have revealed a complex structure with many proximal and distal regulatory elements that mediate constitutive and stimulated regulatory activities [121–125]. Proximal promoter elements are necessary for basal transcriptional activation [126–129] and bind various nuclear factors [126,130] responsible for mediating this activity, including SP1 [131], USF [132,133], and CTCF [134,135]. A 30 bp element in this region mediates cell type-specific transcriptional activation [136]. Proximal regions further upstream also contain regulatory elements important for transcriptional regulation [128]. Negative regulatory elements exist in this region [137,138], as do heat shock elements that bind HSF-1 and mediate transcriptional activity in response to stress and an enhancer element that binds a SP1-like factor [139]. Regulatory elements in the genomic 5'-untranslated region (UTR) also drive promoter activity through a CAGA box [140], thyroid hormone (T3) responsive element [141], and nuclear factor binding domain [142], among others.

Post-transcriptional regulation is also mediated via regulatory elements in the mRNA 5'-UTR, including an iron responsive element (IRE) [143,144] and IL-1 responsive element [145] involved in regulating stimulated translation of the APP transcript. Specifically, the iron responsive element forms a stem-loop that binds to iron regulatory protein 1 (IRP1) under low intracellular iron conditions, thereby inhibiting APP translation. When intracellular iron levels increase, iron binds to IRP1 promoting its release from the APP mRNA 5'-UTR and disinhibiting the translational block [144]. An internal ribosomal entry site has also been described in the 5'-UTR that can also regulate translation of APP independent of cap-dependent translation [146].

The APP 3'-UTR contains several stability control elements that regulate APP mRNA stability. 29-nucleotide (nt) and 52-nt control elements exist that destabilize the transcript [147–149]. Destabilization is attenuated or promoted in a regulated fashion by the binding of various cytosolic factors to these elements, including hnRNP C and nucleolin [150–153]. Polyadenylation of the APP 3'-UTR also regulates transcript stability through the inclusion or exclusion of a specific GG dinucleotide sequence in the various polyadenylated transcripts [154,155].

Finally, interactions between the APP mRNA coding sequence (CDS) and FMRP and hnRNP C competitively regulate translation of APP in response to metabotropic glutamate receptor activity [156,157]. Obviously, regulation of APP expression involves a complex, intertwined network of trans-acting factors working on a dense landscape of cis-acting elements located throughout the APP gene and transcript.

III. Biology of BACE1

A. Biochemical and physiological function of BACE1

The biochemical properties of the β-secretase enzyme had been established well before BACE1 was identified by five independent groups as the β-secretase enzyme in 1999 [158–161]. BACE1 is a type I transmembrane aspartyl protease. Protease activity is optimal when the catalytic site is in a low pH environment. As a result, BACE1 tends to localize in acidic compartments, such as endosome and trans-Golgi network, with its catalytic site oriented towards the lumen [162].

As described above, BACE1 cleaves APP at the aspartate residue that defines the N-terminus of the Aβ domain in the APP protein and is the rate-limiting enzyme for Aβ production. Cleavage at this site liberates sAPPβ into the lumen of the vesicular organelle where the BACE1 enzyme is localized. The C99 CTF remains in the membrane as a substrate for γ-secretase processing. γ-secretase then cleaves at the C-terminal end of the Aβ domain, liberating either Aβ40 or Aβ42. Aβ is a normal physiological product of BACE1 activity, suggesting that it might have a physiological function aside from its pathological role in AD. Indeed, low concentrations of Aβ have been shown to enhance synaptic plasticity and memory [163,164]. This response to Aβ has been described as hormetic in that the opposite effect is observed at higher concentrations [165].

BACE1 has other physiological substrates aside from APP. The protease also cleaves APP-like protein 1 (APLP1) and APLP2 [166,167], the voltage-gated sodium channel β_2 subunit ($Na_v\beta_2$) [168], and neuregulin 1 type III and neuregulin 3 (NRG1 and NRG3) [169,170]. NRG1 and NRG3 processing by BACE1 plays a critical role in normal peripheral myelination [169,170]. Blocking the processing of NRG1 and NRG3 by BACE1 produces reduced myelin thickness at the sciatic nerve. Repair of damaged

sciatic nerve is also impaired when NRG1 processing by BACE1 is inhibited. Cleavage of the $Na_v\beta_2$ subunit, first by BACE1 and then by γ-secretase, results in the release of a short β_2 intracellular fragment that activates $Na_v1.1$ mRNA expression [171]. However, the end result of this process is reduced surface $Na_v1.1$ due to intracellular accumulation. Therefore, BACE1 regulates sodium current densities in the cell.

B. Transcriptional and post-transcriptional control of BACE1 expression

Much like with APP, the spectrum of regulatory schemes utilized by the cell to control BACE1 expression is complex and still not fully clear. The BACE1 promoter has been fairly well characterized [172,173]. In neurons, the BACE1 promoter activity is significantly weaker as compared to the APP promoter [174]. The promoter lacks canonical TATA or CAAT boxes and more closely resembles the promoter of a "housekeeping gene". The core or minimal promoter is located proximally and spans the transcription start site (TSS) with some aspects of the minimal promoter located in the genomic 5'-UTR [172,173]. Both positive and negative regulatory elements have been described in more distal segments up to 4 kb from the TSS.

Multiple predicted transcription factor (TF) binding sites have been reported [172]. Of these, several have been validated in terms of physical interactions and functional effects. Sp1 interacts with the BACE1 promoter and stimulates BACE1 expression [173]. 12/15-lipoxygenase expression in the brain has been linked to AD and causes increased BACE1 expression and Aβ production. This enzyme mediates this effect indirectly by stimulating Sp1 expression [175]. Yin Yang 1 (YY1) binds to a more distal section of the rat promoter and also stimulates BACE1 expression [176]. NF-κB binds to the rat promoter and normally represses BACE1 expression in neurons but activates BACE1 expression in activated astrocytes under AD-type stress conditions [177]. Finally, two CpG sites in the genomic 5'-UTR are typically methylated

and basally inhibit BACE1 transcription [178]. Treatment with the demethylating agent, 5-aza-2'-deoxycytidine, results in increased BACE1 expression mediated specifically through demethylation of these two CpG sites.

Several modes of BACE1 post-transcriptional regulation have also been discovered. One mechanism is mediated through the BACE1 5'-UTR. The 5'-UTR is rather long at 446 nt, has high GC content and multiple predicted upstream AUGs (uAUGs) and open reading frames (uORF) [179]. These are all characteristics typical for gene products under strict translational control, such as proto-oncogenes and stress response proteins. The presence of multiple uAUGs and uORF generally inhibits mRNA translation because ribosomal scanning initiated from the cap will result in binding and translation of the uORF instead of the authentic ORF. Unless the ribosome re-initiates scanning following translational termination of the upstream ORF or simply skips the upstream ORF altogether (i.e leaky scanning), then the authentic AUG cannot serve as a site of translation initiation [180]. Indeed, multiple studies have identified the second uORF in the BACE1 5'-UTR as a potent inhibitor of BACE1 translation [179,181–183]. Interestingly, under conditions of energy deprivation, BACE1 translation is induced via a mechanism that requires the presence of the 5'-UTR and phosphorylation of the translation initiation factor eIF2α [184]. The proposed model for this effect is that phosphorylation of eIF2α creates an environment where ribosomes more readily scan past the uORF, therby increasing the likelihood that the authentic ORF will be recognized.

Another post-transcriptional mechanism employed by human cells to control BACE1 levels is the expression of a BACE1 antisense non-coding RNA [185]. This RNA binds to approximately 106 complementary nucleotides from exon 6 in the BACE1 mRNA and stabilizes the transcript. The mechanism involves protecting a microRNA recognition element (MRE) against targeting by miR-485-5p [186]. Despite containing a

longer 3'-UTR than APP, no novel regulatory mechanisms targeting the 3'-UTR have been described for BACE1.

It is clear that, as with APP, transcriptional and post-transcriptional mechanisms for regulating BACE1 expression in human cells are complex and varied. Our understanding of the full regulatory network is still incomplete. Therefore, continued study of the mechanisms that regulate BACE1 expression in human cells is warranted.

IV. Targeting APP and BACE1 as a therapeutic strategy

As described above, many of the anti-amyloid therapeutic strategies being pursued in the AD preclinical and clinical pipeline are designed to act on protein targets after they have been expressed (e.g. anti-Aβ immunotherapy and small molecule secretase inhibitors). Most of these late-phase clinical trials have generated disappointing results. While some have taken these clinical trial failures as an indictment of the amyloid hypothesis of AD etiology, it is more likely that deficiencies in clinical trial design or the treatment strategies themselves are more likely to blame [187,188]. Therefore, additional strategies and targets are likely needed before safe and effective therapeutics are developed.

As an alternative strategy, modulating *expression* of relevant protein drug targets may prove equally effective (or superior) in some cases. Specifically, APP and BACE1 are attractive candidates for expression modulation. Increased APP expression in DS [30], *APP* gene locus duplication events [47], and as a consequence of *APP* promoter polymorphisms [48,49] is sufficient to cause FAD. BACE1 protein levels are known to be increased in some SAD patients [39,40,189]. Reducing APP and BACE1 expression would be corrective in these cases and would be expected to reduce production of Aβ with presumably anti-amyloidogenic effects in cases where APP and BACE1 levels are not deranged.

It is important to point out that APP has very well established roles in normal neurodevelopment as described above. Therefore, therapeutically targeting APP expression could potentially have deleterious side effects related to inhibition of these neurodevelopmental pathways, aside from the anticipated salutary effects on Aβ production. However, given that neurodevelopmental pathways are likely to be most active during early CNS development, application of APP targeting in later life when amyloid pathology begins to accumulate would presumably have a less malignant effect.

Preclinical studies in rodent animal models using antisense inhibition of APP expression have demonstrated salutary effects following the approach outlined above [190,191]. Other amyloid-independent roles of APP implicated in AD, such as transcriptional effects from the release of AICD and effects on endosomal function [52], would also be altered in a beneficial fashion. A small molecule-based approach for modulating APP expression post-transcriptionally has already been pursued in at least one study [192]. Similarly, knockout of BACE1 expression in the Tg2576 AD mouse model reverses cognitive deficits associated with Aβ accumulation [193]. Systemic delivery to the brain of both a BACE1 siRNA and BACE1 neutralizing monoclonal antibody resulted in decreased BACE1 expression and decreased Aβ levels in the brains of animal models [70,71,194]. Therefore, the evidence supports targeting expression of APP or BACE1 therapeutically as a means to modify Aβ levels in the human brain.

Certain caveats would certainly have to be addressed before translating such an approach to the clinic, such as whether any malignant effects might arise from reducing APP and BACE1 expression and their associated physiological functions in the context of FAD or SAD. APP and BACE1 gene knockout animals have only subtle phenotypic changes, suggesting that side effects of expression reduction would be minimal

[193,195]. Whether this would also translate to humans is not clear and would require further investigation.

Before APP and BACE1 expression can be targeted therapeutically, a clear map of the regulatory network that governs APP and BACE1 expression in the CNS needs to be established. Only then can appropriate targets be selected for therapeutic manipulation. As summarized above, this regulatory network appears to be extensive for both APP and BACE1, with contributions arising at the transcriptional and post-transcriptional levels. MicroRNAs (miRNA) are a relatively new class of biological molecule that mediate potent post-transcriptional effects on gene expression. This class of regulatory molecule will likely be amenable to *in vivo* therapeutic manipulations in the near future and therefore may serve as ideal drug targets for modulating APP and BACE1 expression. Prior to expounding upon the rationale for examining the role of miRNA in regulating expression of APP and BACE1, a sufficient introduction to basic miRNA biology will be presented.

V. Biology of miRNA

A. Discovery, historical perspective and nomenclature

The first miRNA was discovered in 1993 during studies on the temporal control of *Caenorrhabditis elegans* development [196]. *lin-4* was identified as a regulator of the heterochronic gene *lin-14* and originally termed a small temporal RNA (stRNA). Investigators discovered that *lin-4* was not expressed as a protein, but instead as a small RNA consisting of a 61-nt stem-loop precursor that matured to a 22-nt product. This small RNA contained sequences with partial complementarity to sequences in the *lin-14* 3'-UTR known to be important for post-transcriptional regulation of the protein product [197]. Thus, many of the prominent structural and functional principles now

known to be common to all miRNAs were elucidated in these first reports of a single member. A second miRNA (let-7) was not discovered until 2000 [198] and was found to be conserved across a number of species, including vertebrates [199]. Large scale cloning studies later identified a plethora of miRNA that are expressed across many species, including humans, and that fit the miRNA profile: a small RNA sequence that is present in both a stem-loop precursor form (pre-miRNA) and mature single stranded RNA form [200–202]. Many of these miRNAs were also shown to be conserved across numerous species. miRNAs were soon found to negatively regulate both *Drosophila* and vertebrate mRNA targets through complimentary sequence motifs located in the 3'-UTR, just as in *C. elegans* [203,204].

The naming convention adopted in these early studies was to name miRNA numerically in the order they were discovered. Nomenclature is now curated by the miRBase database [205]. Since many miRNA are conserved across species, the same number is given to orthologous miRNA. Species is designated by a three or four letter prefix (e.g. hsa-miR-101 for human miR-101). In most cases, mature miRNA are generated from one strand of the precursor miRNA (guide strand) while the other strand of the stem-loop (passenger strand) is degraded (discussed below). The passenger strand is often designated the "star" strand (e.g. hsa-miR-101*). In some cases, mature miRNA strands are generated from both arms of the stem-loop. These miRNA are given either a -5p or -3p appellation based upon the end of the stem-loop from which they were derived (e.g. miR-339-5p). Finally, gene duplication events and subsequent sequence evolution have generated miRNA paralogs in some cases. These are distinguished by a letter suffix (e.g. hsa-miR-133a and hsa-miR-133b). When the mature miRNA sequences derived from paralogous precursor miRNA are identical, the gene loci from which they are derived are distinguished by a number suffix (e.g. hsa-miR-101-1 and hsa-miR-101-2).

B. Biogenesis

Most miRNAs are transcribed by RNA polymerase II as long primary transcripts (pri-miRNA) that form local stem-loop structures harboring the mature miRNA sequence [206]. Therefore the structure of a transcribed pri-miRNA consists of long ssRNA arms flanking small local stem-loops containing a pre-miRNA and mature miRNA sequence. The genomic location of the pri-miRNA locus can vary from intergenic regions, to intronic or exonic regions of non-coding or protein-coding RNA [207]. When located intergenically, Pol II-based transcription is driven by independent promoter elements. When located within introns, miRNA are often co-transcribed along with the host gene. Following transcription, the pre-miRNA is processed from the intron either before or in conjuction with intron splicing just as if the sequence was an independent pri-miRNA. If the miRNA locus is hosted within a large intron, it is not unreasonable to speculate that distinct internal regulatory elements within the intron may independently drive miRNA expression.

Following pri-miRNA transcription, the nuclear microprocessor complex, consisting of RNaseIII-like Drosha and DiGeorge syndrome critical region 8 (DGCR8) in human cells, recognizes the internal stem-loop and cleaves the pri-miRNA approximately 11 nt from the dsRNA-ssRNA junction, releasing the stem-loop structure (pre-miRNA) from flanking RNA and leaving a 3' 2-nt overhang [208–210]. This newly formed pre-miRNA is exported from the nucleus by exportin-5 [211]. In the cytosol, the complex of Dicer and TAR RNA-binding protein (TRBP) in human cells binds the pre-miRNA at the 2-nt overhang and cleaves the loop approximately 22-nt downstream of the stem terminus [212,213]. TRBP then recruits AGO2 to the Dicer-TRBP-miRNA complex [212]. The miRNA is then incorporated into a microribonucleoprotein (miRNP) complex [214], also termed the RNA induced silencing complex (RISC), via a loading complex as described below [215].

C. Assembly of microribonucleoprotein complex

The core protein of the RISC complex in humans is always a member of the AGO subfamily of Argonaute proteins (AGO1-4), oftentimes being AGO2. AGO2 is the only member of the AGO family to possess “slicer” activity (i.e. endonucleolytic activity). The mature RISC consists of a ssRNA loaded onto AGO2, in complex with other effector proteins. However, the miRNA product of Dicer processing is a dsRNA with 2 nt 3’ overhangs on either end. Therefore, three steps are necessary for proper assembly of the mature RISC [216]. These steps are facilitated by the RISC loading complex (RLC). The RLC can be minimally reconstituted *in vitro* by combining equal stoichiometric amounts of Dicer, TRBP and AGO2 [217]. However, full RLC activity is achieved when the RISC activator C3PO is also a part of the RLC [218].

The first step in assembling the mature RISC is to load the double stranded miRNA onto the AGO protein. Due to the bulky size of the dsRNA, heat shock proteins 90 and 70 (HSP90 and HSP70) chaperone this process by helping to modify the AGO structure such that the dsRNA fits into the AGO protein [219,220]. The 5’ phosphate on the duplex miRNA strand is apparently critical for normal loading into AGO proteins [221]. The choice of strand to be incorporated into the mature RISC is generally based upon the asymmetry rule [222]. The strand with the least thermodynamic stability at its 5’ end generally is loaded and becomes the guide strand.

The next step in assembling a mature RISC is to pry apart the duplex miRNA as the initial step in unwinding the duplex. Recently the N-terminal domain of AGO2 has been implicated in this task [216]. The data suggest that the N-terminal domain either actively or passively wedges the duplex apart during loading.

The final step in assembling a mature RISC is to fully unwind the duplex RNA until only the guide strand remains in complex with AGO. If there is no mismatch in the duplex complementarity at nucleotides 10 – 11, then slicer-dependent unwinding is

employed. AGO2 endonucleolytically nicks the passenger strand while also wedging the sequences apart. C3PO then can exonucleolytically degrade the AGO2-knicked passenger strand [218]. When mismatches in the double stranded miRNA are present at nucleotides 10 – 11, then slicer-independent unwinding is instead employed. Once the single stranded guide strand is loaded into the mature RISC, it guides the RISC to complementary mRNA targets (biogenesis and RISC assembly summarized in Figure 2).

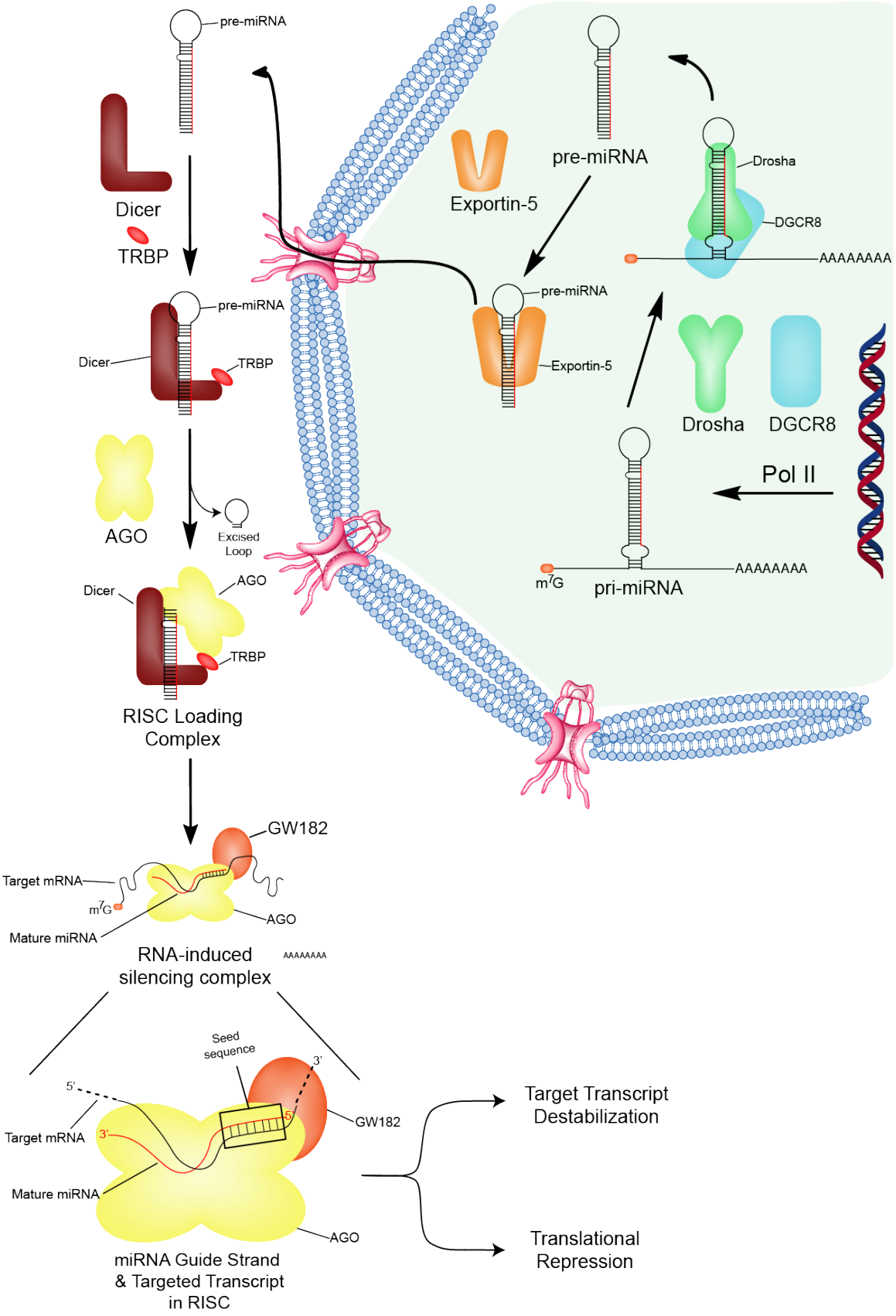
pre-miRNA
Dicer
TRBP
pre-miRNA
Dicer
TRBP
AGO
Excised Loop
Dicer
AGO
TRBP
RISC Loading Complex
GW182
Target mRNA
m7G
AGO
Mature miRNA
AAAAAAAA
RNA-induced silencing complex
Seed sequence
3'
5'
Target mRNA
3'
5'
GW182
Mature miRNA
AGO
miRNA Guide Strand & Targeted Transcript in RISC
Target Transcript Destabilization
Translational Repression
Exportin-5
pre-miRNA
Drosha
DGCR8
AAAAAAAA
pre-miRNA
Exportin-5
Drosha
DGCR8
Pol II
m7G
AAAAAAAA
pri-miRNA

Figure 2: miRNA biogenesis and RISC assembly in human cells. miRNA are initially transcribed as pri-miRNA, processed by the complex of Drosha and DGCR8 to pre-miRNA, exported to the cytosol by exportin-5, and cleaved to a mature miRNA guide strand and passenger strand (miRNA*) by the complex of Dicer and TRBP. For RISC loading, the miRNA duplex is loaded onto an AGO protein and unwound. The passenger strand is degraded while mature guide strand remains (red strand in illustration). The guide strand, AGO and GW182 proteins forms the mature RISC. The guide strand guides RISC to target transcripts by interacting with specific target sites in the 3'-UTR. Near perfect complementarity between the target transcript and the seed sequence of the miRNA is required to effectuate an inhibitory response. GW182 recruits deadenylase complexes and other factors to promote target transcript destabilization and repress translation. Adapted from Long and Lahiri [223]

D. Molecular mechanisms of gene regulation

Most miRNA target sites appear to be located in the 3'-UTR of target transcripts [84], although recent cross-linking experiments suggest interactions with target sites in the CDS and 5'-UTR do occur [85-86]. The primary explanation for why the majority of target sites are restricted to the 3'-UTR across the genome is that active translation of the transcript outside the 3'-UTR reduces the efficacy of target sites in these regions [224] .

Canonical target sites require a near perfect match between the 5' end of the miRNA (seed sequence located at nucleotide 2 – 6 of the miRNA) and target transcript [204]. Less stringency is required at the 3' end of the miRNA. Recently a novel mode for target recognition was described [225]. This new form of target site contains a G bulge in the target mRNA at position 5 of the seed sequence. Apparently this mode of targeting is favored because during the nucleation step, when the miRNA interacts with the G bulge target site, a reaction intermediate with favorable thermodynamics is formed.

Once the mature RISC is targeted to a given mRNA, the physiological response is typically to suppress protein production, although in some rare cases post-transcriptional activation has been reported [226]. The original consensus in the field was that miRNA suppressed protein output in animals primarily by decreasing translational efficiency and occasionally by degrading target mRNA. However, recent microarray and ribosome profiling studies have suggested that mRNA destabilization is the primary factor driving reduced protein output in animals [227,228]. The most recent studies have further clarified the story by suggesting that both decreased translational efficiency and mRNA destabilization occur during mRNA targeting, with the former preceding and often leading to transcript destabilization [229–231].

The mechanisms underlying the repressive effects of RISC targeting are beginning to become clear. AGO proteins serve as central hubs to recruit additional effector complexes that mediate inhibitory effects. Interaction of AGO with GW182 is essential for miRNA-mediated translational repression and, in some cases, mRNA destabilization [232,233]. The primary mechanism for mRNA destabilization is deadenylation of targets transcripts, followed by transcript decapping mediated by DCP2, and then 5'-to-3' exonucleolytic mRNA decay by XRN1 [234–236]. GW182 seems to participate in this pathway by recruiting the CCR4-CAF1-NOT and PAN2-PAN3 deadenylase complexes to the target mRNA [234,237,238]. The mechanisms underlying reduced translational efficiency are not as clear but miRNA targeting inhibits translation at both initiation and elongation steps [239,240]. The mechanism of miRNA-mediated gene repression contrasts to that of widely-used synthetic short interfering RNAs (siRNAs), which hybridize with perfect complementarity to mRNA targets and induce AGO2-mediated endonucleolytic cleavage and degradation of the transcript.

The precise level of miRNA expression necessary for functional regulation is likely to vary for each combination of miRNA and mRNA target and their specific environmental context. Titration experiments have demonstrated that miRNA efficacy is influenced both by the levels of target expression as well as miRNA levels, such that target thresholds are generated around which target levels are highly sensitive to miRNA effects [241,242]. Therefore, there is a complex interplay between target transcript, targeting miRNA and ensuing regulatory effects.

Bioinformatic analyses suggest that each miRNA may target hundreds of mRNA transcripts and that a single mRNA may be targeted by hundreds of targeting miRNA. In fact, more than 60% of all mammalian transcripts appear to have been under evolutionary pressure to maintain miRNA target sites [243]. However, global proteomic analyses following synthetic miRNA delivery suggest that a majority of miRNA-transcript

interactions mediate only subtle effects on protein expression. A much smaller number of targets per miRNA experience strong regulatory pressures [244,245]. Therefore, miRNAs appear to act more like rheostats to fine-tune expression for a majority of targets, with a select few targets under heavier regulatory pressures. Alternative theories posit that many of the miRNA-target interactions predicted by bioinformatic analyses are not physiologically relevant and instead serve to soak up and sequester target miRNAs [246]. By titrating levels of available miRNAs, these sites would control interactions of miRNA with physiologically relevant targets. These have been termed competing endogenous RNA (ceRNA) [247]. Several examples have been described where the presence of ceRNA has significant biological effects [248–250].

E. miRNA stability and turnover

Control of miRNA steady-state levels is a function of pri-miRNA transcription, pri- and pre-miRNA processing by the processing complexes, and regulated turnover of mature miRNA. Unlike miRNA, mRNA are stabilized by the presence of a 5' 7-methylguanylate cap and 3' poly(A) tail that protect against exonuclease activity. Controls on mRNA stability are tightly regulated and mRNA turnover modulates miRNA efficacy. A shorter mRNA half-life generally correlates with reduced miRNA efficacy [251]. Conversely, miRNA termini are exposed and appear to rely on interactions with AGO proteins [252] to stabilize against exonucleolytic degradation [253].

Recent studies have explored the half-life of miRNAs in various cell types and identified great variability. In one study, miRNA half-life was measured in mouse embryonic fibroblasts and bone marrow-derived macrophages following conditional Dicer ablation [254]. The predicted half-life after controlling for dilutional effects of cell proliferation was much longer than that of mRNAs and averaged around 119 hours. Conversely, two recent studies have identified much shorter miRNA half-lives in

neuronal cell types following inhibition of RNA polymerase II-based transcription. Analysis in primary neuronal cell cultures (HN cells) and frozen human brain specimens revealed miRNA half-lives in the range of 1 – 4 hours [255]. Similarly short miRNA half-lives were observed in retinal photoreceptors and cultured hippocampal and cortical neurons [256]. Together, these studies suggest that miRNAs are generally very stable *in vivo* but appear to be under regulatory control in neurons that promotes rapid turnover.

Specific mechanisms by which metazoan cells control miRNA degradation and turnover have been described but are just beginning to be explored [257,258]. In *C. elegans*, mature miRNA degradation was recently shown to be mediated by the 5'-to-3' exoribonuclease XRN-2 following dissociation of miRNA from RISC. Interestingly, increased levels of target mRNA protected against XRN-2 mediated degradation suggesting that duplex formation in RISC may stabilize miRNA. An additional control mechanism that appears to influence miRNA stability is the addition of non-templated terminal nucleotides. The poly(A) polymerase (PAP) GLD-2 monoadenylates miR-122 at the 3' terminus resulting in increased miR-122 stability [259]. Conversely, the non-canonical PAP Tut4 polyuridylates pre-let-7 at the 3' terminus resulting in reduced pre-let-7 stability and reduced mature let-7 levels [260,261]. This interaction requires Lin28 proteins that act as processivity factors for Tut4 [262]. Two recent studies have examined pre-miRNA modifications at the transcriptome level and identified extensive mono and polynucleotide additions and novel cleavage patterns indicating post-transcriptional nuclease modifications [263,264]. These studies demonstrate that post-transcriptional modifications of pre-miRNA are widespread and suggest they may represent a widely employed mechanism for miRNA stability control.

F. miRNA dysregulation in AD and contribution to pathophysiology

Unlike in many cancers, where direct contribution of miRNA dysregulation to disease etiology is well described, comparatively little is in known about the role miRNA play in the development of AD. A small number of studies have reported that miRNA levels are dysregulated in AD brain specimens [189,265–268], in AD CSF [267] and in peripheral blood mononuclear cells (PBMC) from AD patients [269] (for review see ref [270]). Unfortunately, there is very little reproducibility in detected miRNA between these studies. Disease heterogeneity, differences in specimen characteristics and methodological limitations likely underlie this lack of inter-lab reproducibility to varying degrees.

A small number of miRNA targets have been validated across multiple studies and might represent specific AD-dysregulated miRNA. These include miR-107, miR-29a/b, miR-181, miR-9, miR-106, miR-16, miR-15 and miR-146. miR-29a/b inhibits BACE1 expression [189] and is decreased in AD brain possibly contributing to elevated Aβ levels [189,267,268,271,272]. Similarly, miR-107 inhibits BACE1 and cofilin expression and is decreased in early AD [266,273,274]. miR-181c is decreased in AD brain [189,267,268,271], although the pathological relevance of miR-181c targets is still unclear. miR-15a levels are decreased in AD. This is a pro-apoptotic miRNA that inhibits expression of Bcl2 [275], an anti-apoptotic protein whose expression is known to be elevated in AD. miR-9 is highly expressed in the brain and is either decreased or elevated in the AD brain depending on the study [189,255,265,267,268,271]. miR-106b is decreased in AD brain and in AD transgenic animal models [276,277]. This miRNA also targets APP expression [276], perhaps directly promoting Aβ production. Finally, miR-146a is a pro-inflammatory miRNA that is elevated in the AD brain and in AD transgenic animal models possibly contributing to the pro-inflammatory state present in the AD brain [255,267,278,279]. miR-146a expression is stimulated by NF-κB signaling

and, once expressed, inhibits expression of complement factor H, an inflammatory response repressor in the brain [278]. Therefore, this is some precedence for miRNA dysregulation in the AD brain possibly contributing to AD pathophysiology.

G. Role of miRNA in normal and pathological aging

miRNA also appear to be implicated in the the process of physiological aging. The ultimate quantitative measure for effects on aging is life span. *C. elegans* is a commonly used model to assess effects on aging given the naturally short life spans of the worms. Studies have identified a large number of miRNA downregulated in older worms compared to young worms and a smaller number of miRNA that are upregulated with age (e.g. miR-34, miR-246, miR-271, miR-239a/b and others) [280]. When these upregulated miRNA were genetically deleted, the effects on aging varied depending on the identity of the miRNA. Therefore, in *C. elegans*, miRNA can have either promoting or antagonistic effects on life span. One miRNA with elevated expression in these studies was miR-34, a miRNA separately reported to contribute to brain aging [280–282]. Expression changes have also been reported in humans, where nine miRNA were found to be significantly downregulated in PBMC with increasing age [283]. These miRNA were also demonstrated to target gene products with known functions relevant to aging and may therefore play a causative or compensatory role in the aging process. The miRNA identified in these studies may also indirectly contribute to the pathophysiology of AD since the greatest risk factor for developing AD is advanced age.

Aging is often associated with cognitive decline even in the absence of AD, although the molecular processes underlying this phenomenon and general brain aging are not well understood [284]. The pathophysiological process for brain aging appears to be distinct from that of AD or other neurodegenerative disorders since large-scale neuron loss is not a significant component of normal brain aging [285]. Studies in

mouse, rat, chimpanzee and human have revealed that gene expression and biological pathways are altered during normal brain aging, especially those related to inflammatory and stress responses [286–290]. Several recent studies have also identified miRNA that appear to have altered expression patterns in the brain during aging. In the mouse brain, approximately 75 miRNA were found downregulated in old animals compared to young, including miR-34a, mir-101 and miR-124, and a few miRNA were upregulated [281]. Another study also examined miRNA expression changes with aging in rhesus macaque, chimpanzee and human brain and found that only miR-144 was consistently upregulated [291]. The contribution of these miRNA to the aging process and the relevance of their gene targets is still uncertain. A recent study demonstrated that knockdown of miRNA processing in *Drosophila melanogaster* reduced the fly lifespan and accelerated brain aging and degeneration [282]. Interestingly, miR-34a increased with age in these flies and miR-34a knockdown also reduced lifespan and promoted an accelerated brain aging phenotype. Therefore, expression of this miRNA during the aging process is required for normal rate of aging in *Drosophila*. This study also demonstrated that miR-34a likely mediates this effect by inhibiting expression of Eip74EF (E74A isoform), a component of steroid hormone signaling pathways [282]. While the data in this field is still preliminary and lacks consistency and reproducibility, it does suggest that miRNAs likely play a critical role in the normal and pathological aspects of the aging process.

VI. Hypothesis and Aims

Comprehensive knowledge of the physiological state is an essential component for elucidating pathogenic mechanisms. As such, the *overarching goal* of this dissertation is to clarify the normal, physiological pathways utilized by human cells to control expression of APP and BACE1. Given the hypothesized centrality of the Aβ peptide to AD etiology, the expectation is that newly discovered regulatory mechanisms that control expression of two gene products critical to Aβ production might serve as novel therapeutic targets for modulating disease progression. The current state of knowledge suggests that regulation of these two gene products is complex, with regulatory mechanisms existing at both the transcriptional and post-transcriptional level. miRNA are a class of endogenous non-coding RNA molecule with significant post-transcriptional gene silencing properties. Given that these molecules are predicted to regulate expression of the majority of mammalian genes and participate in nearly every biological pathway, it is highly likely that miRNA play an important role in regulating normal expression of APP and BACE1. Therefore, the *objective* of this dissertation is to determine whether miRNA participate in the regulatory networks that govern their expression. The ***central hypothesis*** tested in this dissertation is that specific miRNA species regulate APP and BACE1 expression and, by extension, have Aβ-modifying properties.

This hypothesis was tested by pursuing the following specific aims:

1.) Identify miRNA that endogenously regulate APP expression.
2.) Identify miRNA that endogenously regulate BACE1 expression.
3.) Investigate the relevance of identified microRNA in normal physiology and in pathophysiology of Alzheimer disease.

CHAPTER 2: MATERIALS AND METHODS

I. Tissue culture techniques

A. Culture and maintenance of continuous human cell lines

HeLa, U373, SK-N-SH and NTera2/D1 (NT2) cells were obtained from American Tissue Type Culture (ATCC, Manassas, VA). Standard cell culture procedures were employed in the culture and maintenance of all cell lines. Cells were grown on tissue-culture treated plasticware (Corning, Tewsbury, MA) and maintained at 37°C in a humidified incubator containing 5% CO_2. HeLa, U373 and SK-N-SH were grown in minimum essential media (MEM) (Cellgro, Manassas, VA) supplemented with 10% fetal bovine serum (FBS) (Atlanta Biologicals, Lawrenceville, GA) and 1% penicillin-streptomycin-amphotericin solution (Cellgro, Manassas, VA). NT2 cells were maintained in Dulbecco's modified eagle's media (DMEM) (Cellgro, Manassas, VA) supplemented with 10% FBS and 1% antibiotic cocktail.

Cells were routinely subcultured upon reaching 90% – 100% confluence by first washing cells twice with sterile phosphate buffered saline (PBS; Cellgro, Manassas, VA) and then enzymatically dissociating adherent cells using 0.05% trypsin/0.53 mM EDTA solution (Cellgro, Manassas, VA) for approximately 1 minute. Trypsin was then deactivated by adding an excess volume of serum-supplemented media and the cell suspension centrifuged at 200 g for 2 minutes. Cell pellets were then resuspended in serum-supplemented media and replated on new culture plasticware at 5 – 25% original density.

For certain experiments, precise number of cells were plated as indicated below. To obtain precise cell counts, the trypan blue exclusion method was employed. Cells were first dissociated with trypsin/EDTA as described above. Cell pellets were

resuspended in 1 mL of serum-supplemented media and a small aliquot diluted as needed for ease of cell counting. Diluted cell aliquots were mixed 1:1 with 0.4% trypan blue solution (Sigma-Aldrich, St. Louis, MO) and incubated for 2 – 5 minutes. Cells were then pipetted into a chamber consisting of a hemacytometer slide with an overlying coverslip. Number of cells were counted in five out of nine squares on the hemacytometer (each containing a volume of 0.1 mm^3) and used to estimate the concentration of cells in the original solution. Precise cell numbers were than plated by applying appropriate cell suspension volume.

Differentiated, post-mitotic NT2 neurons (NT2N) were prepared using a well-established protocol [292]. Adherent NT2 cells were cultured in T75 flasks in the presence of retinoic acid (RA) for four weeks with media changes every four days. Cells were then dissociated with trypsin/EDTA and replated to three T175 flasks (1:7 plating density). On each of the next two days, flasks were vigorously tapped along each side to detach loosely adherent cells. Recovered cells were replated on 100 mm dishes coated with 1:30 Matrigel (BD Biosciences, San Jose, CA) and grown in DMEM supplemented with 10% FBS, 1 μM cytosine arabinoside (Sigma-Aldrich, St. Louis, MO), 10 μM fluorodeoxyuridine (Sigma-Aldrich, St Louis, MO) and 10 μM uridine (Sigma-Aldrich, St. Louis, MO) for 1 week. Cells were then transitioned to DMEM supplemented with 10% FBS, 10 μM flurodeoxyuridine and 10 μM uridine for one additional week. Cell clumps were then gently dissociated with trypsin/EDTA and plated in white-walled 96-well tissue-culture treated plates for reporter transfections (see below). Following this protocol, this culture is comprised of greater than 90% post-mitotic neuronal cells resembling immature CNS neurons [292,293]

B. Culture and maintenance of primary human fetal brain cells

The process for culturing primary human fetal brain cells was established and primarily performed by Dr. Balmiki Ray in Dr. Lahiri's lab with assistance from the author. Primary cultures of mixed human fetal brain cells were prepared from the brain parenchyma of aborted fetuses (80 – 100 days gestational age). The tissues were obtained from the Birth Defects Research Laboratory (BDRL) at the University of Washington with approval from the Indiana University Institutional Review Board (IRB). Fetal brain materials (10 – 20 g) were shipped overnight in chilled Hibernate-E medium (Invitrogen, Grand Island, NY) supplemented with 1x B27 serum-free supplement (Invitrogen, Grand Island, NY), 0.5 mM GlutaMAX (Invitrogen, Grand Island, NY) and antibiotic-antimycotic solution (Cellgro, Manassas, VA).

The culture procedures closely followed a similar procedure for establishing primary neuronal cultures from rat cortex [294], with some modifications. The tissues were digested in 0.05% trypsin/0.53 mM EDTA solution and incubated in a shaking water bath (150 RPM) at 37°C for 15 minutes. The trypsin-digested tissues were transferred to Hibernate-E medium and triturated several times using a siliconized, fire-polished pipette followed by centrifugation at 400g for 15 minutes. The cell pellet was resuspended in Hibernate-E medium and triturated once more followed by centrifugation. The pellet was resuspended in culture medium (see below) and cells counted by Trypan blue exclusion method as described above.

The cells were plated at a density of 2 – 4x10^5 cells per well on poly-D-lysine (Sigma-Aldrich, St Louis, MO) coated 24-well plates in Neurobasal medium (Invitrogen, Grand Island, NY), supplemented with 1x B27, 0.5 mM GlutaMAX, 5 ng/mL bFGF (Invitrogen, Grand Island, NY) and antibiotic-antimycotic cocktail. Half media changes were performed every fourth day of culture. Based on preliminary characterizations, the late stage culture (days *in vitro* (DIV) 16 and beyond) contains a mixture of immature

neural stem cells (GFAP-, nestin-, and neuronal marker-positive) and differentiated neurons and astrocytes (positive for a single marker). A brief immunocytochemical characterization of these cultures is described in the Appendix.

C. Transfection of DNA vectors or RNA oligonucleotides into cell lines and primary cultures

Lipofection was employed in these experiments using two separate cationic lipid reagents: Transfectin (Bio-Rad, Hercules, CA) and Lipofectamine RNAiMAX (Invitrogen, Grand Island, NY). A full list of all commercially-obtained miRNA and siRNA molecules transfected in these experiments is included in Table 1. DNA constructs are described in section II below. During all transfections, antibiotics were omitted from cell culture media.

It is important to note that in all experiments where negative control RNA oligonucleotides (i.e miRNA mimics, miRNA inhibitors, target protectors) were transfected, universal negative controls were used. These commercially available universal controls have been designed to be minimally reactive with as few transcripts as possible based on complementarity analyses with mammalian transcriptome databases. These controls are not scrambled sequences and therefore do not necessarily have base composition identical to the experimental oligonucleotides for which they serve as controls.

In many experiments, changes in analytes levels were observed following transfection of negative control constructs as compared to mock transfection conditions. One possible explanation in these experiments is that changes in analyte levels following negative control transfection represent global non-specific or stress-related expression changes secondary to high oligonucleotide burden or interruption of normal metabolic pathways. As such, comparing negative control to experimental condition is

extremely appropriate in this case. An alternative explanation is that the negative control may have an inadvertent effect on analyte levels via sequence-specific complementarity or indirectly by modulating expression of an upstream pathway. In this case, comparison of experimental condition to negative control is likely not appropriate. In general, statistical comparisons were made between the experimental treatment and either the negative control or the mock transfection depending on which control condition exhibited the smallest difference in analyte levels compared to the experimental treatment. This approach was taken to avoid, as much as possible, inappropriate comparison between experimental treatments and negative control transfections.

In one set of experiments, DNA reporter constructs containing luciferase-expressing cassettes were transfected into HeLa, SK-N-SH and NT2N cells. For these experiments, HeLa cells ($5x10^4$ cells per well), SK-N-SH cells ($1x10^5$ cells per well) and NT2N cells ($1.6x10^4$ cells per well) were cultured in white-walled 96 well plates, with each well containing 100 µL of serum-supplemented media per well and transfected with 150 ng – 300 ng of reporter constructs using Transfectin. Transfection complexes were prepared by incubating DNA in a volume of serum-free media equivalent to 20 µL per well with 0.75 µL Transfectin per well for 15 – 20 minutes. Transfection complex-containing solution was then directly added to cells on-plate in serum-containing media. Luciferase assays were normally performed 48 hours after transfection.

In a separate set of experiments, HeLa cells were co-transfected with reporter constructs and miRIDIAN miRNA mimics (Dharmacon, Lafayette, CA). These co-transfections were performed by incubating HeLa cells cultured in 96-well plates ($5x10^4$ cells per well) with 150 ng reporter DNA and 40 nM miRNA mimic using 0.2 µL Transfectin per well. Transfection complexes were prepared as described above.

The remaining experiments were single transfections of Silencer Select siRNA (Applied Biosystems, Carlsbad, CA), miRNA mimics, miRNA locked nucleic acid (LNA) inhibitors (Exiqon, Woburn, MA), or miRNA Target Protectors (Qiagen, Valencia, CA) into HeLa or U373 cells using RNAiMAX reagent (primary human fetal neuron cultures discussed below). For most experiments, HeLa cells ($1.35x10^5$ cells per well) and U373 cells ($7.5x10^4$ cells per well) were cultured in 24-well plates and reverse transfected. In reverse transfections, transfection complexes are added to cultures at the same time as cells are plated. So, in this transfection format, cells are initially transfected in suspension until they settle and adhere to the plate. HeLa cells were generally transfected with 20 nM siRNA, 50 nM miRNA mimic, 100 nM – 1000 nM LNA miRNA inhibitor and 100-1000 nM miRNA Target Protector using 0.5 µL RNAiMAX per well. Transfection complexes were prepared in 50 µL Opti-MEM serum-free media (Invitrogen, Grand Island, NY) with 10 – 15 minute incubation periods prior to mixing with cell suspensions. U373 cells were similarly transfected with 75 nM miRNA mimics using 3.5 µL RNAiMAX per well. In several cases, miRNA mimics were co-transfected into HeLa cells with siRNA or miRNA target protectors. In these cases, RNAiMAX levels were boosted to 1µL per well to account for the increase in nucleic acid content.

Multiple batches of human fetal brain cultures were transfected at DIV 17 in 24-well plates. Cultures were transfected with 20 nM siRNA, 150 nM miRNA mimics, and 1000 nM LNA miRNA inhibitors using 1.25 µL RNAiMAX per well. bFGF was omitted from media during transfections. In one series of experiments, human fetal brain cultures were transfected with miRNA mimics in the presence of 150 µM deferroxamine mesylate (DFO) (Sigma-Aldrich, St Louis, MO). The appropriate volume of DFO was prepared from a 5 mg/mL stock solution in PBS and added to cell culture plates approximately one hour prior to transfection.

In all experiments employing transfection of small RNA oligonucleotides, transfection efficiency was assessed qualitatively by including a siRNA transfection (20 nM) against the gene product of interest. These siRNA were validated in HeLa cells as capable of reducing APP or BACE1 protein and mRNA expression to less than 5% of mock or negative control siRNA transfections.

Table 1: List of transfected siRNA and miRNA molecules

siRNA Reagents		
Targeted mRNA	Vendor	siRNA ID
APP	Applied Biosystems	s1500
BACE1	Applied Biosystems	s24219
Dicer	Applied Biosystems	Custom
AGO2	Applied Biosystems	Custom
IRP1	Applied Biosystems	s672
Negative Control #1	Applied Biosystems	4390843
miRNA Mimics		
miRNA Name	Vendor	Catalog Number
hsa-miR-1	Dharmacon	C-300585-05
hsa-miR-101	Dharmacon	C-300518-07
hsa-miR-153	Dharmacon	C-300615-07
hsa-miR-346	Dharmacon	C-300712-03
hsa-miR-339-5p	Dharmacon	C-300707-07
hsa-miR-29b	Dharmacon	C-300520-05
Negative Control Mimic #1	Dharmacon	CN-001000-01
Negative Control Mimic #2	Dharmacon	CN-002000-01
miRNA Antisense LNA Inhibitors		
Targeted miRNA	Vendor	Catalog Number
miR-101	Exiqon	412942-08
miR-153	Exiqon	410076-08
miR-346	Exiqon	411373-00
Negative Control A	Exiqon	199004-00
Custom miRNA Target Protectors		
miRNA Target Site		Vendor
miR-346 APP Target Site		Qiagen
miR-339-5p BACE1 Target Site 1		Qiagen
miR-339-5p BACE1 Target Site 2		Qiagen
Negative Control Target Protector		Qiagen

D. Harvest and preparation of cell culture lysate for RNA and protein analyses

Culture plates were collected, placed on ice, and allowed to equilibrate to temperature for a few minutes. Conditioned media (CM) from cell cultures were then collected and centrifuged at 200 g for 10 minutes. Cleared supernatant was collected and stored at -20°C for later analysis. Culture plates were then washed once briefly with 5 mL ice-cold PBS followed by aspiration of wash solution.

For downstream protein analyses, 75 – 100 µL of ice-cold mammalian protein extraction reagent (M-PER; Pierce, Rockford, IL) supplemented with 0.1% sodium decyl sulfate (SDS) and 1x protease inhibitor cocktail set III (EMD, Billerica, MA) was added to each well on the plate with shaking for 15 minutes at 4°C. Crude lysates were collected and centrifuged at 30,000 g for 10 minutes. Cleared supernatant was collected and either immediately used in downstream applications or stored at -20°C for later use.

For downstream RNA analyses, 300 – 600 µL ice-cold cell lysis/binding buffer from the miRVana miRNA Isolation kit (Ambion, Grand Island, NY) was added to each well. Cells were immediately washed from the plate by pipette and triturated up and down until no visible cell clumps were apparent. Lysates were stored on ice before proceeding with RNA extractions (described below).

For downstream applications that required both RNA and protein analyses from the same sample, 125 µL ice-cold cell disruption buffer from the miRVana PARIS kit (Ambion, Grand Island, NY) supplemented with 1x protease inhibitor cocktail set III was added to each well. Cells were washed from the plate and triturated by pipet until no visible clumps were apparent. A 50 µL aliquot of lysate was then immediately mixed with equal volume 2x denaturant (from miRVana PARIS kit) supplemented with β-mercaptoethanol (βME). Denaturant-containing lysate was then used for downstream

RNA extraction while the crude lysate was centrifuged at 30,000 g for 10 minutes. Cleared supernatant was collected and stored at -20°C for later protein analyses.

II. Molecular biology techniques

A. PCR amplification of DNA insert and purification

The APP 3'-UTR and BACE1 3'-UTR were amplified by PCR for insertion into the psiCHECK-2 reporter vector (Promega, Madison, WI). The APP 3'-UTR was amplified in both forward and reverse orientation from the pGALA construct (kindly provided by Dr. JT Rogers). The BACE1 3'-UTR was amplified from pooled human genomic DNA (Roche Applied Science, Indianapolis, IN). The DNA templates were amplified using Platinum Taq (Invitrogen, Hercules, CA). This is a "hot start" enzyme mix containing an anti-Taq antibody that must be first heat-denatured during thermocycling for full enzyme activity. All PCR reactions were assembled on ice at a dedicated PCR/RNA workbench with special supplies to prevent DNA or RNA contamination.

Reactions were assembled by combining 1 ng plasmid DNA or 200 ng human genomic DNA with 10x PCR buffer, 1.5 mM $MgCl_2$, 200 µM dNTP mixture, 1 µM forward and reverse orientation PCR primers, Platinum Taq enzyme and molecular-grade water. Reactions were then placed in a thermocyler (Bio-Rad). A preliminary denaturation incubation at 94°C for 2 minutes was followed by 30 cycles of the following protocol: 94°C for 30 seconds, 55°C for 30 seconds, 72°C for 1 minute for the APP 3'-UTR or 4 minutes for the BACE1 3'-UTR.

PCR reactions were then purified using the spin column-based QIAQuick PCR Purification Kit per manufacturer's protocol (Qiagen, Valencia, CA). This kit selectively retains amplicons larger than 100 bp while allowing primers and primer-dimers to wash

through the column. Purified PCR amplicons were analyzed by agarose gel electrophoresis to confirm specific amplification and efficient removal of primers and primer-dimers. Amplicon fragments were quantified by measuring sample absorbance at 260 nm (A260) on a Tecan GENios plate reader and utilized in downstream cloning.

Primers used in PCR reactions in this study were obtained from Integrated DNA Technologies (Coralville, IA) and are listed in Table 2. A requirement of the In-Fusion cloning technique (discussed below) is the addition of a 5' extension on each forward and reverse primer. These extensions are indicated in the table.

A separate insert was generated for cloning a miR-1 MRE into a reporter construct as a positive control. This was accomplished by obtaining sense and antisense oligonucleotides harboring the miR-1 MRE (IDT). These oligonucleotides were annealed by combining the oligonucleotides in 100 µL annealing buffer (10 mM Tris, pH 7.5, 50 mM NaCl, 1 mM EDTA), heating to 95°C in a thermocycler, progressively cooling to 70°C over the course of 5 minutes, and then slowly cooling to 25°C over the course of two hours. Annealed oligonucleotides were then used in downstream cloning. Oligonucleotide sequences included 5' extensions for In-Fusion cloning. Sequences are listed in Table 2.

Table 2: List of PCR primers and oligonucleotides used for generating DNA inserts

Primer/Oligo Description	Orientation	Primer/Oligo Sequence
APP 3'-UTR from pGALA	Forward	5'-*TAGGCGATCGCTCGAG*ATAAAGGCCAAGAAGGGCGGAA-3'
APP 3'-UTR from pGALA	Reverse	5'-*AATTCCCGGGCTCGAG*ATCTTATCATGTCTGCTCGAAGCGGC-3'
BACE1 3'-UTR from human genomic DNA	Forward	5'-*TAGGCGATCGCTCGAG*AGATAGAGATTCCCCTGGAC-3'
BACE1 3'-UTR from human genomic DNA	Reverse	*GGCCGCTCTAGGTTTAAAC*GCCTCAGTATTGTTTTAGCC
Reverse APP 3'-UTR from pGALA	Forward	5'-*TAGGCGATCGCTCGAG*ATCTTATCATGTCTGCTCGAAGCG-3'
Reverse APP 3'-UTR from pGALA	Reverse	5'-*GGCCGCTCTAGGTTTAAAC*ATAAAGGCCAAGAAGGGCGGA-3'
miR-1 MRE Insert[a]	Sense	5'-*TAGGCGATCGCTCGAG*ACTAAATGA**ATACATACTTCTTTACATTCCA**ACCATATGGACA-3'
miR-1 MRE Insert[a]	Antisense	5'-*GGCCGCTCTAGGTTTAAAC*TGTCCATATGGT**TGGAATGTAAAGAAGTATGTAT**TCATTTAGT-3'

a= Oligonucleotides that were annealed and cloned into psiCHECK-2 by In-Fusion cloning
Underlined, italics= 5' extensions required for In-Fusion cloning
Bold= miR-1 MRE sequence

B. Restriction digest of plasmid DNA or amplicon

The parental construct used in cloning 3'-UTR reporter constructs was psiCHECK-2 (Promega, Madison, WI). This plasmid is 6.2 kb in length and contains a Renilla luciferase coding sequence (CDS) driven by the SV40 promoter, a multiple cloning site (MCS) located in the Renilla 3'-UTR, and a synthetic polyadenylation signal to ensure normal transcript processing in the absence of a 3'-UTR insert. A firefly luciferase CDS is located downstream and is driven independently by the HSV-TK promoter. An ampicillin resistance CDS is also incorporated in this vector to provide ampicillin resistance when transformed into bacteria.

Both In-Fusion cloning and standard ligation cloning require that the vector receiving the insert be linearized by restriction enzyme digestion. The cloning procedures used in this study to generate 3'-UTR reporter constructs employed either single digestion with XhoI or double digestion with XhoI and PmeI. All restriction endonucleases employed in this study were obtained from New England BioLabs (Ipswich, MA). Restriction digests were performed in 20 µL final volume by mixing psiCHECK-2 DNA with XhoI with or without PmeI, appropriate digest buffer, 1x bovine serum albumin (BSA) and water. Reactions were incubated at 37°C for 1 – 2 hours. Digests were then resolved by agarose gel electrophoresis using 110V for 45 minutes to 1 hour. Gels were visualized using a UV transilluminator and bands corresponding to linearized psiCHECK-2 were excised. Linearized vector was then extracted from excised gel fragments using QIAquick Gel Extraction kit (Qiagen, Valencia, CA). Eluted vector was quantified by A260 values and utilized in downstream cloning applications.

C. Molecular cloning, bacterial transformation and plasmid preparation

Inserts prepared by PCR amplification or oligonucleotide annealing were cloned into linearized psiCHECK-2 by ligation-independent cloning as implemented in the In-

Fusion cloning system (Clontech, Mountain View, CA). This proprietary enzyme mix contains 3'-5' exonucleolytic activity. Both forward and reverse PCR primers used in this system are designed with 15 bp 5' extensions that are identical in sequence to 15 bp on either side of the restriction sites used to linearize the host vector. Following PCR amplification, amplicons then have 5' and 3' ends that are identical in sequence to the 3' and 5' end of the linearized plasmid, respectively. Incubation of the linearized plasmid and amplicon with the In-Fusion enzyme results in 3'-5' exonucleolytic attack on the exposed ends of both the amplicon and linearized plasmid. Given the sequence identify between the ends of both molecular species, very long complementary sticky ends are created that anneal to one another. Due to the high thermodynamic stability of the annealed vector and amplicon at the extended sticky ends, ligation is unnecessary prior to bacterial transformation. Apparently endogenous nick repair mechanisms in *E. coli* are sufficient to allow propagation of the newly formed recombinant plasmid. A significant advantage of this method is that no restriction digests or other treatments of the insert are necessary prior to cloning. This is highly advantageous, especially when working with long inserts, since the presence of internal restriction sites in the insert itself can be limiting when performing standard ligation cloning.

To perform In-Fusion cloning, insert and linearized psiCHECK-2 (200 ng) were mixed together, generally at a 2:1 molar ratio, along with the In-Fusion enzyme mix, In-Fusion buffer and water in a 10 µL final volume. This reaction mix was incubated at 50°C for 15 minutes before being placed on ice. In every cloning reaction, a negative control reaction with no insert was performed to aid in visual estimation of recombination efficiency following bacterial transformation.

Bacterial transformations were performed using Z-competent DH5α *E. coli*. Z-competent cells were prepared using the Z-Competent *E. Coli* Transformation Kit and Buffer Set (Zymo, Irvine, CA) per manufacturer's protocol. Briefly, an overnight culture

of untransformed DH5α cells was used to seed a 50 mL culture grown in Zymobroth. This culture was shaken and incubated at 250 rpm and 25° – 30°C for approximately seven hours. Culture density was frequently monitored by measuring sample absorbance at 600 nm (A600) on a Milton Roy Spectronic spectrophotometer. Once A600 measurements were between 0.4 – 0.6, the culture was equilibrated to 0°C and spun down at 2500 g for 10 minutes. Cell pellet was washed once with 1x Wash buffer and re-spun at 2500 g for 10 minutes. Cell pellet was then resuspended in 1x Competency buffer, aliquoted, snap-frozen, and stored at -80°C until use.

To perform transformations, an aliquot of Z-competent *E. coli* was first thawed gently on ice. Then approximately 1 µL of In-Fusion reaction mixture was added to the bacterial suspension and the aliquot was gently mixed and incubated on ice for approximately 10 – 15 minutes. Transformed aliquots were plated on pre-warmed LB agar plates supplemented with 100 µg/mL ampicillin sodium salt (Sigma-Aldrich, St Louis, MO) and incubated for 12 – 18 hours at 37°C. Plates that had considerable number of colonies relative to negative control cloning plates were further screened. A number of colonies (ranging from 3 – 15) were picked and grown in 3 mL LB cultures overnight at 37°C. Overnight cultures were then processed using QIAprep Spin Miniprep kits (Qiagen, Valencia, CA) to purify plasmid DNA. Restriction digests were then performed as described above with diagnostic enzymes to confirm plasmid identity. Digests were analyzed by agarose gel electrophoresis and banding patterns visualized by UV transillumination. Expected banding patterns generated from multiple restriction digests was used as confirmation of successful cloning. DNA was also submitted to the Indiana University Sequencing Core for direct sequencing to confirm sequence fidelity.

To prepare sufficient quantities of plasmid DNA for transfections, 150 – 300 mL LB-ampicillin cultures from positive clones were grown overnight at 37°C with shaking

at 250 rpm. A small volume of culture was stored as a glycerol stock for future retrieval. Depending on culture volume, cultures were processed by either NucleoBond Xtra Maxi Plus or Midi Plus kits (Clontech, Mountain View, CA) to purify plasmid DNA per manufacturer's protocol. DNA was then quantified on a Nanodrop 1000 spectrophotometer (Thermo Scientific, Waltham, MA). Table 3 lists the cloned reporter constructs used in this dissertation.

Table 3: Summary of reporter constructs generated for this disseration

Plasmid Insert	Insert Size	Parental Vector	Total Plasmid Size
None	None	psiCHECK-2	6273 bp
APP 3'-UTR	1210 bp	psiCHECK-2	7487 bp
BACE1 3'-UTR	3936 bp	psiCHECK-2	10193 bp
APP 3'-UTR Reverse	1210 bp	psiCHECK-2	7464 bp
miR-1 MRE	36 bp	psiCHECK-2	6305 bp

D. Site-directed and cassette mutagenesis

To prepare mutants at specific miRNA target sites in the APP and BACE1 3'-UTR (and APP 5'-UTR), the QuikChange Lightning Site-Directed Mutagenesis kit (Agilent, Santa Clara, CA) was employed. This kit utilizes mutagenic primer-directed replication to introduce mutations at specific sites. Primers are designed to harbor the mutagenic site in the middle of the primer but with long perfectly complementary flanking regions on either side to anchor the primer to the target sequence. Plasmid amplification with a *Pfu* polymerase is then used to introduce the mutagenic sequence into the original sequence.

Site-directed mutagenesis was performed by first designing optimized mutagenesis primers with the aid of the web-based Agilent QuikChange primer design tool. Some primers were designed to introduce a novel restriction site during mutagenesis to aid in screening for true clones. Primers were obtained commercially (Integrated DNA Technologies, Coralville, IA) and are listed in Table 4. To prepare reactions, 25 ng template DNA was mixed with 125 ng sense and antisense mutagenic primers, QuikSolution, dNTPs, 10x reaction buffer, QuikChange Lightning enzyme mix and water for a final volume of 50 µL. Reactions were placed in the thermocycler and initially denatured at 95°C for 2 minutes followed by 18 cycles of the following protocol: 95°C for 20 seconds, 60°C for 10 seconds, 68°C for 4 minutes for APP 3'-UTR reporter and 7 minutes for BACE1 3'-UTR reporter. Hemimethylated plasmids containing an original, non-mutagenized strand were degraded by DpnI digestion. DpnI-digested samples were then transformed into XL10 ultracompetent DH5α *E. coli* cells from the kit. Cells were heat-shocked followed by a one hour outgrowth in NZY broth prior to plating on LB/ampicillin agar plates. Colonies were picked and cultured in 3 mL LB/ampicillin overnight at 37°C followed by miniprep DNA purification. To screen for true clones, some mutants had newly created restriction sites that were digested to

reveal novel banding patterns on agarose gel electrophoresis not observed in wild-type plasmids. For all other mutants, confirmation was performed by direct sequencing at the Indiana University Sequencing Core. Table 5 lists all sequencing primers utilized to confirm successful mutagenesis.

The pGAL reporter construct was kindly provided by Dr. Jack T Rogers to study regulatory effects on the APP 5'-UTR [143]. Mutagenesis at a predicted miR-346 target site in this 5'-UTR proved refractory to standard site-directed mutagenesis procedures. Therefore, cassette mutagenesis was employed instead. In this form of mutagenesis, the region of plasmid DNA to be mutated is excised by restriction digest. A mutagenized version of this cassette is synthesized, annealed, digested and ligated into the linearized vector. The oligonucletoides to replace the miR-346 target site in the APP 5'-UTR were obtained from Integrated DNA Technologies (Coralville, IA) and are listed in Table 4. To perform cassette mutagenesis, pGAL was first double digested with HindIII and NcoI as described above. The digested plasmid was then resolved by agarose gel electrophoresis, bands containing linearized plasmid excised, and linearized plasmid extracted and purified from gel fragments using QIAQuick Gel Extraction kit. Mutant oligonucleotides were designed so that, once annealed, the 5' and 3' ends would form sticky ends to match the HindIII and NcoI sites in the linearized pGAL. Oligonucleotides were annealed as described above and directly ligated into linearized pGAL by combining annealed cassette, linearized pGAL, T4 ligase buffer, and T4 ligase in a 20 µL final volume and incubating at room temperature for 2 hours. Approximately, 1 µL of ligase reaction mix was then transformed into Z-competent *E. coli* and plated overnight. True clones were confirmed by direct sequencing of plasmid DNA.

Table 4: List of primers and oligonucleotides used for site-directed and cassette mutagenesis

Mutagenic Primer/Cassette Oligos	Orientation	Primer Sequence
miR-101 APP 3'-UTR Target Site 1	Sense	5'-TACATTTTGGTCTCTATACTACATTATTAATGGG TTTTGTG**ATGACAT**AAGAATTTAGCTGTATCAAAC TAGTGCATGAATAGATTCTC3'-
miR-101 APP 3'-UTR Target Site 1	Antisense	5'-GAGAATCTATTCATGCACTAGTTTGATACAGCT AAATTCTT**ATGTCAT**CACAAAACCCATTAATAATGT AGTATAGAGACCAAAATGTA-3'
miR-101 APP 3'-UTR Target Site 2	Sense	5'-GTATTTCAGATGCTTTAGAGAGATTTTTTTTCCA TGACTGCATTT**GTT**T**AA**ACAGATTGCTGCTTCTGC TATAT-3'
miR-101 APP 3'-UTR Target Site 2	Antisense	5'-ATATAGCAGAAGCAGCAATCTGT**TT**A**AAC**AAAT GCAGTCATGGAAAAAAAATCTCTCTAAAGCATCTG AAATAC-3'
miR-153 APP 3'-UTR Target Site	Sense	5'-CAGCTGCTTCTCTTGCCTAAGTATTCCTTTCCT GATCAC**CGCATG**TTTTAAAGTTAAACATTTTTAAGT ATTTCAGATGCTTTAG-3'
miR-153 APP 3'-UTR Target Site	Antisense	5'-CTAAAGCATCTGAAATACTTAAAAATGTTTAACT TTAAAA**CATGCG**GTGATCAGGAAAGGAATACTTAG GCAAGAGAAGCAGCTG-3'
miR-339-5p APP 3'-UTR Target Site 1	Sense	5'-GGAGAGGATGCACAGTTTGCTATTTGCTTTAGA **CGG**A**TCC**ACTGTATAAACAAGCCTAACATTG-3'
miR-339-5p APP 3'-UTR Target Site 1	Antisense	5'-CAATGTTAGGCTTGTTTATACAGT**GGA**T**CCG**TC TAAAGCAAATAGCAAACTGTGCATCCTCTCC-3'
miR-339-5p APP 3'-UTR Target Site 2	Sense	5'-AAGAGGAGAAGGAGAGGGAGTACAAA**CGGA**T**C** **C**AATAGTGGGATCAAAGCTAGGAAAGG-3'
miR-339-5p APP 3'-UTR Target Site 2	Antisense	5'-CCTTTCCTAGCTTTGATCCCACTATT**GGA**T**CCG** TTTGTACTCCCTCTCCTTCTCCTCTT-3'
miR-346 APP 5'-UTR Target Site[a]	Sense	5'-AGCTTAGTTTCCTCGGCAGCGGTAGGCGAGAG CACGCGGAGGAGCGTGCGCGGGGGCCCCGGGA GACGGCGGCGGTGGCGGCGCG**AATGAG**GCAAG GACGCGGCGGATCCCACTCGCACAGCAGCGCAC TCGGTGCCCCGCGCAGGGTCGCGC-3'
miR-346 APP 5'-UTR Target Site[a]	Antisense	5'-CATGGCGCGACCCTGCGCGGGGCACCGAGTG CGCTGCTGTGCGAGTGGGATCCGCCGCGTCCTT GC**CTCATT**CGCGCCGCCACCGCCGCCGTCTCCC GGGGCCCCCGCGCACGCTCCTCCGCGTGCTCTC GCCTACCGCTGCCGAGGAAACTA-3'

a = Cassette mutagenesis oligonucleotides
BOLD RED = target mutation

Table 5: List of sequencing primers used for confirming mutagenesis

Sequencing primer description	Orientation	Primer Sequence
miR-101 APP 3'-UTR Target Sites	Sense	5'-GATGCCTGAACTTGAATTAATCCACAC-3'
miR-153 APP 3'-UTR Target Site	Sense	5'-TTTACATATGCTTTAAGAATCGATGG-3'
miR-346 APP 5'-UTR Target Site	Sense	5'-CTGCTGTGCGAGTGGGAT-3'
miR-339-5p APP 3'-UTR Target Sites	Sense	5'-GGCGTGTGTCCCTGTGGTA-3'
miR-339-5p APP 3'-UTR Target Sites	Antisense	5'-AGCCCTTCCCATCTCACTTT-3'

III. Biochemical techniques

A. Luciferase reporter assay

The normal reaction catalyzed by luciferase exhibits very fast kinetics such that the standard dual luciferase reporter assay generates a rapid rise and fall in luminescence that spans only a few minutes. This reaction system requires the use of an injector system to inject reaction reagents and immediately measure luminescence from each well of a plate. The Dual Glo assay system (Promega, Madison, WI) utilizes a modified reaction system with stabilized reaction kinetics such that the half-life of the luciferase reaction is over 2 hours. This is beneficial when multiple plates are being analyzed simultaneously, as in this study. After adding reagents, a significant time gap is tolerable before taking luminescence readings. Therefore, the Dual Glo assay was employed in these experiments.

HeLa, SK-N-SH or NT2N cells were transfected with reporter constructs either in isolation or in combination with miRNA mimics, as described above. Forty eight hours post-transfection, the *Renilla* and firefly luciferase activity was assayed using the Dual-Glo Reporter system (Promega, Madison, WI). This assay was performed by first removing cell culture media from the plate. 30 µL of PBS was then added, followed by 30 µL Dual-Glo luciferase reagent. Plates were incubated at room temperature for 10 minutes before firefly luminescence readings were taken using a Turner Biosystems Veritas luminomenter. 30 µL of Stop & Glo reagent was then added to each plate followed by 10 minute room temperature incubation. *Renilla* firefly luminescence readings were then taken. Since the reporter constructs contained the APP or BACE1 3'-UTR downstream of the *Renilla* coding sequence, ratios of *Renilla*/firefly luminescence values were calculated to control for variability in cell number and transfection efficiency. When multiple plates were assessed simultaneously, relative

response ratios (RRR) were calculated to control for plate-to-plate variation. The RRR was calculated by scaling *Renilla*/firefly ratios to a positive control reaction (miR-1 co-transfected with miR-1 MRE-containing construct) and negative control reaction (reporter alone without co-transfection) included on every plate.

B. Processing of brain tissue for protein extraction

Frozen human brain specimens from the Harvard Brain Tissue Resource Center and University of Kentucky Alzheimer Disease Center Brain Bank isolated from BA9 of the frontal cortex in age-matched control and AD patients were provided by Dr. P. Hemachandra Reddy and Dr. Peter Nelson, respectively. Sample demographics and post-mortem interval (PMI) are described in more detail in Chapter 3 under Aim 3. Specimens were initially pulverized using a stainless steel pulverizing chamber pre-chilled with liquid nitrogen. Pulverized samples were quickly aliquoted and stored at -80°C, avoiding sample thawing.

One aliquot of each sample was processed for protein analysis. This frozen aliquot was immersed in M-PER supplemented with 0.1% SDS and protease inhibitor cocktail set III and immediately sonicated using a Sonifier Cell Disruptor 350 (Branson, St Louis, MO) until visible clumps were no longer apparent. Lysates were then incubated with 50 U/mL Benzonase enzyme (EMD, Billerica, MA) for 10 minutes at 37°C to reduce nucleic acid content and associated viscosity. Lysates were centrifuged down at 30,000 *g* for 2 h to clear debris. Cleared supernatants were collected and stored at -80°C for future protein analysis.

C. RNA extraction from cell culture and tissue samples

All RNA extraction procedures were performed at a dedicated RNA/PCR workbench under conditions to protect against ribonuclease contamination. Pulverized

brain specimens first underwent a preliminary tissue disruption step. A separate frozen aliquot of pulverized tissue from each specimen was immersed in 200 µL – 1100 µL ice-cold Cell Disruption Buffer from the miRVana miRNA Isolation kit and immediately homogenized using a Polytron (Kinematica, Bohemia, NY). Cell culture lysates for RNA extraction were prepared as described above using either the miRVana miRNA Isolation kit or the miRVana PARIS kit.

Total RNA was extracted using the miRVana miRNA Isolation kit or PARIS kit per manufacturer's instructions. The basis of total RNA extraction in both kits is essentially identical. Lysates are prepared in buffers containing guanidinium salts and other denaturants to inhibit RNase activity. Lysates are then extracted with an equal volume of acid phenol:chloroform. The aqueous layer is recovered and nucleic acid solubility is reduced by the addition of ethanol. Total RNA is then bound to a silica-based spin column. Multiple washes are applied to remove trace phenol and cellular contaminants. Finally, RNA is extracted by adding molecular-grade water preheated to 70°C.

RNA quantity and purity were assessed following purification by measuring sample absorbance across the ultraviolet spectrum using a Nanodrop 1000 (Thermo Scientific, Waltham, MA) and assessing the absorbance ratio of 260 nm versus 280 nm (A260/A280). RNA integrity was assessed by the Center for Medical Genomics through use of on-chip capillary electrophoresis in a Bioanalyzer (Agilent, Santa Clara, CA). The RNA integrity number (RIN) was determined by automated software analysis of the electropherogram. The RIN value is calculated from an empirically-derived algorithm that assesses multiple features of the sample electropherogram and is superior to the ratio of 28S:18S ribosomal RNA for assessing RNA integrity [295]. All cell culture samples had acceptable A260/A280 ratios and RIN values greater than 8.5. RNA quality of the brain specimens was somewhat variable. Specimens from the University

of Kentucky Brain Bank had generally high RIN values, with all but two out of 20 samples having RIN values greater than 6. Several specimens from the Harvard Tissue Resource Center had low RIN values (<6), likely attributable to prior sample processing. There was no detectable association between low RIN value and higher Ct values obtained from quantitative PCR analyses in this collection. Therefore, all samples were included for further analysis.

D. Protein quantification, SDS-PAGE and Western blotting

Lysate protein concentrations were first measured by BCA (Pierce, Rockford, IL) per manufacturer's instructions. This assay is based upon the biuret reaction, whereby Cu^{2+} is reduced to Cu^{1+} via interactions with peptide bonds in the protein sample. Bicinchoninic acid (BCA) included in the assay reagent then complexes with Cu^{1+} producing a stable chromophore that absorbs maximally at 562 nm [296]. This assay has a larger dynamic range and a wider breadth of compatibility with various buffer components as compared to Lowery and Bradford assays. Protein concentrations were measured by incubating 10 µL of lysate with 200 µL of working reagent at 37°C for 30 minutes and then measuring absorbance at 570 nM with a microplate reader (Bio-Rad, Hercules, CA). All samples were analyzed in duplicates and absorbance values averaged. Concentrations were calculated by comparison to a bovine serum albumin (BSA) standard curve included with each new assay.

Lysates were prepared for Western blot analysis by first heating samples to 95°C for 5 minutes in Laemmli sample buffer [297]. An equal amount of lysate protein (ranging from 1 – 5 µg) was loaded onto Bis-Tris XT denaturing 10% polyacrylamide gels containing sodium dodecyl sulfate (SDS) (Bio-Rad, Hercules, CA). Proteins were resolved by SDS-PAGE by applying 200V across the gels for 1.3 hours. Resolved protein bands were then transferred onto PVDF membranes by electroblotting at either

30V for 10 hours or 100V for 1.5 hours. To assess for even transfer, blots were stained with Ponceau-S. Membranes were blocked for 1 h in 5% non-fat milk and then incubated overnight with primary antibodies against APP (22C11, Chemicon, Billerica, MA), BACE1 (3D5, gift from Dr. Robert Vassar), IRP1 (Santa Cruz Biotechnology, Santa Cruz, CA), Dicer (NeuroMAB, Davis, CA), α-tubulin (B-5-1-2, Sigma-Aldrich, St Louis, MO), and β-actin (AC15, Sigma-Aldrich, St Louis, MO). Membranes were then incubated with HRP-conjugated goat anti-mouse secondary antibody (Rockland Immunochemical, Gilbertsville, PA) or HRP-conjugated rabbit anti-goat secondary antibody (Santa Cruz Biotechnology, Santa Cruz, CA) for 1 h. Bands were visualized using ECL reagent (Pierce, Rockford, IL), detected on film and scanned for densitometric analysis

.

E. Aβ ELISA analyses

Aβ analyses were primarily performed by Dr. Balmiki Ray. Levels of Aβ1-40 were measured in the CM of U373 cells and primary human fetal brain cultures using a sensitive and specific commercially available ELISA kit (IBL America, Minneapolis, MN). Equal volume of CM (25μL) was loaded in a plate pre-coated with anti-human Aβ (35 – 40) antibody (clone 1A10) and incubated overnight. This kit uses HRP-conjugated anti-human Aβ (11 – 28) as detection antibody. The overall assay was performed according to manufacturer's instructions. Briefly, CM was added to pre-coated plates and incubated overnight at 4°C. The next day plates were vigorously washed and then incubated with detection antibody for approximately one hour at 4°C. Plates were again vigorously washed and then incubated with chromogenic substrate tetramethylbenzidine for thirty minutes in the dark. Chromogenic reaction was then stopped by the addition of stop solution and absorbance at 450 nm was read using Tecan GENios microplate reader. Absolute Aβ1-40 values (in pg/mL of CM) were

calculated by comparison to an Aβ1-40 standard curve. This value was normalized to the total lysate protein yield from each well to control for variability attributable to differences in cell number and scaled relative to mock transfection values.

F. Reverse transcription quantitative PCR (RT-qPCR) analysis of mRNA and miRNA

Both mRNA and miRNA levels were quantified by reverse transcription quantitative PCR (RT-qPCR). Specific qPCR assays used in this dissertation are listed in Table 6. All RT and qPCR steps were performed at a dedicated PCR/RNA workbench with separate supplies to avoid DNA or RNA contamination. For miRNA quantification, stem-loop TaqMan assays were employed (Applied Biosystems, Carlsbad, CA). This method utilizes miRNA-specific RT primers with complementarity to several ribonucleotides on the 3' end of the targeted miRNA along with a stem-loop structure on the primer 5' end [298]. Since pre-miRNA species have additional nucleotides downstream of the mature sequence, steric hindrance between the RT primer secondary structure and pre-miRNA sequence impedes unwanted pre-miRNA cDNA synthesis. A miRNA-specific forward primer and reverse primer targeting a universal sequence located within the loop of the RT primer are used for qPCR amplification. The assay uses a hydrolysis probe for detecting amplification during qPCR.

Total RNA (10 ng) was first converted to cDNA using TaqMan microRNA Reverse Transcription kit (Applied Biosystems, Carlsbad, CA) by combining RNA, miRNA-specific RT primer, MultiScribe reverse transcriptase, RNase inhibitor enzyme, dNTPs, reaction buffer and water per manufacturer's protocol and incubating reaction mix on a thermocycler at 16°C for 30 minutes, 42°C for 30 minutes and 85°C for 5 minutes. cDNA was then subjected to qPCR analysis using specific TaqMan hydrolysis probe assays (Applied Biosystems, Carlsbad, CA). The RT reaction mix (cDNA) was

combined with TaqMan miRNA assay and TaqMan Universal PCR master mix (Applied Biosystems, Carlsbad, CA) per manufacturer's protocol and analyzed on a 7300 Real-Time PCR instrument (Applied Biosystems, Carlsbad, CA). Each sample was analyzed in duplicate and signals averaged.

For mRNA quantification, standard mRNA TaqMan hydrolysis probe assays were utilized. Total RNA (10 – 75 ng) was converted to cDNA with the High Capacity RNA-to-cDNA kit (Applied Biosystems) by combining total RNA, RT enzyme mix and RT reaction buffer per manufacturer's protocol and incubating reaction mix in a thermocycler at 37°C for 60 minutes and then 95°C for 5 minutes. The RT reaction mix (cDNA) was combined with TaqMan mRNA assay and TaqMan Universal PCR master mix as in miRNA analyses. The PCR reactions were then analyzed on the 7300 Real-Time PCR instrument. Each sample was analyzed in duplicate and signals averaged.

Both relative and absolute quantification methods were employed. Relative quantification was performed using a modified delta-Cq method. The delta-Cq method allows for the determination of relative amplicon levels by first calculating the difference in the crossing threshold cycle (Ct) for a gene of interest in an unknown sample relative to a calibrator sample, i.e. ΔCt. In the simplest form of the delta-Cq method [299], the ΔCt value for the gene of interest in a given sample is then compared to the ΔCt value for a stably expressed reference gene in the same sample by taking the difference, i.e ΔΔCt. Assuming the PCR amplification efficiencies are 100% for both the genes, i.e. the amplicon numbers double after each cycle, then the relative levels of the gene of interest is calculated by the formula $2^{-\Delta\Delta Ct}$. A more sophisticated analysis allows for more precise quantification by incorporating exact amplification efficiencies (E) for each PCR reaction into the calculation [300]. Relative levels are calculated by taking the ratio of $E_x^{\Delta Ct,x}$ for the gene of interest to $E_y^{\Delta Ct,y}$ for the stable reference gene, where E_x and E_y are experimentally-determined PCR amplication efficiencies for the gene of interest and

reference gene, respectively. Studies have demonstrated that relative transcript quantities derived from qPCR analyses are more accurate when normalized to the geometric mean of multiple reference genes [301]. Therefore, the relative quantification scheme employed for relative RT-qPCR analyses in this dissertation took into account experimentally-derived PCR amplification efficiencies and normalization to the geometric mean of multiple reference genes [302]. This scheme is implemented into the qBasePLUS software used for RT-qPCR analyses in these studies. In order to determine amplification efficiencies for each TaqMan assay, aliquots of every RNA sample in a given analysis were pooled and used to create a relative standard curve by serial dilution. This standard curve was then converted to cDNA and analyzed by qPCR in parallel with unknown samples. The slope of the plot of Ct versus standard curve dilutions used to calculate amplification efficiency.

For miRNA relative quantification studies, RNU48, RNU49, RNU6B, and hsa-miR-16 were used for normalization. For mRNA relative quantification studies, GAPDH, B2M, β-actin and TBP were used for normalization.

To perform absolute quantification in miRNA analyses, HPLC-purified synthetic oligoribonucleotide standards were obtained commercially (Sigma, St Louis, MO and Integrated DNA Technologies, Coralville, IA). These oligonucleotides were identical in sequence to human miR-101, miR-153, miR-346, miR-339-5p, miR-124 and miR-1. These oligoribonucleotides were resuspended and exact concentrations measured by A260 measurements. Based on measured concentrations, standard curves with absolute copy counts were prepared by serial dilution. These serially diluted standards were converted to cDNA and analyzed by qPCR in parallel with unknown samples. Copy counts per reaction were then determined based upon standard curve analysis. Given that each reaction mix was loaded with a known amount of total RNA (generally

10 ng), copy counts were then presented as copy counts/15 pg total RNA. This serves as a rough estimate of copy counts per average human cell.

Table 6: List of TaqMan assays utilized in qPCR analyses

miRNA and mRNA qPCR Assays			
Assay Name	Assay RNA Target	Vendor	Assay ID
hsa-miR-101	hsa-miR-101	Applied Biosystems	002253
mmu-miR-153	hsa-miR-153	Applied Biosystems	001191
hsa-miR-346	hsa-miR-346	Applied Biosystems	000553
hsa-miR-339-5p	hsa-miR-339-5p	Applied Biosystems	002257
mmu-miR-124a	hsa-miR-124	Applied Biosystems	001182
hsa-miR-1	hsa-miR-1	Applied Biosystems	002222
hsa-miR-107	hsa-miR-107	Applied Biosystems	000443
hsa-miR-29b	hsa-miR-29b	Applied Biosystems	000413
hsa-miR-16	hsa-miR-16	Applied Biosystems	000391
RNU6B	Human U6B snRNA	Applied Biosystems	001093
RNU48	Human U48 snoRNA	Applied Biosystems	001006
RNU49	Human U49 snoRNA	Applied Biosystems	001005
APP	Human APP	Applied Biosystems	Hs01552282_m1
BACE1	Human BACE1	Applied Biosystems	Hs00201573_m1
GAPDH	Human GAPDH	Applied Biosystems	Hs99999905_m1
ACTB	Human β-actin	Applied Biosystems	4333762T
B2M	Human β-2-microglobulin	Applied Biosystems	Hs99999907_m1
TBP	Human TATA-binding protein	Applied Biosystems	Hs99999910_m1

IV. Data Analysis

Densitometric analysis of Western blots was performed using ImageJ software. qPCR data normalization was performed using qbase^{PLUS} software. Fluoresence micrograph and Western blot image processing was performed using Adobe Photoshop. Western blot images were adjusted for contrast and brightness and some extraneous sections of blots between boxed regions were removed for the sake of clarity. No manipulations have been made to images that alter data quantification or interpretation. All graphs were preared in Prism GraphPad. Error bars represent standard error of the mean (SEM). Statistical analyses were performed using Prism GraphPad and SPSS. For comparison between two categories, two-tailed Student's t-test was performed. For comparison across multiple categories, one-way ANOVA was performed. When ANOVA was significant, post-hoc Dunnett's t-test, Tukey's Honest Significant Difference (HSD) test, or Student-Neuman-Keuls (SNK) test were performed as appropriate to correct for multiple comparisons. The α threshold for statistical significance was set at 0.05.

CHAPTER 3: RESULTS

I. Aim 1: Identify miRNA that endogenously regulate APP expression

To unequivocally identify specific members of the repertoire of miRNA that regulate APP expression, the workflow outlined in Figure 3 was employed throughout this study. This workflow starts from a gene of interest (GOI), in this case APP – or BACE1 in aim 2 – and proceeds as follows: i) identification of putative miRNA target sites within the transcript, ii) functional validation of these putative regulatory interactions, iii) testing the effect on a relevant downstream pathway of interest (i.e. Aβ production), and iv) assessing the physiological relevance of the putative regulatory relationship by blocking endogenous interaction between miRNA and target site.

A. Global knockdown of miRNA function elevates APP expression

To begin to dissect the role that miRNAs play in the basal regulation of APP expression, global miRNA function was inhibited in cultured human fetal brain cells. To accomplish this, AGO2 expression was knocked down using siRNA transfection. Given that AGO family proteins are the core constituent of RISC as previously discussed, this approach would be expected to modulate expression of gene targets that are under direct basal regulation by miRNAs. Also, given the acute nature of the knockdown, the compensatory effect of homeostatic controls on gene expression would be expected to be less vigorous than in long-term or stable AGO2 knock out conditions. Human fetal brain cultures were either mock transfected or transfected with a negative control or AGO2-specific siRNA at DIV 17. Cultures were harvested 48 hours post-transfection (DIV 19) and APP expression assayed by Western blot. APP levels were found to be significantly elevated (1.51±0.09 fold change) following knockdown of AGO2 as compared to negative control siRNA transfection ($p=0.043$ by two-tailed Student's t-

test) (Figure 4A and B). This suggests that APP expression is basally inhibited by the global complement of miRNA in this relevant cell model.

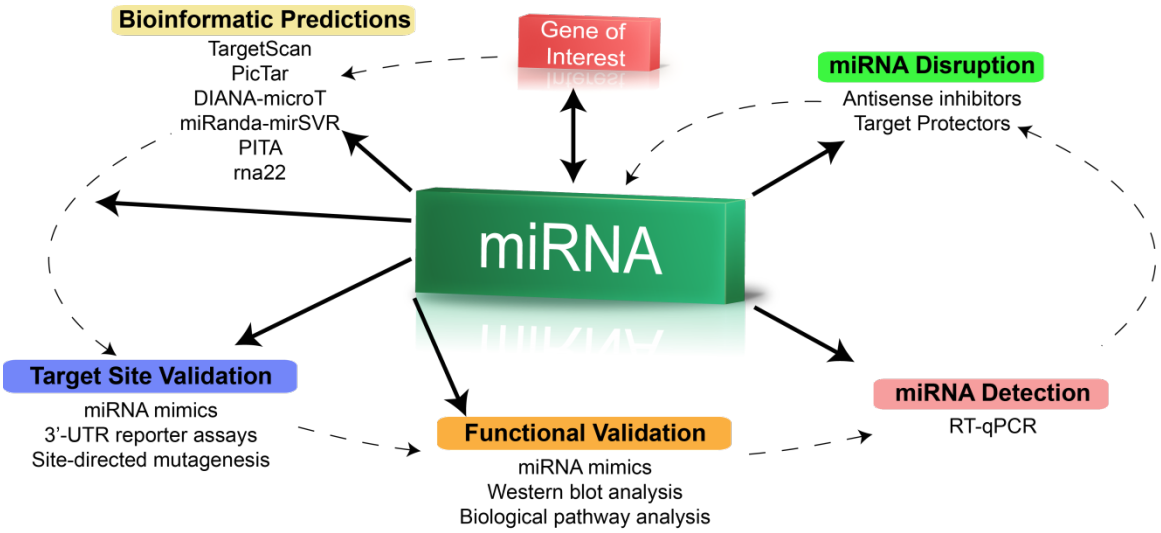

Figure 3: Methodological workflow employed to identify novel AD-relevant miRNA regulators of APP and BACE1 expression. The workflow utilized in this dissertation began with a specific predetermined GOI – in this case APP and BACE1. Putative target sites in the 3'-UTR of the APP and BACE1 transcripts were identified by bioinformatic analysis. Target sites were then validated by both 3'-UTR reporter assays and direct analysis of native protein levels following transfection of putative targeting miRNA. The effect of miRNA-mediated regulation of APP and BACE1 on downstream biological pathways was assessed by measuring levels of Aβ in conditioned media of miRNA-transfected cultures. Endogenous miRNA function was then disrupted to assess whether endogenous miRNAs physiologically regulate expression of APP and BACE1. Originally published in expanded form in Long and Lahiri (2012) [223].

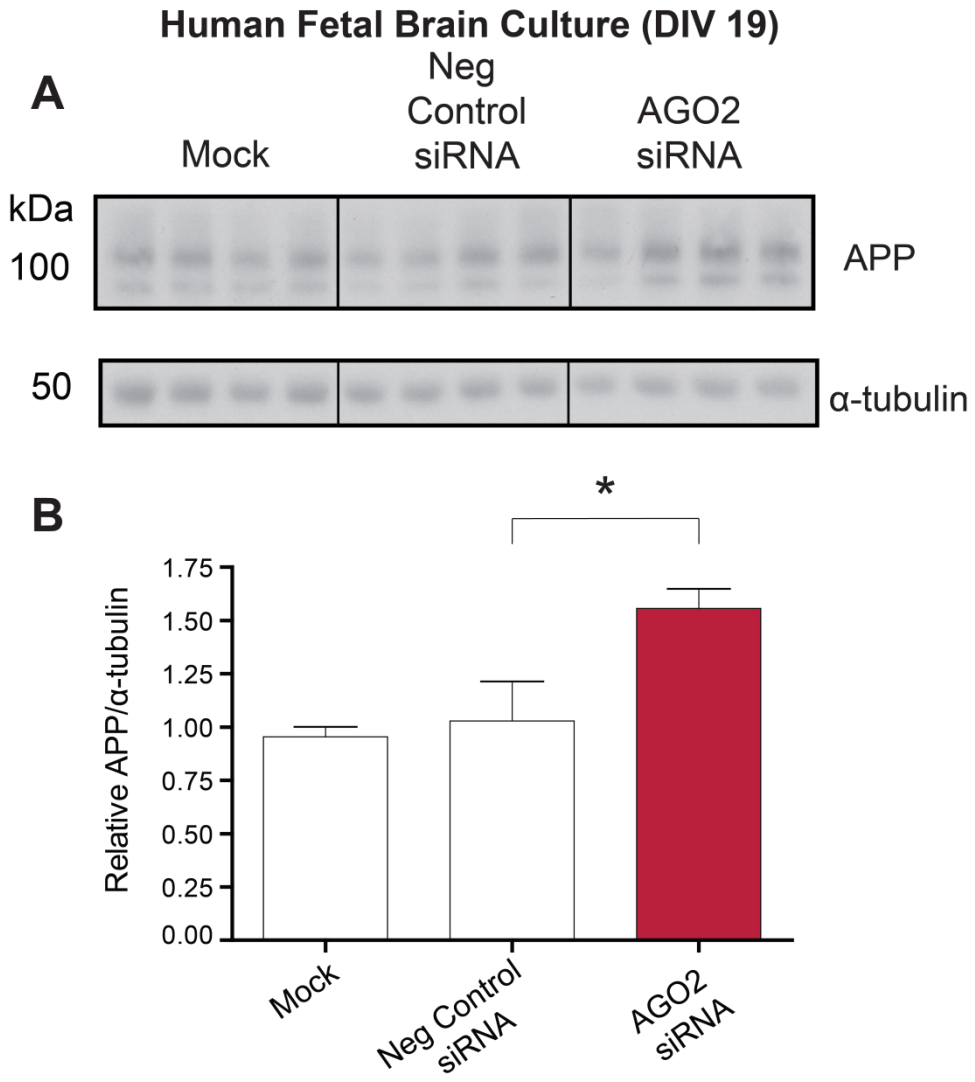

Figure 4: Knockdown of miRNA effector protein AGO2 enhances expression of APP in primary human fetal brain cultures. The effect of disrupting global miRNA functionality on APP expression in primary human fetal brain cultures was assessed by using siRNA-mediated knockdown of AGO2. Cultures were transfected at DIV 17 and lysates prepared 48 hours post-transfection (DIV 19). (A) Levels of APP and α-tubulin were assayed by Western blot. (B) Blots were quantified by densitometric analysis and APP levels normalized to α-tubulin levels and scaled relative to mock transfection (n=4).

B. Bioinformatic analysis of putative miRNA targets in the human APP 3'-UTR

To identify novel miRNA target sites in the human APP 3'-UTR, multiple web-based bioinformatics algorithms were used to predict favorable miRNA interactions. These web-based predictors included TargetScan 6.0 [204,243,303–305], PicTar [306], DIANA-microT v4.0 [307–310], miRANDA-mirSVR [311–314], PITA [315] and rna22 [316]. There are some common parameters that a majority of these algorithms assess to varying degrees when predicting putative target sites. These include seed sequence complementarity, the free energy of duplex formation, cross-species conservation at the target site and local sequence context surrounding the target sites. However, each predictor algorithm includes its own unique combination of parameters making each set of predictions distinct between the predictors. Specific attributes of each predictor are described in Table 7.

miRNA target site predictions in the APP 3'-UTR were extracted from the predictor outputs. Criteria for selecting a given miRNA:target site interaction included relatively high predictor score and known brain expression. Preference was also given to miRNA-target interactions predicted across multiple algorithmic platforms. Table 8 summarizes the identity of the predicted targeting miRNA and the location of the predicted target site in relation to the human APP 3'-UTR, along with the various predictor scores computed for each given target site interaction. In the case of miR-101, two distinct target sites were predicted by multiple algorithms. Since each predictor utilizes a unique algorithm for scoring favorable target site interactions or target site efficacy, it is not meaningful to compare scores between predictors. However, scores can be compared within a prediction set produced by a single predictor. As an example, among all TargetScan predictions listed, miR-101 produced the most favorable context+ score (-0.35) for interaction with the APP 3'-UTR (Table 8).

Table 7: Summary of computational predictor algorithms

Computational Target Site Predictor (URL)	Summary of Key Algorithm Components	References
TargetScanHuman 6.0 (http://www.targetscan.org)	– Perfect seed sequence complementarity – High miRNA-target duplex stability favored – Favored sequence contexts – Target site position within 3'-UTR – Target site cross-species conservation required	[204,243,303–305]
PicTar (http://pictar.mdc-berlin.de)	– Imperfect seed sequence complementarity tolerated – High miRNA-target duplex stability favored – Target site cross-species conservation required – Probability-based combinatorial scoring matrix	[306]
DIANA-microT v4.0 (http://diana.cslab.ece.ntua.gr/DianaTools/index.php?r=microtv4)	– Imperfect seed sequence complementarity tolerated – High miRNA-target duplex stability favored – Target site cross-species conservation incorporated into algorithm but not strictly required	[307–310]
miRanda-mirSVR (http://www.microrna.org)	– Dynamic programming alignment weighted for seed sequence complementarity – High miRNA-target duplex stability favored – Target site cross-species conservation required – Machine learning algorithm for predicting miRNA efficacy	[311–314]
PITA (http://genie.weizmann.ac.il/pubs/mir07/index.html)	– High miRNA-target duplex stability favored – Low stability of secondary structure near target site favored (i.e. site accessibility favored)	[315]
rna22 (http://cbcsrv.watson.ibm.com/rna22.html)	– Pattern recognition algorithm that identifies sequence motifs from miRNA sequences – Identifies target islands in 3'-UTR complementary to these sequence motifs	[316]

Table 8: Selected APP 3'-UTR miRNA Target Site Predictions and Scores

miRNA	*Computational Predictor Scores*						Target Site[g]
	Target Scan[a]	PicTar[b]	DIANA-microT v4[c]	miRanda miRSVR[d]	PITA[e]	rna22[f]	
miR-101[h]	-0.35	5.13	0.307	-1.278	2.45	***	242-248
	-0.05	5.13	0.226	-0.150	***	***	532-538
miR-153	-0.22	2.50	0.414	-1.256	-3.91	-21.3	457-463
miR-106a	-0.12	2.35	0.436	-0.703	-6.58	-27.4	710-716
miR-106b	-0.12	1.82	0.414	-0.703	0.21	-27.4	710-716
miR-20a	-0.10	2.35	0.414	-0.707	-6.56	-27.5	710-716
miR-20b	-0.10	***	0.414	-0.707	-6.66	-28.6	710-716
miR-17-5p	-0.12	2.35	0.414	-0.703	-6.58	-29.4	710-716
miR-483-3p	***	***	***	***	-16.99	-43.6	720-740
miR-520c-3p	-0.13	***	0.467	-0.723	3.18	-28.7	709-715
let-7g	***	***	***	***	***	-37.2	532-553

Reported scores: [a]context+ score, [b]PicTar score, [c]Site score, [d]mirSVR score, [e]ddG score, [f]folding energy in kCal/mol, M=14, G=0, E=-20 Kcal/mol; [g]Target site position relative to start of APP 3'-UTR; [h]miR-101 has two distinct predicted target sites in APP 3'-UTR; *** = target site not predicted by algorithm

C. APP 3'-UTR reporter validation of putative miRNA targets in APP 3'-UTR

To rapidly screen the functionality and efficacy of the various predicted miRNA:3'-UTR interactions in the APP 3'-UTR, a reporter construct was prepared containing the full length APP 3'-UTR. The APP mRNA consists of a 144 bp 5'-UTR, 2.3 kb coding sequence (CDS) and 1.2 kb 3'-UTR (Figure 5A). The full length APP 3'-UTR was PCR-amplified from the pGALA construct [143] (provided by Dr. Jack T Rogers) and inserted downstream of a Renilla luciferase CDS in the psiCHECK-2 vector. The psiCHECK-2 vector contains the Renilla luciferase cassette driven by the SV40 promoter and a separate firefly luciferase CDS under independent transcriptional control by the HSV-TK promoter that serves as an internal control in dual reporter assays (Figure 5B). A positive control vector was also constructed by inserting annealed oligonucleotides containing a MRE perfectly complementary to miR-1 into the same psiCHECK-2 vector (Figure 2B). This positive control vector was used to confirm effective miRNA delivery and repressive activity in subsequent co-transfection experiments.

Prior to performing APP 3'-UTR reporter and miRNA co-transfections to screen for functional interactions, the regulatory influence of the APP 3'-UTR on basal reporter expression was first tested. Three different human cell lines (human cervical epithelial [HeLa], human neuroblastoma [SK-N-SH] and human neuronally differentiated embryonal carcinoma [NT2N]) were transfected with either the empty psiCHECK-2 vector or the APP 3'-UTR reporter vector (Figure 5C). Despite the 3'-UTR being a general hub for MREs with inhibitory influences on protein expression, the presence of the APP 3'-UTR significantly stimulated reporter expression in HeLa cells (1.42±0.08 fold change compared to empty; $p=0.002$ by post-hoc Dunnett's t-test) and differentiated NT2 neurons (2.73±0.39 fold change compared to empty; $p=0.003$ by post-hoc Dunnett's t-test) (Figure 5C). There was also a trend for increased reporter

expression in response to the APP 3'-UTR in SK-N-SH cells but this was not statistically significant. To confirm the specificity of this response, cells were also transfected with a reporter construct containing the APP 3'-UTR sequence inserted into psiCHECK-2 in reverse orientation. This sequence had no stimulatory effect on reporter expression in any of cell lines tested (Figure 5C). Therefore, these data suggest that under basal transfection conditions the APP 3'-UTR contains response elements that increase reporter gene transcription, enhance mRNA stability or stimulate mRNA translation.

To validate the functionality of putative miRNA:APP 3'-UTR interactions as predicted by the various algorithms, a medium-throughput reporter screen was employed as schematically illustrated in Figure 6A. HeLa cells were co-transfected with both the APP 3'-UTR reporter construct and miRNA mimics listed in Table 8. A negative control co-transfection was performed with a commercial mimic not predicted to target mammalian mRNA transcripts. A positive control was performed by co-transfecting the positive control reporter construct from figure 6B and miR-1 mimic. Forty eight hours post-transfection, reporter expression was determined using a dual luciferase reporter assay. Reporter expression values were calculated as normalized ratios of Renilla-to-firefly luciferase activity. HeLa cells were primarily utilized because of high transfection efficiencies and highly reproducible cellular responses. Their lack of neuronal phenotype was not a significant concern since HeLa cells have a functional miRNA:AGO apparatus [317] and both reporter construct and miRNA were exogenously supplied in this particular experiment.

Co-transfection of miR-106a, miR-106b, miR-153, miR-101 and miR-20b with the APP 3'-UTR reporter construct all resulted in significantly reduced reporter expression compared to co-transfection with negative control miRNA mimic or transfection with the APP 3'-UTR reporter vector alone (fold change in comparison to reporter alone: miR-106a, 0.788±0.014 fold; miR-106b, 0.652±0.038 fold; miR-153,

0.741±0.024; miR-101, 0.572±0.023 fold; miR-20b, 0.825 ± 0.018 fold; $p<0.01$ in all cases as determined by post-hoc Dunnett's t-test). Co-transfection with miR-520c-3p resulted in significantly increased reporter expression compared to co-transfection with negative control miRNA mimic (1.219 ± 0.014 fold change compared to negative control; $p<0.01$ by post-hoc Dunnett's t-test). Data in figure 6B are scaled such that transfection of APP 3'-UTR reporter alone is set to one and the co-transfection of the positive control construct from Figure 6B and miR-1 is set to zero. Scaling is necessary to control for plate-to-plate variation between reporter assays.

The strongest inhibitory effect on reporter expression was observed following co-transfection with miR-101, miR-106b and miR-153. Further, miR-520c-3p co-transfection significantly elevated reporter expression. Regulatory effects of miR-106b on APP expression were previously reported in the literature [276] and APP protein expression in response to miR-520c overexpression has been reported to be decreased, not increased [318]. Therefore, follow-up experiments from this set of miRNA were restricted to miR-101 and miR-153 to focus on novel putative regulatory interactions.

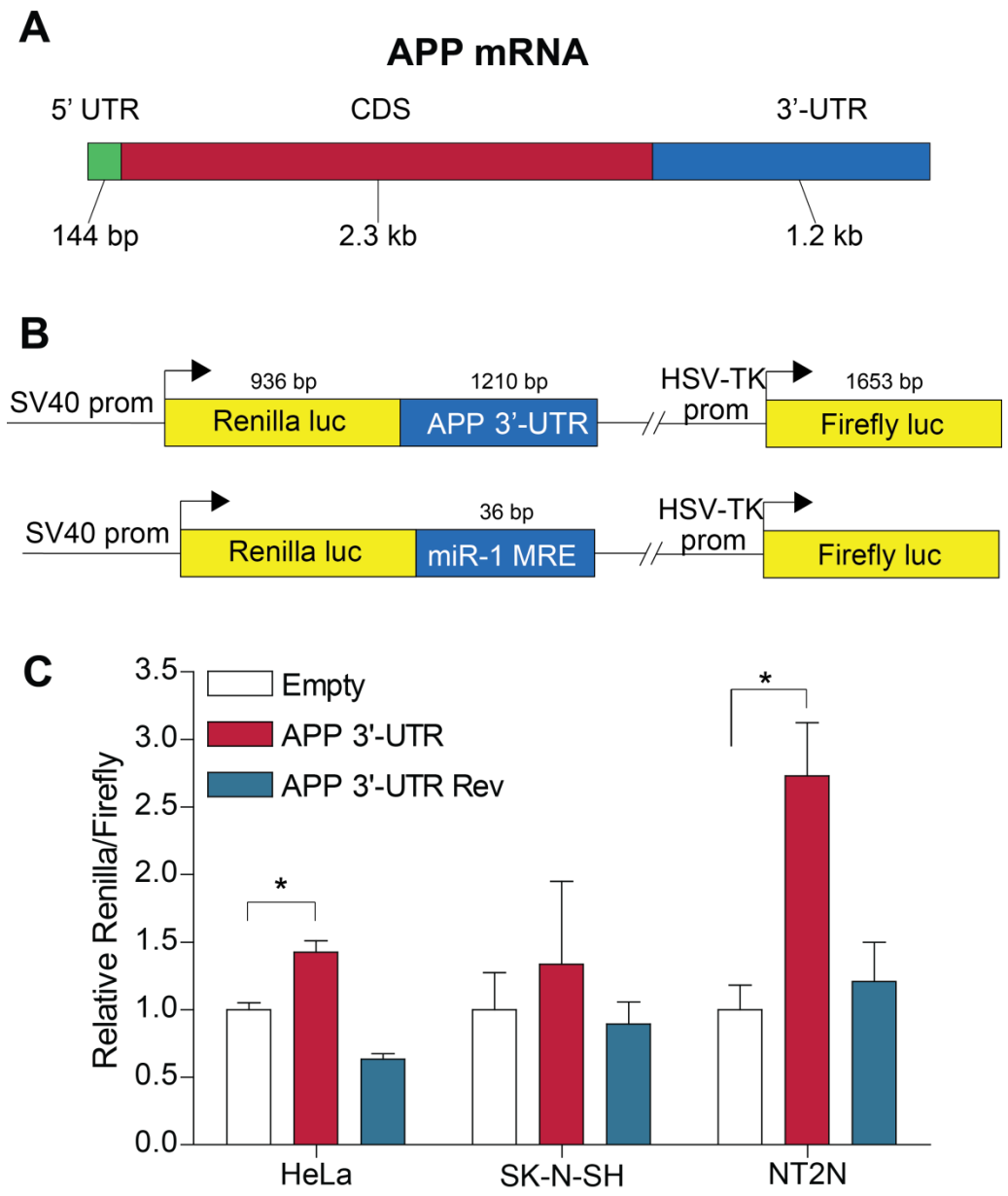

Figure 5: APP 3'-UTR stimulates basal reporter expression in multiple human cell types. (A) Schematic of the APP mRNA demonstrating sizes of the 5'-UTR, CDS and 3'-UTR. (B) Schematic of the reporter constructs used to validate putative miRNA target sites in the APP 3'-UTR. The APP 3'-UTR was PCR-amplified from the pGAL construct and inserted into the psiCHECK-2 vector downstream of the Renilla luciferase (luc) CDS. A positive control construct containing a site perfectly complementary to miR-1

was constructed by inserting annealed oligonucleotides containing this MRE into psiCHECK-2 downstream of Renilla luc. prom=promoter (C) The regulatory effect of the APP 3'-UTR on reporter expression was tested by transfecting either the empty psiCHECK-2 vector, the APP 3'-UTR reporter construct or vector containing the APP 3'-UTR in reverse orientation into HeLa, SK-N-SH or differentiated NT2 neuronal cells and assaying basal reporter expression. Assay values are reported as the ratio of Renilla to luciferase luminescence scaled relative to empty vector (n=5; *$p<0.01$).

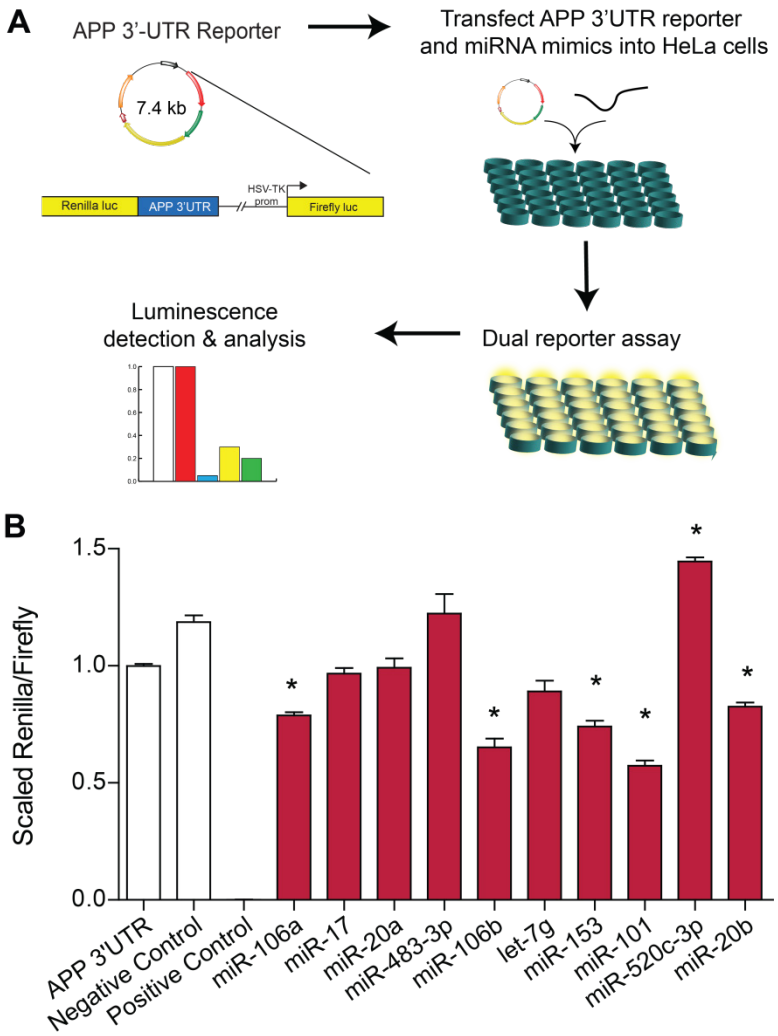

Figure 6: Multiple miRNA modulate APP3'-UTR reporter expression in HeLa cells. (A) Schematic of the methodological workflow employed to validate putative miRNA regulatory interactions with target sites in the APP 3'-UTR. The APP 3'-UTR reporter construct was co-transfected into HeLa cells along with miRNA mimics predicted to target the 3'-UTR. Reporter expression was then assayed using a dual luciferase reporter assay and luminescence detected and analyzed as the normalized and scaled ratio of Renilla to firefly luciferase. (B) The APP 3'-UTR reporter construct and miRNA mimics (40 nM) were co-transfected and Renilla to firefly luciferase ratios computed as described above. Data are presented as RRR (see Materials and Methods).

D. miR-101 negatively regulates APP expression

The APP 3'-UTR reporter assay results above demonstrated that co-transfection of miR-101 significantly downregulated reporter expression. miR-101 has two predicted target sites in the APP 3'-UTR as predicted by TargetScan, PicTar, DIANA-microT, and miRanda-miRSVR. PITA predicts only the first site. The approximate locations of these two predicted target sites are schematically illustrated in Figure 7A. The precise location of each target site in the human APP 3'-UTR, their sequences and predicted interactions with miR-101, and a limited mammalian multiple sequence alignment pulled from TargetScan are indicated in Figure 7B. The scores for each site prediction where the predictor discriminates between multiple target sites gave a "stronger" score for the first site (Table 8). Further, the conserved branch length metric employed in TargetScan to assess conservation of each site [243] demonstrated stronger conservation at the first site as compared to the second site (1.619 for site 1 vs 0.859 for site 2). This suggests that the first site has been under heavier evolutionary pressure to maintain target site sequence fidelity.

To confirm that the inhibitory effect of miR-101 on APP 3'-UTR reporter expression was mediated specifically via one of two predicted miR-101 target sites located in the APP 3'-UTR, mutations were introduced separately in the seed sequences of both target sites in the reporter construct (Figure 7C). These mutant reporter constructs were then co-transfected along with miR-101 mimic into HeLa cells and reporter expression compared to wild-type reporter (Figure 7D). This reporter assay replicated the original finding, demonstrating reduced reporter expression when the wild-type reporter was co-transfected with miR-101 as compared to co-transfection with negative control miRNA (0.604±0.013 fold change; $p<0.01$ by post-hoc Dunnett's t-test). Mutation of site 1 eliminated the inhibitory effect of miR-101 mimic on reporter expression, whereas mutation of site 2 had no effect on this response (0.596±0.062 fold

change compared to co-transfection with negative control miRNA; $p<0.01$ by post-hoc Dunnett's t-test). Therefore, miR-101 regulates reporter expression specifically via site 1 in the APP 3'-UTR.

Reporter assays allow for rapid and sensitive detection of miRNA-mediated effects on reporter expression but are indirect measures of the effect on APP expression. Therefore, to directly examine whether miR-101 reduces endogenous APP levels, miR-101 mimic was transfected into HeLa cells and APP protein levels directly assayed by Western blot (Figure 8A and B). In response to miR-101 transfection, APP protein levels were significantly reduced as compared to HeLa cells transfected with negative control mimic or mock-transfected cells (0.383±0.056 fold change compared to mock transfection; $p=0.0011$ by Student's t-test). Therefore, endogenous APP levels are inhibited by miR-101 in human HeLa cells. Effective delivery of mimic into HeLa was confirmed by RT-qPCR (Figure 8D). Notably, APP mRNA levels measured by RT-qPCR were significantly decreased following miR-101 transfection as compared to negative control miRNA (0.663±0.030 fold change; $p= 0.0009$ by two-tailed Student's t-test) (Figure 8C). This response is consistent with that expected from a miRNA that mediates strong inhibitory control on gene expression [227].

To confirm that the inhibitory effect of miR-101 on APP levels was not limited to HeLa cells, the human glioblastoma cell line U373 (Figure 9A and B) and primary human fetal brain cultures (Figure 9C and D) were transfected with miR-101 mimic and APP levels assayed by Western blot. In both culture systems, APP protein levels were significantly reduced following miR-101 transfection (fold change compared to mock transfection: U373, 0.715±.025; human fetal brain culture, 0.756±0.038; $p<0.05$ by Student's t-test). Therefore, the inhibitory effect on APP levels is not limited only to human epithelial HeLa cells but is also apparent in transformed human astroglial cells and primary human brain cells.

An expected outcome of reducing APP protein output would be a reduction in its neurotoxic metabolite – secreted Aβ protein. To test whether miR-101 delivery reduces Aβ secretion, primary human fetal brain cultures and U373 cells were transfected with miR-101 mimic and conditioned media (CM) collected after 48 hours. Levels of Aβ1-40 were then assayed by ELISA and absolute values (pg/mL) corrected for well-to-well variations in cell number by either normalizing to total protein yield of crude cell lysates (human fetal brain cultures) or to a measure of cell viability (Cell Titer Glo for U373). Aβ1-40 levels were significantly decreased in the CM of primary human fetal brain cultures transfected with miR-101 as compared to cultures transfected with a negative control miRNA (0.367±0.031 fold change; p=0.0012 by Student's t-test) (Figure 10A). Aβ1-40 levels were similarly decreased (but not statistically significant) in the CM of primary human fetal brain cultures transfected with miR-101 (0.817±0.059 fold change compared to negative control transfection; p=0.052 by Student's t-test) (Figure 10B).

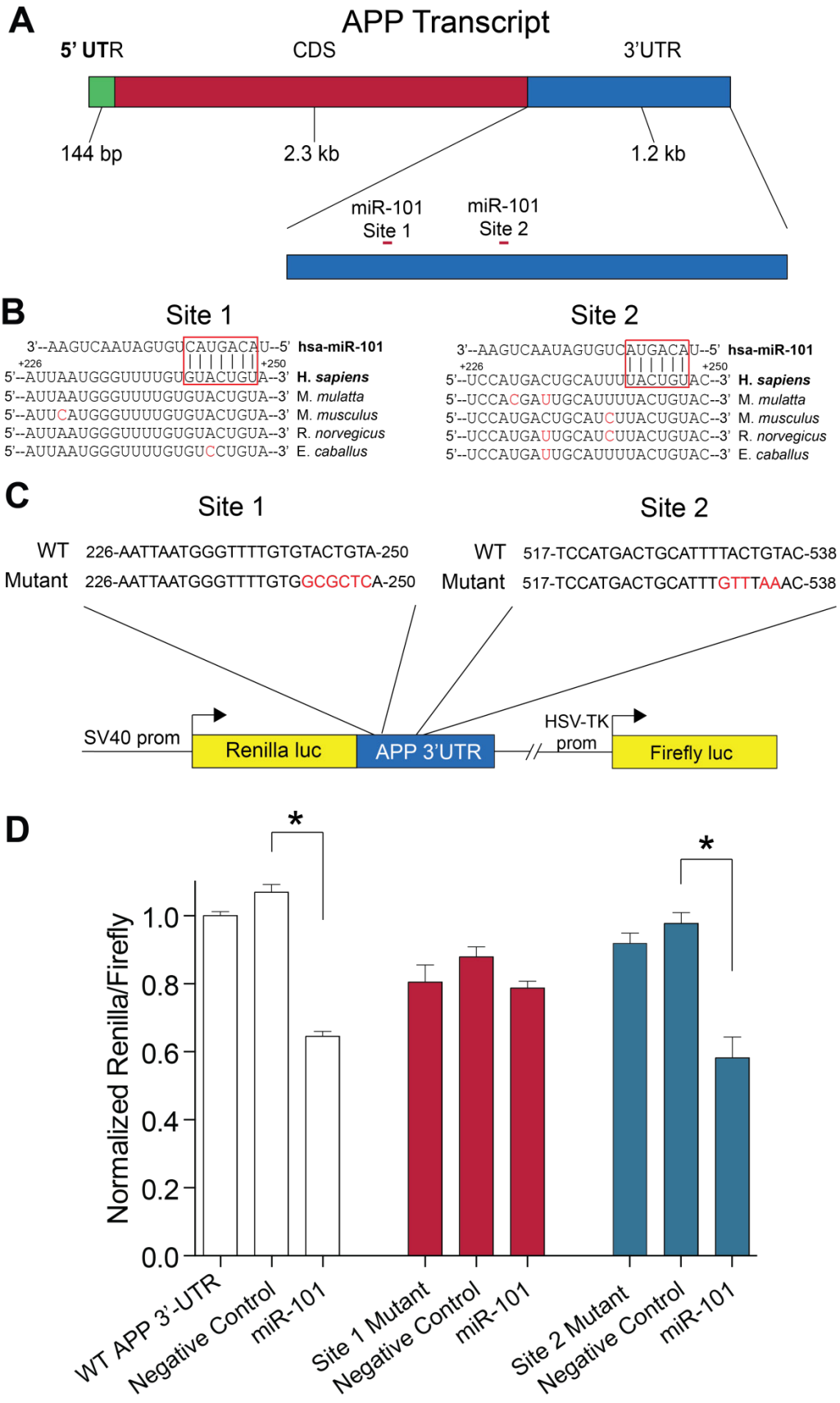
A
APP Transcript
5' UTR
CDS
3'UTR
144 bp
2.3 kb
1.2 kb
miR-101 Site 1
miR-101 Site 2
B
Site 1
3'--AAGUCAAUAGUGUCAUGACAU--5' hsa-miR-101
+226
+250
5'--AUUAAUGGGUUUUGUGUACUGUA--3' H. sapiens
5'--AUUAAUGGGUUUUGUGUACUGUA--3' M. mulatta
5'--AUUCAUGGGUUUUGUGUACUGUA--3' M. musculus
5'--AUUAAUGGGUUUUGUGUACUGUA--3' R. norvegicus
5'--AUUAAUGGGUUUUGUGUCCUGUA--3' E. caballus
Site 2
3'--AAGUCAAUAGUGUCAUGACAU--5' hsa-miR-101
+226
+250
5'--UCCAUGACUGCAUUUUACUGUAC--3' H. sapiens
5'--UCCACGAUUGCAUUUUACUGUAC--3' M. mulatta
5'--UCCAUGACUGCAUCUUACUGUAC--3' M. musculus
5'--UCCAUGAUUGCAUCUUACUGUAC--3' R. norvegicus
5'--UCCAUGAUUGCAUUUUACUGUAC--3' E. caballus
C
Site 1
WT 226-AATTAATGGGTTTTGTGTACTGTA-250
Mutant 226-AATTAATGGGTTTTGTGGCGCTCA-250
Site 2
WT 517-TCCATGACTGCATTTTACTGTAC-538
Mutant 517-TCCATGACTGCATTTGTTTAAAC-538
SV40 prom
Renilla luc
APP 3'UTR
HSV-TK prom
Firefly luc
D
Normalized Renilla/Firefly
0.0
0.2
0.4
0.6
0.8
1.0
*
*
WT APP 3'-UTR
Negative Control
miR-101
Site 1 Mutant
Negative Control
miR-101
Site 2 Mutant
Negative Control
miR-101

Figure 7: miR-101 targets human APP 3'-UTR via a conserved site. (A) Schematic of the APP transcript demonstrating location of two putative miR-101 target sites in the 3'-UTR predicted by the TargetScan, PicTar, DIANA-microT, rna22, miRanda-mirSVR, and PITA algorithms. (B) Sequence and predicted base-pairing of human miR-101 with its two predicted target sites in the human APP 3'-UTR, including seed sequence interactions (red boxes). To assess site conservation, multiple genome alignments for mammalian species were pulled from TargetScan. Sequences from rhesus macaque, mouse, rat, and horse from positions orthologous to the predicted miR-101 target site in the human APP 3'-UTR are shown. Red text highlights nucleotide differences compared to the human sequence. (C) Two predicted target sites in the APP 3'-UTR reporter construct were mutated by site-directed mutagenesis. Red text highlights mutations introduced in seed sequence. (D) Wild-type and target site mutant reporter constructs were transfected into HeLa cells either alone or along with 50 nM negative control and miR-101 mimic. Luciferase expression was assessed 48 hours post-transfection. * $p<0.05$, $n=6$.

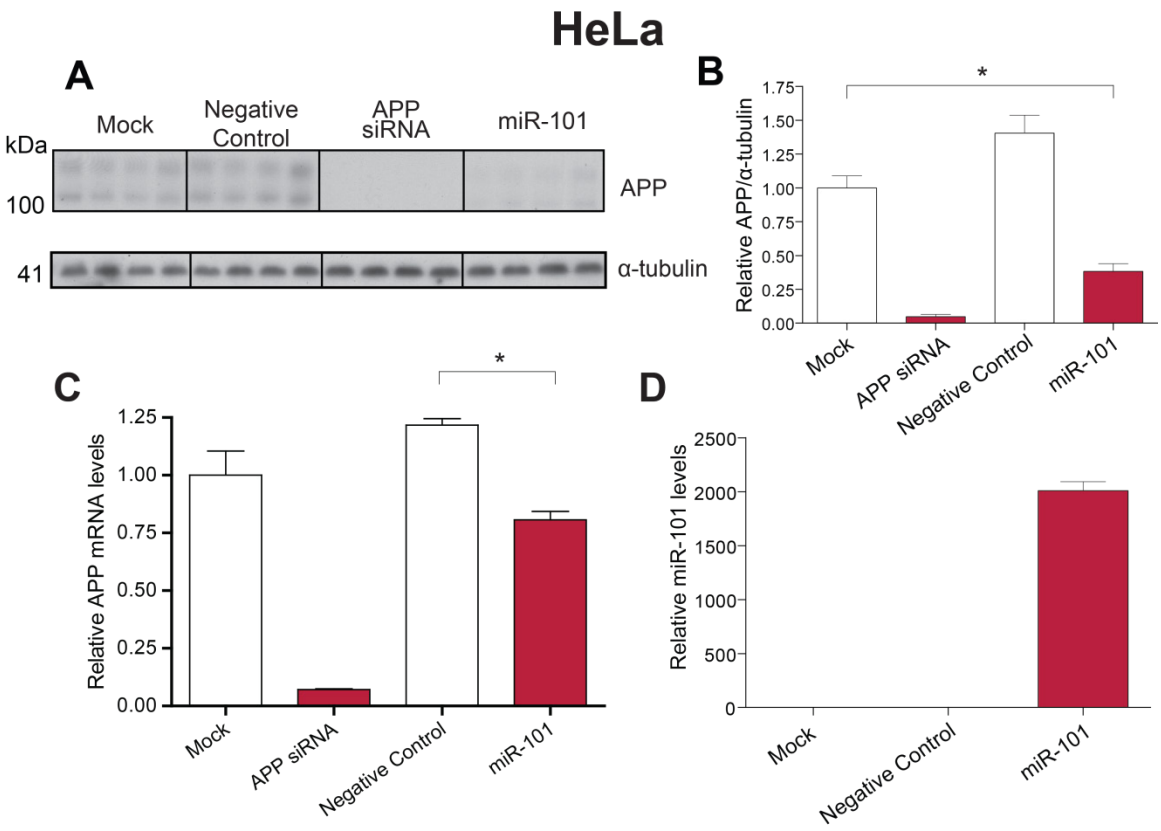

Figure 8: miR-101 delivery downregulates APP expression in HeLa cells. (A) HeLa cells were transfected with 50 nM miR-101 mimic or negative control and APP levels assayed 72 hours post-transfection by Western blot. siRNA (20 nM) transfection included as delivery control (n=4). (B) Blots were quantified by densitometric analysis and APP levels normalized to α-tubulin levels and scaled relative to mock transfection (n=4). (C) APP mRNA levels in HeLa cells were assayed by RT-qPCR 48 hours post-transfection (n=3). RT-qPCR expression levels were normalized to the geometric mean of β-actin, B2M, GAPDH and TBP expression levels and further scaled relative to mock-transfected levels. (D) Efficient delivery of miR-101 into HeLa cells confirmed by RT-qPCR 72 hours post-transfection (two technical replicates). RT-qPCR expression levels were normalized to the geometric mean of RNU48, RNU6B and hsa-miR-16 expression levels and further scaled relative to mock-transfected levels. * $p<0.05$ relative to mock-transfected or negative control-trasfected cells.

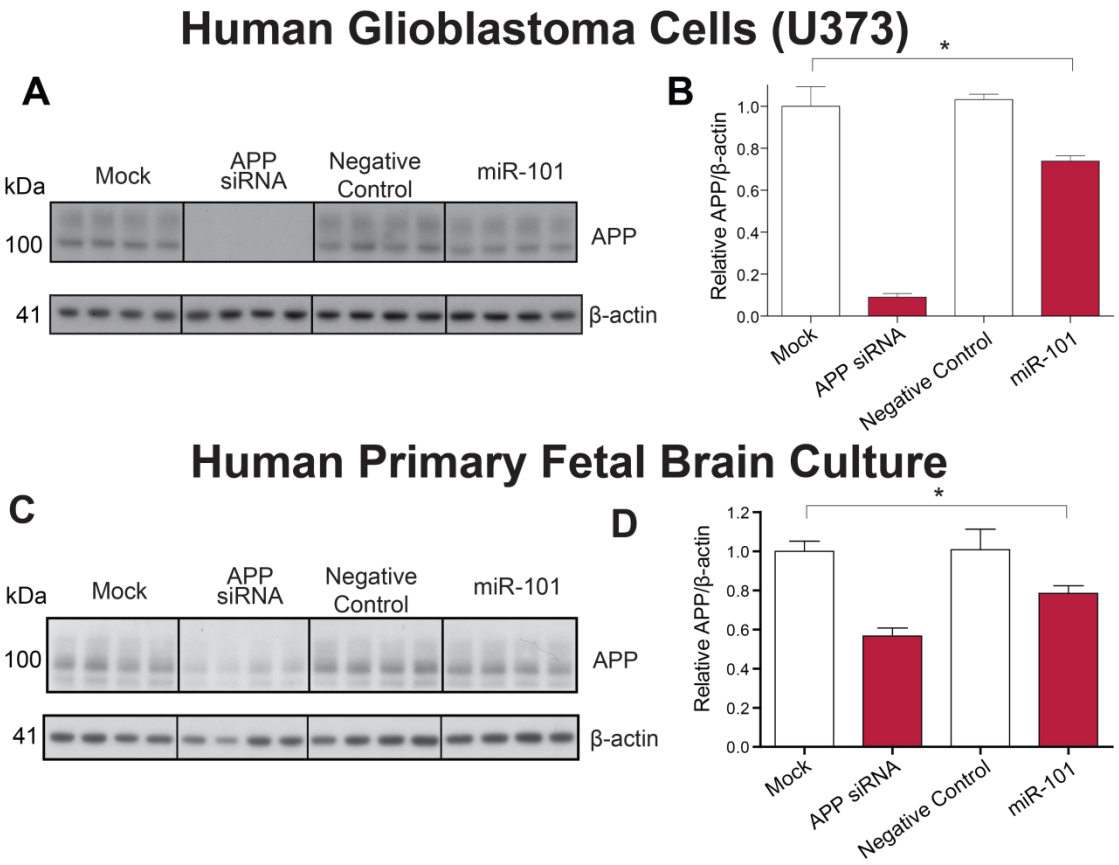

Figure 9: miR-101 delivery downregulates APP expression in U373 cells and primary human fetal brain cultures. (A) U373 cells were transfected with 75 nM miR-101 mimic or negative control and APP levels assayed 72 hours post-transfection by Western blot. siRNA (20 nM) transfection included as delivery control (n=4). (B) Blots from panel (A) were quantified by densitometric analysis and APP levels normalized to β-actin levels and scaled relative to mock transfection. (C) Primary human fetal brain cultures were transfected with 150 nM miR-101 mimic or negative control at DIV 17 and lysates prepared 48 hours post-transfection (DIV 19). siRNA (20 nM) transfection included as delivery control. Levels of APP and α-tubulin were assayed by Western blot. (D) Blots from panel (C) were quantified by densitometric analysis and APP levels normalized to β-actin levels and scaled relative to mock transfection. * $p<0.05$ relative to mock-transfected cells; n=4

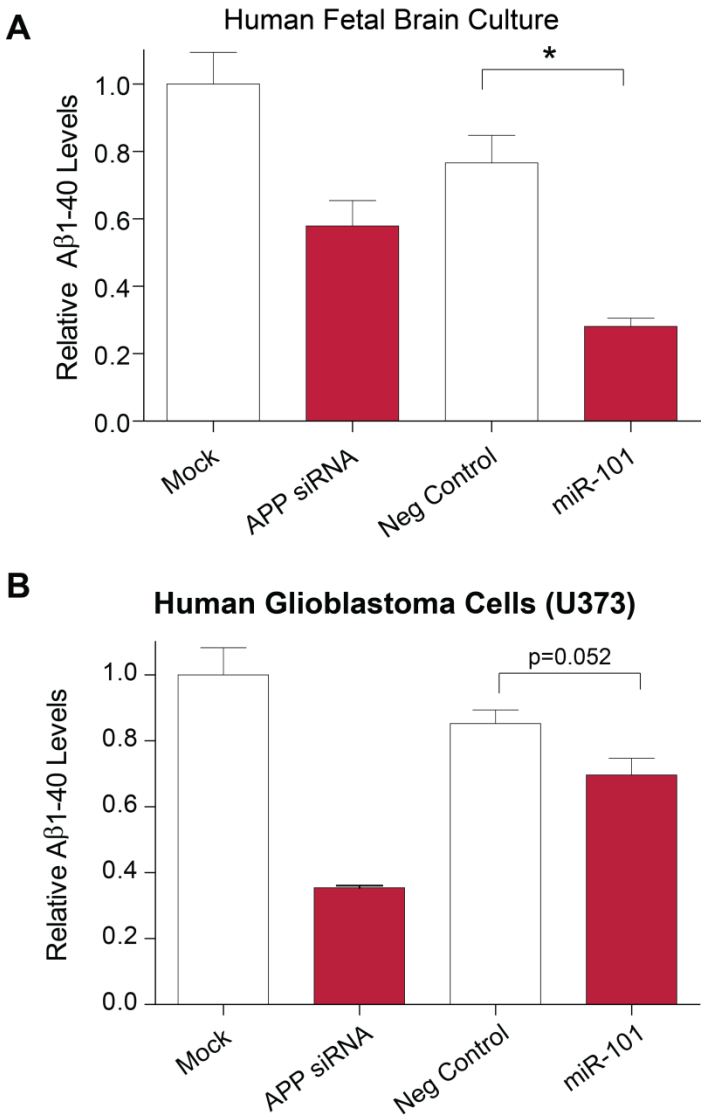

Figure 10: miR-101 delivery reduces secretion of Aβ1-40 into the CM of primary human fetal brain cultures and U373 cells. Primary human fetal brain cultures at DIV 17 and U373 cells were either mock-transfected, transfected with 20 nM APP siRNA, transfected with negative control or miR-153 mimic (75 nM for U373; 150 nM for human fetal brain cultures). CM were collected 48 h post-transfection. Aβ1-40 levels were measured in CM by ELISA. Absolute values (pg/mL) were normalized to either the total protein yield of crude cell lysates for primary human fetal brain cultures or to Cell Titer Glo values for U373 cells and scaled relative to mock transfection to account for

variability associated with differences in cell number and viability. (*p<0.01 by Student's t-test; n=4)

E. Other predicted targets of miR-101

A frequent critique of pursuing miRNA modulation as a therapeutic strategy in the diseased state is that physiological miRNA targeting is so promiscuous that it would surely result in adverse off-targeting effects during therapeutic manipulation. Given the promise of miR-101 as a putative therapeutic target for modulating APP expression, the extent of possible promiscuity associated with miR-101 was examined. Datasets containing human transcriptome-wide miR-101 target site predictions compiled by the TargetScan algorithm were pulled from the TargetScan website.The data were filtered by context+ score. The context+ scoring system assesses the predicted efficacy of a given target site by assessing the seed sequence type, degree of target site complementarity to miRNA 3' end, presence of optimal local AU bases, and position of target site along the transcript 3'-UTR. Table 9 lists all transcripts containing miR-101 target sites with context+ scores suggesting equal or more efficacious (more negative) miR-101 targeting than APP. Aggregate P_{CT} (probability of conserved targeting) scores are also listed for each target site. The aggregate P_{CT} score is a quantitative measure of the level of cross-species conservation across all miR-101 target sites in a given transcript.

One hundred transcripts have putative miR-101 target sites with context+ scores equal to or more favorable than the predicted miR-101 target sites in APP transcript. It is important to keep in mind that the context+ scoring system considers all predicted miR-101 target sites along a given transcript 3'-UTR, even false positive sites such as the second predicted miR-101 target site in APP shown above to be non-functional. Therefore, the number of true miR-101 targets in this list is likely overestimated. Enriched among the listed transcripts are tumor suppressor genes, including validated targets *MYCN* and *EZH2* [319–321]. Therefore, therapeutically elevating miR-101 expression levels would not be expected to promote carcinogenesis. Also of note are

validated transcript targets with roles in autophagy (e.g. *RAB5A*) and spinocerebellar ataxia (i.e. *ATXN1*) [291,322,323]. Inhibition of these transcripts by therapeutically elevating miR-101 levels might potentially have synergistic effects on anti-amyloidogenic APP metabolism as further discussed in the Discussion section. Therefore, promiscuity and off-target effects of miRNA targeting are not exclusively deleterious and in some cases may prove synergisitic and beneficial.

Table 9: List of transcripts containing TargetScan-predicted miR-101 target sites

Target gene	Gene name	Total context+ score[a]	Aggregate P_{CT}
FAM108C1	family with sequence similarity 108, member C1	-0.84	0.60
GLTSCR1	glioma tumor suppressor candidate region gene 1	-0.81	0.98
ZNF654	zinc finger protein 654	-0.78	0.99
EYA1	eyes absent homolog 1 (Drosophila)	-0.76	0.32
FLRT3	fibronectin leucine rich transmembrane protein 3	-0.76	0.95
CDYL	chromodomain protein, Y-like	-0.76	0.65
TNPO1	transportin 1	-0.71	0.78
LCOR	ligand dependent nuclear receptor corepressor	-0.69	0.97
MYCN	v-myc myelocytomatosis viral related oncogene, neuroblastoma derived (avian)	-0.67	0.90
TET2	tet oncogene family member 2	-0.66	0.67
UBE2D1	ubiquitin-conjugating enzyme E2D 1	-0.65	0.79
SIX4	SIX homeobox 4	-0.64	0.97
MFSD6	major facilitator superfamily domain containing 6	-0.63	0.86
TSHZ3	teashirt zinc finger homeobox 3	-0.63	0.93
FZD4	frizzled family receptor 4	-0.58	0.95
STC1	stanniocalcin 1	-0.58	0.85
MYRIP	myosin VIIA and Rab interacting protein	-0.58	0.84
FAT3	FAT tumor suppressor homolog 3 (Drosophila)	-0.57	0.89
GLCCI1	glucocorticoid induced transcript 1	-0.57	0.47
SEL1L	sel-1 suppressor of lin-12-like (C. elegans)	-0.56	0.77
PPARGC1B	peroxisome proliferator-activated receptor gamma, coactivator 1 beta	-0.56	> 0.99
ZBTB41	zinc finger and BTB domain containing 41	-0.56	0.62
ATXN1	ataxin 1	-0.55	0.98
TMEM65	transmembrane protein 65	-0.55	0.77
ZNF295	zinc finger protein 295	-0.55	0.16
NSD1	nuclear receptor binding SET domain protein 1	-0.55	0.91
MOBKL3	MOB1, Mps One Binder kinase activator-like 3 (yeast)	-0.55	0.87
HSPE1-MOBKL3	HSPE1-MOBKL3 readthrough	-0.55	0.87
ASPN	asporin	-0.55	0.65
KBTBD8	kelch repeat and BTB (POZ) domain containing 8	-0.54	0.79
SLC12A2	solute carrier family 12 (sodium/potassium/chloride transporters), member 2	-0.54	0.56
FAM73A	family with sequence similarity 73, member A	-0.54	0.31
EZH2	enhancer of zeste homolog 2 (Drosophila)	-0.54	0.81
RBM25	RNA binding motif protein 25	-0.54	0.31
ZMAT3	zinc finger, matrin-type 3	-0.53	0.79
SLC39A10	solute carrier family 39 (zinc transporter), member 10	-0.51	0.81
ZFHX4	zinc finger homeobox 4	-0.51	0.83
BEAN1	brain expressed, associated with NEDD4, 1	-0.51	0.86
ZNF532	zinc finger protein 532	-0.51	0.63
PIKFYVE	phosphoinositide kinase, FYVE finger containing	-0.50	< 0.1
MKL2	MKL/myocardin-like 2	-0.50	0.93
PLEKHG1	pleckstrin homology domain containing, family G (with RhoGef domain) member 1	-0.50	0.48
DCBLD2	discoidin, CUB and LCCL domain containing 2	-0.50	0.99
NEK7	NIMA (never in mitosis gene a)-related kinase 7	-0.50	0.87
HTRA3	HtrA serine peptidase 3	-0.49	0.94
IKZF4	IKAROS family zinc finger 4 (Eos)	-0.49	0.90
ZDHHC21	zinc finger, DHHC-type containing 21	-0.49	0.31
CBFA2T2	core-binding factor, runt domain, alpha subunit 2; translocated to, 2	-0.48	0.88
INO80D	INO80 complex subunit D	-0.48	0.93
SHISA6	shisa homolog 6 (Xenopus laevis)	-0.47	0.91

UGGT1	UDP-glucose glycoprotein glucosyltransferase 1	-0.47	0.52
RAB5A	RAB5A, member RAS oncogene family	-0.47	0.63
NPNT	nephronectin	-0.47	0.87
FZD6	frizzled family receptor 6	-0.47	0.57
CACNB2	calcium channel, voltage-dependent, beta 2 subunit	-0.47	0.99
BTBD3	BTB (POZ) domain containing 3	-0.46	0.85
PBX3	pre-B-cell leukemia homeobox 3	-0.46	0.76
SUB1	SUB1 homolog (S. cerevisiae)	-0.46	0.70
ZFP36L2	zinc finger protein 36, C3H type-like 2	-0.45	0.81
C3orf58	chromosome 3 open reading frame 58	-0.45	0.36
UBE2D2	ubiquitin-conjugating enzyme E2D 2	-0.45	< 0.1
ACVR2B	activin A receptor, type IIB	-0.45	0.96
H2AFV	H2A histone family, member V	-0.44	0.91
PDS5B	PDS5, regulator of cohesion maintenance, homolog B (S. cerevisiae)	-0.44	0.30
USP47	ubiquitin specific peptidase 47	-0.43	0.88
DIP2B	DIP2 disco-interacting protein 2 homolog B (Drosophila)	-0.43	0.91
ASAP1	ArfGAP with SH3 domain, ankyrin repeat and PH domain 1	-0.43	0.60
ICK	intestinal cell (MAK-like) kinase	-0.43	0.85
SGK1	serum/glucocorticoid regulated kinase 1	-0.43	0.63
TCF4	transcription factor 4	-0.43	0.48
SH2B3	SH2B adaptor protein 3	-0.43	0.88
ANKRD11	ankyrin repeat domain 11	-0.43	0.87
ATXN1L	ataxin 1-like	-0.43	0.87
ZNF746	zinc finger protein 746	-0.43	0.84
NACC2	NACC family member 2, BEN and BTB (POZ) domain containing	-0.42	0.91
AP1S3	adaptor-related protein complex 1, sigma 3 subunit	-0.42	0.50
PROK2	prokineticin 2	-0.42	0.31
SULT4A1	sulfotransferase family 4A, member 1	-0.42	0.83
SRGAP1	SLIT-ROBO Rho GTPase activating protein 1	-0.42	0.87
SMARCA5	SWI/SNF related, matrix associated, actin dependent regulator of chromatin, subfamily a, member 5	-0.42	0.88
RAB39B	RAB39B, member RAS oncogene family	-0.42	0.47
MTSS1L	metastasis suppressor 1-like	-0.42	0.31
TGFA	transforming growth factor, alpha	-0.42	0.84
KCNH7	potassium voltage-gated channel, subfamily H (eag-related), member 7	-0.42	0.76
FAM108B1	family with sequence similarity 108, member B1	-0.41	0.65
RAB3GAP2	RAB3 GTPase activating protein subunit 2 (non-catalytic)	-0.41	< 0.1
SSX2IP	synovial sarcoma, X breakpoint 2 interacting protein	-0.41	0.31
COL10A1	collagen, type X, alpha 1	-0.41	0.68
NLK	nemo-like kinase	-0.41	0.76
CDH5	cadherin 5, type 2 (vascular endothelium)	-0.41	0.84
ADAMTSL3	ADAMTS-like 3	-0.41	0.59
PRKCE	protein kinase C, epsilon	-0.41	0.86
CEP350	centrosomal protein 350kDa	-0.40	0.93
RAP1B	RAP1B, member of RAS oncogene family	-0.40	0.71
BEGAIN	brain-enriched guanylate kinase-associated homolog (rat)	-0.40	0.31
RORA	RAR-related orphan receptor A	-0.40	0.97
FGA	fibrinogen alpha chain	-0.40	0.86
GSK3B	glycogen synthase kinase 3 beta	-0.40	0.86
SACM1L	SAC1 suppressor of actin mutations 1-like (yeast)	-0.40	< 0.1
APP	amyloid beta (A4) precursor protein	-0.40	0.66

[a]Context+ score threshold for inclusion in table set equal to or less than (more favorable) APP score of -0.40

F. miRNA-153 negatively regulates APP expression

Unlike miR-101, miR-153 has only one predicted target site in the APP 3'-UTR as predicted by TargetScan, PicTar, DIANA-microT, and miRanda-miRSVR, PITA, and rna22. Approximate location of the predicted target site is schematically illustrated in Figure 11A. Location, exact sequence and predicted interaction of the target site in the human APP 3'-UTR with miR-153 are indicated in Figure 11B, as is a limited mammalian multiple sequence alignment. Specific scores produced by each predictor for this target site are indicated in Table 8. This specific site is considered strongly conserved according to the conserved branch length metric employed in TargetScan (1.864 vs 1.619 for conserved miR-101 site 1). This suggests that, as with the functional miR-101 site, this particular target site has been under heavy evolutionary pressure to maintain perfect target site sequence identity.

To confirm that the inhibitory effect of miR-153 on APP 3'-UTR reporter expression was mediated specifically by the predicted miR-153 target site, mutations were introduced into the seed sequence of the target site in the reporter construct (Figure 11C). The mutant reporter construct was co-transfected along with miR-153 mimic into HeLa cells and reporter expression compared to wild-type reporter (Figure 11D). The original finding was replicable – wild-type reporter co-transfection with miR-153 was significantly reduced as compared to transfection of the reporter alone (0.832±0.017 fold change; $p<0.0004$ by Student's t-test). Target site mutation eliminated the inhibitory effect of miR-153 delivery on reporter expression. Therefore, miR-153 regulates reporter expression specifically via the predicted site in the APP 3'-UTR.

miR-153 mimic was transfected into HeLa cells and APP protein levels directly assayed by Western blot to directly examine whether miR-153 reduces endogenous APP levels (Figure 12A and B). APP protein levels were significantly reduced as

compared following transfection with miR-153 as compared to HeLa cells transfected with negative control mimic (0.661±0.096 fold change; p=0.0059 by Student's t-test). Therefore, endogenous APP levels are inhibited by miR-153 in human HeLa cells. Effective delivery of mimic into HeLa was confirmed by RT-qPCR (~220,000 fold change relative to mock) (Figure 12D). APP mRNA levels measured by RT-qPCR were significantly decreased following miR-153 transfection as compared to negative control miRNA or mock transfection (0.601±0.053 fold change compared to mock transfection; p=0.0050 by Student's t-test) (Figure 12C), suggesting a post-transcriptional mechanism that does likely involve a degree of mRNA destabilization, perhaps in addition to direct inhibition of protein translation.

As with miR-101, other human cell types were transfected to confirm that the inhibitory effect of miR-153 on APP levels was not limited to HeLa cells. U373 cells (Figure 13A and B) and primary human fetal brain cultures (Figure 13 and D) were transfected with miR-153 mimic and APP levels assayed by Western blot. In both culture systems, APP protein levels were significantly reduced following miR-153 transfection as compared to transfection with a negative control miRNA (fold change compared to negative control transfection: U373, 0.762±.039; human fetal brain culture, 0.790±0.104; $p<0.05$ by Student's t-test). Therefore, the inhibitory effect on APP levels is not limited only to human epithelial HeLa cells but is also apparent in transformed human astroglial cells and highly relevant primary human brain cells.

To test whether miR-153 also delivery reduces Aβ secretion, primary human fetal brain cultures were transfected with miR-153 mimic and CM collected after 48 hours. Levels of Aβ1-40 were then assayed by ELISA and absolute values (pg/mL) corrected for well-to-well variations in cell number by normalizing to total protein yield of crude cell lysates. Aβ1-40 levels were significantly decreased in the CM of primary human fetal brain cultures transfected with miR-153 as compared to cultures

transfected with a negative control miRNA (0.717±0.054 fold change; p=0.0436 by Student's t-test) (Figure14).

To establish whether miR-153 participates in the regulatory network that controls APP expression in human neurons, a miRNA antisense inhibitor was utilized to bind to and disrupt the interaction of miR-153 with mRNA targets. Primary human fetal brain cultures were transfected with miR-153 inhibitor and APP expression assayed by Western blot. Transfection of miR-153 inhibitor significantly increased APP expression relative to negative control inhibitor transfection (1.317±0.099 fold change; p=0.026) (Figure 15). Therefore, endogenous miR-153 actively inhibits APP expression in human fetal brain cultures under physiological culture conditions.

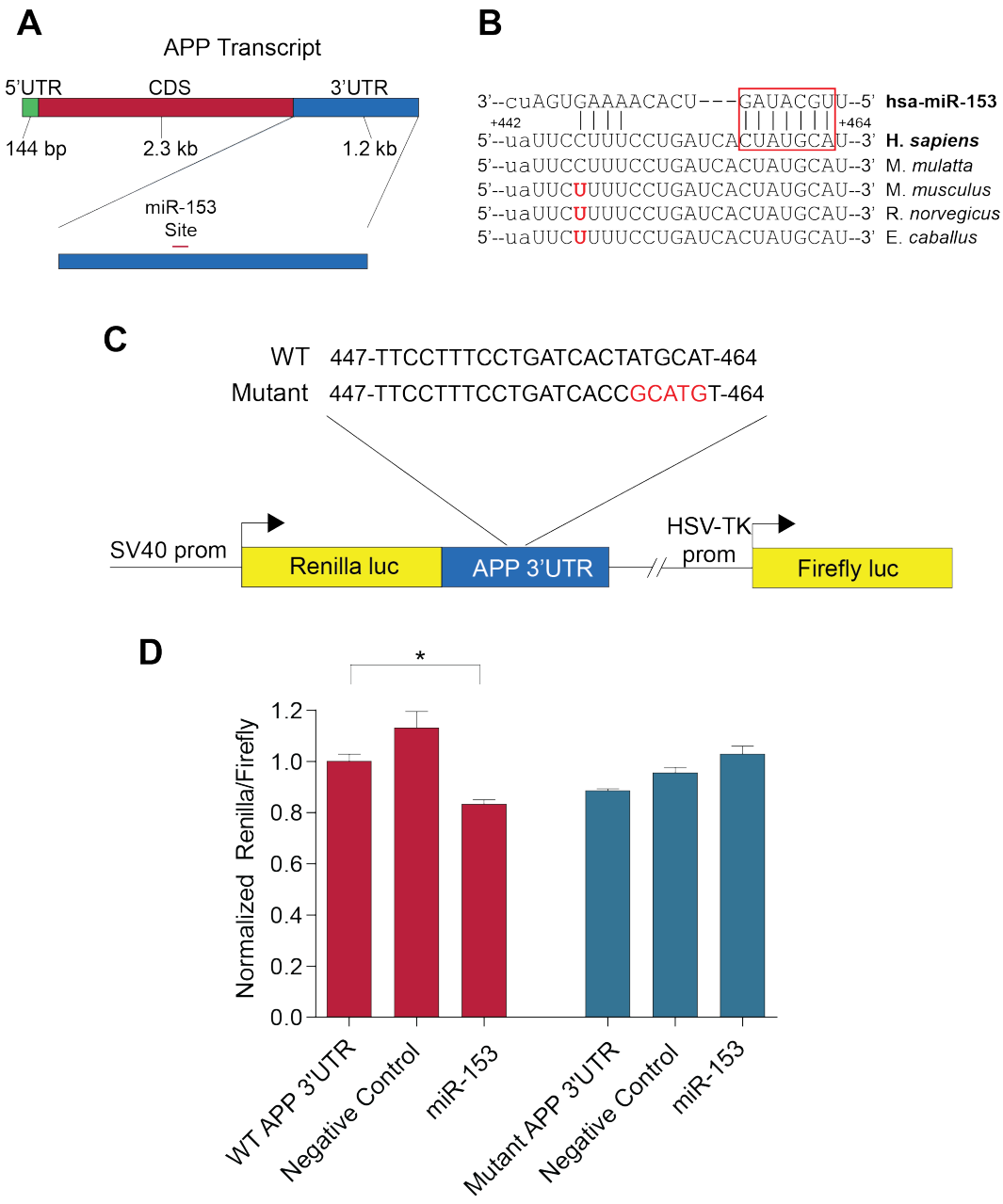

Figure 11: miR-153 targets human APP 3'-UTR via a conserved site. (A) Schematic of the APP transcript demonstrating location of a putative miR-153 target site in the 3'-UTR predicted by the TargetScan, PicTar, DIANA-microT, rna22, miRanda-mirSVR, and PITA algorithms. (B) Sequence and predicted base-pairing of human miR-153 with its predicted target site in the human APP 3'-UTR, including the seed sequence interaction (red box). To assess site conservation, multiple genome alignments for

mammalian species were pulled from TargetScan. Sequences from rhesus macaque, mouse, rat, and horse from positions orthologous to the predicted miR-153 target site in the human APP 3'-UTR are shown. Red text highlights nucleotide differences compared to the human sequence. (C) The predicted target site in the APP 3'-UTR reporter construct was mutated by site-directed mutagenesis. Red text highlights mutations introduced in seed sequence. (D) Wild-type and target site mutant reporter constructs were transfected into HeLa cells either alone or along with 50 nM negative control and miR-153 mimic. Luciferase expression was assessed 48 hours post-transfection. * $p<0.05$, $n=6$.

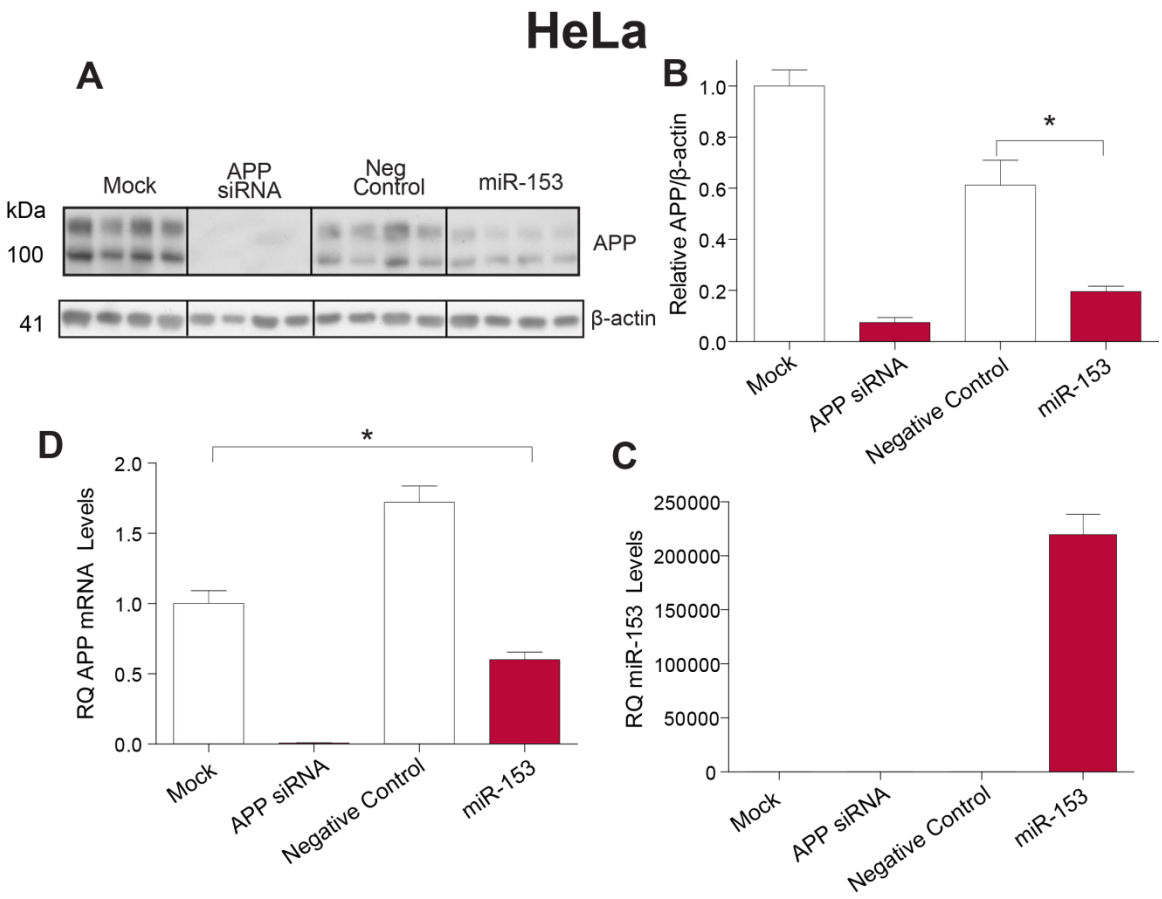

Figure 12: miR-153 delivery downregulates APP expression in HeLa cells. (A) HeLa cells were transfected with 50 nM miR-153 mimic or negative control and APP levels assayed 72 hours post-transfection by Western blot. siRNA (20 nM) transfection included as delivery control (n=4). (B) Blots were quantified by densitometric analysis and APP levels normalized to α-tubulin levels and scaled relative to mock transfection (n=4). (C) APP mRNA levels in HeLa cells were assayed by RT-qPCR 48 hours post-transfection (n=3). RT-qPCR expression levels were normalized to the geometric mean of β-actin, B2M, GAPDH and TBP expression levels and further scaled relative to mock-transfected levels. (D) Efficient delivery of miR-153 into HeLa cells confirmed by RT-qPCR 48 hours post-transfection (n=3). RT-qPCR expression levels were normalized to the geometric mean of RNU48, RNU6B and hsa-miR-16 expression

levels and further scaled relative to mock-transfected levels. RQ=relative quantity; * $p<0.05$ relative to mock-transfected cells.

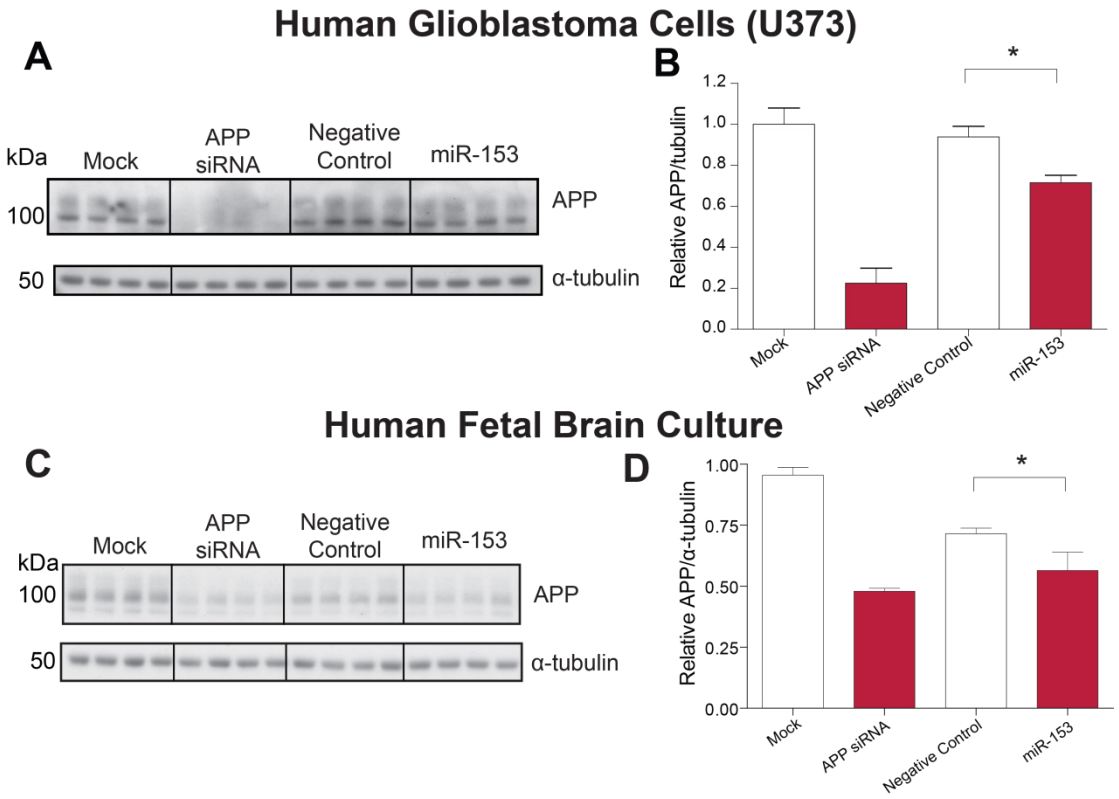

Figure 13: miR-153 delivery downregulates APP expression in U373 cells and primary human fetal brain cultures. (A) U373 cells were transfected with 75 nM miR-153 mimic or negative control and APP levels assayed 72 hours post-transfection by Western blot. siRNA (20 nM) transfection included as delivery control (n=4). (B) Blots from panel (A) were quantified by densitometric analysis and APP levels normalized to α-tubulin levels and scaled relative to mock transfection. (C) Primary human fetal brain cultures were transfected with 150 nM miR-153 mimic or negative control at DIV 17 and lysates prepared 48 hours post-transfection (DIV 19). siRNA (20 nM) transfection included as delivery control. Levels of APP and α-tubulin were assayed by Western blot. (D) Blots from panel (C) were quantified by densitometric analysis and APP levels normalized to β-actin levels and scaled relative to mock transfection. * $p<0.05$ relative to negative control-transfected cells; n=4

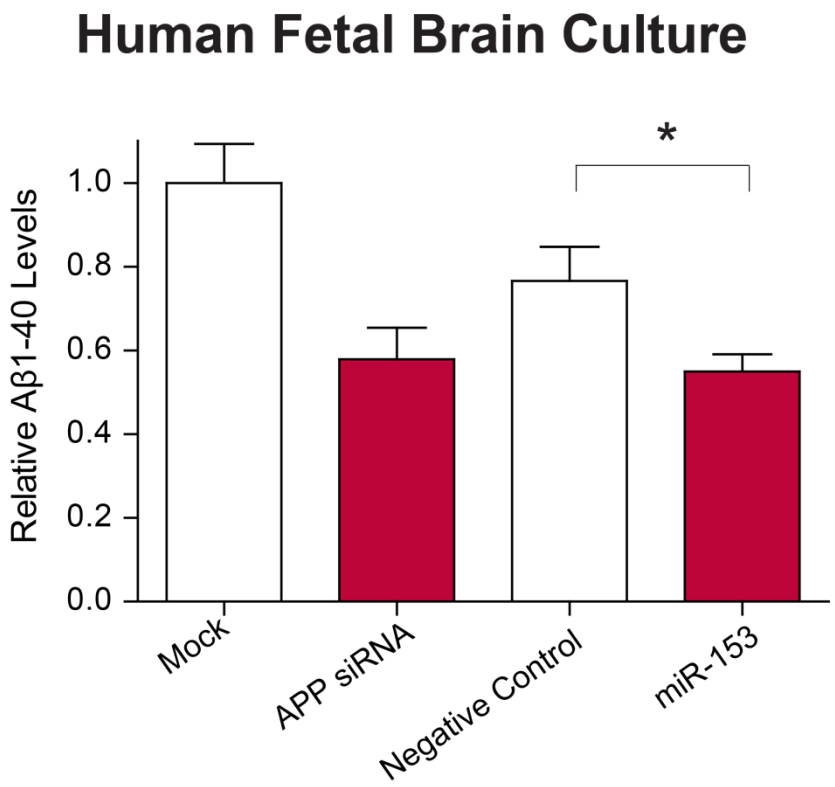

Figure 14: miR-153 reduces secretion of Aβ1-40 into the CM of primary human fetal brain cultures. Primary human fetal brain cultures at DIV 17 were either mock-transfected, transfected with 20 nM APP siRNA, transfected with 150 nM negative control or miR-153 mimic. CM were collected 48 h post-transfection. Aβ1-40 levels were measured in CM by ELISA. Absolute values (pg/mL) were normalized to the total protein yield of crude cell lysates and scaled relative to mock transfection to account for variability associated with differences in cell number. Transfection of miR-153 significantly reduced levels of Aβ1-40 released in the CM of primary human fetal brain cultures as compared to negative control-transfected cultures. * $p<0.05$ relative to negative control-transfected cells; n=4.

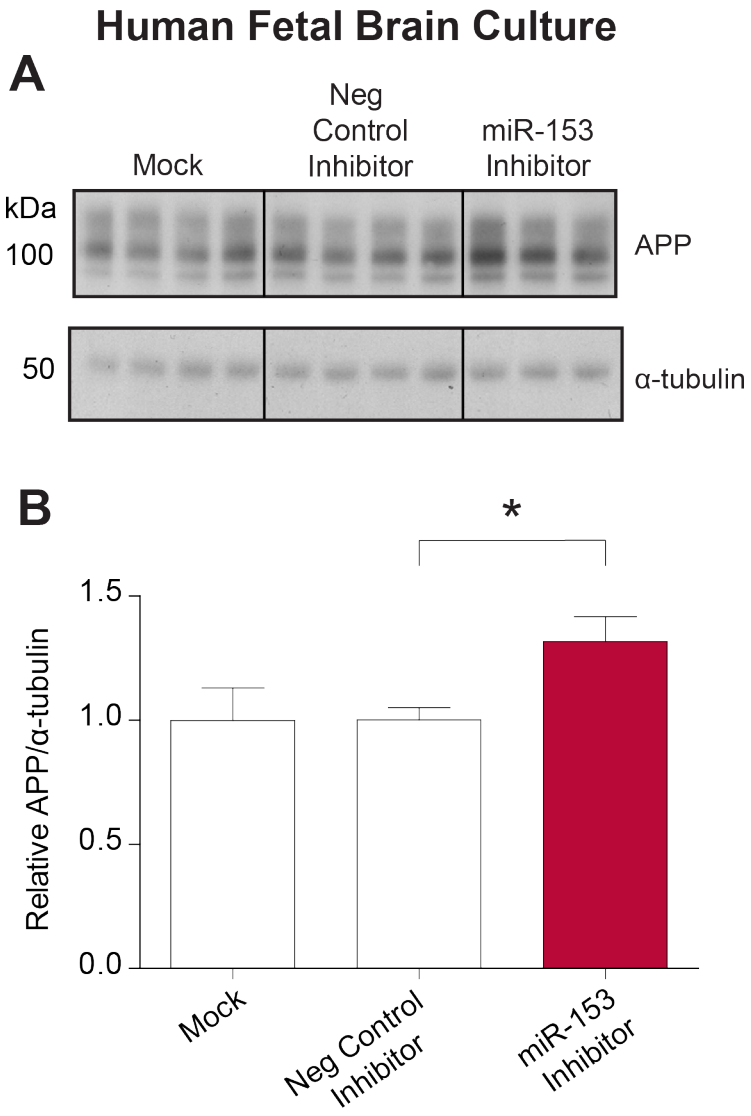

Figure 15: Blocking miR-153 interaction with the APP mRNA 3'-UTR elevates basal APP protein levels. (A) Western blot analysis of APP and α-tubulin levels in transfected primary human fetal brain cultures. Fetal brain cultures at DIV 17 were either mock-transfected or transfected with 1000 nM negative control or miR-153 antisense inhibitor. Cell lysates for proteins were prepared 24 h post-transfecton. (B) Densitometric analysis of APP normalized to α-tubulin demonstrated that miR-153 inhibitor significantly increased APP expression in primary human fetal brain cells. * $p<0.05$ relative to negative control inhibitor-transfected cells; n=3 – 4.

G. miRNA-346 positively regulates APP expression

While the great majority of miRNA:mRNA interactions detected in global analyses are restricted to the mRNA 3'-UTR [303,304], there is significant evidence that functional regulatory interactions also occur in the 5'-UTR and CDS [186,245,324,325]. To expand the scope of potential miRNA:APP mRNA interactions, the complete APP transcript sequence was scanned using the miRanda algorithm as implemented on the RegRNA web server [326] against a set of complete human miRNA sequences. This implementation utilizes the basic features of the miRanda algorithm [311], including the dynamic programming local alignment and thermodynamic stability assessment. It does not filter for target site cross-species conservation or utilize machine learning algorithms to predict site efficacy as implemented in the miRanda-miRSVR web server (this server limits searches to 3'-UTR only).

Many putative miRNA:APP mRNA interactions were predicted by this algorithm, including several 3'-UTR interactions predicted by the algorithms in Table 8 (e.g. miR-101, miR-153, miR-106a/b, miR-20a/b). A predicted interaction between miR-346 and the APP 5'-UTR (Figure 16A) was noted due to high overlap with a known IRE stem-loop structure previously shown to mediate translational control of APP expression in response to changes in intracellular iron homeostasis [143,144]. This site is also directly upstream of a known IL-1 acute box domain previously shown to post-transcriptionally stimulate APP mRNA translation [145]. The predicted interaction of miR-346 with the APP 5'-UTR sequence is indicated in Figure 16B, along with a limited mammalian multiple sequence alignment. The predicted interaction produced a complementarity score of 153 and minimum free energy (ΔG) of -26.3 kcal/mol, indicating high level of complementarity and stable duplex formation. Based on high level of complementarity and possibility for direct interaction with known functional regulatory elements in the 5'-

UTR, it was hypothesized that miR-346 regulates APP expression through interaction with its predicted site in the APP 5'-UTR.

To test for regulatory effects of miR-346 mediated via the APP 5'-UTR, the pGAL construct was utilized (provided by Dr. Jack T Rogers) [143]. This construct contains the complete 144 bp APP 5'-UTR inserted upstream of the firefly luciferase CDS in pGL3 (Promega). The predicted miR-346 target site in pGAL was mutated by cassette mutagenesis as indicated in Figure 16C. The wild-type and mutant pGAL constructs were co-transfected with miR-346. A Renilla luciferase construct (pRLSV40) was also co-transfected as an internal control to allow for dual reporter normalization. Surprisingly, transfection of miR-346 significantly induced reporter expression as compared to transfection with reporter construct alone (1.701±0.034. fold change; $p<0.0001$ by two-tailed Student's t-test) (Figure 16D). When the putative miR-346 target site in the APP 5'-UTR reporter, co-transfection with miR-346 no longer had a stimulatory effect on reporter expression and instead repressed reporter expression (0.630±0.027 fold change; $p<0.0001$ by two-tailed Student's t-test). Since this region of the APP 5'-UTR has known promoter activity [140], a separate strategy was employed to test the specificity of the putative target site without mutating a known promoter sequence. miR-346 was co-transfected with WT reporter along with either a negative control target protector or a custom target protector designed to block interaction of miR-346 with the putative target site in the APP 5'-UTR.While the negative control target protector had minimal effect, the custom miR-346-APP 5'-UTR target protector significantly reduced the stimulatory effect of miR-346 on APP 5'-UTR reporter expression (0.724±0.024 fold change compared to miR-346 transfection alone; $p<0.01$) (Figure 16E).Therefore,miR-346 stimulates APP 5'-UTR reporter expression in HeLa cells through a predicted target site in the APP 5'-UTR.

miR-346 mimic was transfected into HeLa cells and APP protein levels directly assayed by Western blot to directly examine whether miR-346 stimulates endogenous APP levels (Figure 17A and B). APP protein levels were dramatically and significantly elevated following transfection with miR-346 as compared to HeLa cells transfected with negative control mimic (3.035±0.109 fold change; $p<0.0001$ by Student's t-test). Therefore, endogenous APP levels are elevated by miR-346 in human HeLa cells. Effective delivery of mimic into HeLa was confirmed by RT-qPCR (~29,000 fold change relative to negative control miRNA) (Figure 17D). APP mRNA levels measured by RT-qPCR were not significantly increased following miR-346 transfection as compared to negative control miRNA or mock transfection (Figure 17C), suggesting a post-transcriptional mechanism that does not likely involve mRNA stabilization but instead direct stimulation of protein translation.

Given the non-canonical location of the miR-346 target site and non-canonical effect on APP protein expression, an additional experiment was performed to verify the specificity of the 5'-UTR target site for mediating this stimulatory effect. The target protector designed to block the interaction of miR-346 with its putative target site in the APP 5'-UTR was co-transfected into HeLa cells at increasing concentrations (0 nM-1000 nM) while holding the concentration of miR-346 mimic steady (15 nM). An potential unwanted consequence of increasing the concentration of target protector while holding the miR-346 mimic concentration steady is that competition for transfection reagent could reduce delivery of miR-346 and the resulting effect on APP expression. To control for this, negative control target protector was also co-transfected at decreasing concentration (1000 nM – 0 nM) such that the total target protector concentration was constant in all transfection conditions. Following miR-346 co-transfection with negative control target protector, APP expression was significantly elevated compared to mock transfection (2.574±0.304 fold change; $p=0.0021$ by

Student's t-test). Co-transfection of miR-346 mimic with miR-346 target protector demonstrated a concentration-dependent decrease in APP levels relative to 0 nM miR-346 target protector. At 1000 nM miR-346 target protector, APP expression was significantly decreased relative to 0 nM miR-346 target protector (0.606±0.074 fold change; $p<0.01$ by post-hoc Dunnett's t-test) (Figure 18A and B). Therefore, the stimulatory effect of miR-346 on endogenous APP protein expression at least partially requires the specific interaction of miR-346 with the APP 5'-UTR target site.

While the general mechanisms underlying the inhibitory effects of miRNA on target protein output, including mRNA deadenylation, mRNA decay and translational repression, are fairly well characterized [227,229,230,238,240,327], there is no characterized mechanistic precedent to serve as basis for explaining the stimulatory effect of miR-346 on APP expression. To begin to explore underlying mechanism, the role of endogenous miRNA processing and effector machinery was examined. HeLa cells were co-transfected with miR-346 and siRNA against Dicer or AGO2. Consistent with above experiments, co-transfection of miR-346 with negative control siRNA resulted in significantly elevated APP levels compared to negative control siRNA transfection alone (2.028±0.067 fold change; $p<0.0001$ by Student's t-test) (Figure 19A). To compare the effect of miR-346 delivery on APP levels after Dicer and AGO2 siRNA knockdown, the fractional increase in APP levels following miR-346 co-transfection with siRNA was calculated relative to transfection with siRNA alone independently for each siRNA. The fractional increase was then expressed as percent increase relative to negative control siRNA co-transfection (100±6.5%) (Figure 19B). The increase in APP expression following miR-346 delivery was significantly attenuated with knockdown of Dicer (61.55±3.90%; $p<0.05$ by post-hoc Dunnett's t-test) or AGO2 (40.03±11.24%; $p<0.01$ by post-hoc Dunnett's t-test). Therefore, the presence of both

Dicer and AGO2 is at least partially required for the stimulatory effect of miR-346 on APP expression.

As previously mentioned, the miR-346 target site in the APP 5'-UTR directly overlaps with a known IRE [143]. This IRE is known to bind IRP1 in the absence of iron, resulting in translational inhibition [144]. In the presence of iron, IRP1 dissociates from the IRE, thereby promoting APP mRNA translation. Therefore, it was hypothesized that miR-346 may partially mediate its stimulatory effect on APP expression by interfering or otherwise modulating with the interaction of IRP1 with its regulatory element in the APP 5'-UTR. To test this hypothesis, IRP1 expression was knocked down in HeLa cells by siRNA transfection. Western analysis confirmed successful knockdown in IRP1 following siRNA transfection (Figure 20). To assess the effect of IRP1 knockdown on induced APP expression following miR346 delivery, percent increase in APP levels following miR-346 delivery was calculated as discussed in Figure 18, with the exception that negative control miRNA mimic was included in place of mock transfection. IRP1 knockdown significantly attenuated the stimulatory effect of miR-346 on APP expression as compared to negative control siRNA co-transfection (55.48±4.39%; $p=0.0488$ by Student's t-test) (Figure 20A and B). Therefore, in addition to Dicer and AGO2, the presence of IRP1 is at least partially required for the stimulatory effect of miR-346 on APP expression.

To test whether the stimulatory effect of miR-346 on APP expression extended to primary human brain cells, human fetal brain cultures were transfected at DIV 19 with negative control miRNA or miR-346 mimic. No effect on APP expression was observed following miR-346 transfection (Figure 21A and B). Given the suggestive evidence in Figure 21 that miR-346 may mediate its effect on APP by cross-talking with IRP1 at the levels of the APP transcript, one possible explanation for the lack of response in primary human fetal brain cultures is that IRP1 binding to APP mRNA may be reduced

due to saturated intracellular iron binding to IRP1. To test this hypothesis, intracellular iron was first chelated using deferroxamine mesylate (Dfo). APP expression was significantly reduced in cultures treated with 150 μM Dfo for 48 hours relative to vehicle-treated cells (0.639±0.023 fold change; p=0.0477) (Figure 21C and D). This indicates that under basal conditions, intracellular iron disinhibits the repressive action of IRP1 on APP translation in primary human fetal brain cultures – a finding consistent with previous publications [143,144]. To test whether intracellular iron chelation might unveil the stimulatory effect of miR-346 on APP expression in human fetal brain cultures, negative control and miR-346 mimics were transfected into primary human fetal brain cultures at DIV 19 under continuous Dfo co-treatment for 48 hours. APP expression following miR-346 delivery was significantly increased relative to negative control miRNA transfection (1.235±0.057 fold change; p=0.0122) (Figure 21E and F). Therefore, miR-346 delivery does stimulate APP expression in primary human fetal brain cultures, but the effect is only apparent after basal intracellular iron concentrations are reduced by chelation.

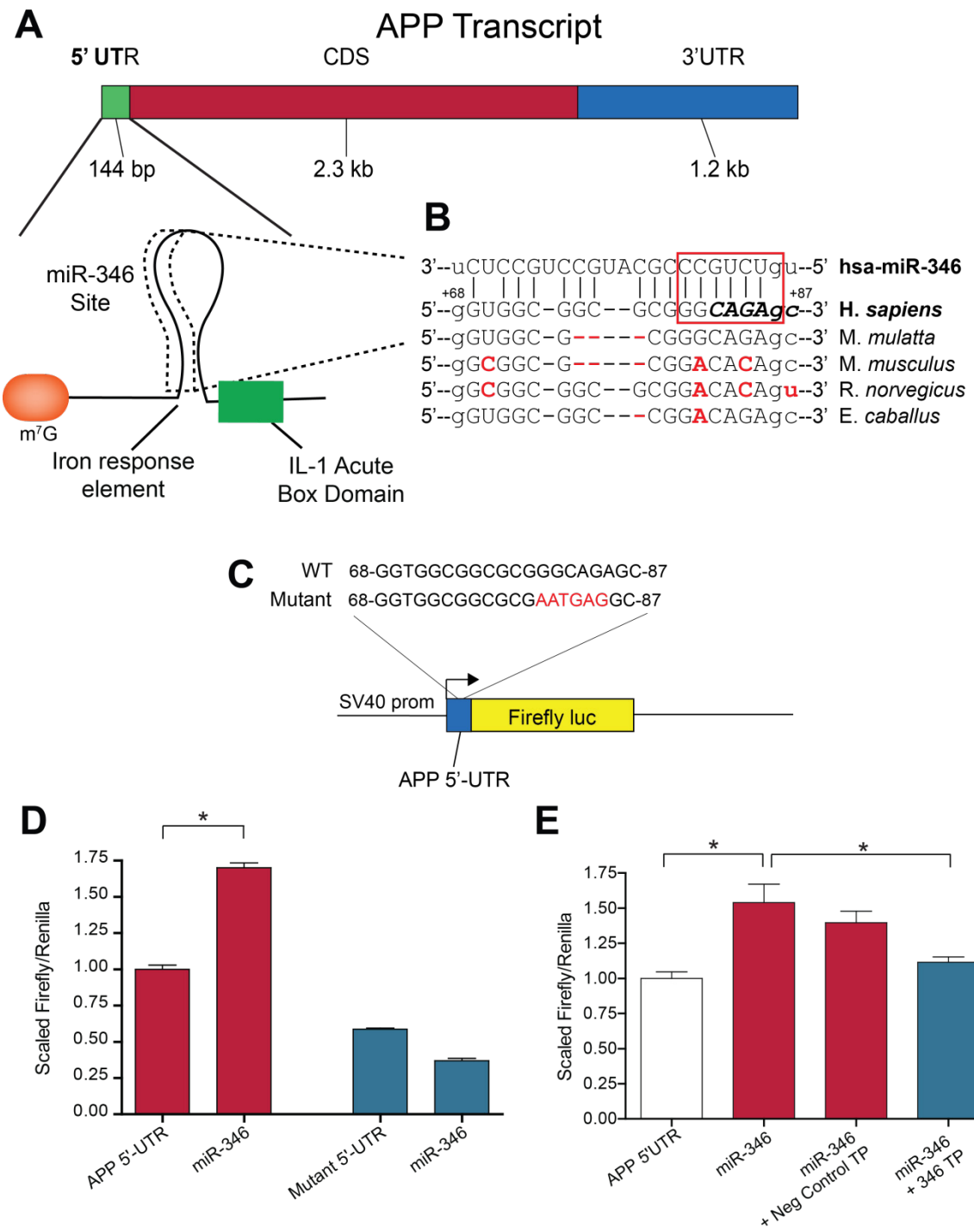

Figure 16: miR-346 targets human APP 5'-UTR via a target site overlapping a known IRE. (A) Schematic of the APP transcript demonstrating location of a putative miR-346 target site in the 5'-UTR directly overlapping with a known IRE stem-loop. The APP 5'-UTR was scanned using the miRanda algorithm on the RegRNA web server to

identify the putative miR-346 site. Dashed black rectangle encompasses approximate location of predicted miR-346 target site in known IRE stem-loop structure. (B) Sequence and predicted base-pairing of human miR-346 with its predicted target site in the human APP 5'-UTR, including the seed sequence interaction (red box). To assess site conservation, multiple genome alignments for mammalian species were pulled from the UCSC Genome Browser. Sequences from rhesus macaque, mouse, rat, and horse from positions orthologous to the predicted miR-346 target site in the human APP 5'-UTR are shown. Red text highlights nucleotide differences compared to the human sequence. Bold, italicized, black text in human APP 5'-UTR sequence represents functional IRE consensus sequence. (C) APP 5'-UTR reporter construct containing the APP 5'-UTR sequence inserted upstream of a firefly luciferase CDS was utilized to probe sequence specificity. The predicted target site in the 5'-UTR reporter construct was mutated by cassette mutagenesis. Red text highlights mutations introduced in seed sequence. (D) Wild-type and target site mutant reporter constructs were transfected into HeLa cells either alone or along with 50 nM miR-346 mimic. Luciferase expression was assessed 48 hours post-transfection and data presented as scaled Firefly/Renilla luminescence. (E) As a separate strategy to probe site specificity, the WT 5'-UTR APP reporter construct was co-transfected with miR-346 along with either 200 nM negative control target protector or putative miR-346-APP 5'-UTR target protector. Luciferase expression was assessed 48 hours post-transfection and data presented as scaled Firefly/Renilla luminescence. * $p<0.05$, $n=6$.

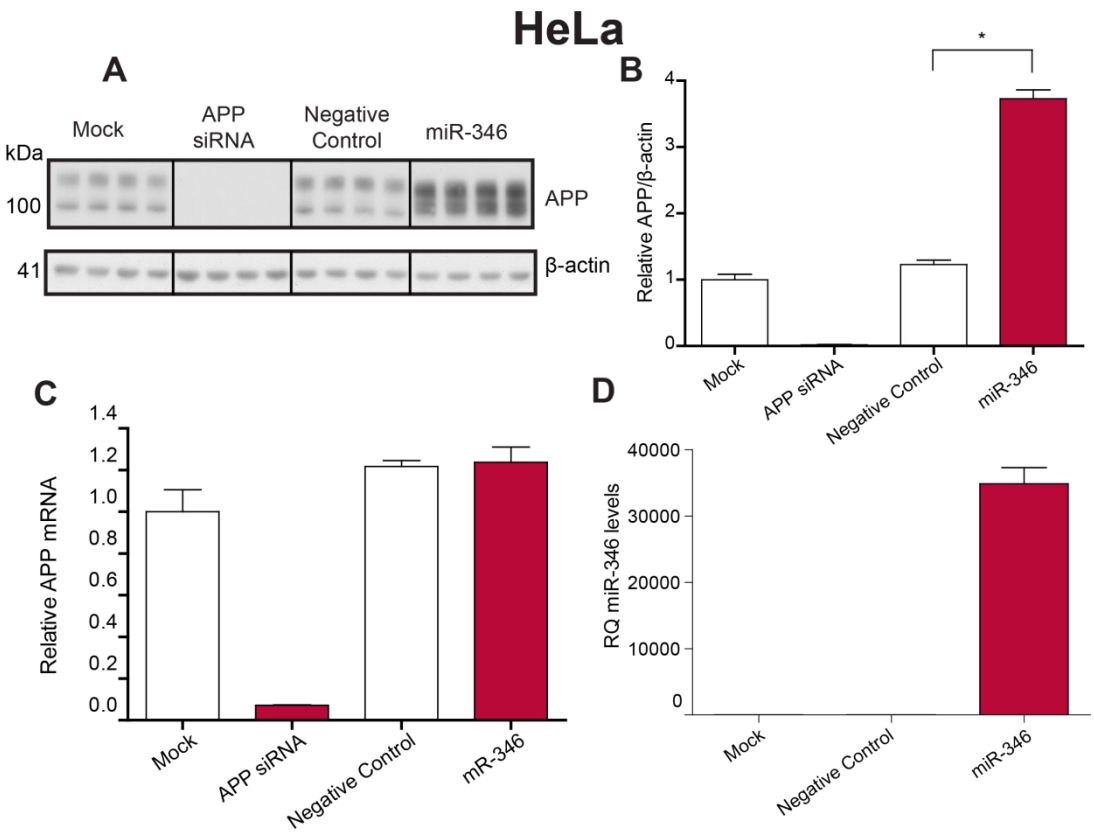

Figure 17: miR-346 delivery dramatically stimulates APP expression in HeLa cells. (A) HeLa cells were transfected with 50 nM miR-346 mimic or negative control and APP levels assayed 72 hours post-transfection by Western blot. siRNA (20 nM) transfection included as delivery control (n=4). (B) Blots were quantified by densitometric analysis and APP levels normalized to β-actin levels and scaled relative to mock transfection (n=4). (C) APP mRNA levels in HeLa cells were assayed by RT-qPCR 48 hours post-transfection (n=3). RT-qPCR expression levels were normalized to the geometric mean of β-actin, B2M, GAPDH and TBP expression levels and further scaled relative to mock-transfected levels. (D) Efficient delivery of miR-346 into HeLa cells confirmed by RT-qPCR 48 hours post-transfection (two technical replicates). RT-qPCR expression levels were normalized to the geometric mean of RNU48, RNU6B and hsa-miR-16 expression levels and further scaled relative to mock-transfected levels. RQ=relative quantity; * $p<0.05$ relative to negative control-transfected cells.

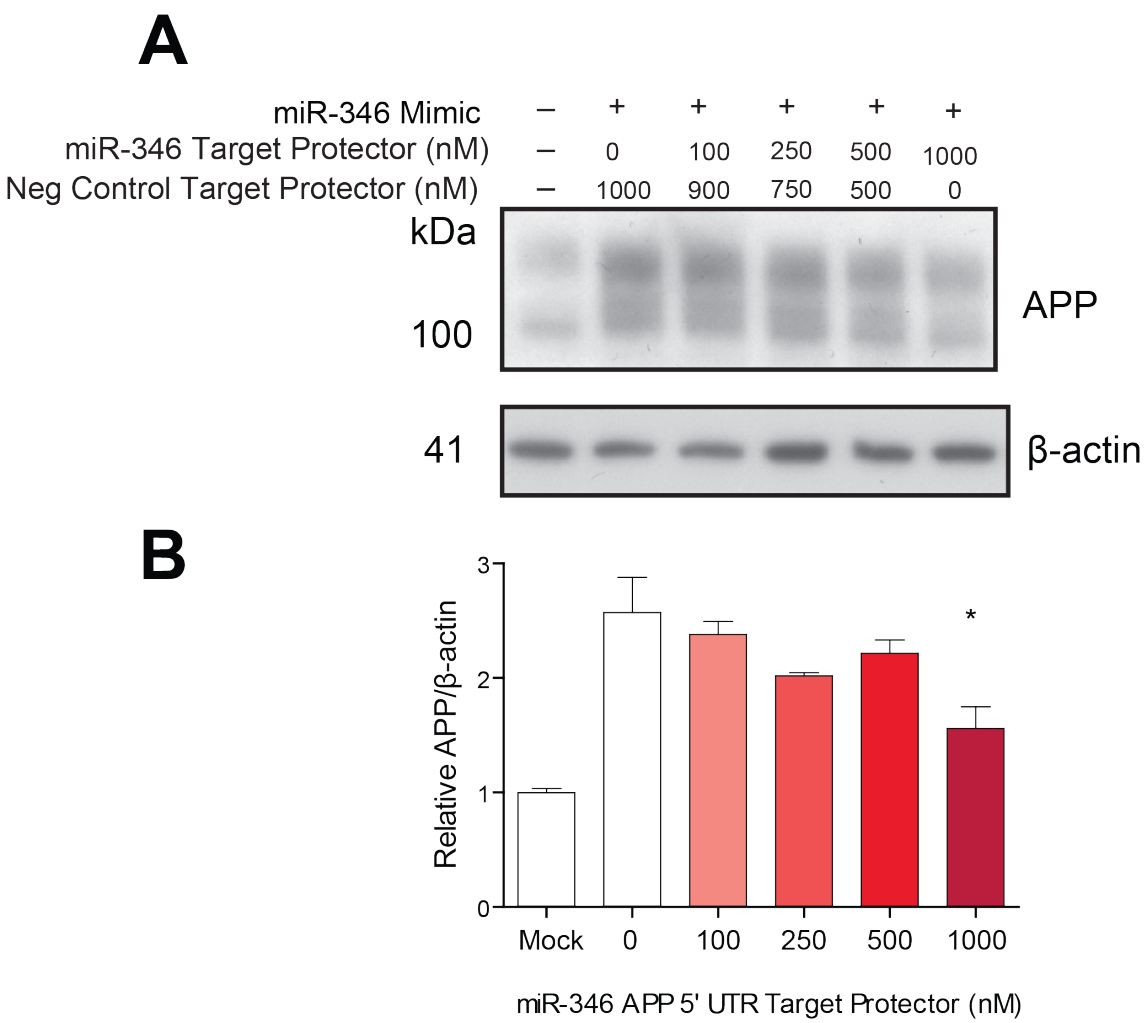

Figure 18: Induction of APP expression in HeLa by miR-346 delivery is reversed when interaction with the predicted target site in the APP 5'-UTR is blocked. HeLa cells were transfected with 15 nM miR-346 along with increasing concentrations of a target protector designed to protect the APP 5'-UTR miR-346 target site from interaction with miR-346. Total transfected nucleic acid concentration was held constant by adding adjusted amounts of negative control target protector. (A) APP levels were assayed 72 hours post-transfection by Western blot. (B) Blots were quantified by densitometric analysis and APP levels normalized to β-actin levels and scaled relative to mock transfection (n=4). *$p < 0.01$ relative to 0 nM miR-346 target protector.

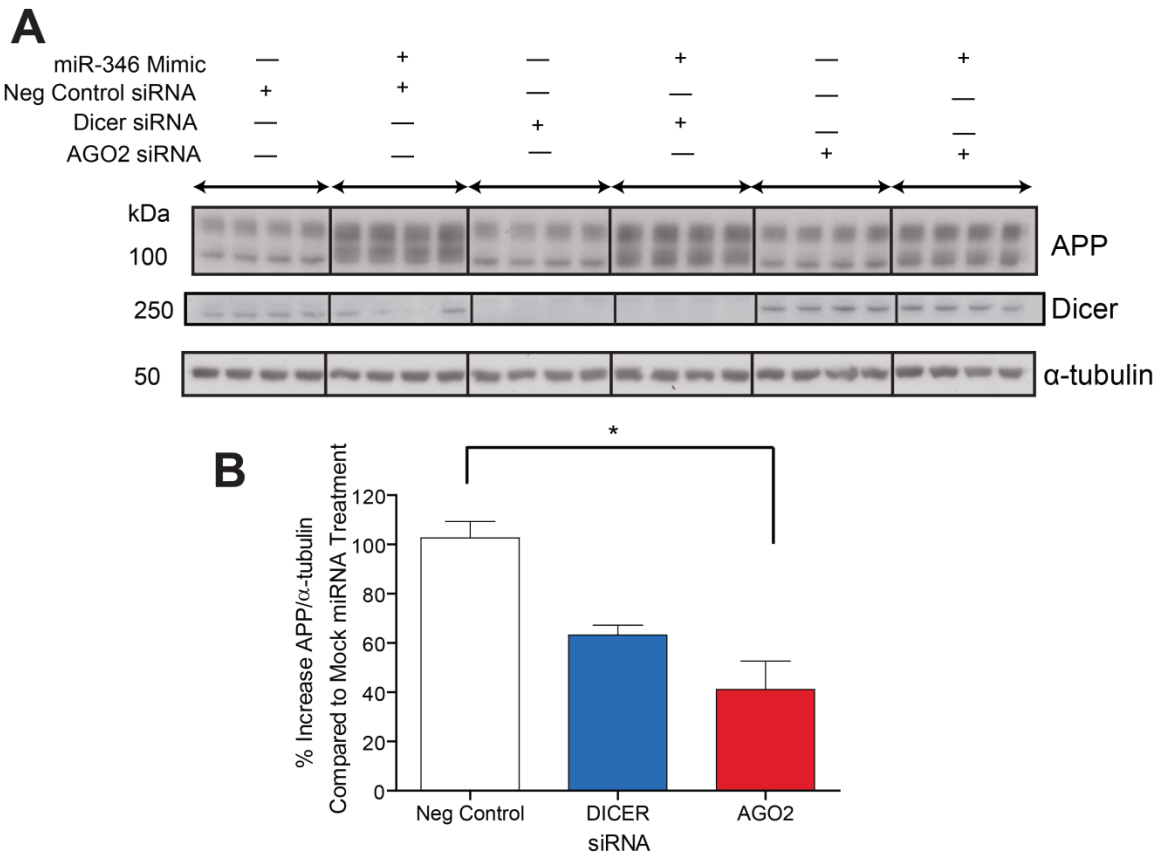

Figure 19: Knockdown of Dicer and AGO2 attenuates the stimulatory effect of miR-346 on APP expression. HeLa cells were co-transfected with or without miR-346 mimic along with either negative control siRNA, Dicer siRNA or AGO2 siRNA. (A) APP levels were assayed 72 hours post-transfection by Western blot. (B) Blots were quantified by densitometric analysis and APP levels normalized to β-actin levels. Percent increase was then calculated by subtracting the average signal of each mock condition (without miR-346) from the miR-346-transfected signal for each siRNA transfection group and then scaling as percent increase relative to the mock condition.

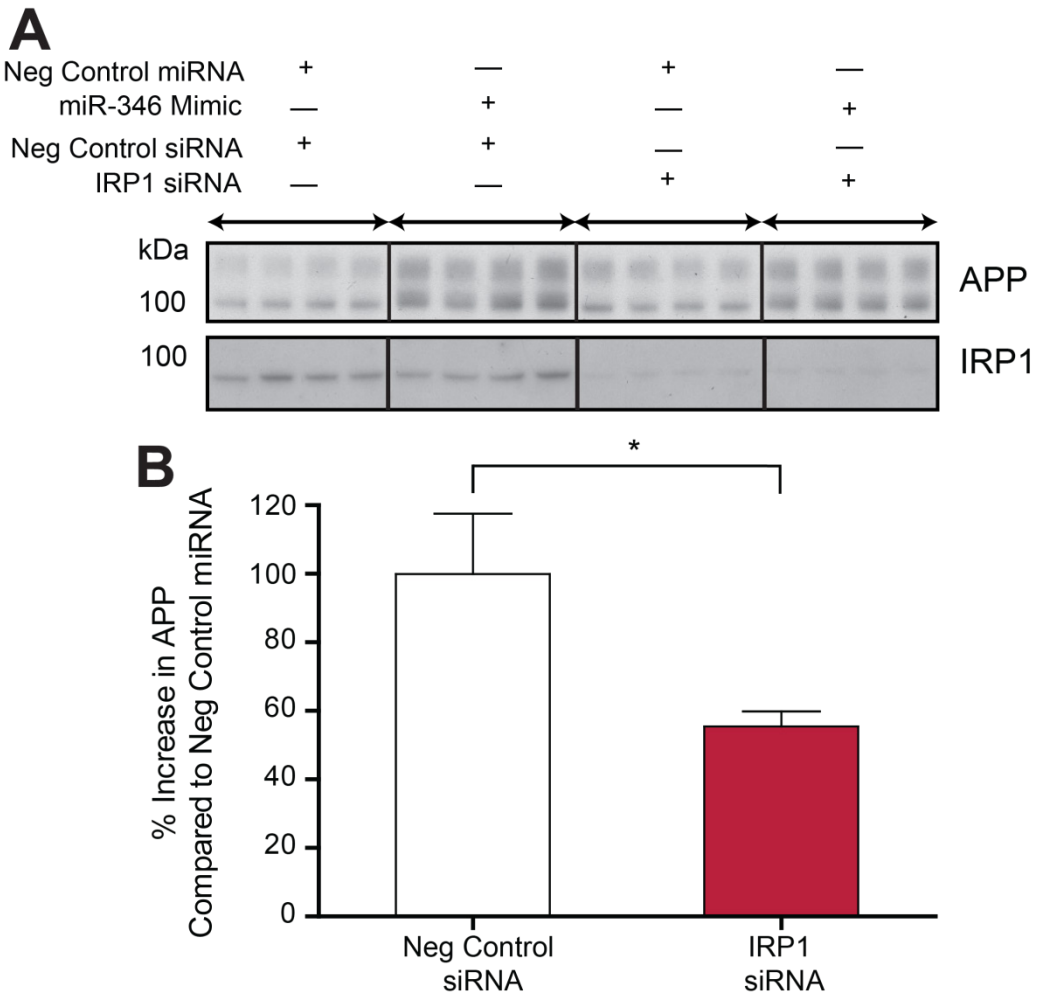

Figure 20: Knockdown of IRP1 attenuates the stimulatory effect of miR-346 on APP expression. HeLa cells were co-transfected with negative control miRNA mimic or miR-346 mimic along with either negative control siRNA or IRP1 siRNA. (A) APP levels were assayed 48 hours post-transfection by Western blot. (B) Blots were quantified by densitometric analysis. Percent increase was calculated by subtracting the average signal of the negative control mimic transfections from the miR-346-transfected signal for both siRNA transfection groups and then scaling as percent increase relative to the negative control mimic condition.

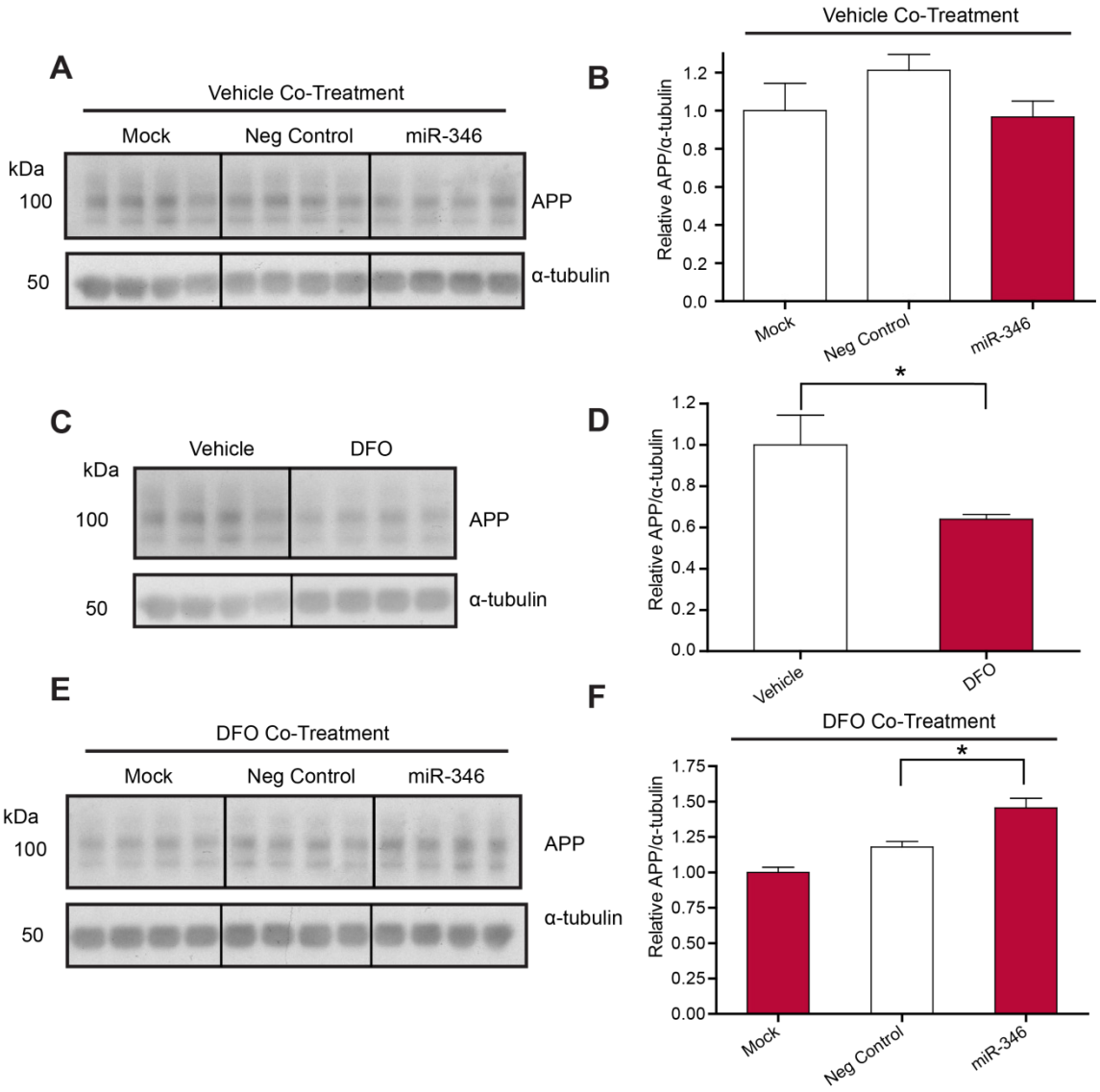

Figure 21: Stimulatory effect of miR-346 on APP expression in human fetal brain cultures only apparent after iron chelation. Human fetal brain cultures were transfected with negative control mimic or miR-346 mimic either in the presence of vehicle (A) or presence of 150 μM DFO (E). Vehice and DFO treatments were also compared in mock-transfected cells (C). APP levels were assayed 48 hours post-transfection by Western blot. (B, D, F) Blots were quantified by densitometric analysis and APP levels normalized to β-actin levels.

II. Aim 2: Identify miRNA that endogenously regulate BACE1 expression

A. Global knockdown of miRNA function elevates BACE1 expression

A similar strategy to that used in the APP-focused studies described above was employed for investigating miRNA regulatory effects on BACE1 expression. To begin, the effect of inhibiting global miRNA function on BACE1 levels was tested in cultured human fetal brain cells. Human fetal brain cultures were either mock transfected or transfected with a negative control or AGO2-specific siRNA at DIV 18. Cultures were harvested 48 hours post-transfection (DIV 20) and BACE1 expression assayed by Western blot. BACE1 levels were significantly elevated following knockdown of AGO2 as compared to negative control siRNA transfection (1.318±0.051 fold change; $p=0.043$ by two-tailed Student's t-test) (Figure 22A and B). As with APP expression, this suggests that the global complement of miRNA act to basally inhibit BACE1 expression in cultured human brain cells.

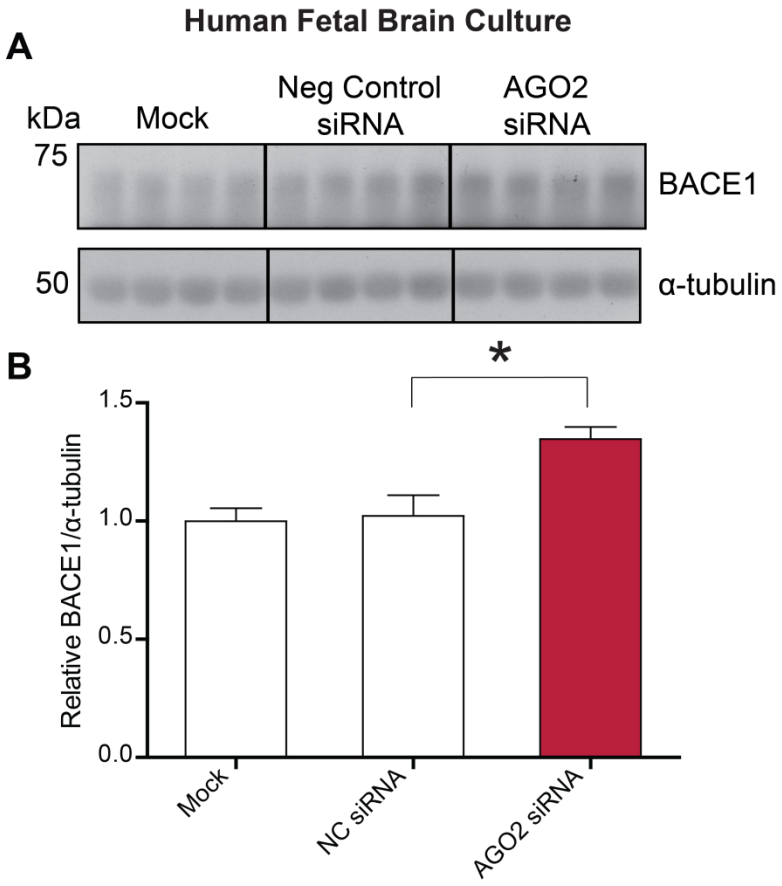

Figure 22: Knockdown of miRNA effector protein AGO2 enhances expression of BACE1 in primary human fetal brain cultures. The effect of disrupting global miRNA functionality on BACE1 expression in primary human fetal brain cultures was assessed by using siRNA-mediated knockdown of AGO2. Cultures were transfected at DIV 17 and lysates prepared 48 hours post-transfection (DIV 19). (A) Levels of BACE1 and β-actin were assayed by Western blot. (B) Blots were quantified by densitometric analysis and BACE1 levels normalized to β-actin levels and scaled relative to negative control transfection. BACE1 levels were significantly increased in primary human fetal brain cultures transfected with an AGO2 siRNA as compared to transfection with a negative control siRNA (n=4). BACE1 siRNA reduced BACE1 expression confirming partial delivery of siRNA in these cultures. * p=0.048 by one-tailed Student's t-test.

B. Bioinformatic analysis of putative miRNA targets in BACE1 3'-UTR

To identify novel miRNA target sites in the human BACE1 3'-UTR, the same set of web-based bioinformatics algorithms described in APP-focused studies above and summarized in Table 7 were used to predict favorable miRNA interactions. miRNA target site predictions in the BACE1 3'-UTR were extracted from the predictor outputs. Criteria for selecting a given miRNA:target site interaction included relatively high predictor score and known brain expression. Preference was also given to miRNA-target interactions predicted across multiple algorithmic platforms. Table 10 summarizes the identity of the predicted targeting miRNA and the location of the predicted target site in relation to the human BACE1 3'-UTR, along with the various predictor scores computed for each given target site interaction. Two distinct target sites were predicted for miR-29a/b, miR-570, miR-133a/b and miR-339-5p by multiple algorithms.

Table 10: Selected BACE1 3'-UTR miRNA target site predictions and scores

	Computational Predictor Scores						
miRNA	Target Scan[a]	PicTar[b]	DIANA-microT v4[c]	miRanda miRSVR[d]	PITA[e]	rna22[f]	Target Site[g]
miR-107	***	6.16	0.307	***	***	-26.2	267-273
miR-29a[h]	-0.07	2.46	0.281	***	***	-26.2	1052-1058
	-0.07	2.46	0.234	***	***	***	1793-1799
miR-29b[h]	-0.02	3.97	0.281	***	***	***	1052-1058
	-0.02	3.97	0.234	***	***	-30.4	1793-1799
miR-298	***	***	***	***	***	-27.8	466-471
miR-328	***	***	***	***	***	-30.6	91-96
miR-570[h]	-0.18	***	***	***	***	***	720-727
	-0.14	***	***	***	***	***	729-735
miR-339-5p[h]	-0.37	***	***	-0.2873	-5.2	-31.8	484-491
	-0.34	***	0.177	-0.6294	***	-33.6	611-618
miR-133a[h]	-0.06	***	***	***	***	***	755-761
	-0.02	***	***	***	-6.58	-38.8	1500-1506
miR-133b[h]	-0.06	***	***	***	***	***	755-761
	-0.02	***	***	***	-6.58	-38.8	1500-1506
miR-769-3p	-0.08	***	***	***	***	-28.7	3423-3429

Reported scores: [a]context+ score, [b]PicTar score, [c]Site score, [d]mirSVR score, [e]ddG score, [f]folding energy in kCal/mol, M=14, G=0, E=-20 Kcal/mol; [g]Target site position relative to start of BACE1 3'-UTR; [h]Two distinct target sites are predicted in the BACE1 3'-UTR; *** = target site not predicted by algorithm

C. Reporter validation of putative miRNA targets in BACE1 3'-UTR

The BACE1 mRNA consists of a 460 bp 5'-UTR, 1.5 kb coding sequence (CDS) and 3.9 kb 3'-UTR (Figure 23A). To screen for functional miRNA interactions, a reporter construct was prepared containing the full length BACE1 3'-UTR. This reporter was generated by PCR amplifying the BACE1 3'-UTR from human genomic DNA and inserting the amplicon downstream of the Renilla luciferase CDS in the psiCHECK-2 vector. This reporter has an identical arrangement to the APP 3'-UTR reporter used in aim 1 and is schematically illustrated in Figure 23B.

The regulatory influence of the BACE1 3'-UTR on basal reporter expression was tested prior to screening for functional miRNA interactions. HeLa, SK-N-SH and differentiated NT2 neurons were transfected with either the empty psiCHECK-2 vector or the BACE1 3'-UTR reporter vector (Figure 23C). The presence of the BACE1 3'-UTR significantly repressed reporter expression in HeLa cells (0.391±0.009 fold change compared to empty; p=0.0001 by Student's t-test), SK-N-SH cells (0.251±0.091 fold change compared to empty; p=0.0002 by Student's t-test) and differentiated NT2 neurons (0.425±0.067 fold change compared to empty; p=0.0176 by Student's t-test) (Figure 23C). These data suggest that under basal transfection conditions the BACE1 3'-UTR contains inhibitory response elements, completely consistent with the presence of possible inhibitory MRE.

To validate the functionality of putative miRNA:BACE1 3'-UTR interactions as predicted by the various algorithms, HeLa cells were co-transfected with both the BACE1 3'-UTR reporter construct and miRNA mimics listed in Table 10 (Figure 24). Negative control and positive control co-transfections were performed identically to the experiment previously discussed in Figure 6. Forty eight hours post-transfection, reporter expression was determined using a dual luciferase reporter assay. Reporter

expression values were calculated as normalized ratios of Renilla-to-firefly luciferase activity.

Co-transfection of miR-339-5p, miR-29a, miR-29b, miR-570, miR-133a, miR-133b and miR-769-3p with the BACE1 3'-UTR reporter construct all resulted in significantly reduced reporter expression compared to co-transfection with negative control miRNA mimic (fold change in comparison to negative control miRNA transfection: miR-339-5p, 0.551±0.021 fold; miR-29a, 0.880±0.038 fold; miR-29b, 0.575±0.036; miR-570, 0.717±0.027 fold; miR-133a, 0.803 ± 0.044 fold, miR-133b, 0.793 ± 0.023 fold, miR-769-3p, 0.816 ± 0.030 fold; $p<0.05$ in all cases as determined by post-hoc Dunnett's t-test). Data in Figure 24 are presented as RRR to control for plate-to-plate variation as previously described in the discussion for Figure 6.

Co-transfection with miR-29a/b both produced inhibitory effects on reporter expression. Importantly, this regulatory interaction has been independently validated [189], highlighting the reproducibility and validity of the reporter assessment. The strongest inhibitory effect on reporter expression was observed following co-transfection with miR-339-5p. Therefore, follow-up experiments from this set of miRNA were restricted to 339-5p.

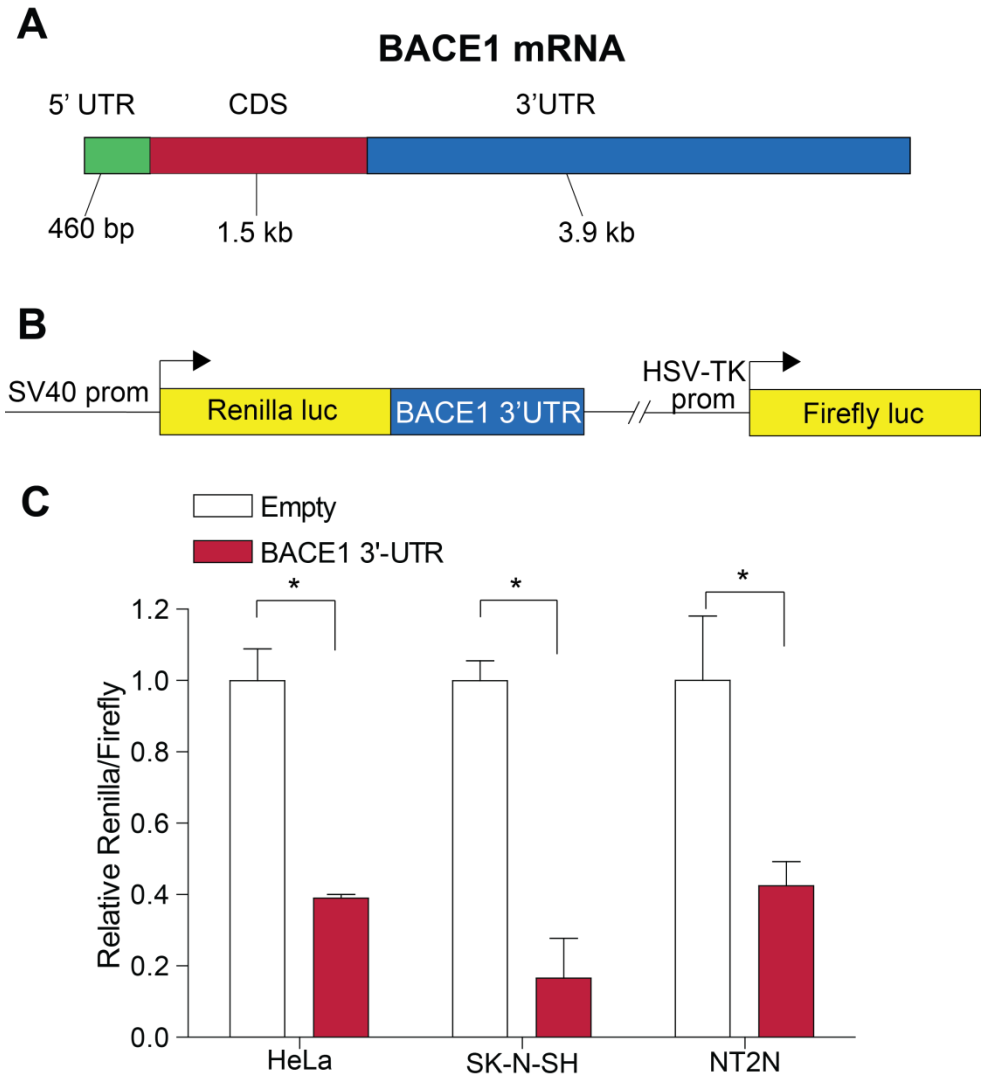

Figure 23: BACE1 3'-UTR inhibits basal reporter expression across multiple human cell types. (A) Schematic of the BACE1 mRNA demonstrating sizes of the 5'-UTR, coding sequence (CDS) and 3'-UTR. (B) Schematic of the reporter constructs used to validate putative miRNA target sites in the BACE1 3'-UTR. The BACE1 3'-UTR was PCR amplified from human genomic DNA and inserted into the psiCHECK-2 vector downstream of the Renilla luciferase (luc) CDS. The positive control construct was the same as in Figure 3B. (C) The regulatory effect of the BACE1 3'-UTR on reporter expression was tested by transfecting either the empty psiCHECK-2 vector or vector

containing the BACE1 3'-UTR into HeLa, SK-N-SH or differentiated NT2 neuronal cells and assaying basal reporter expression. Assay values are reported as the ratio of Renilla to luciferase luminescence scaled relative to empty vector (n=5; *p<0.05).

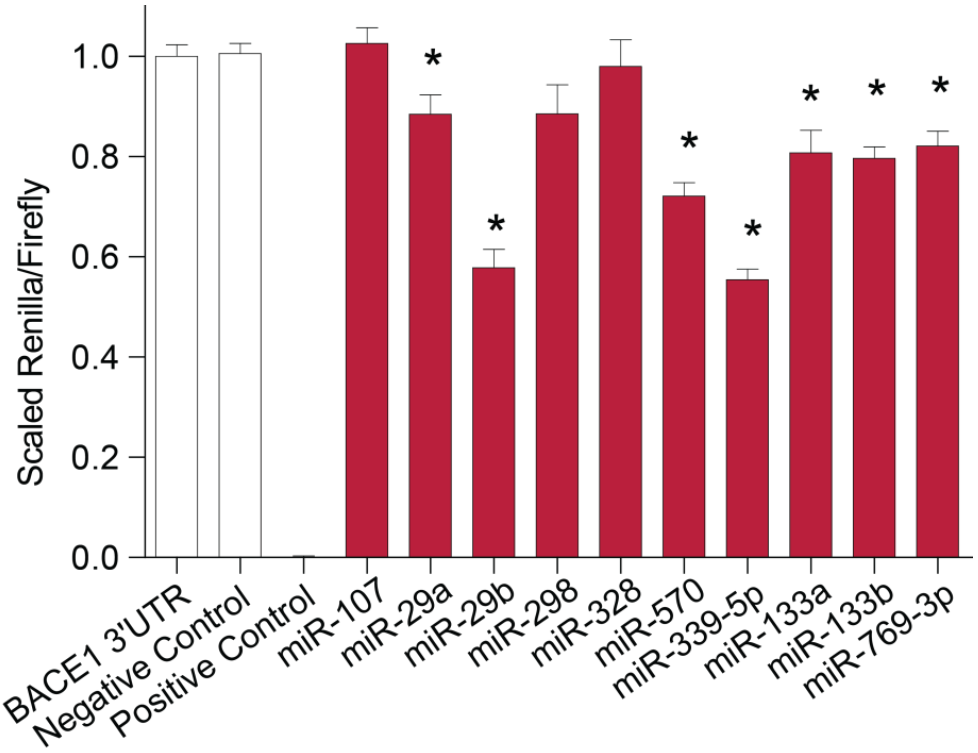

Figure 24: Multiple miRNA modulate BACE1 3'-UTR reporter expression levels in HeLa cells. The BACE1 3'-UTR reporter construct and miRNA mimics (40 nM) were co-transfected into HeLa cells. Renilla and firefly luciferase activity were assayed 48 hours post-transfection. Data are presented as scaled relative response ratios of Renilla to firefly luciferase (n=5; *p<0.05).

D. miR-339-5p negatively regulates BACE1 expression

miR-339-5p has two predicted target sites in the BACE1 3'-UTR as predicted by TargetScan, miRanda-miRSVR, and rna22. Approximate locations of the predicted target sites in the BACE1 transcript are schematically illustrated in Figure 25A. The predicted interaction of each target site in the human BACE1 3'-UTR with miR-339-5p are indicated in Figure 25B, along with a limited mammalian multiple sequence alignment. Both sites are considered poorly conserved according to the conserved branch length metric employed in TargetScan (0.212 for miR-339-5p site 1 and 0.595 for miR-339-5p site 2). This suggests a lack of evolutionary pressure to maintain sequence identity at these two sites. Therefore, if a physiologically relevant interaction exists at either of these sites, the interaction may be an evolutionarily new phenomenon.

To confirm that the inhibitory effect of miR-339-5p on BACE1 3'-UTR reporter expression was mediated specifically via one of two predicted miR-339-5p target sites located in the BACE1 3'-UTR, mutations were introduced separately in the seed sequences of both target sites in the reporter construct (Figure 25C). A double mutant reporter was also constructed containing both target site mutations. These mutant reporter constructs were then co-transfected along with miR-339-5p mimic into HeLa cells and reporter expression compared to wild-type reporter (Figure 25D). This reporter assay replicated the original finding, demonstrating reduced reporter expression when the wild-type reporter was co-transfected with miR-339-5p as compared to co-transfection with negative control miRNA (0.53±0.025 fold change; $p<0.0001$ by two-tailed Student's t-test). Due to technical issues with the site 1 mutant clone, the effect of miR-339-5p co-transfection on reporter expression could not be determined. Mutation of site 2 partially eliminated the inhibitory effect of miR-339-5p mimic on reporter expression (0.731±0.011 fold change compared to negative control reporter; $p=0.0001$

by two-tailed Student's t-test), whereas mutation of both sites completely reversed the miR-339-5p response (p=0.2192 by Student's t-test). Therefore, miR-339-5p most likely regulates reporter expression by interacting with two distinct target sites in the BACE1 3'-UTR.

The next step was to directly examine whether miR-339-5p reduces endogenous BACE1 levels. BACE1 expression is so low in HeLa that it is not readily detectable by Western blot using 3D5 antibody. It is readily detected in U373 and primary human fetal brain cultures. Therefore, miR-339-5p mimic was transfected into both U373 cells (Figure 26A and B) and human fetal brain cultures at DIV 17 (Figure 26C and D). U373 cells were also transfected with miR-29b as a positive control transfection. miR-29b has been previously shown to downregulate endogenous BACE1 protein expression [189]. BACE1 protein levels were then directly assayed by Western blot. BACE1 expression in U373 cells was significantly reduced following transfection with both miR-29b (0.125±0.013 fold change; $p<0.01$ by post-hoc Dunnett's t-test) and miR-339-5p (0.373±0.038 fold change; $p<0.01$ by post-hoc Dunnett's t-test) as compared to transfection with negative control miRNA mimic. Similarly, BACE1 protein levels were significantly reduced following transfection with miR-339-5p in human fetal brain cultures as compared to transfection with negative control miRNA mimic (0.873±0.019 fold change; p=0.0381 by two-tailed Student's t-test). Therefore, endogenous BACE1 levels are inhibited by miR-339-5p delivery in human U373 and primary fetal brain cells.

To establish whether endogenous miR-339-5p regulates BACE1 expression by interacting with the two reporter-validated target sites in human fetal brain cells, two separate custom target protectors were utilized to block the interaction of miR-339-5p with each validated BACE1 3'-UTR target site. Primary human fetal brain cultures were transfected with miR-339-5p target protectors at DIV 17 and BACE1 expression

assayed by Western blot 48 hours post-transfection. Transfection of miR-339-5p site 1 target protector elevated BACE1 expression, but the increase was not statistically significant compared to transfection with negative control target protector (1.351±0.139 fold change). Transfection of miR-339-5p site 2 target protector significantly elevated BACE1 expression compared to transfection with negative control target protector (1.499±0.101 fold change) (Figure 27). Therefore, endogenous miR-339-5p actively inhibits BACE1 expression in human fetal brain cultures under physiological culture conditions and does so by potentially interacting with site 1 and definitely interacting with site 2 in the BACE1 3'-UTR. Of note is that site 2, though itself poorly conserved by TargetScan standards, exhibits a higher level of cross-species conservation than does site 1. Therefore, the reduced efficacy of the site 1 target protector in modulating BACE1 expression and the lower level of site 1 cross-species conservation may suggest that this site is less physiological relevant than site 2.

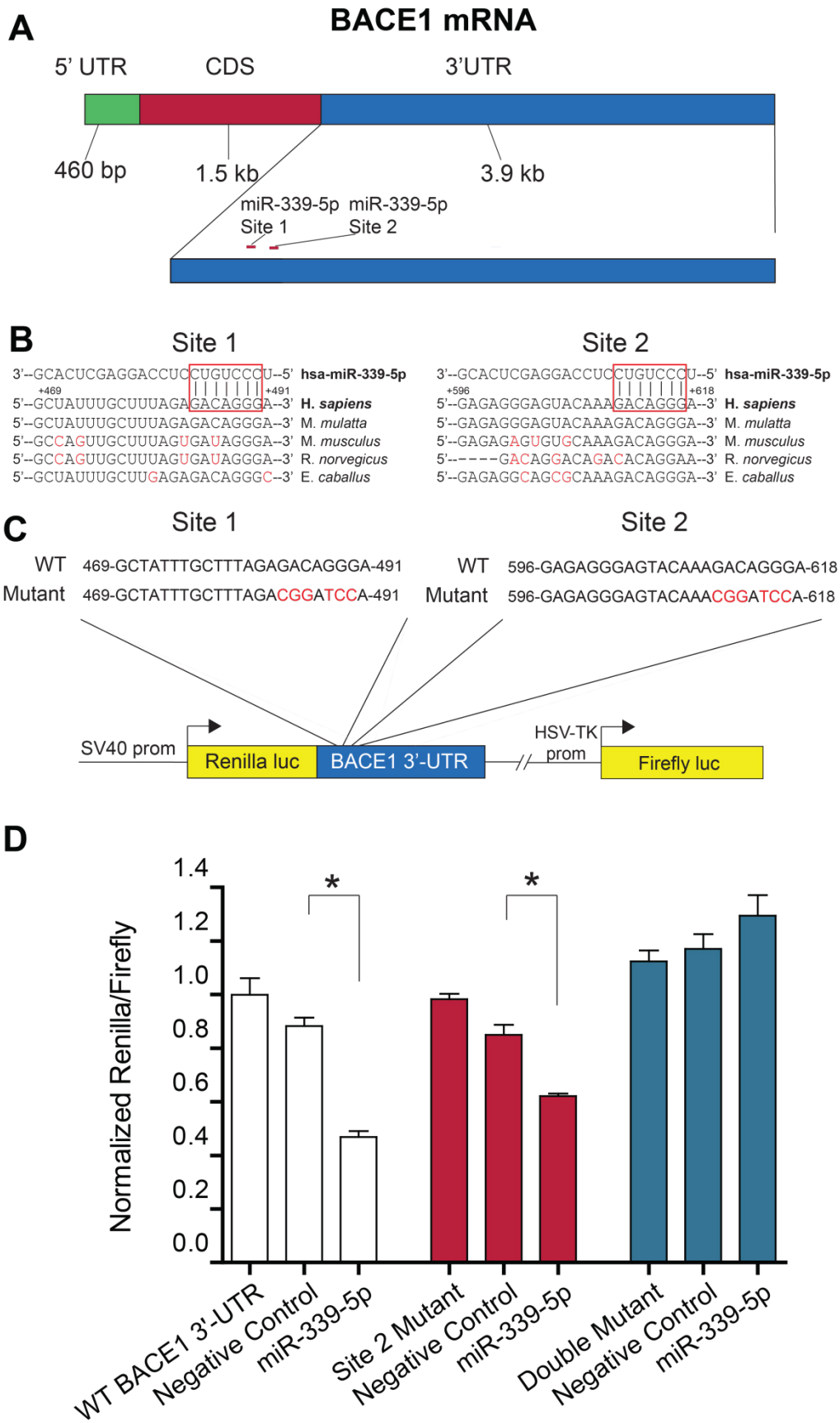
A
BACE1 mRNA
5' UTR
CDS
3'UTR
460 bp
1.5 kb
3.9 kb
miR-339-5p Site 1
miR-339-5p Site 2
B
Site 1
3'--GCACUCGAGGACCUCCUGUCCCU--5' hsa-miR-339-5p
+469 +491
5'--GCUAUUUGCUUUAGAGACAGGGA--3' H. sapiens
5'--GCUAUUUGCUUUAGAGACAGGGA--3' M. mulatta
5'--GCCAGUUGCUUUAGUGAUAGGGA--3' M. musculus
5'--GCCAGUUGCUUUAGUGAUAGGGA--3' R. norvegicus
5'--GCUAUUUGCUUGAGAGACAGGGC--3' E. caballus
Site 2
3'--GCACUCGAGGACCUCCUGUCCCU--5' hsa-miR-339-5p
+596 +618
5'--GAGAGGGAGUACAAAGACAGGGA--3' H. sapiens
5'--GAGAGGGAGUACAAAGACAGGGA--3' M. mulatta
5'--GAGAGAGUGUGCAAAGACAGGGA--3' M. musculus
5'-----GACAGGACAGACACAGGAA--3' R. norvegicus
5'--GAGAGGCAGCGCAAAGACAGGGA--3' E. caballus
C
Site 1
WT 469-GCTATTTGCTTTAGAGACAGGGA-491
Mutant 469-GCTATTTGCTTTAGACGGATCCA-491
Site 2
WT 596-GAGAGGGAGTACAAAGACAGGGA-618
Mutant 596-GAGAGGGAGTACAAACGGATCCA-618
SV40 prom
Renilla luc
BACE1 3'-UTR
HSV-TK prom
Firefly luc
D
Normalized Renilla/Firefly
1.4
1.2
1.0
0.8
0.6
0.4
0.2
0.0
*
*
WT BACE1 3'-UTR
Negative Control
miR-339-5p
Site 2 Mutant
Negative Control
miR-339-5p
Double Mutant
Negative Control
miR-339-5p

Figure 25: miR-339-5p targets human BACE1 3'-UTR via poorly conserved sites. (A) Schematic of the BACE1 transcript demonstrating location of two putative miR-339-5p target sites in the 3'-UTR predicted by the TargetScan, rna22, miRanda-mirSVR, and PITA algorithms. (B) Sequence and predicted base-pairing of human miR-339-5p with its two predicted target sites in the human BACE1 3'-UTR, including the seed sequence interactions (red boxes). To assess site conservation, multiple genome alignments for mammalian species were pulled from TargetScan. Sequences from rhesus macaque, mouse, rat, and horse from positions orthologous to the predicted miR-339-5p target sites in the human BACE1 3'-UTR are shown. Red text highlights nucleotide differences compared to the human sequence. (C) The predicted target sites in the BACE1 3'-UTR reporter construct were mutated by site-directed mutagenesis. A double mutant containing both mutations was also constructed. Red text highlights mutations introduced in seed sequence. (D) Wild-type and target site mutant reporter constructs were transfected into HeLa cells either alone or along with 50 nM negative control and miR-339-5p mimic. Luciferase expression was assessed 48 hours post-transfection. * $p<0.0005$, $n=5$.

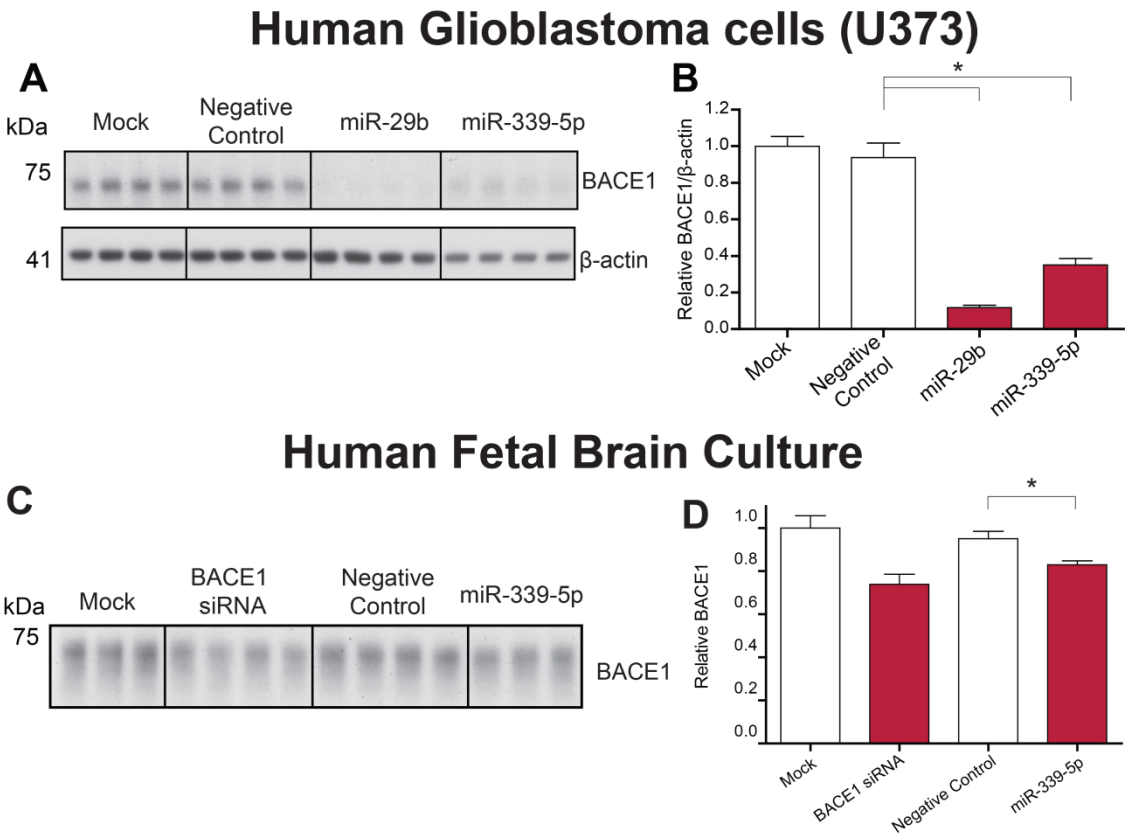

Figure 26: miR-339-5p delivery downregulates BACE1 expression in U373 cells and primary human fetal brain cultures. (A) U373 cells were transfected with 150 nM miR-29b (positive control) and miR-339-5p mimic or negative control and BACE1 levels assayed 72 hours post-transfection by Western blot (n=4). (B) Blots from panel (A) were quantified by densitometric analysis and BACE1 levels normalized to β-actin levels and scaled relative to mock transfection. (C) Primary human fetal brain cultures were transfected with 150 nM miR-339-5p mimic or negative control at DIV 17 and lysates prepared 48 hours post-transfection (DIV 19). siRNA (20 nM) transfection included as delivery control. Levels of BACE1 were assayed by Western blot. (D) Blots from panel (C) were quantified by densitometric analysis and BACE1 levels scaled relative to mock transfection (n=3 – 4). * $p<0.05$

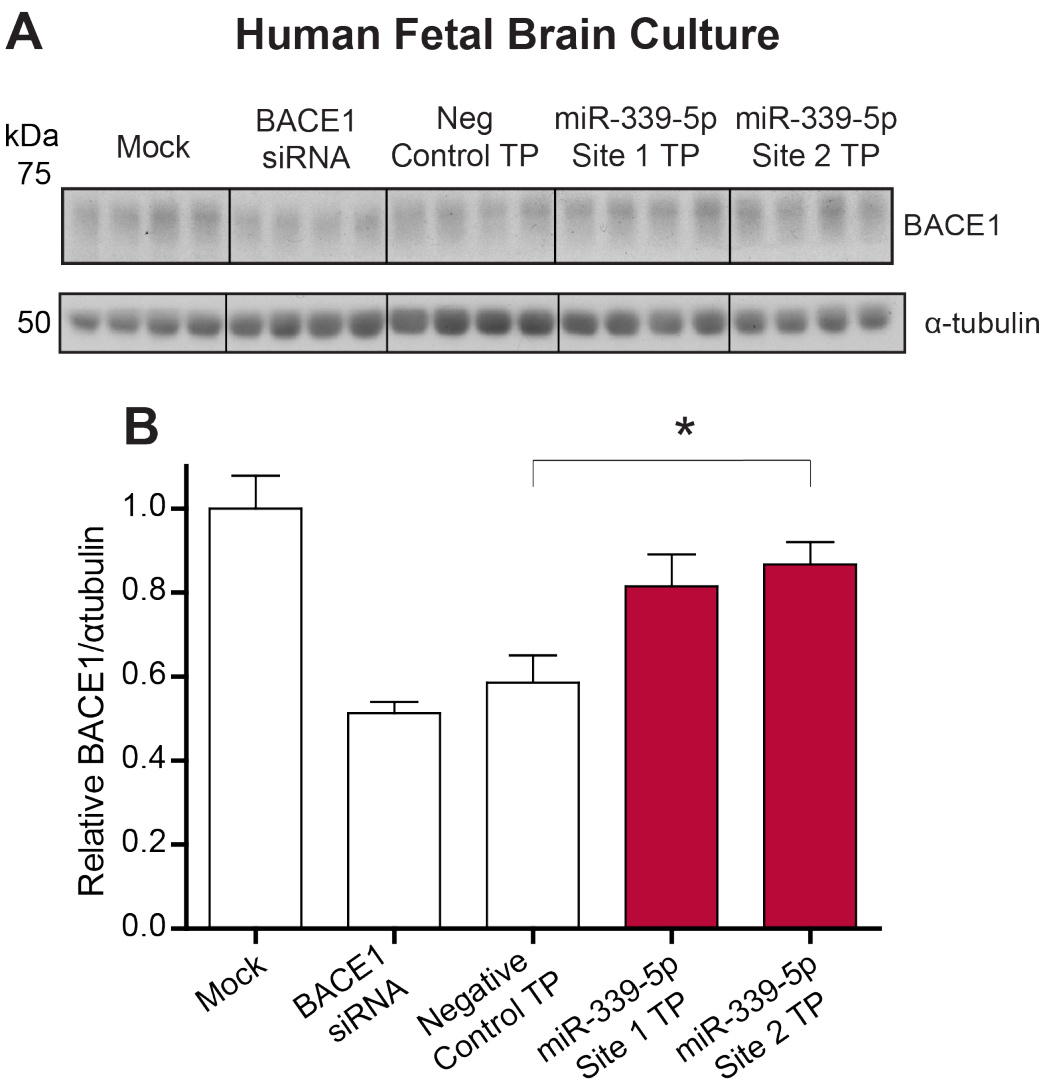

Figure 27: Blocking miR-339-5p interaction individually with each of two predicted target sites in the BACE1 mRNA 3'-UTR elevates basal BACE1 protein levels. (A) Western blot analysis of BACE1 and α-tubulin levels in transfected primary human fetal brain cultures. Primary human fetal brain cultures at DIV 17 were either mock-transfected or transfected with 1000 nM negative control target protector or custom-designed target protectors designed to inhibit interaction of miR-339-5p specifically with predicted site 1 or site 2 in the BACE1 mRNA 3'-UTR. BACE1 siRNA (20 nM) transfection was included as a delivery control. Cell lysates for proteins were

prepared 48 h post-transfecton. (B) Densitometric analysis of blots from panel A. * $p<0.05$; n=4. TP = target protector.

III. Aim 3: Investigate the relevance of identified miRNA in normal physiology and in pathophysiology of Alzheimer disease

A. Expression analysis of miRNA and protein targets in primary human fetal mixed brain cultures suggest co-regulation

One characteristic of a physiologically relevant miRNA:mRNA regulatory relationship is concordant changes in miRNA and protein expression during a cellular response. Therefore, the next question addressed was whether APP and its targeting miRNA identified in aims 1 and 2 are co-regulated during the maturation of a primary human fetal brain culture. Mixed brain cultures were established from the brain parenchyma of aborted fetuses as previously described. Cultures were maintained for 7, 10, 14, 18, 22 and 26 DIV before harvest.

The analysis compared APP protein levels and miR-153 and miR-346 levels as measured from the same sample by Western blot and RT-qPCR, respectively. miR-101 expression analysis was not completed in this experimentdue to technical complications. APP expression was significantly higher at DIV 7 as compared to all other time points and then rapidly plateaued with lowest expression levels observed at DIV 18 ($p<0.01$ for DIV7 compared to all time points by post-hoc Tukey's HSD test) (Figure 28A and B). Interestingly, miR-153 had a somewhat inverse expression pattern, with highest expression levels at DIV 18, though no differences in expression were statistically significant (Figure 28C). Correlation analysis of miR-153 levels versus APP levels revealed no significant correlation ($p=0.4112$), though linear regression produced a (non-significant) slope consistent with inverse expression patterns (Figure 28D). miR-346 exhibited an expression pattern similar to that exhibited by APP with highest expression at DIV 7 that plateaued with lower expression levels at DIV ($p<0.01$ for DIV 7 as compared to DIV 14, 18, 22 and 26 by post-hoc Tukey's HSD test) (Figure 28E).

Correlation analysis revealed significant positive correlation between miR-346 levels and APP levels ($p=0.001$) (Figure 28F). Linear regression also produced a significant non-zero slope consistent with increasing APP levels as a function of increasing miR-346 levels. These data demonstrate that, in maturing human fetal mixed brain cultures, both miR-153 and miR-346 exhibit expression patterns that are perfectly concordant with their anticipated regulatory effect on APP expression. Therefore, it is reasonable to speculate that the regulatory effect of miR-153 and miR-346 may contribute to the pattern of APP expression observed in this culture system.

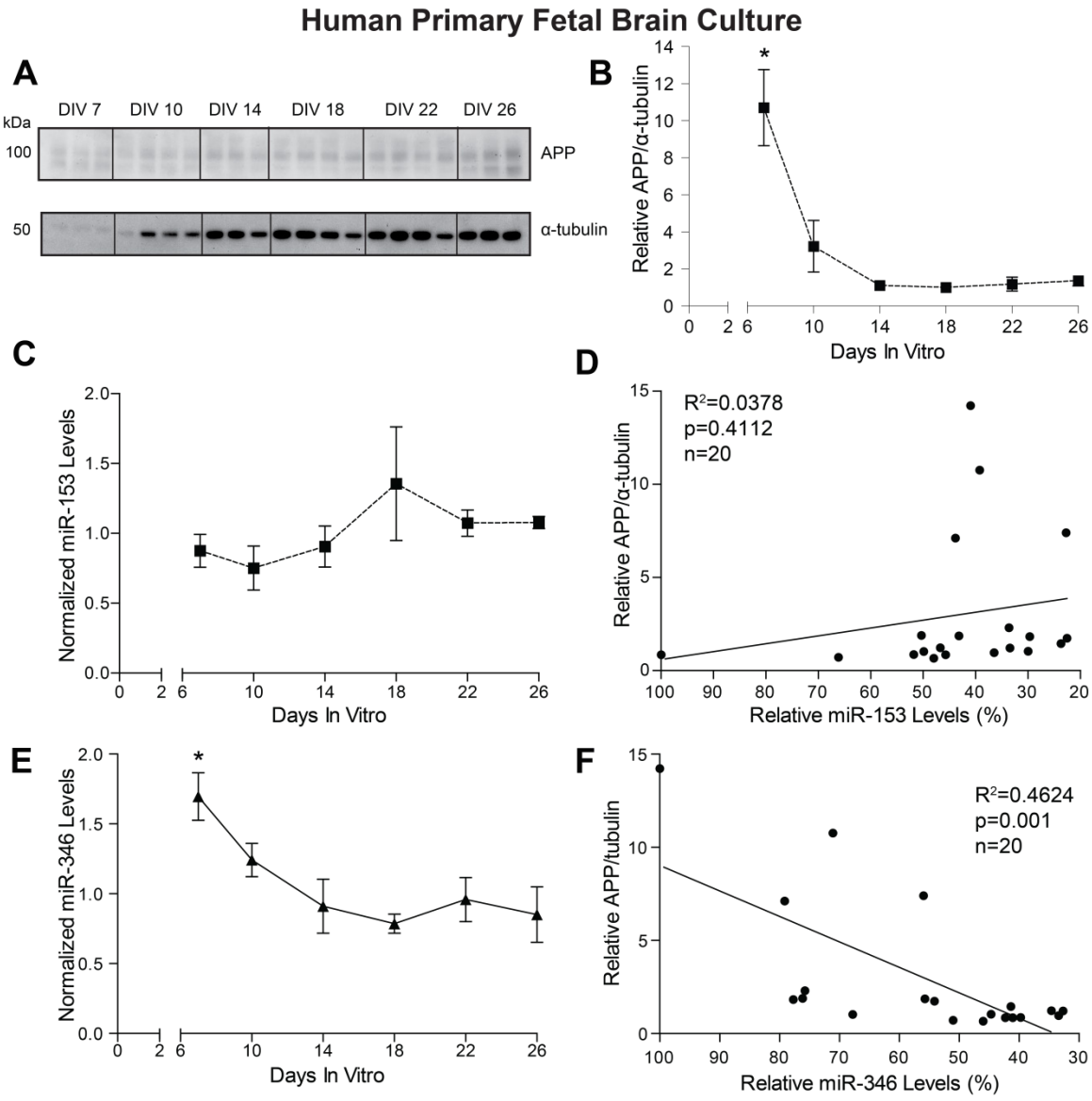

Figure 28: Time profile of APP protein levels and miR-153 and miR-346 levels in human fetal brain cultures suggests possible co-regulation. (A) Western blot analysis of APP and α-tubulin levels across time (DIV 7 to DIV 26) in a primary human fetal brain culture. (B) Blot from panel A was densitometrically analyzed and APP levels normalized to α-tubulin and scaled relative to DIV 18 levels (*p<0.001 vs. all time points by post-hoc Tukey's HSD; n=3 – 4). (C) RT-qPCR analysis of miR-153 levels across time in the same primary human fetal brain culture as in A & B. Expression levels were normalized to the geometric mean of expression levels for endogenous controls

RNU6B, RUN48 and miR-16. (p values to be determined; n=2 – 4). (D) Scatter plot of normalized APP levels versus relative miR-153 levels. miR-153 levels presented as percent of highest expressing sample. Pearson's correlation coefficient analysis used to determine R^2 and p-value. Data fitted by linear regression. (E) RT-qPCR analysis of miR-346 levels as performed in panel (C). (F) Scatter plot of normalized APP levels versus relative miR-346 levels. Analysis performed as in panel (D). (*p<0.001 vs. DIV 14, 18, 22 and 26 by post-hoc Tukey's HSD; n=2 – 4).

B. Expression analysis of miRNA and protein targets in brain specimens from unaffected and Alzheimer disease-affected patients

The miRNA identified in aims 1 and 2 represent putative drug targets based on their ability to modulate gene products essential to the production of Aβ. If these miRNA are also dysregulated in the AD brain, they become even more attractive drug targets. Discovery of their dysregulation might also provide valuable insights into the underlying molecular etiology of AD. Therefore, the next set of experiments sought to examine the expression patterns of these miRNA in the AD brain as compared to the non-demented brain.

Two independent cohorts of brain specimens were utilized in this study. The first set of specimens was provided by Dr. Peter T Nelson from the University of Kentucky Alzheimer Disease Brain Bank. These specimens were isolated from BA9 of the frontal cortex and consisted of both control (n=5) and AD (n=15) specimens. Demographic details for these specimens are listed in Table 11. These specimens were age-matched with a mean age for control specimens of 84.0±2.2 years and 80.8±1.7 years for AD specimens. All AD specimens had advanced AD neuropathology (Braak stage VI [13] and CERAD score C [328]). Importantly, all specimens were collected following a short PMI (range 1.75 hr – 8 hr). Finally, the AD component of this cohort consisted of three subgroups defined by history of treatment with AD medications: no history of AD medication (No Rx; n=5), history of treatment with rivastigmine but not memantine (n=5), and history of treatment with memantine but not rivastigmine (n=5). In these experiments, analyses were restricted to the full AD cohort or the No Rx cohort.

The second set of specimens originated from the Harvard Tissue Resource Center and was provided by Dr. P Hemachandra Reddy. These specimens were also isolated from BA9 of the frontal cortex and consisted of control (n=5) and AD (n=15) specimens. Demographic details from this cohort are listed in Table 12 and were

previously published [329]. The AD group was further subdivided into three groups defined by stage of neurofibrillary pathology: Braak stage I/II (early AD; n=5), Braak stage III/IV (definite AD; n=5), and Braak stage V/VI (severe AD; n=5). Therefore, this group consisted of specimens spanning the stages of AD progression. Analyses of this cohort was performed either by making comparisons across all Braak stages or by combining control and stage I/II and stage III – VI into two distinct groupsfor comparison. The rationale for consolidating groups was to increase power of analysis by increasing sample size. Given that stage I/II specimens have only very mild AD pathology and represent a very early stage of the clinical disease, the assumption is that control and stage I/II specimens are more biochemically similar to one another than to either stage III/IV or V/VI specimens.

This cohort was age-matched across groups: controls (77.6±3.8 years), stage I/II (73.2±1.7 years), stage III/IV (77.6±2.5 years), stage V/VI (86.0±3.3 years). Only stage I/II and stage V/VI subgroups demonstrated any significant difference in age (ANOVA $p=0.0476$) by post hoc Tukey's HSD test ($p<0.05$). PMI was significantly higher for cohort 2 but did not vary significantly between groups (ANOVA $p=0.1409$).

Table 11: Demographics and neuropathological assessments of post-mortem specimens[a] constituting cohort 1

Diagnosis	Rx History[b]	Age	Sex	PMI (h)	Braak Stage[c]	CERAD Score[d]	NIA-Reagan Assessment[e]
Control	No Rx	F	79	1.75	I	0	No disease
Control	No Rx	F	92	8	II	0	No disease
Control	No Rx	F	84	5	III	0	No disease
Control	No Rx	M	81	2.83	II	A	Low likelihood
Control	No Rx	M	84	1.5	II	C	Low likelihood
AD	No Rx	M	76	4.25	VI	C	High likelihood
AD	No Rx	F	91	7.5	V	C	High likelihood
AD	No Rx	F	86	4	VI	C	High likelihood
AD	No Rx	F	80	3.83	VI	C	High likelihood
AD	No Rx	M	74	3	VI	C	High likelihood
AD	Rivastigmine, No memantine	M	88	3.75	V	C	High likelihood
AD	Rivastigmine, No memantine	M	96	3.5	V	C	High likelihood
AD	Rivastigmine, No memantine	F	83	3.5	VI	C	High likelihood
AD	Rivastigmine, No memantine	M	65	4	VI	C	High likelihood
AD	Rivastigmine, No memantine	M	69	4	VI	C	High likelihood
AD	Memantine, no rivastigmine	F	92	3.5	V	C	High likelihood
AD	Memantine, no rivastigmine	F	79	3.75	VI	C	High likelihood
AD	Memantine, no rivastigmine	M	84	5.25	VI	C	High likelihood
AD	Memantine, no rivastigmine	F	65	4.25	VI	C	High likelihood
AD	Memantine, no rivastigmine	F	82	6.25	VI	C	High likelihood

[a]Brain specimens provided by Dr. Peter T Nelson from the University of Kentucky Alzheimer Disease Center Brain Bank

[b]History of cholinesterase inhibitor or memantine therapy, No Rx means no history of treatment with cholinesterase inhibitors or memantine

[c] Braak staging of neurofibrillary tangles as described in [13];

[d]Neuritic plaque density scores from the Consortium to Establish a Registry for Alzheimer's Disease as described in [328], 0=no disease, A=possible AD, C=definite AD

[e]Assessement of AD pathology based on National Institute of Aging-Reagan Institute consensus recommendations as described in [330]

Table 12: Demographics for post-mortem specimens[a] constituting cohort 2

Diagnosis	Braak Stage	Sex	Age	PMI (h)
Control	0	M	68	21
Control	0	M	82	17
Control	0	F	74	23
Control	0	M	74	15
Control	0	F	90	12
AD	I/II	F	74	12
AD	I/II	F	67	10
AD	I/II	F	76	24
AD	I/II	M	77	18
AD	I/II	F	72	12
AD	III/IV	M	69	18
AD	III/IV	M	75	24
AD	III/IV	M	82	19
AD	III/IV	M	80	19
AD	III/IV	F	82	18
AD	V/VI	M	77	11
AD	V/VI	F	83	18
AD	V/VI	M	83	19
AD	V/VI	F	92	5
AD	V/VI	F	95	8

[a]Specimens from the Harvard Tissue Resource Center were provided by Dr. P Hemachandra Reddy and demographic details previously published [329].

Prior to assessing for dysregulated miRNA expression in pathological specimens, miRNA levels were measured by absolute quantification RT-qPCR in control specimens from each cohort to test whether basal expression levels in the adult human brain are in the range sufficient for mediating regulatory effects. Previous studies have demonstated that thresholds for functional miRNA activity in a cell can be as low as ~ 100 copies per cell [242]. Absolute miRNA copy counts were measured using RT-qPCR by analyzing miRNA standard curves prepared from synthetic oligoribonucleotides. miRNA expression levels were measured for miR-101, miR-153, miR-346 and miR-339-5p and normalized to copies per 15 pg total RNA. This amount of total RNA approximates the amount present in a single human cell. Therefore, miRNA copies as presented in Figure 29 roughly approximate the amounts per cell. However, post-mortem RNA degradation in brain specimens prior to freezing likely significantly underestimates actual copy counts per cell. For comparison to a known highly expressed brain miRNA, miR-124 copy counts were also quantified [331,332].

In cohort 1 (Figure 29A), miR-124 was the most highly expressed (71340±13550 copies/15 pg total RNA). Expression levels of other miRNA were significantly lower than miR-124 and varied in the following order: miR-101 (6195±452 copies/15 pg total RNA), miR-153 (994±314 copies/15 pg total RNA), miR-346 (194±77 copies/15 pg total RNA), and miR-339-5p (58±19 copies/15 pg total RNA). Cohort 2 was similarly examined, with the exception being that miR-124 was not quantified in specimens from this cohort. Expression levels for miRNA varied in the same order for cohort 2 as in cohort 1: miR-101 (1203±225 copies/15 pg total RNA), miR-153 (260 ±52 copies/15 pg total RNA), miR-346 (63 ±23 copies/15 pg total RNA), miR-339-5p (26±5 copies/15 pg total RNA). Notably, the absolute copy counts were significantly lower for each miRNA assayed in cohort 2 specimens relative to cohort 1. This likely reflects the fact that PMI was

significantly longer in cohort 2 and is further reflected by the lower RIN values observed in some samples from cohort 2.

In summary, miR-101, miR-153, miR-346 and miR-339-5p are expressed in the human brain to varying extents. Given the degree of underestimation of actual copy counts per cell inherent in analyzing a post-mortem specimen, the expression levels of each tested miRNA in the human brain are expected to be sufficient to mediate functional effects on gene expression observed in aims 1 and 2.

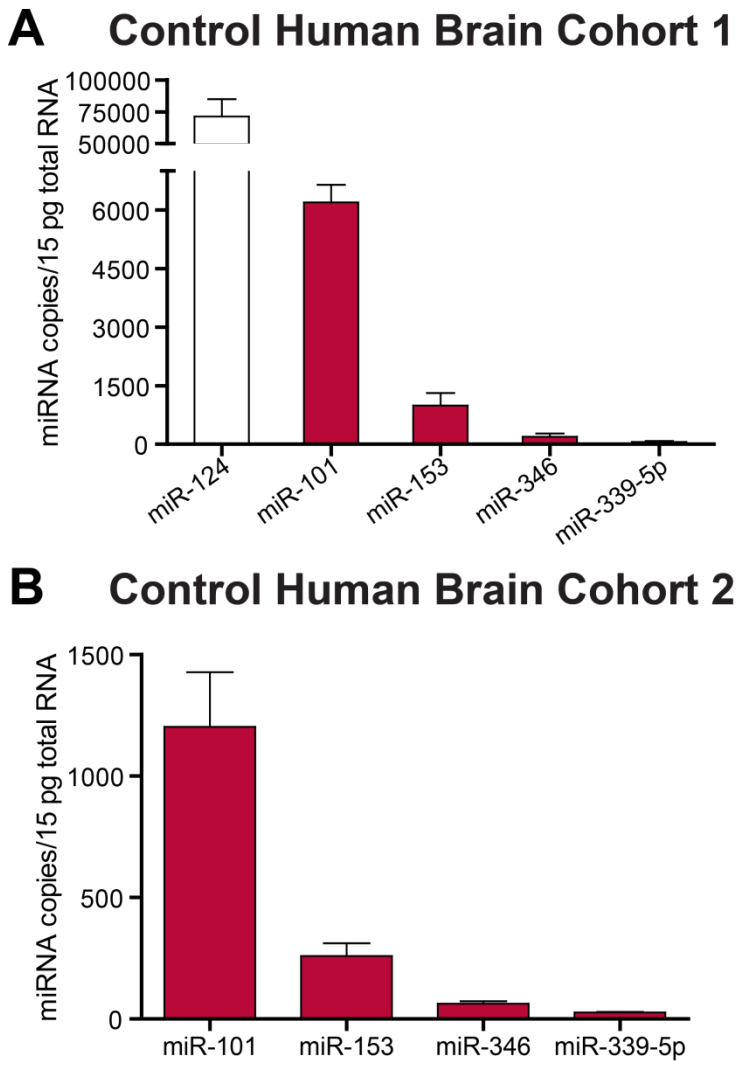

Figure 29: Absolute quantification of miRNA levels in control human brain specimens confirms physiologically relevant expression. Absolute miRNA copy counts per 15 pg of total RNA in control brain specimens from two independent cohorts were analyzed by RT-qPCR. Copy counts were calculated from standard curves prepared from serial dilutions of miRNA oligonucleotide standards with known concentrations. Control reactions lacking template did not demonstrate any amplification. miR-124 is a highly expressed, brain-expressed miRNA and was analyzed for comparison to a known highly expressed brain miRNA. (n=5 for each cohort)

Specimens from each brain cohort were next examined for dysregulation of APP, BACE1 or their targeting miRNA in AD. APP levels were measured by Western blot and levels of miRNA by RT-qPCR. Both relative quantification (normalized to the geometric mean of RNU6B, RNU48, RNU49 and miR-16 expression levels) and absolute quantification (normalized as copy counts per 15 pg total RNA) of miRNA levels were performed. In both cohorts, APP levels were not significantly different in the AD specimens (or No Rx AD subgroup) as compared to control brain specimens (Figure 31A and B). Next, expression of APP-targeting miRNA was assessed. Levels of miR-101 were significantly decreased in both the AD specimens (0.688±0.051 fold change; p=0.009 by Student's t-test) and the No Rx subgroup (0.624±0.070 fold change; p=0.0176 by Student's t-test) as compared to control specimens by relative quantification (Figure 10A). The same decrease in miR-101 levels in AD (0.588±0.054 fold change by Student's t-test) and the No Rx subgroup (0.650±0.010 fold change; p=0.0223 by Student's t-test) were observed when quantified in absolute terms (Figure 31B).

Simlarly, miR-346 expression was significantly decreased in both the full AD group (0.338±0.077 fold change; $p<0.05$ by ANOVA and post hoc Dunnett's t-test) and No Rx subgroup (0.228±0.050 fold change; $p<0.51$ by ANOVA and post-hoc Dunnett's t-test) by relative quantification (Figure 31E). This finding was also apparent when miR-346 expression levels were compared by absolute quantification between the full AD group (0.256±0.023 fold change; $p<0.01$ by ANOVA and post hoc Dunnett's t-test) and the controls and for the No Rx subgroup (0.228±0.027 fold change) as compared to controls (Figure 31F).

No significant difference in miR-153 (Figure 31Cand D) levels were observed between AD (or No Rx) and control specimens, whether quantified in relative or

absolute terms. Therefore, miR-101 and miR-346 levels are negatively dysregulated in AD specimens from this cohort

Next, expression levels of BACE1 and BACE1-targeting miRNA were assessed. Levels of BACE1 were not significantly different in AD (or No Rx) specimens as compared to control specimens (Figure 32A and B). miR-339-5p levels were significantly decreased compared to controls but only in the full AD group and onlywith absolute quantification (0.549±0.045 fold change; p=0.033 by two-tailed Student's t-test) (Figure 33B). Expression levels of several additional miRNA not specifically tested for BACE1-regulating effects in these studies but previously reported to regulate BACE1 expression were also assessed: miR-124 [333], miR-107 [266], and miR-29b [189]. There were no significant differences in miR-124 (Figure 33C and D), miR-107 (Figure 33E) or miR-29b levels (Figure 33F) in AD or No Rx subgroup specimens as compared to negative control specimens. However, all trended toward decreased expression despite not reaching statistical significance. Therefore, miR-339-5p levels may be negatively dysregulated in AD specimens from this cohort.

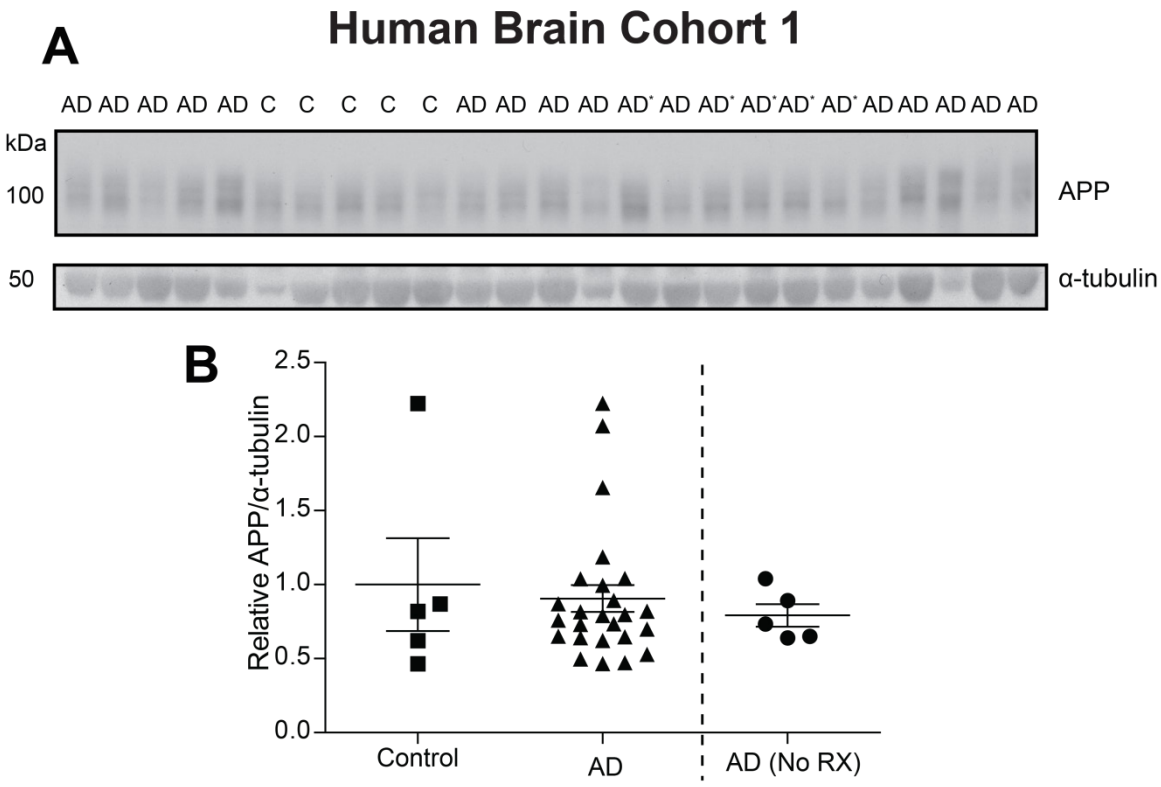

Figure 30: Analysis APP protein levels in control and AD human brain specimens from cohort 1. (A) Western blot analysis of APP and α-tubulin levels in brain specimens from AD and control patients in cohort 1. (B) Blot from panel A was densitometrically analyzed and APP levels normalized to α-tubulin and scaled relative to control APP levels. AD (No Rx) represents a subgroup of patients from the AD group that had no history of treatment with cholinesterase inhibitors or memantine. C, control group; AD, AD group; AD*, AD (No Rx) subgroup.

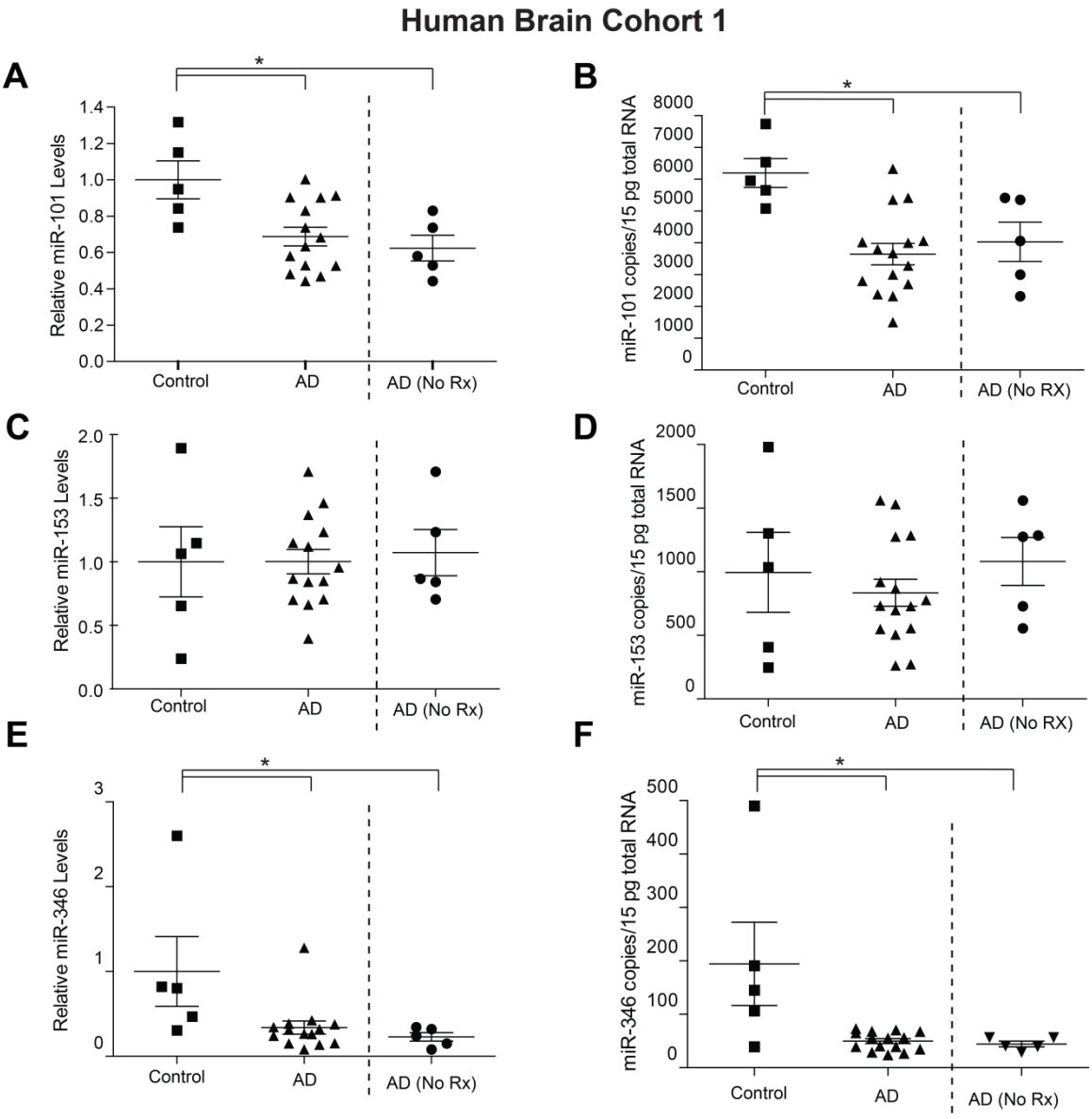

Figure 31: Analysis of validated APP-regulating miRNA expression levels in control and AD human brain specimens from cohort 1. RT-qPCR analysis of expression levels for miR-101 (A and B), miR-153 (C and D), and miR-346 (E and F) in brain specimens from AD and control patients in cohort 1. AD (No Rx) represents a subgroup of patients from the AD group that had no history of treatment with cholinesterase inhibitors or memantine. In panels A, C and E, expression levels were determined using the modified delta C_q relative quantification method as implemented in qBase^{PLUS} software [301,302]. Expression levels were normalized to the geometric

mean of four endogenous controls: RNU6B, RNU48, RNU49 and miR-16. In panels B, D, and F, expression levels were quantified in absolute terms as miRNA copy counts per 15 pg of total RNA. Copy counts were calculated from standard curves prepared from serial dilutions of miRNA oligonucleotide standards with known concentrations. (*$p<0.05$; n=5 for controls, n=14 for AD, n=5 for AD (No Rx)).

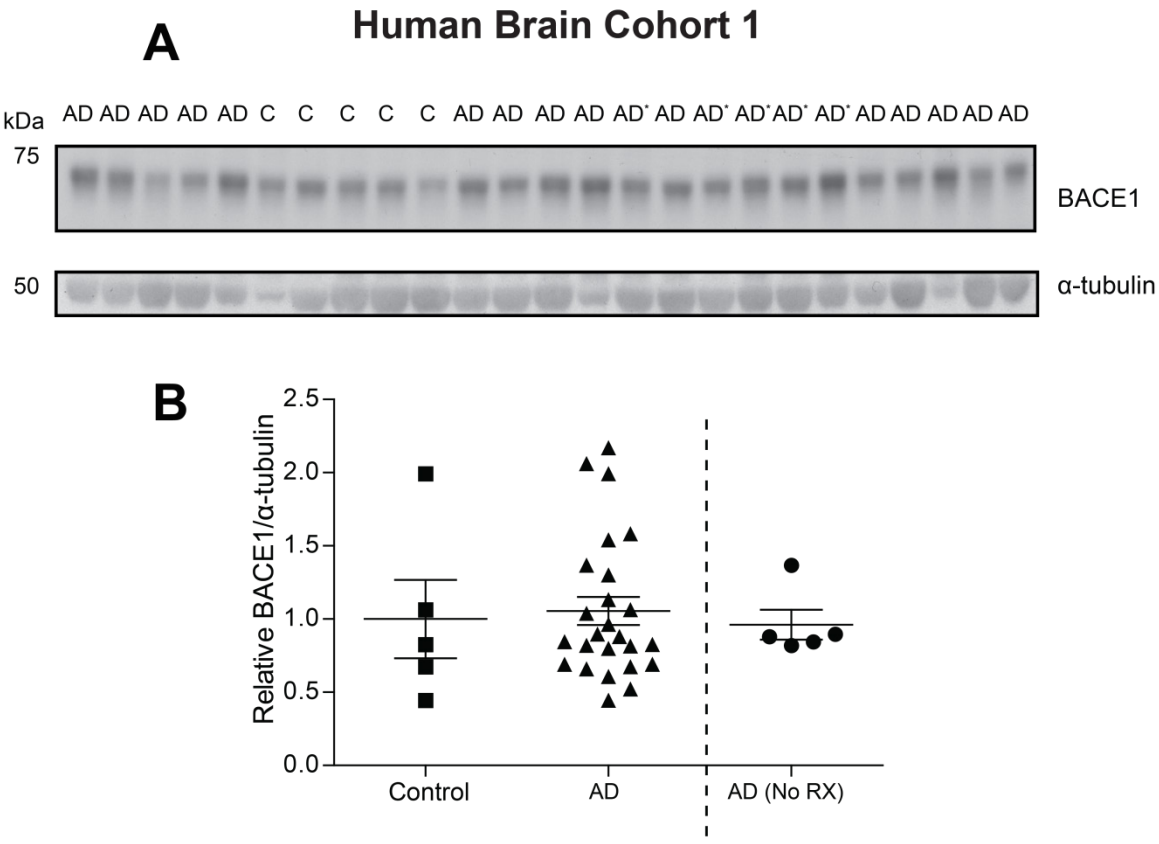

Figure 32: Analysis of BACE1 protein levels in control and AD human brain specimens from cohort 1. (A) Western blot analysis of BACE1 and α-tubulin levels in brain specimens from AD and control patients in cohort 1. (B) Blot from panel A was densitometrically analyzed and BACE1 levels normalized to α-tubulin and scaled relative to control BACE1 levels. C, control group; AD, AD group; AD*, AD (No Rx) subgroup

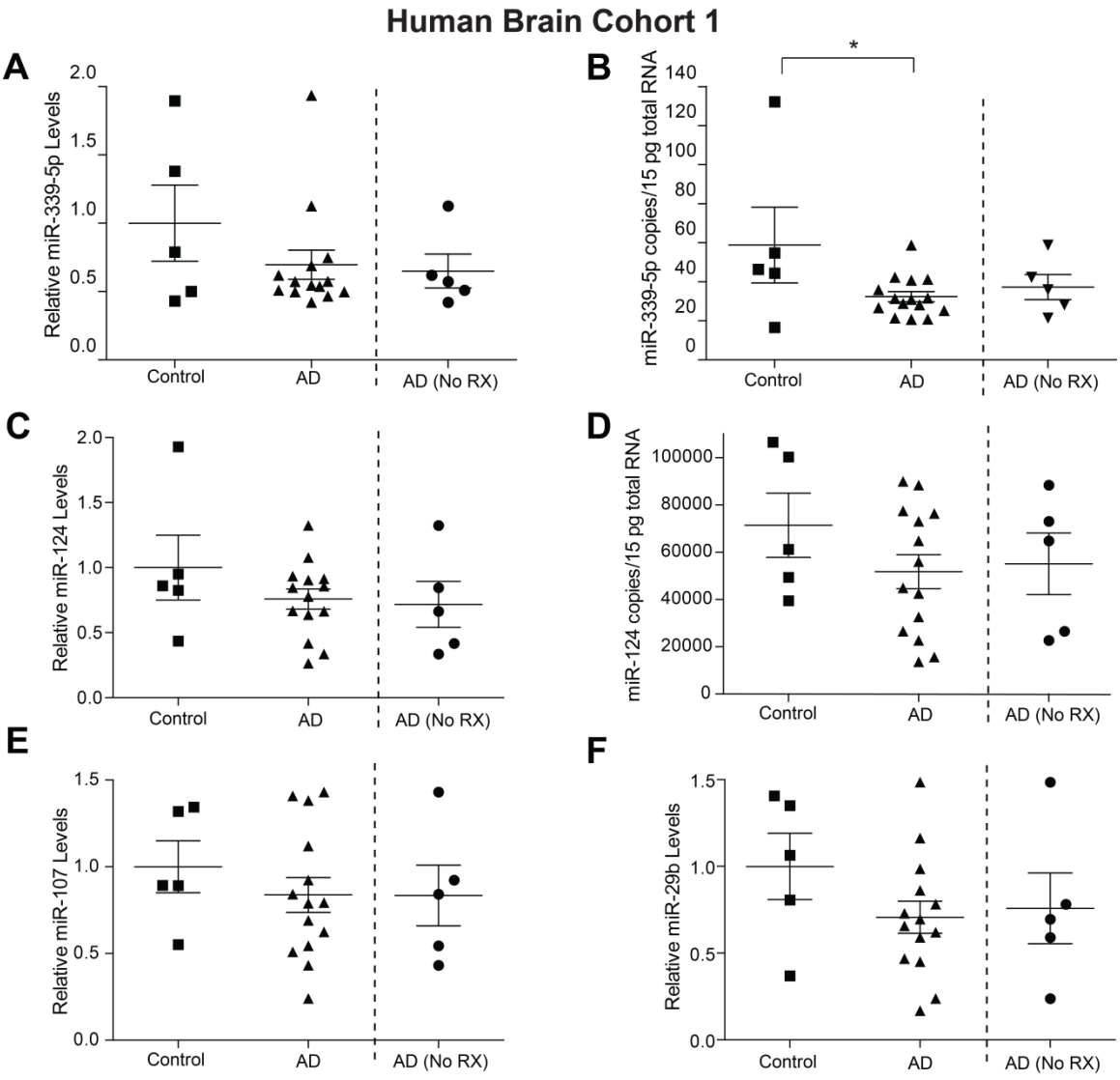

Figure 33: Analysis of validated BACE1-regulating miRNA expression levels in control and AD human brain specimens from cohort 1. RT-qPCR analysis of expression levels for miR-339-5p (A and B), miR-124 (C and D), miR-107 (E) and miR-29b (F) in brain specimens from AD and control patients in cohort 1. In panels A, C, E and F, expression levels were determined using the modified comparative C_q relative quantification method as implemented in qBase^{PLUS} software [301,302] . Expression levels were normalized to the geometric mean of four endogenous controls: RNU6B, RNU48, RNU49 and miR-16. In panels B and D, expression levels were quantified in absolute terms as miRNA copy counts per 15 pg of total RNA. Copy counts were

calculated from standard curves prepared from serial dilutions of miRNA oligonucleotide standards with known concentrations. (*$p<0.05$; n=5 for controls, n=14 for AD, n=5 for AD (No Rx)).

A similar set of analyses were performed on independent cohort 2. Unlike the specimens in the previous cohort that exhibited only severe AD pathology, these specimens ranged across the pathological stages of the disease (Braak stage 0, I/II, III/IV and V/VI). Specimens were also grouped into two higher level categories for analysis: 1) control and Braak stage I/II specimens, and 2) Braak stage III, IV, V and VI specimens. The rationale for comparing these two supergroups is that neurofibrillary tangle (NFT) pathology (the basis of Braak staging) does not progress into the neocortex until Braak stages III and IV [13]. Since specimens analyzed here are from BA9 of the neocortex, the progression from Braak stage II to stage III delineates a distinct transition in the pathogenic environment of this region of the brain. Clinicopathological correlation studies have also demonstrated that the progression of NFT in the neocortex better correlates with cognitive decline than stages of disease where NFT are restricted to the allocortex [334]. Grouping also served to enhance the power of analysis by increasing sample size of each group to ten.

APP levels were quantified by Western blot (Figure 34). When compared across Braak stages, APP levels were significantly increased in Braak stage III/IV AD samples ($p=0.041$ by post-hoc Tukey's HSD; $n=5$) (Figure 34B). When compared between the two supergroups, APP expression was also significantly elevated in specimens with the presence of neocortical NFT pathology (stages III – VI) and a significant increase was observed in stage III/IV specimens as compared to stage I/II ($p=0.048$ by Student's t-test) (Figure 34C). Levels of APP-targeting miRNA were investigated next. miR-101 levels were not found to be significantly altered across any groups by either relative or absolute quantification methods (Figure 35 A – D). Interestingly, miR-153 levels were significantly decreased in specimens from combined Braak stages III/IV and V/VI as compared to combined control and Braak stage I/II specimens following both relative quantification (0.460 ± 0.104 fold change; $p=0.024$ by two-tailed Student's t-test) (Figure

36B and D) and absolute quantification (0.497±0.117 fold change; p=0.035 by two-tailed Student's t-test). The inverse pattern of APP and miR-153 dysregulation in Braak stage III/IV AD specimens suggests that decreased miR-153 levels may contribute to elevated APP in these specimens.

miR-346 levels were also found to be significantly decreased in combined AD specimens from Braak stage III/IV and V/VI as compared to combined control and stage I/II specimens by both relative (0.547±0.079 fold change; p=0.0109 by two-tailed Student's t-test) (Figure 37A and B) and absolute quantification methods (0.530±0.088 fold change; p=0.0038 by two-tailed Student's t-test) (Figure 37C and D).This is notable because the same alteration in miR-346 expression was observed in cohort 1 providing extra validitiy to this finding.

Finally, levels of BACE1 and BACE1-targeting miRNA were assessed in cohort 2. BACE1 levels demonstrated a trend towards elevated expression in Braak stage III/IV specimens, however this trend was not significant (ANOVA p=0.2648) (Figure 38A and B). miR-339-5p levels were then quantified by relative (Figure 39A and B) and absolute (Figure 39C and D) quantification. No alterations in miR-339-5p levels between any groups were detected by any quantification scheme.

Collectively these data indicate that miR-101, miR-153, miR-346 and potentially miR-339-5p are dysregulated in the brains of at least a subset of moderate to severe sporadic AD patients.

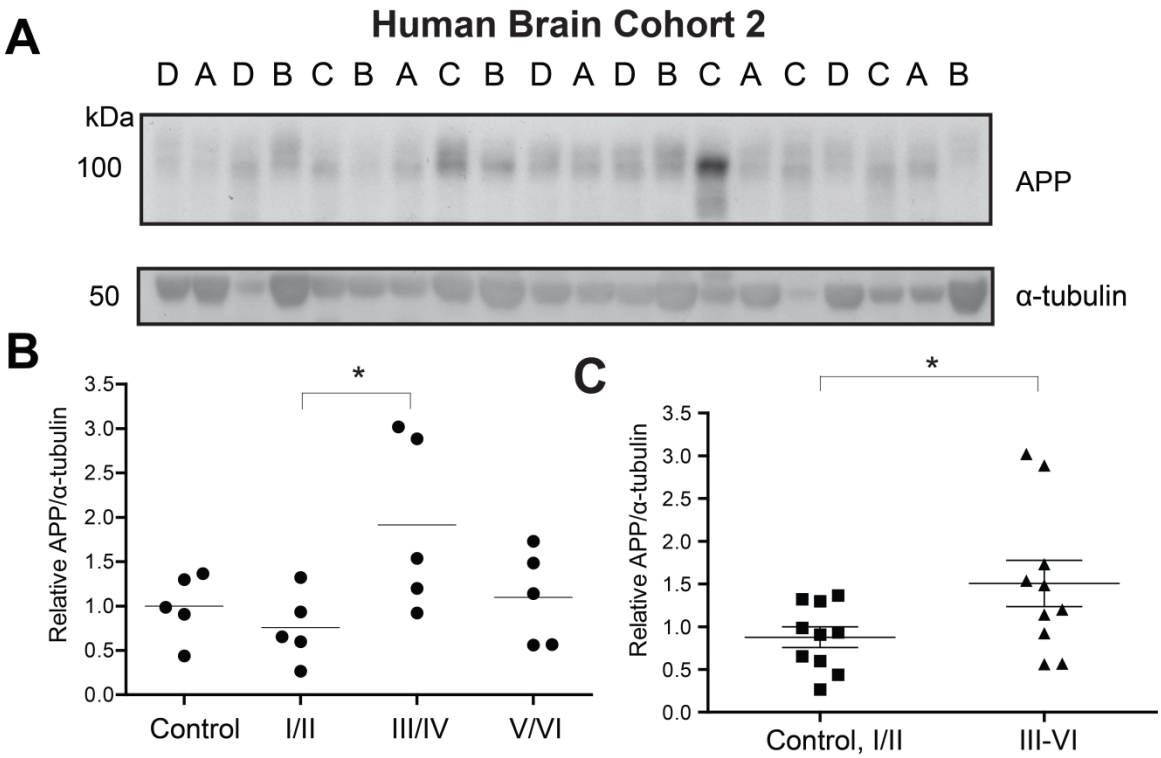

Figure 34: Analysis of APP protein levels in control and AD human brain specimens across Braak stages from cohort 2. (A) Western blot analysis of APP and α-tubulin levels in control, early (Braak stage I/II), definite (Braak stage III/IV) and severe (Braak stage V/VI) AD brain specimens in cohort 2. In panel (B), expression levels were compared across control and Braak stage I/II, III/IV, and V/VI specimens. In panel (C), similar groups were combined to increase the power of analysis. Control and Braak stage I/II specimens were grouped together and Braak stage III – VI were grouped together for analysis. Blot abbreviations: A, control specimens; B, early AD specimens (stage I/II); C, definite AD specimens (stage III/IV); D, severe AD specimens (stage V/VI). *$p<0.05$; n=5 – 10 for each group

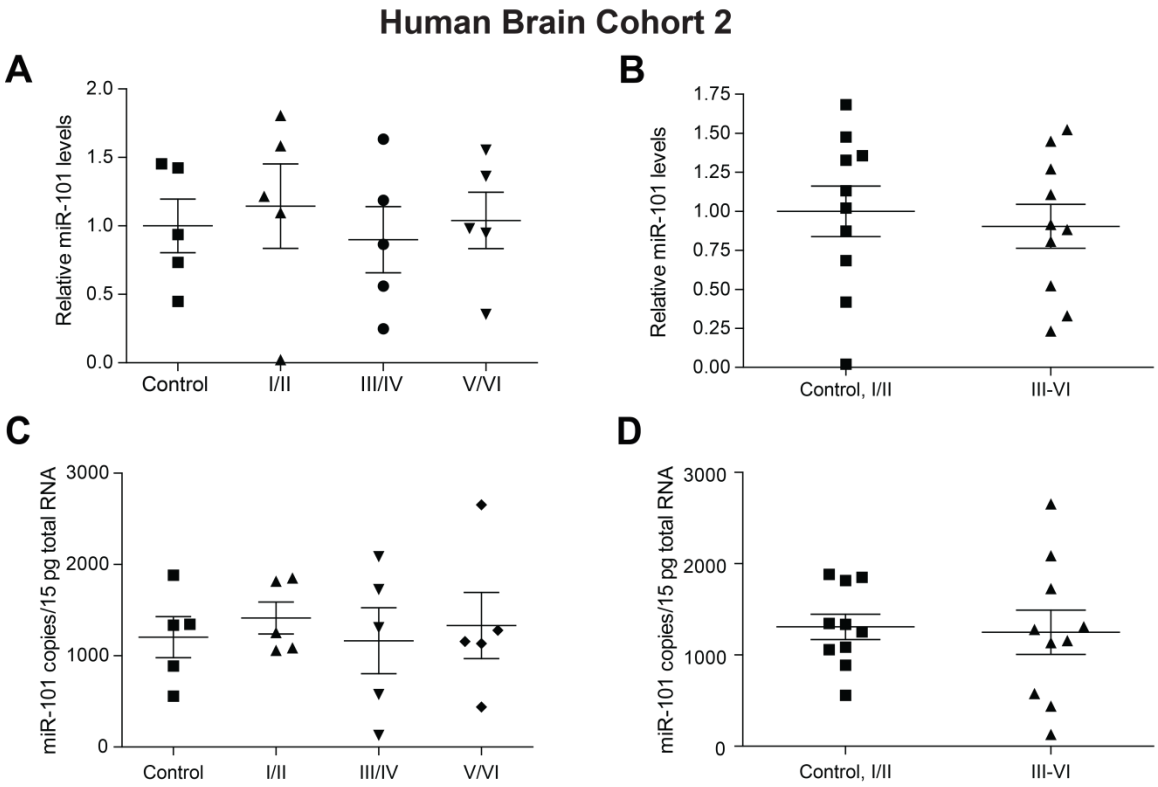

Figure 35: Analysis of miR-101 expression levels in control and AD human brain specimens across Braak stages from cohort 2. RT-qPCR analysis of expression levels for miR-101. In panel A and B, expression levels were determined relative to the geometric mean of four endogenous controls: RNU6B, RNU48, RNU49 and miR-16. In panels C and D, expression levels were quantified in absolute terms as miRNA copy counts per 15 pg of total RNA using standard curves prepared from serial dilutions of miRNA oligonucleotide standards with known concentrations. In panels A and C, expression levels were compared across control and Braak stage I/II, III/IV, and V/VI specimens. In panels B and D, similar groups were combined to increase the power of analysis. Control and Braak stage I/II specimens were grouped together and Braak stage III-VI were grouped together for analysis. (*$p<0.05$; n=5 – 10 for each group).

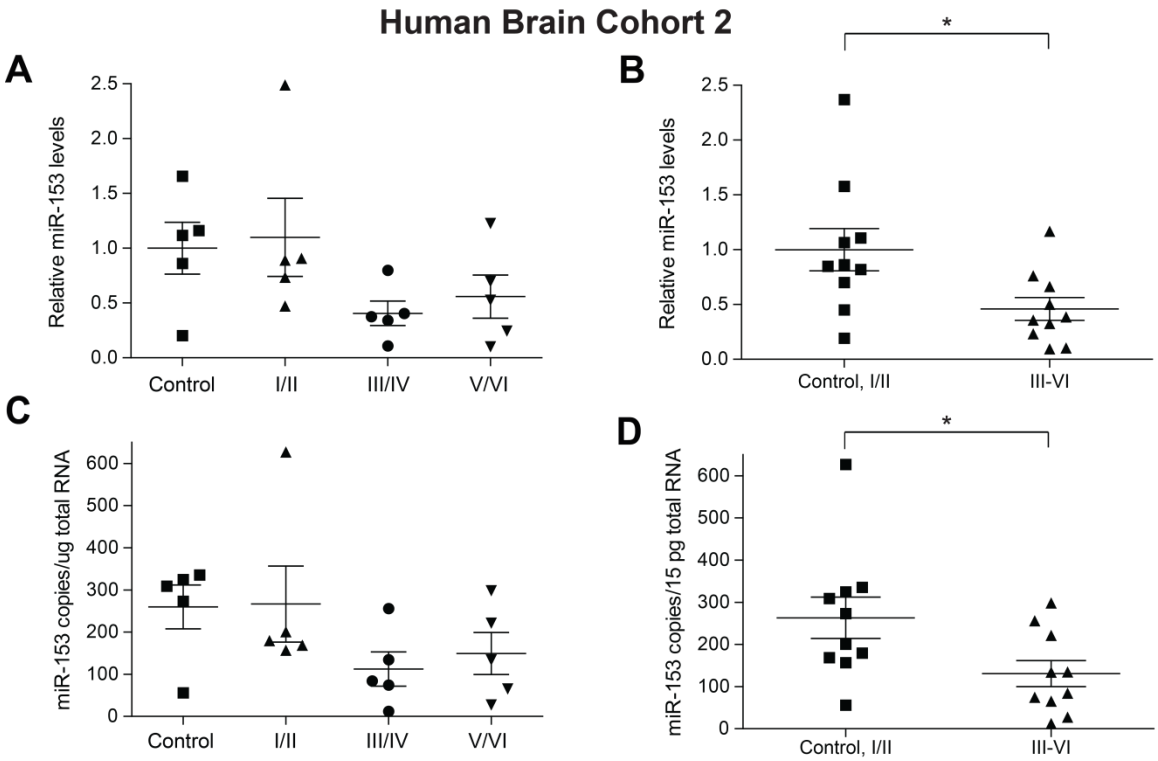

Figure 36: Analysis of miR-153 expression levels in control and AD human brain specimens across Braak stages from cohort 2. RT-qPCR analysis of expression levels for miR-153. In panels A and B, expression levels were determined relative to the geometric mean of four endogenous controls: RNU6B, RNU48, RNU49 and miR-16. In panels C and D, expression levels were quantified in absolute terms as miRNA copy counts per 15 pg of total RNA using standard curves prepared from serial dilutions of miRNA oligonucleotide standards with known concentrations. In panels A and C, expression levels were compared across control and Braak stage I/II, III/IV, and V/VI specimens. In panels B and D, similar groups were combined to increase the power of analysis. Control and Braak stage I/II specimens were grouped together and Braak stage III – VI were grouped together for analysis. (*$p<0.05$; $n=5 – 10$ for each group).

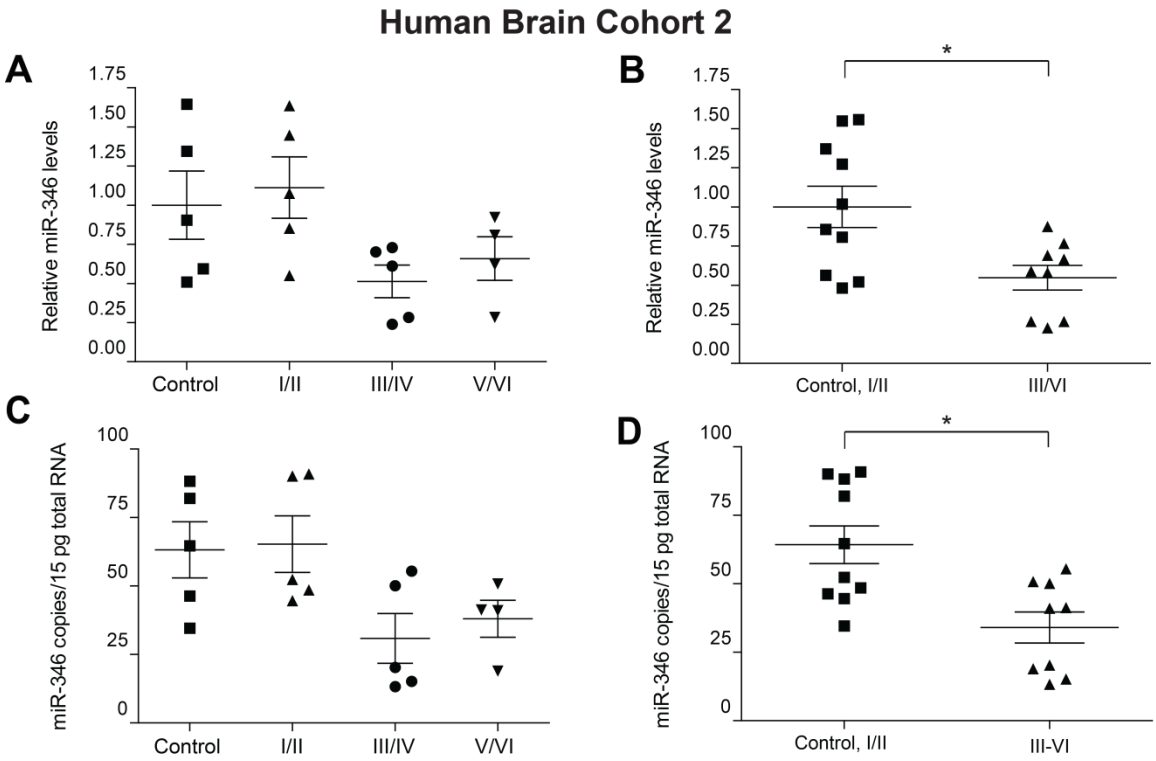

Figure 37: Analysis of miR-346 expression levels in control and AD human brain specimens across Braak stages from cohort 2. RT-qPCR analysis of expression levels for miR-346. In panel A and B, expression levels were determined relative to the geometric mean of four endogenous controls: RNU6B, RNU48, RNU49 and miR-16. In panels C and D, expression levels were quantified in absolute terms as miRNA copy counts per 15 pg of total RNA using standard curves prepared from serial dilutions of miRNA oligonucleotide standards with known concentrations. In panels A and C, expression levels were compared across control and Braak stage I/II, III/IV, and V/VI specimens. In panels B and D, similar groups were combined to increase the power of analysis. Control and Braak stage I/II specimens were grouped together and Braak stage III – VI were grouped together for analysis (n=5 for each Braak stage). (*$p<0.05$; n=5 for each group).

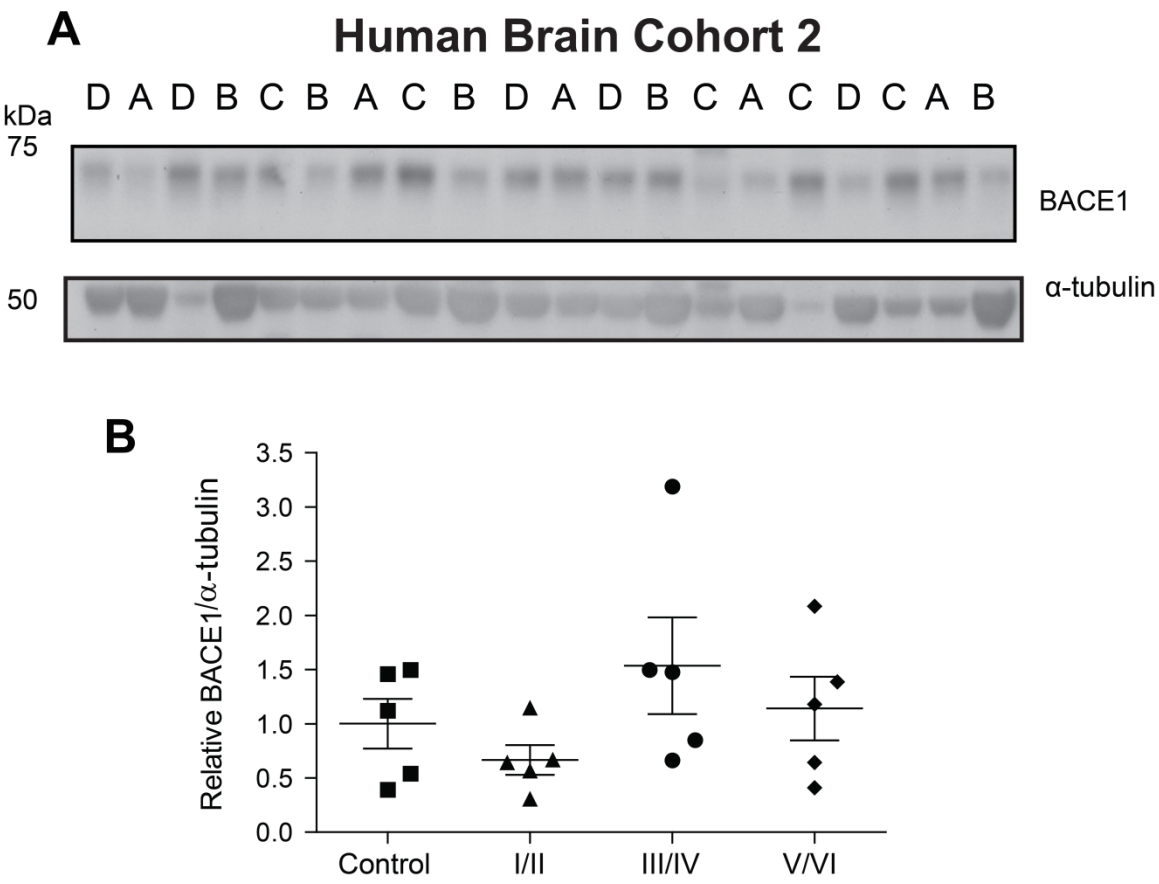

Figure 38: Analysis of BACE1 protein expression levels in control and AD human brain specimens across Braak stages from cohort 2. (A) Western blot analysis of BACE1 and α-tubulin levels in control, early (Braak stage I/II), definite (Braak stage III/IV) and severe (Braak stage V/VI) AD brain specimens in cohort 2. (B) Blot from panel A was densitometrically analyzed and BACE1 levels normalized to α-tubulin and scaled relative to control BACE1 levels. Blot abbreviations: A, control specimens; B, early AD specimens (stage I/II); C, definite AD specimens (stage III/IV); D, severe AD specimens (stage V/VI).

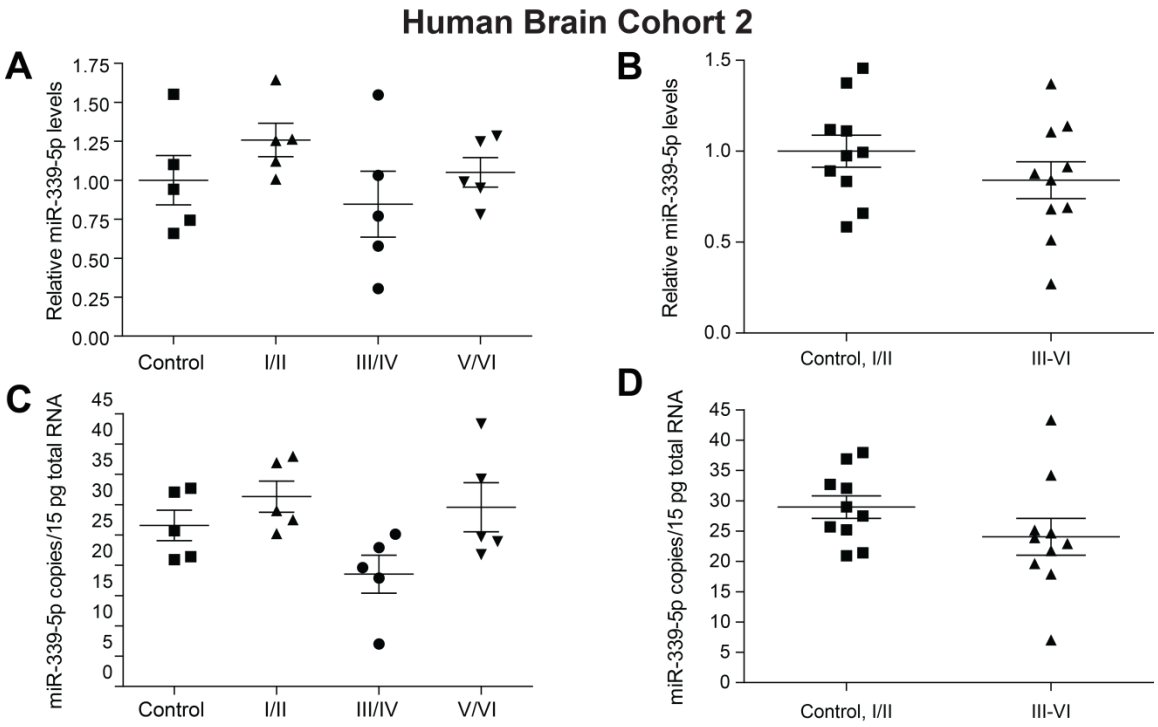

Figure 39: Analysis of miR-339-5p expression levels in control and AD human brain specimens across Braak stages from cohort 2. RT-qPCR analysis of expression levels for miR-339-5p. In panel A and B, expression levels were determined relative to the geometric mean of four endogenous controls: RNU6B, RNU48, RNU49 and miR-16. In panels C and D, expression levels were quantified in absolute terms as miRNA copy counts per 15 pg of total RNA using standard curves prepared from serial dilutions of miRNA oligonucleotide standards with known concentrations. In panels A and C, expression levels were compared across control and Braak stage I/II, III/IV, and V/VI specimens. In panels B and D, similar groups were combined to increase the power of analysis. Control and Braak stage I/II specimens were grouped together and Braak stage III – VI were grouped together for analysis (n=5 for each Braak stage).

CHAPTER 4: DISCUSSION

The overarching goal of the studies described in this disseration was to identify novel regulators of gene expression for gene products critical to the production of Aβ in the human brain. Given the presumed centrality of Aβ to AD pathogenesis [27], these novel regulators might then be pursued as novel drug targets based on their Aβ-modulating activities. APP and BACE1 were chosen as the gene products of interest given their role as the Aβ parental molecule [92] and rate-limiting enzyme for Aβ production [158], respectively. Also, they both exhibit elevated expression contributing to disease in sporadic AD or rare genetic variants of AD [30,47–49,335].The novel regulators that were the focus of these studies were miRNA. The hypothesis that miRNA regulate the expression of APP and BACE1 was based upon systems-level analyses that demonstrate most mammalian transcripts are miRNA targets [243] and by the fact that knockdown of a central RISC protein essential for global miRNA function (AGO2) resulted in elevated levels of APP and BACE1 protein (Figures 1 and 21). Therefore, experiments were pursued that identified physiologically relevant APP and BACE1 mRNA:miRNA regulatory interactions, demonstrated the Aβ-modifying properties of some of these miRNA, and established dysregulation of several miRNA in the AD brain.

I. Novel miRNA interactions with the APP mRNA regulate APP expression

A. The APP 3'-UTR stimulates basal expression

Reporter expression under the regulatory influence of the APP 3'-UTR was elevated as compared to reporter expression in the absence of the APP 3'-UTR, suggesting the presence of regulatory elements in the APP 3'-UTR that either stabilize

the reporter transcript or promote reporter transcript translation. This stimulatory effect is consistent with previous reports [336]. Several trans-acting factors have been previously reported to interact with cis-elements in the APP 3'-UTR promoting APP mRNA stability. A 29-nt sequence in the 3'-UTR normally acts as an instability element, however hnRNP C binding to this element enhances transcript stability [147,150]. A 52-nt element located immediately downstream of the APP stop codon basally enhances transcript stability and appears to do so by binding multiple RNA-binding proteins, including rck/p54 [149,151]. An 81-nt element downstream of the two previous elements responds to TGF-β1 signaling by significantly enhancing APP transcript stability [337].

Any or all of these elements might contribute to the stimulatory effect of the APP 3'-UTR on reporter expression observed in this study. Additional elements not yet described may also significantly contribute. Aside from the exact mechanism, it is clear that with the reporter system tested here the integrated response of the APP 3'-UTR across multiple cellular environments is to enhance expression. Importantly, the observed effect does not preclude the possibility of distinct negative regulatory influences being mediated by 3'-UTR cis-elements, such as MRE.

B. Bioinformatic analyses reveal putative APP 3'-UTR:miRNA interactions

As a first step in identifying miRNA that regulate APP expression, bioinformatic predictors were employed to predict putative APP 3'-UTR:miRNA interactions. A more unbiased workflow would make no assumptions about putative miRNA target sites and simply screen a complete library of all known miRNAs for regulatory effects on APP expression using an optimized high throughput assay. However, the costs, logistics, and time required for assay optimization are extensive. Further, this approach does not provide a sorting mechanism to distinguish effects that are indirect from those that are mediated by direct interaction with the APP transcript. Therefore, mechanism would be

difficult to dissect. Bioinformatic-based predictions are useful in that they provide preliminary evidence for direct interaction of a predicted miRNA with the target transcript. Thus, once miRNA regulatory effects on target gene expression are validated, a hypothesis regarding mechanism can be immediately tested by mutating target site sequences. Additionally, recent proteomic analyses of protein expression changes following transfection of synthetic miRNAs have demonstrated that bioinformatic predictions capture many experimentally confirmed regulatory relationships [244,245]. Therefore, in this study, the following predictors were used: TargetScan 6.0, PicTar, DIANA-microT v.4.0, miRanda-mirSVR, PITA and rna22 (Table 7 for summary). These algorithms output a set of miRNA predicted to target the APP 3'-UTR. The validity of this approach as a starting point for identifying miRNA regulators of APP expression is highlighted by the fact that several miRNA in this set were subsequently shown in independent labs to mediate inhibitory effects on APP expression: miR-20a [338], miR-20b, miR-106a [276] and miR-520c-3p [318].

Despite their ease of use and general success in identifying true interactions between miRNA and mRNA target sites, predictor algorithms are not unassailable tools in the hunt for physiologically relevant regulatory interactions. The same proteomic studies cited above also indicate that these tools generate very high levels of false positives despite continued improvement in algorithmic design [244,245]. Therefore, a set of miRNA predicted to target APP transcript can be expected to include many physiologically irrelevant members (false positive) and exclude many physiologically relevant members not detected by the predictor algorithm (false negatives). Other disadvantages underlying exclusive use of web-based predictors is that most have pre-assembled prediction sets that are limited to 3'-UTR only. New experimental approaches have identified functional interactions with target sites in the CDS and 5'-UTR of mRNAs [225,325,339]. Therefore, exclusive use of computational methods for

target site identification is likely to miss out on some important functional interactions that occur outside the 3'-UTR (e.g. miR-346 data presented in this dissertation). Finally, the requirement for cross-species conservation at putative target sites serves as a useful filter for enriching for functional sites but is also likely to eliminate the detection of species-specific miRNA:mRNA target interactions. Therefore, future studies that continue the search for miRNA regulators of APP expression might be well served to incorporate new state-of-the-art experimental techniques that directly identify physical interactions between miRNA and target mRNA. Examples of such techniques include RIP-Chip [340], TAP-Tar [341], HITS-CLIP [225] and PAR-CLIP [339]. These techniques are based on the pulldown of a ternary complex consisting of AGO2, miRNA and target mRNA via immunoprecipitation of AGO2.

C. APP expression is negatively regulated by miR-101 and miR-153 via target sites in the APP 3'-UTR

Efficacy of predicted miRNA:APP 3'-UTR interactions was tested by 3'-UTR reporter assays. Multiple miRNA were found to inhibit reporter expression following co-transfection with an APP 3'-UTR reporter. The focus of subsequent investigations was on miR-101 and miR-153 given the strong inhibitory effect on reporter expression. The inhibitory effect of both miRNA on reporter expression required seed sequence fidelity at the specific predicted target sites in the APP 3'-UTR, suggesting that miR-101 and miR-153 mediate their inhibitory effect by direct interaction with these sites. For miR-101, two target sites were predicted in the APP 3'-UTR but only the most strongly conserved site was found to be functionally active. Both miR-101 and miR-153 inhibit APP protein expression and Aβ production in multiple human cell types, including AD-relevant human primary fetal mixed brain cultures. Importantly, endogenous miR-153

regulates basal expression in human cells, as evidenced by elevated APP expression following delivery of either antisense inhibitors that disrupt interaction of the miRNA with their APP 3'-UTR target sites. In toto, these data suggest that miR-101 and miR-153 are bona fide drug targets that might be targeted therapeutically to reduce APP expression in AD by either stimulating their endogenous expression in the brain or by direct delivery of synthetic miRNA.

Both miR-101 and miR-153 have ascribed functions and targets apart from their ability to regulate APP expression. miR-153 targets a gene product especially relevant to AD and Parkinson's disease (PD): α-synuclein (SNCA) [342]. In the cited study they demonstrate that endogenous miR-153 regulates *SNCA* in rodent neurons. SNCA is an abundant component of the Lewy bodies (LB) found in PD and dementia with Lewy bodies (DLB) [343]. Therefore, miR-153 negatively regulates two gene products implicated in two of the most common neurodegenerative diseases. LB are also found on autopsy in a common subtype of AD known as the Lewy body variant (AD-LBV) [344–347]. This subtype has been associated with more rapid cognitive decline compared to "pure" AD [348,349], along with lower levels of pre-synaptic proteins [350]. A recent animal model of AD-LBV created by crossing 3xTg-AD mice with A53T *SNCA* transgenic mice revealed accelerated amyloid, tau and Lewy body pathology in the AD-LBV animals as compared to the parental strains, suggesting synergistic effects between SNCA, Aβ and tau in promoting pathology [351]. These relationships only strengthen the attractiveness of miR-153 as a potential therapeutic target. Enhancing miR-153 levels would be expected to reduce the expression of two gene products (APP and SNCA) and downstream metabolies (e.g. Aβ peptides) that may have synergistic roles in promoting AD pathology and cognitive decline. An interesting question is whether miR-153 expression might be decreased more substantially in the brains of

AD-LBV patients relative to AD patients. A meaningful follow-up study would measure levels of miR-153 levels in these patients.

miR-101 also targets other gene products or biological pathways with neurodegenerative relevance. A recent study demonstrated that miR-101 is a potent inhibitor of autophagy, the process utilized by cells to degrade cellular material and organelles in lysosomes [322]. In this study, miR-101 inhibited autophagy through negative regulation of gene products implicated in various aspects of autophagy biology: Stathmin/Oncoprotein18 (*STMN1*), Rab5a and ATG4D. Interestingly, autophagy appears to be impaired in AD. Autophagic vesicles have been found to accumulate in dystrophic neurites of the AD brain and in AD animal models [352,353]. Further, acutely inducing autophagy in APP-overproducing cells results in excess Aβ production, suggesting that Aβ may be produced from APP cleavage in the proteolytic environment of the autophagosome [353]. This being the case, enhancing miR-101 levels might be expected to have synergistic effects on Aβ production by inhibiting both APP expression and a cellular process that may promote its production (autophagy). It is important to note that there is conflicting data regarding the role of autophagy in AD; is it protective or pathological [354]? Some studies suggest that autophagy induction protects cells from Aβ neurotoxicity [355]. Others even contradict previous data by suggesting that activation of autophagy decreases APP and Aβ levels [356].

An additional CNS-relevant and validated miR-101 target is ataxin 1 (*ATXN1)* [291,323]. A gain-of-function mutation leading to a polyglutamine (polyQ) tract expansion in *ATXN1* leads to spinocerebellar ataxia type I, a neurodegenerative disorder characterized by ataxia, motor dysfunction and cerebellar Purkinje neuron loss [357]. miR-101 antisense inhibition was shown to enhance the toxicity of polyQ-expanded ATXN1 expression in human cells [323]. A recent genome-wide association study identified *ATXN1* as a SAD candidate gene [358]. Interestingly, loss of *ATXN1*

function has been shown to promote amyloidogenic processing of APP, thereby increasing Aβ production [359]. Therefore, it might be expected that the negative regulatory effect mediated by miR-101 on APP (and therefore Aβ production) might be negated by the opposing effect mediated by *ATXN1* inhibition. However, in the studies presented here, the overall response to miR-101 delivery in U373 cells and primary human fetal brain cultures was a reduction in Aβ levels in the conditioned media.

TargetScan predicts that both miR-101 and miR-153 target the APP paralog, amyloid precursor-like protein 2 (APLP2). This prediction has significant biological implications given the redundancy in function between APP and APLP2. Single gene knockout of either *APP* or *APLP2* results in only a subtle phenotype. But an *APP-APLP2* double gene knock-out is perinatal lethal [360]. The exact function and pathways in which APP and APLP2 serve redundant roles is still unknown but are likely critical for normal CNS development. It is tempting to speculate that miR-101 and miR-153 may target both of these gene products as an evolutionarily conserved mechanism to regulate certain biological pathways in which they both participate. A very recent report has validated the regulatory relationship between miR-153 and APLP2 [361]. Validation of the miR-101 APLP2 target site is still required.

Aside from CNS-relevant functions, both miR-101 and miR-153 have tumor suppressor functions. miR-101 expression is significantly reduced in multiple types of cancers, including prostate [321], colon [362], hepatocellular carcinoma [363], gastric [364], anaplastic large cell lymphoma [365] and lung squamous cell carcinoma [366,367]. Consistent with these findings, functional studies have clearly demonstrated that miR-101 acts as a tumor suppressor by inhibiting expression of the oncogenes *EZH2*, *COX2*, *FOS*, *MYCN* and *MCL-1* [319–321,362–364,368,369]. miR-153 also has low expression in cancer cell lines versus normal tissue [370,371] and overexpression of miR-153 reduces cancer cell line viability [372]. This tumor suppressor activity may

be mediated by inhibitory targeting of anti-apoptotic and pro-survival pathways. Two demonstrated targets of miR-153 in glioblastoma multiforme cell lines include B-cell lymphoma 2 (Bcl-2) and myeloid cell leukemia sequence 1 (Mcl-1), two anti-apoptotic proteins [372]. miR-153 also downregulates insulin receptor substrate 2 (Irs2), thereby inhibiting the pro-survival effect of the PI3K/Akt signaling pathway [373]. In drug-resistant leukemic cancer cells, miR-153 has been shown to be downregulated. Restoring miR-153 levels in these cells was shown to sensitive them to As_2O_3-induced apoptosis [374]. Finally, in an experimental model of pulmonary fibrosis, miR-153 was upregulated, with its pro-apoptotic activity hypothesized to contribute to disease etiology [375].

D. APP expression is stimulated by miR-346 via a non-canonical target site in the APP 5'-UTR

While most miRNA regulatory interactions are limited to the mRNA 3'-UTR [245,303,376] primarily due to the abrogating effect of translation on the efficacy of miRNA target sites [224], there are many reported examples of effective miRNA targeting in the 5'-UTR or CDS [324,325,377–380]. Therefore, the complete APP 3'-UTR sequence was scanned for potential miRNA target sites using the RegRNA web server. A putative target site for miR-346 in the APP 5'-UTR was noted for its exact overlap with a known IRE stem-loop sequence previously shown to regulate APP translation in response to iron homeostasis [143,144]. miR-346 strongly upregulated expression of an APP 5'-UTR reporter and endogenous APP protein in HeLa cells. Site mutagenesis and target protector transfections demonstrated that these effects were mediated by specific interaction with the predicted 5'-UTR target site. This regulatory effect was also observed in primary human fetal brain mixed cultures but only after iron chelation with deferroxamine. Therefore, miR-346 has non-canonical regulatory effects

(stimulation) on APP expression via a non-canonical target site in the APP 5'-UTR. Inhibiting this interaction might be a viable strategy for reducing APP expression and resulting Aβ production in the AD brain.

While the vast majority of validated miRNA:mRNA target interactions involve inhibition of target expression, there are several examples in the literature of stimulatory effects on target expression (for review, see [226]). In fact, Tsai et al. report that miR-346 has a very similar regulatory relationship with receptor interacting protein 140 (RIP140) as that observed here with APP [380]. Specifically, they demonstrated that the *RIP140* 5'-UTR stimulates RIP140 translation and contains a non-canonical miR-346 target site. miR-346 antisense inhibition reduced the stimulatory action of this sequence segment. They further demonstrated that miR-346 directly binds to the *RIP140* 5'-UTR via the predicted target site. Therefore, positive regulation of mRNA targets by miR-346 via 5'-UTR target sites may represent a common mechanism employed by human cells for regulating gene expression.

Other examples of stimulatory miRNA interactions have also been reported. The transition of proliferative HEK293 and HeLa cells to a quiescent state (i.e. G0 state) following serum starvation triggers a switch in the regulatory program for several miRNA:mRNA target interactions from translational repression to translational activation [381]. This phenomenon of switching between repression and activation depending on cell cycle state was observed for interactions between miR-369-3p and *TNFα* 3'-UTR AU-rich element (ARE) and for let-7 and the *HMGA2* 3'-UTR. The activating state requires the interaction of AGO2 with FXR1a [381]. Similarly, in xenopus oocytes (i.e. naturally quiescent cells) miR-16 activates *Myt1* expression by interacting with the 3'-UTR [382]. Upregulation of this kinase maintains the induced quiescent state of the oocyte. miR-466l interacts with an ARE in the *IL-10* 3'-UTR of TLR-triggered macrophages and upregulates IL-10 expression by stabilizing the transcript [383]. The

mechanism of this effect involves the competition of miR-466l with tristetraprolin (TTP), a RNA-binding protein that normally binds the ARE and promotes mRNA degradation. miR-34a and miR-34b-5p bind to the 3'-UTR of an alternatively polyadenylated mouse β-actin transcript and upregulate translation [384]. Finally, many ribosomal protein mRNAs harbor a 5' terminal oligopyrimidine (TOP) motif that mediates inhibitory effects on translation during cell cycle arrest or during nutritional deprivation. miR-10a binds to the 5'-UTR of many of these transcripts downstream of the 5'TOP motif and stimulates translation, a phenomenon with significant implications for global protein synthesis [324]. While miRNA:mRNA interactions that activate expression represent only a small minority of all miRNA:mRNA regulatory interactions, there are clearly a number of precedents for this type of biological function.

Aside from its role in upregulating APP and RIP140 expression, miR-346 has been implicated in other biological pathways. miR-346 inhibits the release of TNFα from synovial cells by stimulating the expression of TTP that binds to the TNFα ARE and promotes mRNA degradation [385]. miR-346 appears to stimulate TTP expression by inhibiting the transcription of Bruton's tyrosine kinase (Btk), perhaps by negatively regulating a transcription factor involved in Btk transcriptional regulation. As a result, miR-346 has been ascribed immunomodulatory functions [385,386]. miR-346 is also overexpressed in follicular thyroid carcinoma [387]. Overexpression of miR-346 induces cell proliferation in human cell lines, suggesting that miR-346 may promote carcinogenesis. An analysis of predicted miRNA:mRNA interactions for schizophrenia-associated gene products revealed that miR-346 contains a higher rate of predicted interactions than expected by chance [388]. miR-346 expression was also found to be decreased in the brains of schizophrenic and bipolar patients relative to control patients. Interestingly, pri-miR-346 is hosted in intron 2 of a known schizophrenia susceptibility gene, glutamate receptor delta 1 subunit (GRID1) [389]. However, expression of miR-

346 appears to be driven independently from GRID1 expression based on miR-346-GRID1 correlation analyses [386,388].

Finally, miR-346 has been implicated in the unfolded protein response (UPR) [386]. This biological pathway is induced under conditions of ER stress that result in accumulation of unfolded proteins in the ER. Activation of this pathway results in the inhibition of global protein production (to reduce ER protein load) and targeted induction of gene expression for products that increase ER protein folding capacity [390]. The expression of miR-346 is increased following the induction of UPR via a mechanism involving transcriptional induction by UPR-linked transcription factor XBP1 [386]. Interestingly, this leads to decreased expression of TAP1 through direct interactions between miR-346 and the *TAP1* 3'-UTR. TAP1 is an ATP-binding cassette transporter that translocates antigens derived from proteasomal processing into the ER lumen for loading onto MHC antigen receptors. miR-346 also decreases MHC class I gene expression via indirect interactions, further implicating miR-346 as an immunomodulatory miRNA.

Neurons in the AD brain are often invested with NFT consisting of aggregated hyperphosphorylated tau protein that might be expected to induce ER stress. Indeed, recent studies suggest that UPR is activated in pretangle neurons [391,392]. Given that UPR is active in the AD brain and that APP expression is elevated following UPR activation [393], it is reasonable to speculate that miR-346 expression may also be induced in certain cells of the AD brain and drive APP expression in pretangle neurons. Future studies investigating the regulatory relationship between miR-346 and APP during UPR are warranted.

E. Mechanism underlying stimulatory effect of miR-346 on APP expression

Mechanisms involved in post-transcriptional miRNA-mediated inhibitory regulation are fairly universal and well described [327]. Generally, AGO2 as a member of the ternary miRISC recruits GW182 to the target transcript promoting further protein interactions that lead to translational inhibition and transcript deadenylation and degradation [227,229,230,237,238,240]. However, mechanisms underlying post-transcriptional miRNA-mediated stimulatory gene regulation are poorly understood and each example may invoke a distinct mechanism involving different mediators and molecular interactions.

To explore the mechanism underlying the stimulatory effect of miR-346 on APP expression, the involvement of proteins implicated in canonical miRNA biogenesis (Dicer) and function (AGO2) was first tested. The stimulatory response of APP to miR-346 was significantly abrogated when expression of either Dicer or AGO2 was knocked down. This is in contrast to RIP140, where AGO2 was dispensable for the stimulatory effect mediated by miR-346 [380]. In this study, AGO2 knockdown almost completely abolished the increase in APP expression following miR-346 delivery, suggesting that AGO2 is required for this effect. Interestingly, AGO2 was originally discovered as a component of a molecular complex involved in translation initiation [394]. This function has since gone largely unexplored. Given the location of the miR-346 target site in the APP 5'-UTR, near the site of ribosome assembly, one possible explanation for the requirement of AGO2 is that it may mediate the stimulatory effect via its functionality in the process of translation initiation. Another possibility (discussed below) is that AGO2 may be required to sterically inhibit interactions between trans-factors and the APP 5'-UTR IRE.

At first glance it seems curious that Dicer depletion reduced APP stimulation following miR-346 delivery since only mature miRNA mimics were transfected (i.e.

downstream of Dicer processing). However, Dicer along with TRBP is a component of the RISC-loading complex (RLC) involved in loading mature miRNA onto AGO proteins [212,395]. In this study, Dicer depletion have may resulted in less efficient loading of miR-346 mimic onto AGO proteins, thereby explaining the effect of Dicer knockdown on APP stimulation. It should be noted that not all studies are in agreement on the role of Dicer as a necessary component for small RNA loading onto AGO proteins [396].

Since the miR-346 target site in the APP 5'-UTR directly overlaps with a known IRE, the hypothesis that miR-346 interferes with normal iron-based regulation of APP expression was next tested. Jack Rogers and colleagues previously demonstrated that the APP 5'-UTR IRE forms a stem-loop structure that binds to IRP1 but not IRP2 [143,144]. IRP1 inhibits APP translation when bound to the 5'-UTR IRE. When iron levels are increased, IRP1 binds free iron and dissociates from the APP mRNA allowing translation to proceed uninhibited. When iron levels are decreased (such as with iron chelation), free iron dissociates from IRP1 allowing IRP1 to bind to the APP 5'-UTR IRE and inhibit APP translation. IRP1 knockdown significantly (but not completely) attenuated the stimulatory effect of miR-346 on APP expression, confirming that functional IRP1 is essential for miR-346 stimulation of APP expression. This strongly supports the hypothesis that miR-346 stimulates APP expression by competing with IRP1 for interaction at the APP 5'-UTR IRE (i.e. relief of repression). A model of this posited interaction is illustrated in Figure 40.

If this hypothesis is correct, one implication is that iron treatment would be expected to reduce the stimulatory effect of miR-346, whereas iron chelation would be expected to augment the stimulatory effect due to enhanced IRP1 association with IRE. Indeed, in primary human fetal brain mixed cultures, miR-346 transfection under normal culture conditions had little effect on APP expression. However, after iron chelation, miR-346 delivery significantly enhanced APP expression. Again, this is consistent with

the hypothesis that miR-346 stimulates APP expression via interactions with IRP1. While this data is highly suggestive, it does not directly confirm the validity of the model presented in Figure 40. Future experiments to confirm that IRP1 interaction with the APP IRE is disrupted by miR-346 delivery and to test whether miR-346 inhibition alters APP expression under conditions of iron treatment or chelation are warranted.

One explanation as to why iron homeostasis might regulate APP levels is that APP has ferroxidase activity [397]. This activity oxidizes ferrous iron (Fe^{2+}), the form that participates in the Fenton reaction producing hydroxyl radicals, to the less toxic ferric form (Fe^{3+}) without producing reactive oxygen species (ROS). Additionally, this ferroxidase activity promotes the export of iron from the cytosol to the extracellular space. Therefore, enhancing APP expression in the presence of elevated iron levels would help to maintain iron homeostasis and prevent oxidative stress. Aside from the role of iron in regulating APP expression, iron is known to accumulate in amyloid plaques of the AD brain [398,399]. Iron binds to Aβ and slows the normal ordered progression of Aβ to higher ordered aggregates, such as fibrils. This altered aggregation process in the presence of iron promotes Aβ toxicity in neuronal cells [400]. Iron bound to Aβ also accelerates the formation of ROS through various redox chemistries resulting in lipid peroxidation and other oxidative insults [401–403]. As such, therapies that modulate iron homeostasis in the AD brain have been proposed as a means of reducing Aβ-associated iron toxicity and reducing APP translation and Aβ production [404,405].

General iron chelation therapy in AD is likely a poor strategy since global effects are likely to arise, such as iron-deficiency anemia. However, metal-complexing agents that have more targeted and less systemic effects on metal ion binding and redistribution have been synthesized and are termed metal-protein attenuating compounds (MPAC) [404,406]. As an example, XH1 is a compound containing both Aβ-

binding moieties and metal chelating moieties that are covalently linked. Therefore, chelating properties of XH1 are targeted to regions where this activity is salutary. XH1 has been shown to reduce APP protein expression in neuronal cells [407].

Based on the results presented in this dissertation, it is reasonable to speculate that therapeutic reduction of intracellular iron in the AD brain as a means to reduce APP translation might be mitigated by endogenous miR-346 expression and its competitive interactions with IRP1 binding at the APP 5'-UTR IRE. Therefore, miR-346 inhibition is likely to synergize with therapeutic strategies to modulate intracellular iron homeostasis as a means to reduce APP translation.

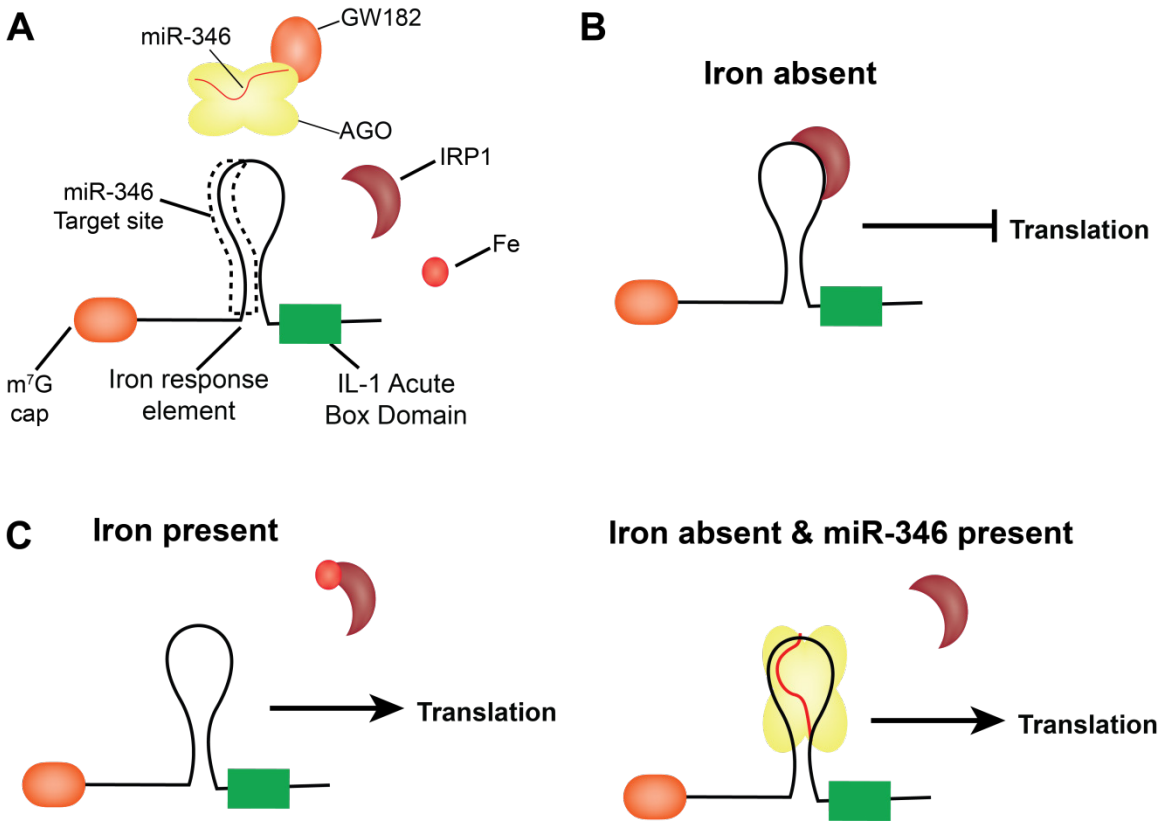

Figure 40: Speculative model of predicted miR-346 interaction with IRP1 in the APP 5'-UTR. (A) Schematic of APP 5'-UTR with the approximate locations of the miR-346 target site and IRE along with other molecular players including miR-346 loaded into RISC, IRP1 and free iron (Fe). (B) In the case when free intracellular iron levels and miR-346 levels are low, IRP1 binds to the IRE and inhibits mRNA translation. (C) When iron is present, IRP1 dissociates from the APP IRE and translation is disinhibited. (D) When iron is absent, IRP1 would normally bind and inhibit translation. But when miR-346 levels are appreciable, its interactionwith the 5'-UTR target site might sterically interfere with IRP1 binding and promote translation.

F. Other APP-targeting miRNA

miR-101, miR-153 and miR-346 are not likely to mediate their regulatory effects on APP expression in isolation. Indeed, regulatory interactions between APP and other miRNA have already been reported (as reviewed in [408,409]). The studies presented in this dissertation focused on miR-101 and miR-153 have been previously published in part [410,411]. Importantly other labs have independently verified the results presented here for miR-101 and miR-153 [361,412,413]. Other miRNAs reported to negatively regulate APP expression include miR-147 [413], the miR-20a family (miR-20a, -17, -106b) [276,338], miR-106a, miR-520c [318], and miR-16 [414]. Some, but not all, of these studies have demonstrated *physiological* regulation of APP expression by these miRNA. The presence of AD-specific SNPs in the APP 3'-UTR has been shown to interfere with the ability of several miRNA to regulate APP expression [413]. Finally, miR-124 has been shown to direct neuron-specific APP mRNA alternative splicing [274]. Apparently human cells utilize an extensive repertoire of miRNA, including miR-101, miR-153 and miR-346, to regulate APP expression and processing. Elucidating this complete network is still an ongoing effort.

II. Novel miRNA interactions with the APP mRNA regulate BACE1 expression

A. The BACE1 3'-UTR inhibits basal expression

The presence of the human BACE1 3'-UTR inhibited reporter expression in three different human cell lines tested, consistent with reports on the mouse BACE1 3'-UTR [415]. This is in contrast to the APP 3'-UTR, which stimulated reporter expression. One possible explanation for the regulatory effect of the BACE1 3'-UTR on reporter expression is the presence of multiple MRE located in the 3'-UTR interacting in a synergistic fashion with endogenously expressed miRNA. The presence of other

inhibitory or stimulatory regulatory elements in the 3'-UTR cannot be ruled out but none have been reported thus far in the literature. An important distinction between the APP 3'-UTR and BACE1 3'-UTR is length. The BACE1 3'-UTR is significantly longer than the APP 3'-UTR (3.9 kb vs 1.2 kb), providing a more expansive UTR workspace upon which favored regulatory interactions between various trans-acting factors (e.g. miRISC) and cis regulatory elements (e.g MRE) may have been molded by evolutionary pressures. Specific mechanism aside, the general integrated response of all regulatory influences directed through the BACE1 3'-UTR in human cells appears to be reduction in transcript translation or stability.

B. BACE1 expression is inhibited by miR-339-5p via target sites in the BACE1 3'-UTR

In silico analyses identified multiple putative miRNA target sites in the BACE1 3'-UTR. Of these predicted interactions, miR-339-5p potently inhibited BACE1 3'-UTR reporter expression. This functional activity of miR-339-5p was mediated via interaction with two poorly conserved target sites in the BACE1 3'-UTR. BACE1 protein levels were dramatically decreased following miR-339-5p transfection in U373 cells and less potently so in primary human fetal brain cultures. Finally, endogenous miR-339-5p regulates basal BACE1 expression in primary human fetal cultures as evidenced by elevated BACE1 expression following target protector transfection. Therefore, miR-339-5p is a putative drug target for AD. Direct miR-339-5p delivery or targeting pathways that elevate expression of endogenous miR-339-5p may represent viable therapeutic strategies.

miR-339-5p has been implicated in other physiological and pathological roles aside from its regulatory effects on BACE1 expression, including hematopoiesis, various cancers and neural tube defects (NTD). More specifically, miR-339-5p expression was shown to vary during the course of *in vitro* erythroid differentiation and

is predicted to target gene products (EpoR and STAT-5) previously implicated in erythroid differentiation [416].

The role of miR-339-5p in cancer is still unsettled and may vary by tissue origin. miR-339-5p expression is significantly upregulated in B-cell precursor acute lymphoblastic leukemia [417]. In contrast, its expression is significantly decreased in highly invasive breast cancer cell lines (MDA-MB-231 and MDA-MB-468) as compared to poorly invasive cell lines (MCF7) [418]. Reduced expression was also observed in breast cancer tissue with lymph node metastasies as compared to breast cancer tissue without node metastases. This study also showed that miR-339-5p had no effect on cell proliferation but that overexpression inhibited breast cancer cell migration while inhibition enhanced migration. This effect may be mediated by the inhibitory effect of miR-339-5p against BCL6. Finally, endogenously expressed miR-339-5p in colorectal cancer cell lines and glioblastoma multiforme cell lines apparently reduces susceptibility of malignant cells to cytolysis by cytotoxic T lymphocytes (CTL) by inhibiting expression of ICAM1 [419,420]. ICAM1 expression in malignant cells is necessary for proper adhesion of CTL to antigen-presenting malignant cells. *In toto*, these studies suggest that miR-339-5p suppresses the malignant potential of transformed cells in some forms of cancer but not necessarily others.

miR-339-5p may play a detrimental role in NTD. A NTD-prone animal model, *Splotch* (*Pax3* -/-), that can be rescued from NTD development by folate supplementation was shown to have reduced expression of a lysine-specific demethylase, KDM6B [421]. Repressed KDM6B expression was shown to inhibit gene expression of several genes essential for normal neural tube formation (*Hes1* and *Neurog2)* by promoting histone methylation at the promoters of these genes. Reduced expression of KDM6B in *Splotch* animals was likely mediated by increased expression of several miRNA, including miR-339-5p, that repressed KDM6B levels via interactions

with its 3'-UTR. Folate supplementation reversed dysregulated miR-339-5p expression, KDM6B expression, promoter methylation and Hes1 and Neurog2 expression in these animals [421].

C. Other BACE1-targeting miRNA

As with APP, there is likely an extensive network of miRNA that act in collaboration with miR-339-5p to modulate BACE1 expression. While the full repertoire has not been elucidated, several BACE1-targeting miRNA have been described in the literature. miR-107 regulates BACE1 expression via interaction with a 3'-UTR target site and is downregulated early in the temporal cortex of the AD brain [266,273]. miR-107 also associates with progranulin (PRGN) mRNA in the RISC complex and downregulates expression via interaction with a target site in the PRGN CDS [325]. This interaction is relevant because mutations in *PRGN* have been previously linked to frontotemporal dementia (FTD) [422,423]. miR-29a/b both downregulate BACE1 expression via 3'-UTR target sites [189], and both have been reported to be downregulated in the AD brain [189,272]. Surprisingly, miR-29b has also been shown to downregulate PRGN expression but via interactions in the 3'-UTR, as compared to the CDS for miR-107 [424]. miR-29c also downregulates BACE1 expression in both cell culture and *in vivo* miR-29c transgenic animal models via a 3'-UTR target site [425]. miR-124 overexpression downregulates BACE1 expression while inhibition elevates BACE1 levels [333]. This finding has significant implications because miR-124 is one of the most abundant neuronal miRNAs and is decreased in the AD brain [265,274]. Additionally, it functions to regulate neuronal APP mRNA splicing as described above [274]. Finally, mouse (mmu) miR-298 and miR-328 also downregulate BACE1 via mouse BACE1 3'-UTR target sites [415].

III. APP and BACE1-targeting miRNA are dysregulated in the AD brain

A. APP and BACE1-targeting miRNA exhibit correlative expression patterns with their target proteins consistent with co-regulation

Experiments in aim 1 and 2 provided strong evidence that miR-101, miR-153, miR-346 and miR-339-5p regulate basal expression of APP or BACE1. Experiments in aim 3 added further evidence that these miRNA are physiologically relevant regulators of APP and BACE1 levels. This was first achieved by analyzing expression levels of miRNAs and APP or BACE1 during *in vitro* development of a human primary fetal brain mixed culture. These experiments demonstrated that the expression pattern of miR-346 and, to a lesser extent, miR-153 correlated with the expression patterns of their APP target in a manner concordant with their expected regulatory effect on expression. Stated alternatively, the data support the supposition that changes in miR-153 and miR-346 levels during *in vitro* development of this culture system aid in driving changes in APP or BACE1 expression.

More specifically, miR-153 levels were highest at a time point in culture (DIV18) when APP levels were lowest. Therefore, it might seem reasonable to hypothesize that miR-153 contributes to the decrease in APP levels at later time points in culture. It is important to note, however, that the correlation coefficient for this analysis was non-significant, as was the trend for increased miR-153 levels across time points. So, while the expression patterns are concordant with miR-153 repression of APP expression, statistical analysis does not support this interpretation. Analysis of miR-153 expression levels across various organs at different developmental time points in relation to another target, SNCA, demonstrated that miR-153 and SNCA were co-expressed rather than inversely expressed [342]. The study concluded that miR-153 was expressed as a component of a feedforward loop to fine-tune SNCA expression rather than completely

block expression. Further experiments would be required to determine whether a similar regulatory relationship exists between miR-153 and APP.

In contrast, miR-346 patterns very similarly mirrored the pattern of APP levels across time in culture. Expression levels across time were significantly different for both miR-346 and APP, with highest levels at DIV 7. Correlation analysis of miR-346 and APP levels produced a non-zero correlation coefficient suggesting co-regulation. Since miR-346 stimulates APP expression, a reasonable hypothesis is that APP levels during culture development may be significantly driven by changes in miR-346 levels with time.

B. APP and BACE1-targeting miRNA are expressed at functionally relevant levels in human brain

Data from aims 1 and 2 demonstrate that miR-101, miR-153 and miR-346 regulate APP levels and miR-339-5p regulates BACE1 levels in multiple human cell cultures. However, for these miRNA to be targeted therapeutically in AD, they must be expressed at relevant levels in the human brain. Therefore, absolute quantification miRNA expression analyses were performed on control specimens from two separate brain specimen cohorts. miR-124 exhibited highest expression levels of all the miRNAs tested. This is consistent with previous studies that have reported miR-124 as either the most abundant miRNA in brain or somewhere among the top ten [225,331,426]. Levels of miR-101 were significantly lower than miR-124 but still expressed at very high levels in the human brain. Global miRNA analyses in the human and rodent brain have also found that miR-101 is among the top 20 most abundant miRNA [225,426–428]. miR-153 levels were lower than miR-101 levels but still present at significantl levels. miR-346 and miR-339-5p levels were significantly lower than miR-153 levels. However, the actual copy counts per cell for each of these miRNA are still likely high enough to mediate regulatory effects. This statement is based upon the fact that expression levels

here were measured in post-mortem brain specimens, where miRNA decay is known to be rapid [255]. Given that PMI were fairly high in some specimens, especially in cohort 2, it is likely that miRNA copy counts in living CNS cells are much higher than detected here.Consistent with the data reported here, studies suggest that miR-346 is highly enriched in the human brain with significantly higher expression than in other tested tissues [429]. Therefore, all miRNA examined were expressed and detectable in the human brain to varying degrees.

The precise level of miRNA expression necessary for functional regulation is likely to vary for each combination of miRNA and mRNA target and their specific environmental context. Titration experiments have demonstrated that miRNA efficacy is influenced both by the levels of target expression as well as miRNA levels, such that target thresholds are generated around which target levels are highly sensitive to miRNA effects [241,242]. However, in some conditions as few as 100 miRNA copies per cell have been reported to be sufficient for repression [242]. By this standard, expression levels of miR-101, miR-153, miR-346 and miR-339-5p in the human brain would be sufficient to mediate their regulatory effects on APP and BACE1 expression. To confirm this would require *in vivo* miRNA inhibition experiments in animal models.

C. APP and BACE1-targeting miRNA are dysregulated in AD brain specimens

Given that miR-101, miR-153, miR-346 and miR-339-5p regulate APP and BACE1 expression and subsequent Aβ production, they might be considered novel drug targets for AD. If their expression is also dysregulated in AD, they represent even more attractive candidates since therapeutic targeting would also correct disease-specific derangements in their expression levels. Therefore, expression analyses for these miRNA were extended to analyze for differential expression in AD samples versus controls. Both absolute and relative quantification schemes were employed to

ensure that normalization strategy did not bias results. Two separate and independent cohorts were analyzed. The first cohort consisted of low PMI specimens from non-demented patients and patients with advanced AD pathology (Braak stage VI). The second cohort consisted of specimens spanning the range of Braak stages (control, Braak stage I/II[early AD], Braak stage III/IV[definite AD], Braak stage V/VI [severe AD]) but with significantly longer PMI on average compared to cohort 1.

Both miR-101 and miR-346 expression levels were significantly decreased in AD specimens compared to control specimens in cohort 1. This trend remained significant when the control specimens were compared among a subset of AD patients that had not been treated with AD therapeutics (NoRx). Also, the trend was observed using both relative and absolute quantification strategies, indicating that the difference could not be explained by normalization bias. Decreased miR-339-5p expression was also observed in AD specimens from this cohort, but only with absolute quantification and not relative quantification strategies.

Interestingly, decreased miR-101 expression in AD specimens is a consistently observed phenomenon, having been reported in three independent microarray-based studies [189,268,430]. On the other hand, to the author's knowledge there are no reports in the literature of differentially expressed miR-346 or miR-339-5p in the AD brain. One potential explanation is that most studies have employed global miRNA analyses that must be statistically corrected for a high number of multiple comparisons. Therefore, the statistical power of these analyses may have been too low to detect the decrease observed here. Alternatively, CNS expression levels of miR-346 and miR-339-5p may be too low to readily detect using probe-based microarray protocols.

Importantly, the finding of decreased miR-346 expression in AD specimens was also observed in independent cohort 2. Surprisingly, no differences in miR-101 or miR-339-5p levels were observed in cohort 2 samples. However, the specimens in this

cohort are very different in that the AD specimens have on average less pathology and were obtained at earlier stages of disease progression than the average AD specimen from cohort 1. Therefore, it may not be reasonable to expect cohort 2 to exactly replicate the expression patterns in cohort 1.

In cohort 2, miR-153 levels were significantly decreased in postmortem brain specimens containing more advanced NFT pathology (Braak stage III – VI) as compared to specimens with none or only mild NFT pathology. Interestingly, APP levels were significantly increased in Braak stage III/IV specimens. This raises the intriguing possibility that the decrease in miR-153 in these specimens may at least partially underlie the elevated APP levels. One might question why dysregulated expression of miR-153 and APP is not represented progressively across Braak stages. One consideration in response is that all these specimens were derived from the frontal cortex (BA9) – a region that only begins to become invested with neurofibrillary pathology (the basis for Braak staging) in stages III and IV of the disease [13]. A second consideration is that changes in miR-153 and APP expression would be expected to contribute to amyloid pathology in the AD brain. The development of amyloid and neurofibrillary pathology do not initially overlap anatomically and do not progress with direct linear correlations between each other in the AD brain [12]. Therefore, one might not expect dysregulation of APP and miR-153 to vary linearly with Braak staging.

This author is not aware of any previous study that has identified miR-153 as being dysregulated in AD. One study specifically measured miR-153 levels in AD brain using a DNA dot blot array but was unable to detect any miR-153 expression in specimens due to low sensitivity [265]. Since most of these studies did not segment brain specimens by severity of NFT pathology (Braak staging), one would not necessarily expect that the decrease in miR-153 expression observed here would be replicated in these studies.

Despite reports of elevated BACE1 expression in AD brain specimens [189,431], no significant differences in BACE1 or APP expression were observed in either cohort. As such, no correlations between miRNA expression and APP or BACE1 expression were present. However, built in redundancies that homeostatically control gene expression are likely to be utilized by cells, especially in chronic pathological conditions like AD, to reduce the impact of changes in any given regulator of gene expression. Given this layer of complexity, it may not be reasonable to expect a simple inverse relationship between miRNA and target expression patterns in the AD specimens analyzed here.

Certain caveats in this analysis should be addressed. First, the sample size here is small (n=5 – 10 per group for cohort 2; n=5 – 15 for cohort 1) and the reliability of the findings would be greatly aided if they were observed in independent cohorts of larger sample size. Second, RNA integrity of some samples in cohort 2 was rather low due to prior processing of specimens, possibly introducing bias into the analysis. However, specimens in the late stage AD categories (Braak stage III – VI) were not preferentially represented among the low RNA integrity extracts. The low integrity extracts also did not demonstrate detectably higher Ct values or lower normalized miR-153 expression values (data not shown). Again, replication of these findings in an independent cohort of low PMI specimens and high RNA quality extracts would address these concerns. It should also be noted that procuring a large sample of high quality, low PMI AD brain tissue spread across Braak stages is a significant challenge. A final caveat is that one cannot rule out that the “dysregulation” of miR-101, miR-346, miR-339-5p and miR-153 along with APP in cohort 2 might be an epiphenomenal manifestation of cell type distribution changes that occurs during the progression of AD. During the course of disease, neurons are lost and astrogliosis results in increased relative numbers of glia to neurons [432]. Therefore, changes at the molecular levels may simply reflect

changes in cell types. However, both APP [433] and miR-153 [342] are more highly expressed in neurons than astrocytes suggesting that the changes observed in cohort 2 cannot be solely explained by changes in cell type distribution. Clarification could be provided by the analysis of miR-101, miR-346, miR-339-5p and miR-153 by in situ hybridization (ISH) and APP by immunohistochemistry (IHC) in sections from specimens across Braak stages. ISH and IHC allows for cellular level resolution of miRNA and protein levels, respectively.

Other studies have profiled miRNA expression in the AD brain [189,265–268,274,276] and in peripheral blood mononuclear cells [269] and identified miRNA that are dysregulated (e.g. miR-107, miR-29a/b, miR-106b, miR-124, etc.) [see [270] for review]. miR-107, miR-29b and miR-124 were all assayed in cohort 1 of this study as well. While all demonstrated a decreasing trend in expression from these AD specimens, these trends were not statistically significant. This either suggests that the sample size in this study was too low to detect true expression changes or that the AD cohorts analyzed here have different underlying molecular etiologies contributing to miRNA dysregulation as those analyzed in earlier studies.

It is important to point out that not all aspects of study design were completely optimal in the brain cohort analyses presented here. Great lengths were taken to obtain cohort samples isolated following short PMI with high quality RNA extracts. Also, both relative and absolute quantification strategies were employed to prevent bias associated with a specific normalization method. These strategies were successful in allowing the detection of statistically significant changes in miRNA expression levels between AD and control specimens. However, these studies were necessarily limited to inter-subject comparisons between control specimens and diseased specimens. A more robust study design would allow for within-subject comparisons between affected and

unaffected regions to normalize for inherent variation in specimen characteristics and PMI.

In an optimally designed study, tissue from the entorhinal cortex (EC) and dentate gyrus (DG) would be analyzed from each subject. The entorhinal cortex is one of the cortical regions first affected in AD, as determined by previous functional imaging and neuropathological observations [12,13,434,435]. Therefore, derangements in miRNA expression that contribute to AD pathogenesis or progression would be expected to occur most significantly and at the earliest time points in the EC. In comparison, the DG exhibits age-dependent decreases in functionality with age but, unlike the EC, is relatively spared functional deficits and pathological abnormalities associated with AD [4]. Importantly, the EC and DG share the same vascular supply and should experience the same levels of hypoperfusion or oxygen deficit that occur immediately prior to and after death. Given that the physiological changes associated with death can dramatically alter gene expression and are highly variable depending on the cause death, within-subject comparisons of differential gene expression in the EC versus the DG would be most likely to discriminate betwen true miRNA expression changes associated with AD from noise accompanying the death process. Such approaches have been successfully used in microarray studies of differential mRNA expression in AD [436,437]. A two-way mixed model ANOVA to identify miRNA expression changes differentially expressed in EC relative to DG specific to AD-derived specimens could then be implemented.

IV. Special considerations for therapeutically targeting miR-101, miR-153, miR-346 and miR-339-5p in AD

The results of this dissertation suggest that miR-101, miR-153, miR-346 and miR-339-5p represent novel targets for the therapeutic modulation of APP, BACE1 and

Aβ levels in AD. These are especially attractive candidates given that their levels are decreased in at least a subset of AD patients. Assuming that this decrease is pathological and not compensatory, modulating their levels would produce salutary effects not only on Aβ but also on other mRNA targets whose levels might be deranged as a result. Prior to pursuing therapeutic modulation of any of these miRNA, validation of beneficial effects on AD-like pathology or cognition in appropriate AD animal models would be instructive.

An important consideration when manipulating miRNA levels is that miRNA targeting can be quite promiscuous (i.e. hundreds of predicted targets for each miRNA). This might be seen as both a negative and positive attribute from the perspective of miRNA therapeutics. miRNA level manipulation might produce unanticipated side effects resulting from regulatory actions on gene products outside of AD-implicated biological pathways. However, recent studies suggest that many predicted miRNA target sites may not be physiologically active and instead interact with and competitively sequester away miRNA from *bona fide* targets [246,247,438]. Further, a majority of miRNA:mRNA interactions lead to only subtle effects of protein output [245]. Therefore, the extent of unwanted effects resulting from miRNA promiscuity may not be as extensive as first appears based on the number of predicted interactions. miRNA level manipulation might also produce synergistic salutary effects if multiple gene products implicated in the same biological pathway or pathological process are targeted by a given miRNA either by chance or as a result of evolutionary pressures. In this case, therapeutically modulating the levels of a single miRNA may have more profound disease-antagonizing effects than miRNA targeting a single transcript. Potential examples of this scenario have been highlighted above, such as miR-153 targeting both APP and SNCA or miR-101 targeting both APP and autophagy pathways.

An analysis of predicted transcript targets of miR-101 listed in Table 9 revealed many targets with sites more favorable than the miR-101 site in APP. This list may at first glance suggest that miR-101 off-targeting effects would be too great for therapeutic manipulation. However, among these targets included tumor suppressor genes, autophagy genes and genes involved in neurodegenerative processes. For these specific targets, therapeutically elevating miR-101 expression might be expected to have synergistic effects on amyloidogenic processing of APP. Therefore, the anticipated results of therapeutically modulating miRNA expression cannot be assumed by default to be deleterious. Instead, careful observation of phenotypic changes in animal models following therapeutic modulation would be necessary to discriminate deleterious versus beneficial outcomes of off-target effects.

Strategies that increase intracellular levels of miR-101, miR-153 and miR-339-5p and that decrease levels of miR-346 or inhibit miR-346 interaction with the APP transcript in the human brain would be necessary to decrease APP or BACE 1 levels. Combining miR-346 inhibition with MPAC therapy would also be expected to have more robust APP-modulating effects, as described above. Direct delivery of miRNA mimics, antisense miRNA inhibitors or miRNA target protectors into cells is one strategy. Direct delivery of these therapeutics by systemic injection can be achieved for organ systems such as the liver [439], heart [440] and lungs [441] where parenchymal cells are in close communication with the systemic blood circulation. Modifications that stabilize the oligonucleotides in circulation (e.g. 2'O-methyl modifications, phosphothiorate linkages, locked nucleic acids (LNA), peptide nucleic acids) or promote cellular uptake (e.g. cholesterol conjugation) are generally employed [438,442,443]. As an example, liver-expressed miR-122 promotes hepatitis C virus (HCV) RNA replication and its accumulation in hepatocytes [444]. This has been exploited therapeutically to reduce HCV viral load in infected chimpanzees by inhibiting miR-122 with intravenously

injected LNA antisense inhibitors [445,446]. This LNA-based anti-HCV therapeutic (miravirsen) is now being developed for use in humans and is the first miRNA-based therapeutic to enter clinical trials (ClinicalTrials.gov). Other strategies for delivering miRNA mimics or inhibitors in the periphery include loaded nanoparticles [447,448] and transgene-expressing viral particles [449,450], among others.

Delivery of oligonucleotide-based therapeutics to the CNS remains difficult because few viable strategies have been devised to effectively mobilize the molecule across the blood-brain barrier (BBB). This would remain the biggest impediment to any attempt to modulate levels of miR-101, miR-153, miR-346 or miR-339-5p therapeutically in AD. Most methods for delivery in the brain experimentally require direct intracranial injection, either as synthetic nucleotides [414] or transgene-expressing viral particles [451]. A recent, innovative strategy employs dendritic cell-derived exosomoes engineered to express Lamp2b-rabies virus glycoprotein (RVG) fusion protein [194]. The exosome preparation is then loaded with small RNA molecules by electroporation, followed by systemic intravenous administration in mouse. The RVG peptide directs the exosome across the BBB with specific uptake by CNS neurons [194]. This study demonstrated that BACE1 expression was specifically knocked down in the mouse brain following systemic administration of BACE1 siRNA-loaded exosomes [194]. Such a strategy might be pursued for delivery of miRNA therapeutics in the human CNS.

An alternative strategy for modulating miR-101, miR-153, miR-346 and miR-339-5p activity is to identify small molecules that either inhibit or augment specific miRNA function, either by altering expression or otherwise modifying biological behavior. Of course, this is not a straightforward proposition and rational design of small molecules for this purpose may be impossible. Recent high throughput screening approaches have identified small molecules from large libraries that do exhibit miRNA

modulating properties [452,453]. Additionally, two recent studies have demonstrated that treating transformed cell lines with chromatin-modifying drugs can induce miR-153 expression by demethylating the miR-153 promoter and promoting histone acetylation [373,454]. How these manipulations would translate to neurons, where miR-153 expression is relatively high and chromatin structure might already favor transcription, is yet to be determined. Regardless of application to neurons, these studies demonstrate proof-of-principle for modifying miR-153 and potentially other miRNA therapeutically by small molecules.

CHAPTER 5: FUTURE DIRECTIONS

While the results presented here are compelling, functional data are restricted to the *in vitro* setting. Several future studies are therefore essential for further evaluating the therapeutic suitability of miR-101, miR-153, miR-346 and miR-339-5p in AD. These experiments would explore the effect of manipulating miRNA levels in AD animal models. Appropriate AD animal models for these experiments must fulfill certain criteria. First, the animal models must obviously replicate aspects of AD pathology. Second, the animal models would ideally express human forms of APP and BACE1 mRNA, since some target sites identified above are poorly conserved across species (e.g. miR-346 target site in APP 5'-UTR and miR-339-5p target sites in BACE1 3'-UTR). Finally, the animal models should express the full length transcripts so that 5'-UTR and 3'-UTR miRNA target sites are expressed. Most AD transgenic mouse models primarily employ overexpression of mutant human APP (hAPP), mutant human presenilin, mutant human tau or a combination thereof. Most also do not express full-length hAPP cDNA [455,456]. Therefore, the most commonly used AD animal models would not be appropriate for testing the therapeutic suitability of miR-101, miR-153, miR-346 and miR-339-5p.

An appropriate AD model for testing *in vivo* modulation of miR-101, miR-153 and miR-346 is the R1.40 model. This model was created by genomic integration of a yeast artificial chromosome encoding the complete hAPP gene sequence containing the FAD Swedish mutation, plus large tracts of flanking DNA on either side of the hAPP gene [457]. Crucially, this model overexpresses full-length APP transcripts, including the 5'-UTR and 3'-UTR, and is driven by the natural human APP promoter. Therefore, this model would allow for direct assessment of miRNA modulation on hAPP expression. Due to the presence of the Swedish mutation, these animals preferentially produce Aβ42 at high levels and develop cortical neuritic plaques and dystrophic

neurites that exhibit some degree of tau hyperphosphorylation [457]. These animals also exhibit deficits in long-term retention memory and working memory that correlates with the levels of Aβ pathology [459]. Therefore, all criteria are fulfilled by this model system.

For testing miR-339-5p modulation of BACE1 expression *in vivo*, a bacterial artificial chromosome transgenic has been created that contains the complete human BACE1 gene and large flanking regions [460]. When crossed with Tg2576 mice, the resulting mice demonstrate enhanced AD pathology. Therefore, this animal could be potentially used as a model system for testing therapeutic modulation of miR-339-5p.

Experiments utilizing these animal models would test for corrections of AD pathology and cognitive deficits following delivery of miRNA mimics or inhibitors. Methods for delivery have been described above and include direct intracranial injection of synthetic molecules, transgene-expressing viral particles, loaded nanoparticles, or neutral lipid emulsions and systemic, intravenous injection of miRNA-loaded exosomes engineered for CNS delivery. Following delivery, brain specimens would be analyzed for changes in APP or BACE1 expression and the extent of AD-like pathology. Improvements in cognitive functioning could also be tested using behavioral paradigms, such as the spontaneous alteration Y-maze test and Morris water maze, as previously described [459].

CHAPTER 6: SUMMARY

This dissertation tested the hypothesis that miRNA are relevant regulators of APP and BACE1 expression. The results demonstrate that miR-101, miR-153 and miR-346 regulate APP expression in cultured cells from the fetal human brain by interacting with specific sites in the APP 5'-UTR and 3'-UTR. For miR-101 and miR-153, this effect on APP expression modulates Aβ production. While miR-101 and miR-153 inhibit APP expression, miR-346 stimulates APP expression through a mechanism that may involve competition with components of the iron regulatory system. This work also demonstrates that miR-339-5p regulates BACE1 expression via specific sites in the BACE1 3'-UTR and is expected to modulate Aβ production. Expression levels of miR-153 and miR-346 co-vary with their target, APP, during the course of *in vitro* development of primary human brain cultures, suggesting co-regulation. miR-101, miR-153, miR-346 and miR-339-5p are all expressed to varying degrees in the human brain, with miR-101, miR-346 and miR-153 dysregulated in the AD brain at different stages of the disease. Based on their Aβ-modulating properties, these miRNA might be viable AD drug targets, with miR-101, miR-153 and miR-346 especially attractive based on dysregulated levels in the AD brain. In the future, a series of feasible experiments in relevant AD animal models should further clarify the suitability of miR-101, miR-153, miR-346 and miR-339-5p as *bona fide* therapeutic targets.

APPENDIX

Immunocytochemical characterization of primary human fetal brain cultures

Note: Most of the experimentation described in this appendix was performed by Dr. Ray Balmiki, with additional data analysis provided by the author.

Method

Human fetal brain cultures were fixed in 4% paraformaldehyde for 15 minutes, washed three times with chilled PBS, and then permeabilized with 0.12% Triton X-100 (Sigma-Aldrich, St Louis, MO) for 10 minutes. Permeabilized cells were blocked with 10% horse serum for 15 minutes followed by overnight incubation with primary antibodies.

Primary antibodies used in this study include a mouse pan-neuronal antibody cocktail (Millipore) active against neurites, neuronal nuclei and neuronal cell bodies, rabbit anti-GFAP (Sigma-Aldrich, St Louis, MO) for astrocyte labeling, and rabbit anti-nestin (Sigma-Aldrich, St Louis, MO) for neural stem cell labeling. Cells were incubated for 1 hr in secondary antibodies: biotin-conjugated donkey anti-mouse (Jackson ImmunoResearch, West Grove, PA) and Cy3-conjugated donkey anti-rabbit (Jackson ImmunoResearch, West Grove, PA). Fluorescein-conjugated streptavidin (Jackson ImmunoResearch, West Grove, PA) was employed to label biotin-conjugated secondary antibody. Nuclei were visualized using Hoechst stain (Sigma-Aldrich, St Louis, MO) and labeled cells were examined under a Leica DMIL HC inverted fluorescence microscope (Leica Microsystems, Germany). Images were captured using a SPOT RT-SE digital camera (SPOT Imaging, Sterling Heights, MI).

Results

To better characterize the distribution of cellular phenotypes in primary human fetal brain cultures, cells were fixed at specific time intervals during culture ranging from day *in vitro* (DIV) 8 to DIV 24. One set of cells was co-labeled with the combination of a pan-neuronal antibody cocktail designed to label neurites, cell soma and nucleus and anti-GFAP. A second set was co-labeled with anti-nestin and anti-GFAP.

Early cultures (i.e. DIV 8) consisted almost entirely of cells co-expressing GFAP, nestin and neuronal markers (Figure A1 and A2). Later stage cultures (e.g. DIV 20) consisted of a mixture of cells. Some cells co-expressed GFAP and neuronal markers (Figure A1) or GFAP and nestin (Figure A2). Other cells expressed only neuronal markers, GFAP or nestin.

Given that radial glia represent the predominant neural stem cell in the developing human cortex [461] and that nestin is a known marker of neural stem cells [462], the late stage culture likely contains a mixture of immature neural stem cells (GFAP-, nestin-, and neuronal marker-positive) and differentiated neurons and astrocytes (positive for a single marker). The persistence of neural stem cells in the culture might be explained by the maintenance of bFGF in the medium throughout culture. A previous study has also described a similar mixture of cultured cells derived from human fetal brain parenchyma [463]. Importantly, this primary human fetal brain culture closely mimics the *in vivo* fetal brain cellular network.

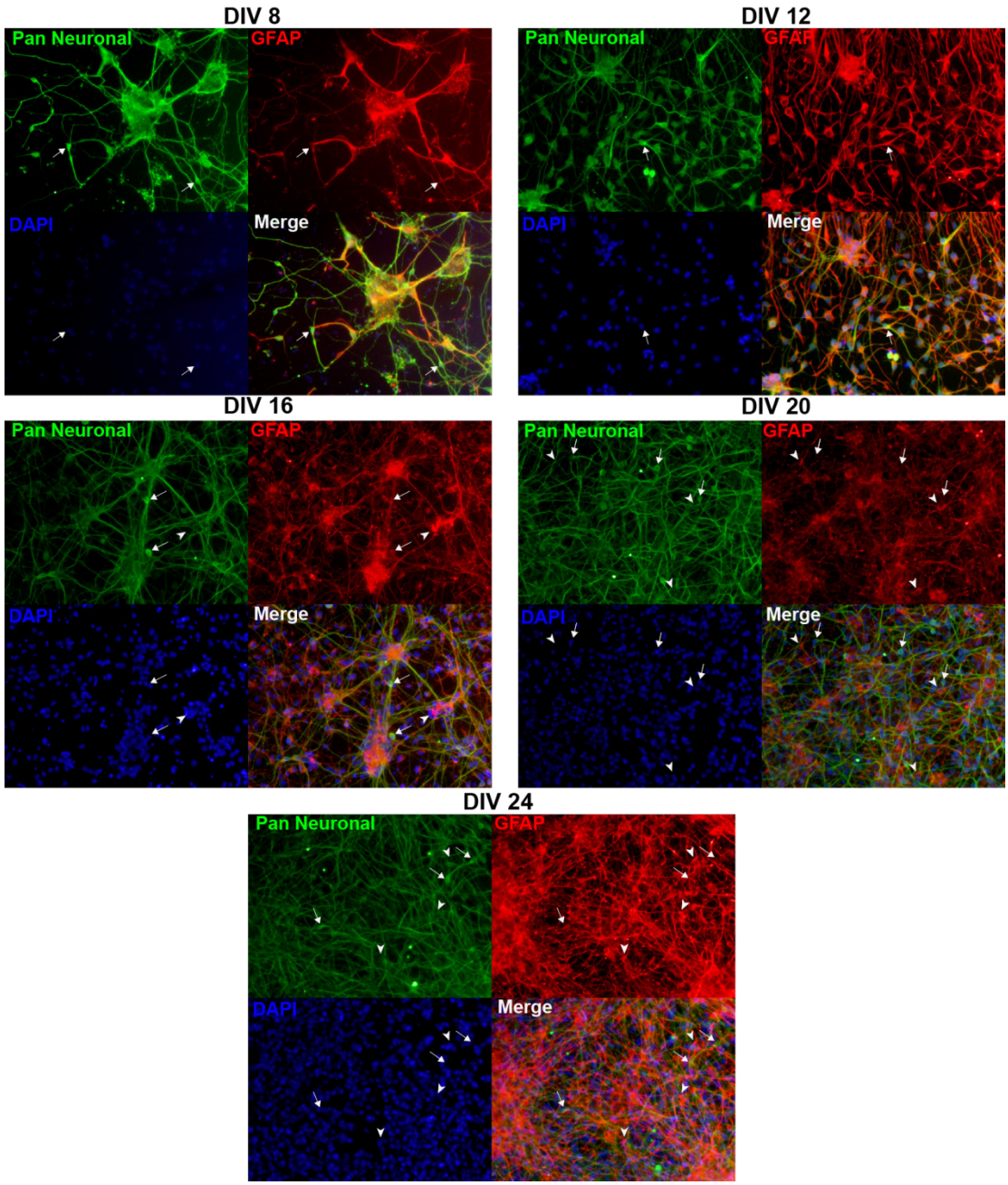

Figure A1: Immunocytochemical characterization of neuronal and glial markers in human primary fetal brain cultures during *in vitro* development. Primary human fetal brain cultures at DIV 8 to DIV 24 following continuous bFGF exposure were co-labeled with a pan-neuronal antibody cocktail and anti-GFAP Arrows point to cells only labeled with the pan neuronal cocktail. Arrowheads point to cells only labeled by anti-GFAP.

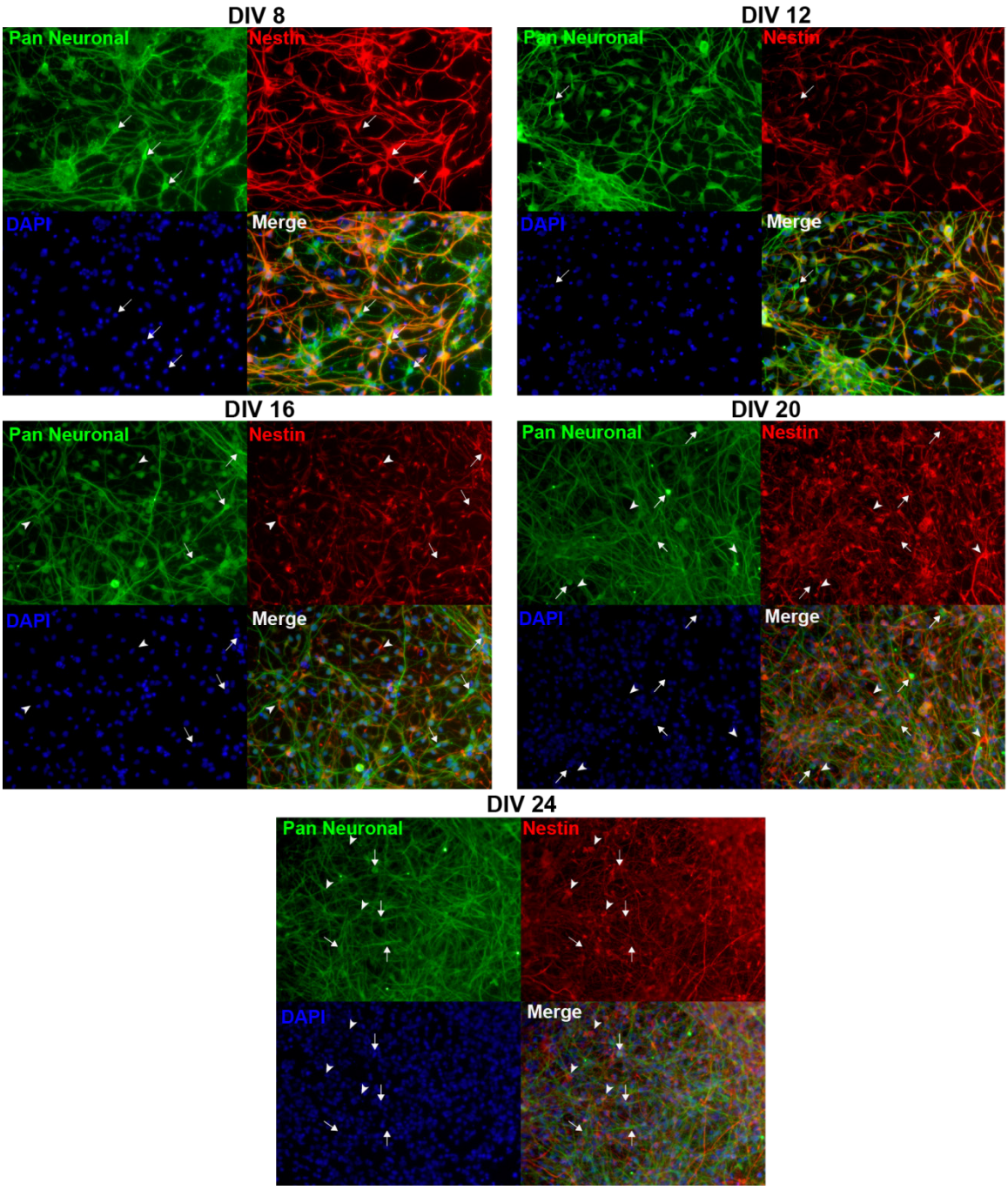

Figure A2: Immunocytochemical characterization of neuronal and neuroprogenitor markers in human primary fetal brain cultures during *in vitro* development. Primary human fetal brain cultures at DIV 8 to DIV 24 following continuous bFGF exposure were co-labeled with a pan-neuronal antibody cocktail and

anti-nestin Arrows point to cells only labeled with the pan neuronal cocktail. Arrowheads point to cells only labeled by anti-nestin.

REFERENCES

[1] Alzheimer's Association 2012 Alzheimer's disease facts and figures. *Alzheimers Dement* **2012**, *8*, 131–168.

[2] Hebert, L. E.; Scherr, P. A.; Bienias, J. L.; Bennett, D. A.; Evans, D. A. Alzheimer disease in the US population: prevalence estimates using the 2000 census. *Archives of Neurology* **2003**, *60*, 1119.

[3] Mayeux, R. Clinical practice. Early Alzheimer's disease. *N. Engl. J. Med.* **2010**, *362*, 2194–2201.

[4] Ballard, C. G.; Bannister, C.; Oyebode, F. Depression in dementia sufferers. *Int. J. Geriatr. Psychiatry* **1996**, *11*, 507–515.

[5] Robins Wahlin, T.-B.; Byrne, G. J. Personality changes in Alzheimer's disease: a systematic review. *Int J Geriatr Psychiatry* **2011**, *26*, 1019–1029.

[6] Mitchell, S. L.; Teno, J. M.; Kiely, D. K.; Shaffer, M. L.; Jones, R. N.; Prigerson, H. G.; Volicer, L.; Givens, J. L.; Hamel, M. B. The clinical course of advanced dementia. *N. Engl. J. Med.* **2009**, *361*, 1529–1538.

[7] Larson, E. B.; Shadlen, M.-F.; Wang, L.; McCormick, W. C.; Bowen, J. D.; Teri, L.; Kukull, W. A. Survival after initial diagnosis of Alzheimer disease. *Ann. Intern. Med.* **2004**, *140*, 501–509.

[8] Helzner, E. P.; Scarmeas, N.; Cosentino, S.; Tang, M. X.; Schupf, N.; Stern, Y. Survival in Alzheimer disease: a multiethnic, population-based study of incident cases. *Neurology* **2008**, *71*, 1489–1495.

[9] Alzheimer, A.; Stelzmann, R. A.; Schnitzlein, H. N.; Murtagh, F. R. An English translation of Alzheimer's 1907 paper, "Uber eine eigenartige Erkankung der Hirnrinde."*Clin Anat* **1995**, *8*, 429–431.

[10] Glenner, G. G.; Wong, C. W. Alzheimer's disease: initial report of the purification and characterization of a novel cerebrovascular amyloid protein. *Biochem. Biophys. Res. Commun.* **1984**, *120*, 885–890.

[11] Bancher, C.; Brunner, C.; Lassmann, H.; Budka, H.; Jellinger, K.; Wiche, G.; Seitelberger, F.; Grundke-Iqbal, I.; Iqbal, K.; Wisniewski, H. M. Accumulation of abnormally phosphorylated tau precedes the formation of neurofibrillary tangles in Alzheimer's disease. *Brain Res.* **1989**, *477*, 90–99.

[12] Nelson, P. T.; Braak, H.; Markesbery, W. R. Neuropathology and cognitive impairment in Alzheimer disease: a complex but coherent relationship. *J. Neuropathol. Exp. Neurol.* **2009**, *68*, 1–14.

[13] Braak, H.; Braak, E. Neuropathological stageing of Alzheimer-related changes. *Acta Neuropathol.* **1991**, *82*, 239–259.

[14] Squire, L. R.; Stark, C. E. L.; Clark, R. E. The medial temporal lobe. *Annu. Rev. Neurosci.* **2004**, *27*, 279–306.

[15] Thal, D. R.; Rüb, U.; Orantes, M.; Braak, H. Phases of A beta-deposition in the human brain and its relevance for the development of AD. *Neurology* **2002**, *58*, 1791–1800.

[16] Terry, R. D.; Masliah, E.; Salmon, D. P.; Butters, N.; DeTeresa, R.; Hill, R.; Hansen, L. A.; Katzman, R. Physical basis of cognitive alterations in Alzheimer's disease: synapse loss is the major correlate of cognitive impairment. *Ann. Neurol.* **1991**, *30*, 572–580.

[17] Davies, P.; Maloney, A. J. Selective loss of central cholinergic neurons in Alzheimer's disease. *Lancet* **1976**, *2*, 1403.

[18] Francis, P. T.; Palmer, A. M.; Snape, M.; Wilcock, G. K. The cholinergic hypothesis of Alzheimer's disease: a review of progress. *J. Neurol. Neurosurg. Psychiatr.* **1999**, *66*, 137–147.

[19] Colom, L. V.; Castaneda, M. T.; Hernandez, S.; Perry, G.; Jaime, S.; Touhami, A. Intrahippocampal amyloid-β (1-40) injections injure medial septal neurons in rats. *Curr Alzheimer Res* **2011**, *8*, 832–840.

[20] Trojanowski, J. Q.; Vandeerstichele, H.; Korecka, M.; Clark, C. M.; Aisen, P. S.; Petersen, R. C.; Blennow, K.; Soares, H.; Simon, A.; Lewczuk, P.; Dean, R.; Siemers, E.; Potter, W. Z.; Weiner, M. W.; Jack, C. R., Jr; Jagust, W.; Toga, A. W.; Lee, V. M.-Y.; Shaw, L. M. Update on the biomarker core of the Alzheimer's Disease Neuroimaging Initiative subjects. *Alzheimers Dement* **2010**, *6*, 230–238.

[21] Risacher, S. L.; Shen, L.; West, J. D.; Kim, S.; McDonald, B. C.; Beckett, L. A.; Harvey, D. J.; Jack, C. R., Jr; Weiner, M. W.; Saykin, A. J. Longitudinal MRI atrophy biomarkers: relationship to conversion in the ADNI cohort. *Neurobiol. Aging* **2010**, *31*, 1401–1418.

[22] Saykin, A. J.; Shen, L.; Foroud, T. M.; Potkin, S. G.; Swaminathan, S.; Kim, S.; Risacher, S. L.; Nho, K.; Huentelman, M. J.; Craig, D. W.; Thompson, P. M.; Stein, J. L.; Moore, J. H.; Farrer, L. A.; Green, R. C.; Bertram, L.; Jack, C. R.; Weiner, M. W. Alzheimer's Disease Neuroimaging Initiative biomarkers as quantitative phenotypes: Genetics core aims, progress, and plans. *Alzheimers Dement* **2010**, *6*, 265–73.

[23] Hampel, H.; Frank, R.; Broich, K.; Teipel, S. J.; Katz, R. G.; Hardy, J.; Herholz, K.; Bokde, A. L. W.; Jessen, F.; Hoessler, Y. C.; Sanhai, W. R.; Zetterberg, H.; Woodcock, J.; Blennow, K. Biomarkers for Alzheimer's disease: academic, industry and regulatory perspectives. *Nat Rev Drug Discov* **2010**, *9*, 560–574.

[24] Albert, M. S.; DeKosky, S. T.; Dickson, D.; Dubois, B.; Feldman, H. H.; Fox, N. C.; Gamst, A.; Holtzman, D. M.; Jagust, W. J.; Petersen, R. C.; Snyder, P. J.; Carrillo, M. C.; Thies, B.; Phelps, C. H. The diagnosis of mild cognitive impairment due to Alzheimer's disease: recommendations from the National Institute on Aging-Alzheimer's Association workgroups on diagnostic guidelines for Alzheimer's disease. *Alzheimers Dement* **2011**, *7*, 270–279.

[25] Tschanz, J. T.; Welsh-Bohmer, K. A.; Lyketsos, C. G.; Corcoran, C.; Green, R. C.; Hayden, K.; Norton, M. C.; Zandi, P. P.; Toone, L.; West, N. A.; Breitner, J. C. S. Conversion to dementia from mild cognitive disorder: the Cache County Study. *Neurology* **2006**, *67*, 229–234.

[26] Hardy, J. A.; Higgins, G. A. Alzheimer's disease: the amyloid cascade hypothesis. *Science* **1992**, *256*, 184–5.

[27] Hardy, J.; Selkoe, D. J. The amyloid hypothesis of Alzheimer's disease: progress and problems on the road to therapeutics. *Science* **2002**, *297*, 353–356.

[28] Querfurth, H. W.; LaFerla, F. M. Alzheimer's disease. *N Engl J Med* **2010**, *362*, 329–44.

[29] Sambamurti, K.; Suram, A.; Venugopal, C.; Prakasam, A.; Zhou, Y.; Lahiri, D. K.; Greig, N. H. A partial failure of membrane protein turnover may cause Alzheimer's disease: a new hypothesis. *Curr Alzheimer Res* **2006**, *3*, 81–90.

[30] Rumble, B.; Retallack, R.; Hilbich, C.; Simms, G.; Multhaup, G.; Martins, R.; Hockey, A.; Montgomery, P.; Beyreuther, K.; Masters, C. L. Amyloid A4 protein and its precursor in Down's syndrome and Alzheimer's disease. *N. Engl. J. Med.* **1989**, *320*, 1446–1452.

[31] Portelius, E.; Bogdanovic, N.; Gustavsson, M. K.; Volkmann, I.; Brinkmalm, G.; Zetterberg, H.; Winblad, B.; Blennow, K. Mass spectrometric characterization of brain amyloid beta isoform signatures in familial and sporadic Alzheimer's disease. *Acta Neuropathol.* **2010**, *120*, 185–193.

[32] Tanzi, R. E.; Bertram, L. Twenty years of the Alzheimer's disease amyloid hypothesis: a genetic perspective. *Cell* **2005**, *120*, 545–55.

[33] Bentahir, M.; Nyabi, O.; Verhamme, J.; Tolia, A.; Horré, K.; Wiltfang, J.; Esselmann, H.; De Strooper, B. Presenilin clinical mutations can affect gamma-secretase activity by different mechanisms. *J. Neurochem.* **2006**, *96*, 732–742.

[34] Kumar-Singh, S.; Theuns, J.; Van Broeck, B.; Pirici, D.; Vennekens, K.; Corsmit, E.; Cruts, M.; Dermaut, B.; Wang, R.; Van Broeckhoven, C. Mean age-of-onset of familial alzheimer disease caused by presenilin mutations correlates with both increased Abeta42 and decreased Abeta40. *Hum. Mutat.* **2006**, *27*, 686–695.

[35] Citron, M.; Oltersdorf, T.; Haass, C.; McConlogue, L.; Hung, A. Y.; Seubert, P.; Vigo-Pelfrey, C.; Lieberburg, I.; Selkoe, D. J. Mutation of the beta-amyloid precursor protein in familial Alzheimer's disease increases beta-protein production. *Nature* **1992**, *360*, 672–674.

[36] Suzuki, N.; Cheung, T. T.; Cai, X. D.; Odaka, A.; Otvos, L., Jr; Eckman, C.; Golde, T. E.; Younkin, S. G. An increased percentage of long amyloid beta protein secreted by familial amyloid beta protein precursor (beta APP717) mutants. *Science* **1994**, *264*, 1336–1340.

[37] Lahiri, D. K.; Maloney, B.; Zawia, N. H. The LEARn model: an epigenetic explanation for idiopathic neurobiological diseases. *Mol. Psychiatry* **2009**, *14*, 992–1003.

[38] Gatz, M.; Reynolds, C. A.; Fratiglioni, L.; Johansson, B.; Mortimer, J. A.; Berg, S.; Fiske, A.; Pedersen, N. L. Role of genes and environments for explaining Alzheimer disease. *Arch. Gen. Psychiatry* **2006**, *63*, 168–174.

[39] Yang, L.-B.; Lindholm, K.; Yan, R.; Citron, M.; Xia, W.; Yang, X.-L.; Beach, T.; Sue, L.; Wong, P.; Price, D.; Li, R.; Shen, Y. Elevated beta-secretase expression and enzymatic activity detected in sporadic Alzheimer disease. *Nat. Med.* **2003**, *9*, 3–4.

[40] Holsinger, R. M. D.; McLean, C. A.; Beyreuther, K.; Masters, C. L.; Evin, G. Increased expression of the amyloid precursor beta-secretase in Alzheimer's disease. *Ann. Neurol.* **2002**, *51*, 783–786.

[41] Castellano, J. M.; Kim, J.; Stewart, F. R.; Jiang, H.; DeMattos, R. B.; Patterson, B. W.; Fagan, A. M.; Morris, J. C.; Mawuenyega, K. G.; Cruchaga, C.; Goate, A. M.; Bales, K. R.; Paul, S. M.; Bateman, R. J.; Holtzman, D. M. Human apoE isoforms differentially regulate brain amyloid-β peptide clearance. *Sci Transl Med* **2011**, *3*, 89ra57.

[42] Strittmatter, W. J.; Saunders, A. M.; Schmechel, D.; Pericak-Vance, M.; Enghild, J.; Salvesen, G. S.; Roses, A. D. Apolipoprotein E: high-avidity binding to beta-amyloid and increased frequency of type 4 allele in late-onset familial Alzheimer disease. *Proc. Natl. Acad. Sci. U.S.A.* **1993**, *90*, 1977–1981.

[43] Jiang, Q.; Lee, C. Y. D.; Mandrekar, S.; Wilkinson, B.; Cramer, P.; Zelcer, N.; Mann, K.; Lamb, B.; Willson, T. M.; Collins, J. L.; Richardson, J. C.; Smith, J. D.; Comery, T. A.; Riddell, D.; Holtzman, D. M.; Tontonoz, P.; Landreth, G. E. ApoE promotes the proteolytic degradation of Abeta. *Neuron* **2008**, *58*, 681–693.

[44] Harold, D.; Abraham, R.; Hollingworth, P.; Sims, R.; Gerrish, A.; Hamshere, M. L.; Pahwa, J. S.; Moskvina, V.; Dowzell, K.; Williams, A.; Jones, N.; Thomas, C.; Stretton, A.; Morgan, A. R.; Lovestone, S.; Powell, J.; Proitsi, P.; Lupton, M. K.; Brayne, C.; Rubinsztein, D. C.; Gill, M.; Lawlor, B.; Lynch, A.; Morgan, K.; Brown, K. S.; Passmore, P. A.; Craig, D.; McGuinness, B.; Todd, S.; Holmes, C.; Mann, D.; Smith, A. D.; Love, S.; Kehoe, P. G.; Hardy, J.; Mead, S.; Fox, N.; Rossor, M.; Collinge, J.; Maier, W.; Jessen, F.; Schürmann, B.; van den Bussche, H.; Heuser, I.; Kornhuber, J.; Wiltfang, J.; Dichgans, M.; Frölich, L.; Hampel, H.; Hüll, M.; Rujescu, D.; Goate, A. M.; Kauwe, J. S. K.; Cruchaga, C.; Nowotny, P.; Morris, J. C.; Mayo, K.; Sleegers, K.; Bettens, K.; Engelborghs, S.; De Deyn, P. P.; Van Broeckhoven, C.; Livingston, G.; Bass, N. J.; Gurling, H.; McQuillin, A.; Gwilliam, R.; Deloukas, P.; Al-Chalabi, A.; Shaw, C. E.; Tsolaki, M.; Singleton, A. B.; Guerreiro, R.; Mühleisen, T. W.; Nöthen, M. M.; Moebus, S.; Jöckel, K.-H.; Klopp, N.; Wichmann, H.-E.; Carrasquillo, M. M.; Pankratz, V. S.; Younkin, S. G.; Holmans, P. A.; O'Donovan, M.; Owen, M. J.; Williams, J. Genome-wide association study identifies variants at CLU and PICALM associated with Alzheimer's disease. *Nat. Genet.* **2009**, *41*, 1088–1093.

[45] Lambert, J.-C.; Heath, S.; Even, G.; Campion, D.; Sleegers, K.; Hiltunen, M.; Combarros, O.; Zelenika, D.; Bullido, M. J.; Tavernier, B.; Letenneur, L.; Bettens, K.; Berr, C.; Pasquier, F.; Fiévet, N.; Barberger-Gateau, P.; Engelborghs, S.; De Deyn, P.; Mateo, I.; Franck, A.; Helisalmi, S.; Porcellini, E.; Hanon, O.; de Pancorbo, M. M.; Lendon, C.; Dufouil, C.; Jaillard, C.; Leveillard, T.; Alvarez, V.; Bosco, P.; Mancuso, M.; Panza, F.; Nacmias, B.; Bossù, P.; Piccardi, P.; Annoni, G.; Seripa, D.; Galimberti, D.; Hannequin, D.; Licastro, F.; Soininen, H.; Ritchie, K.; Blanché, H.; Dartigues, J.-F.; Tzourio, C.; Gut, I.; Van Broeckhoven, C.; Alpérovitch, A.; Lathrop, M.; Amouyel, P. Genome-wide association study identifies variants at CLU and CR1 associated with Alzheimer's disease. *Nat. Genet.* **2009**, *41*, 1094–1099.

[46] Seshadri, S.; Fitzpatrick, A. L.; Ikram, M. A.; DeStefano, A. L.; Gudnason, V.; Boada, M.; Bis, J. C.; Smith, A. V.; Carassquillo, M. M.; Lambert, J. C.; Harold, D.; Schrijvers, E. M. C.; Ramirez-Lorca, R.; Debette, S.; Longstreth, W. T., Jr; Janssens, A. C. J. W.; Pankratz, V. S.; Dartigues, J. F.; Hollingworth, P.; Aspelund, T.; Hernandez, I.; Beiser, A.; Kuller, L. H.; Koudstaal, P. J.; Dickson, D. W.; Tzourio, C.; Abraham, R.; Antunez, C.; Du, Y.; Rotter, J. I.; Aulchenko, Y. S.; Harris, T. B.; Petersen, R. C.; Berr, C.; Owen, M. J.; Lopez-Arrieta, J.; Varadarajan, B. N.; Becker, J. T.; Rivadeneira, F.; Nalls, M. A.; Graff-Radford, N. R.; Campion, D.; Auerbach, S.; Rice, K.; Hofman, A.; Jonsson, P. V.; Schmidt, H.; Lathrop, M.; Mosley, T. H.; Au, R.; Psaty, B. M.; Uitterlinden, A. G.; Farrer, L. A.; Lumley, T.; Ruiz, A.; Williams, J.; Amouyel, P.; Younkin, S. G.; Wolf, P. A.; Launer, L. J.; Lopez, O. L.; van Duijn, C. M.; Breteler, M. M. B. Genome-wide analysis of genetic loci associated with Alzheimer disease. *JAMA* **2010**, *303*, 1832–1840.

[47] Rovelet-Lecrux, A.; Hannequin, D.; Raux, G.; Le Meur, N.; Laquerrière, A.; Vital, A.; Dumanchin, C.; Feuillette, S.; Brice, A.; Vercelletto, M.; Dubas, F.; Frebourg, T.; Campion, D. APP locus duplication causes autosomal dominant early-onset Alzheimer disease with cerebral amyloid angiopathy. *Nat. Genet.* **2006**, *38*, 24–26.

[48] Theuns, J.; Brouwers, N.; Engelborghs, S.; Sleegers, K.; Bogaerts, V.; Corsmit, E.; De Pooter, T.; van Duijn, C. M.; De Deyn, P. P.; Van Broeckhoven, C. Promoter mutations that increase amyloid precursor-protein expression are associated with Alzheimer disease. *Am. J. Hum. Genet.* **2006**, *78*, 936–946.

[49] Lahiri, D. K.; Ge, Y.-W.; Maloney, B.; Wavrant-De Vrièze, F.; Hardy, J. Characterization of two APP gene promoter polymorphisms that appear to influence risk of late-onset Alzheimer's disease. *Neurobiol. Aging* **2005**, *26*, 1329–1341.

[50] Kim, J.; Basak, J. M.; Holtzman, D. M. The role of apolipoprotein E in Alzheimer's disease. *Neuron* **2009**, *63*, 287–303.

[51] Walsh, D. M.; Selkoe, D. J. Aβ oligomers - a decade of discovery. *J Neurochem* **2007**, *101*, 1172–84.

[52] Pimplikar, S. W.; Nixon, R. A.; Robakis, N. K.; Shen, J.; Tsai, L. H. Amyloid-independent mechanisms in Alzheimer's disease pathogenesis. *J Neurosci* **2010**, *30*, 14946–54.

[53] Salehi, A.; Delcroix, J. D.; Belichenko, P. V.; Zhan, K.; Wu, C.; Valletta, J. S.; Takimoto-Kimura, R.; Kleschevnikov, A. M.; Sambamurti, K.; Chung, P. P.; Xia, W.; Villar, A.; Campbell, W. A.; Kulnane, L. S.; Nixon, R. A.; Lamb, B. T.; Epstein, C. J.; Stokin, G. B.; Goldstein, L. S.; Mobley, W. C. Increased App expression in a mouse model of Down's syndrome disrupts NGF transport and causes cholinergic neuron degeneration. *Neuron* **2006**, *51*, 29–42.

[54] Jiang, Y.; Mullaney, K. A.; Peterhoff, C. M.; Che, S.; Schmidt, S. D.; Boyer-Boiteau, A.; Ginsberg, S. D.; Cataldo, A. M.; Mathews, P. M.; Nixon, R. A. Alzheimer's-related endosome dysfunction in Down syndrome is Aβ-independent but requires APP and is reversed by BACE-1 inhibition. *Proc Natl Acad Sci U S A* **2010**, *107*, 1630–5.

[55] Cataldo, A. M.; Petanceska, S.; Peterhoff, C. M.; Terio, N. B.; Epstein, C. J.; Villar, A.; Carlson, E. J.; Staufenbiel, M.; Nixon, R. A. App gene dosage modulates endosomal abnormalities of Alzheimer's disease in a segmental trisomy 16 mouse model of down syndrome. *J Neurosci* **2003**, *23*, 6788–92.

[56] Farlow, M. R.; Cummings, J. L. Effective pharmacologic management of Alzheimer's disease. *Am. J. Med.* **2007**, *120*, 388–397.

[57] Alley, G. M.; Bailey, J. A.; Chen, D.; Ray, B.; Puli, L. K.; Tanila, H.; Banerjee, P. K.; Lahiri, D. K. Memantine lowers amyloid-beta peptide levels in neuronal cultures and in APP/PS1 transgenic mice. *J. Neurosci. Res.* **2010**, *88*, 143–154.

[58] Bailey, J. A.; Ray, B.; Greig, N. H.; Lahiri, D. K. Rivastigmine lowers Aβ and increases sAPPα levels, which parallel elevated synaptic markers and metabolic activity in degenerating primary rat neurons. *PLoS ONE* **2011**, *6*, e21954.

[59] Bailey, J. A.; Lahiri, D. K. A novel effect of rivastigmine on pre-synaptic proteins and neuronal viability in a neurodegeneration model of fetal rat primary cortical cultures and its implication in Alzheimer's disease. *J Neurochem* **2010**, *112*, 843–53.

[60] Raina, P.; Santaguida, P.; Ismaila, A.; Patterson, C.; Cowan, D.; Levine, M.; Booker, L.; Oremus, M. Effectiveness of cholinesterase inhibitors and memantine for treating dementia: evidence review for a clinical practice guideline. *Ann. Intern. Med.* **2008**, *148*, 379–397.

[61] Schneider, L. S.; Insel, P. S.; Weiner, M. W. Treatment with cholinesterase inhibitors and memantine of patients in the Alzheimer's Disease Neuroimaging Initiative. *Arch. Neurol.* **2011**, *68*, 58–66.

[62] Greig, N. H.; Utsuki, T.; Ingram, D. K.; Wang, Y.; Pepeu, G.; Scali, C.; Yu, Q. S.; Mamczarz, J.; Holloway, H. W.; Giordano, T.; Chen, D.; Furukawa, K.; Sambamurti, K.; Brossi, A.; Lahiri, D. K. Selective butyrylcholinesterase inhibition elevates brain acetylcholine, augments learning and lowers Alzheimer beta-amyloid peptide in rodent. *Proc Natl Acad Sci U S A* **2005**, *102*, 17213–8.

[63] Liu, D.; Pitta, M.; Lee, J. H.; Ray, B.; Lahiri, D. K.; Furukawa, K.; Mughal, M.; Jiang, H.; Villarreal, J.; Cutler, R. G.; Greig, N. H.; Mattson, M. P. The KATP channel activator diazoxide ameliorates amyloid-beta and tau pathologies and improves memory in the 3xTgAD mouse model of Alzheimer's disease. *J Alzheimers Dis* **2010**, *22*, 443–57.

[64] Ray, B.; Chauhan, N. B.; Lahiri, D. K. Oxidative insults to neurons and synapse are prevented by aged garlic extract and S-allyl-L-cysteine treatment in the neuronal culture and APP-Tg mouse model. *J. Neurochem.* **2011**, *117*, 388–402.

[65] Ray, B.; Chauhan, N. B.; Lahiri, D. K. The "aged garlic extract:" (AGE) and one of its active ingredients S-allyl-L-cysteine (SAC) as potential preventive and therapeutic agents for Alzheimer's disease (AD). *Curr. Med. Chem.* **2011**, *18*, 3306–3313.

[66] Ono, K.; Hasegawa, K.; Naiki, H.; Yamada, M. Curcumin has potent anti-amyloidogenic effects for Alzheimer's beta-amyloid fibrils in vitro. *J Neurosci Res* **2004**, *75*, 742–50.

[67] Ray, B.; Bisht, S.; Maitra, A.; Lahiri, D. K. Neuroprotective and neurorescue effects of a novel polymeric nanoparticle formulation of curcumin (NanoCurc) in the neuronal cell culture and animal model: implications for Alzheimer's disease. *J Alzheimers Dis* **2011**, *23*, 61–77.

[68] Ghosh, A. K.; Kumaragurubaran, N.; Hong, L.; Koelsh, G.; Tang, J. Memapsin 2 (beta-secretase) inhibitors: drug development. *Curr Alzheimer Res* **2008**, *5*, 121–31.

[69] Ghosh, A. K.; Gemma, S.; Tang, J. beta-Secretase as a therapeutic target for Alzheimer's disease. *Neurotherapeutics* **2008**, *5*, 399–408.

[70] Atwal, J. K.; Chen, Y.; Chiu, C.; Mortensen, D. L.; Meilandt, W. J.; Liu, Y.; Heise, C. E.; Hoyte, K.; Luk, W.; Lu, Y.; Peng, K.; Wu, P.; Rouge, L.; Zhang, Y.; Lazarus, R. A.; Scearce-Levie, K.; Wang, W.; Wu, Y.; Tessier-Lavigne, M.; Watts, R. J. A therapeutic antibody targeting BACE1 inhibits amyloid-β production in vivo. *Sci Transl Med* **2011**, *3*, 84ra43.

[71] Yu, Y. J.; Zhang, Y.; Kenrick, M.; Hoyte, K.; Luk, W.; Lu, Y.; Atwal, J.; Elliott, J. M.; Prabhu, S.; Watts, R. J.; Dennis, M. S. Boosting brain uptake of a therapeutic antibody by reducing its affinity for a transcytosis target. *Sci Transl Med* **2011**, *3*, 84ra44.

[72] Mangialasche, F.; Solomon, A.; Winblad, B.; Mecocci, P.; Kivipelto, M. Alzheimer's disease: clinical trials and drug development. *Lancet Neurol* **2010**, *9*, 702–716.

[73] Eriksen, J. L.; Sagi, S. A.; Smith, T. E.; Weggen, S.; Das, P.; McLendon, D. C.; Ozols, V. V.; Jessing, K. W.; Zavitz, K. H.; Koo, E. H.; Golde, T. E. NSAIDs and enantiomers of flurbiprofen target gamma-secretase and lower Abeta 42 in vivo. *J. Clin. Invest.* **2003**, *112*, 440–449.

[74] Wilcock, G. K.; Black, S. E.; Hendrix, S. B.; Zavitz, K. H.; Swabb, E. A.; Laughlin, M. A. Efficacy and safety of tarenflurbil in mild to moderate Alzheimer's disease: a randomised phase II trial. *Lancet Neurol* **2008**, *7*, 483–493.

[75] Green, R. C.; Schneider, L. S.; Amato, D. A.; Beelen, A. P.; Wilcock, G.; Swabb, E. A.; Zavitz, K. H. Effect of tarenflurbil on cognitive decline and activities of daily living in patients with mild Alzheimer disease: a randomized controlled trial. *JAMA* **2009**, *302*, 2557–2564.

[76] Bateman, R. J.; Siemers, E. R.; Mawuenyega, K. G.; Wen, G.; Browning, K. R.; Sigurdson, W. C.; Yarasheski, K. E.; Friedrich, S. W.; Demattos, R. B.; May, P. C.; Paul, S. M.; Holtzman, D. M. A gamma-secretase inhibitor decreases amyloid-beta production in the central nervous system. *Ann. Neurol.* **2009**, *66*, 48–54.

[77] Siemers, E.; Henley, D.; Sundell, K.; Sethuraman, G.; Dean, R.; Wrobleski, K.; Mohs, R. Evaluating semagacestat, a gamma-secretase inhibitor, in a phase III trial. *Alzheimers Dement.* **2011**, *7*, S484–S485.

[78] Sambamurti, K.; Greig, N. H.; Utsuki, T.; Barnwell, E. L.; Sharma, E.; Mazell, C.; Bhat, N. R.; Kindy, M. S.; Lahiri, D. K.; Pappolla, M. A. Targets for AD treatment: conflicting messages from γ-secretase inhibitors. *J. Neurochem.* **2011**, *117*, 359–374.

[79] Gervais, F.; Paquette, J.; Morissette, C.; Krzywkowski, P.; Yu, M.; Azzi, M.; Lacombe, D.; Kong, X.; Aman, A.; Laurin, J.; Szarek, W. A.; Tremblay, P. Targeting soluble Abeta peptide with Tramiprosate for the treatment of brain amyloidosis. *Neurobiol. Aging* **2007**, *28*, 537–547.

[80] Aisen, P. S.; Saumier, D.; Briand, R.; Laurin, J.; Gervais, F.; Tremblay, P.; Garceau, D. A Phase II study targeting amyloid-beta with 3APS in mild-to-moderate Alzheimer disease. *Neurology* **2006**, *67*, 1757–1763.

[81] Aisen, P. S.; Gauthier, S.; Ferris, S. H.; Saumier, D.; Haine, D.; Garceau, D.; Duong, A.; Suhy, J.; Oh, J.; Lau, W. C.; Sampalis, J. Tramiprosate in mild-to-moderate Alzheimer's disease - a randomized, double-blind, placebo-controlled, multi-centre study (the Alphase Study). *Arch Med Sci* **2011**, *7*, 102–111.

[82] Orgogozo, J.-M.; Gilman, S.; Dartigues, J.-F.; Laurent, B.; Puel, M.; Kirby, L. C.; Jouanny, P.; Dubois, B.; Eisner, L.; Flitman, S.; Michel, B. F.; Boada, M.; Frank, A.; Hock, C. Subacute meningoencephalitis in a subset of patients with AD after Abeta42 immunization. *Neurology* **2003**, *61*, 46–54.

[83] Salloway, S.; Sperling, R.; Gilman, S.; Fox, N. C.; Blennow, K.; Raskind, M.; Sabbagh, M.; Honig, L. S.; Doody, R.; van Dyck, C. H.; Mulnard, R.; Barakos, J.; Gregg, K. M.; Liu, E.; Lieberburg, I.; Schenk, D.; Black, R.; Grundman, M. A phase 2 multiple ascending dose trial of bapineuzumab in mild to moderate Alzheimer disease. *Neurology* **2009**, *73*, 2061–2070.

[84] Siemers, E. R.; Friedrich, S.; Dean, R. A.; Gonzales, C. R.; Farlow, M. R.; Paul, S. M.; Demattos, R. B. Safety and changes in plasma and cerebrospinal fluid amyloid beta after a single administration of an amyloid beta monoclonal antibody in subjects with Alzheimer disease. *Clin Neuropharmacol* **2010**, *33*, 67–73.

[85] Dodel, R.; Neff, F.; Noelker, C.; Pul, R.; Du, Y.; Bacher, M.; Oertel, W. Intravenous immunoglobulins as a treatment for Alzheimer's disease: rationale and current evidence. *Drugs* **2010**, *70*, 513–28.

[86] Relkin, N. R.; Szabo, P.; Adamiak, B.; Burgut, T.; Monthe, C.; Lent, R. W.; Younkin, S.; Younkin, L.; Schiff, R.; Weksler, M. E. 18-Month study of intravenous immunoglobulin for treatment of mild Alzheimer disease. *Neurobiol. Aging* **2009**, *30*, 1728–1736.

[87] Dodel, R.; Balakrishnan, K.; Keyvani, K.; Deuster, O.; Neff, F.; Andrei-Selmer, L.-C.; Röskam, S.; Stüer, C.; Al-Abed, Y.; Noelker, C.; Balzer-Geldsetzer, M.; Oertel, W.; Du, Y.; Bacher, M. Naturally occurring autoantibodies against beta-amyloid: investigating their role in transgenic animal and in vitro models of Alzheimer's disease. *J. Neurosci.* **2011**, *31*, 5847–5854.

[88] Esch, F. S.; Keim, P. S.; Beattie, E. C.; Blacher, R. W.; Culwell, A. R.; Oltersdorf, T.; McClure, D.; Ward, P. J. Cleavage of amyloid beta peptide during constitutive processing of its precursor. *Science* **1990**, *248*, 1122–1124.

[89] Seubert, P.; Oltersdorf, T.; Lee, M. G.; Barbour, R.; Blomquist, C.; Davis, D. L.; Bryant, K.; Fritz, L. C.; Galasko, D.; Thal, L. J. Secretion of beta-amyloid precursor protein cleaved at the amino terminus of the beta-amyloid peptide. *Nature* **1993**, *361*, 260–263.

[90] Zhang, H.; Ma, Q.; Zhang, Y.; Xu, H. Proteolytic processing of Alzheimer's β-amyloid precursor protein. *J. Neurochem.* **2012**, *120 Suppl 1*, 9–21.

[91] Wolfe, M. S.; Xia, W.; Ostaszewski, B. L.; Diehl, T. S.; Kimberly, W. T.; Selkoe, D. J. Two transmembrane aspartates in presenilin-1 required for presenilin endoproteolysis and gamma-secretase activity. *Nature* **1999**, *398*, 513–517.

[92] Thinakaran, G.; Koo, E. H. Amyloid precursor protein trafficking, processing, and function. *The Journal of Biological Chemistry* **2008**, *283*, 29615–29619.

[93] Saitoh, T.; Sundsmo, M.; Roch, J. M.; Kimura, N.; Cole, G.; Schubert, D.; Oltersdorf, T.; Schenk, D. B. Secreted form of amyloid beta protein precursor is involved in the growth regulation of fibroblasts. *Cell* **1989**, *58*, 615–622.

[94] Schubert, D.; Jin, L. W.; Saitoh, T.; Cole, G. The regulation of amyloid beta protein precursor secretion and its modulatory role in cell adhesion. *Neuron* **1989**, *3*, 689–694.

[95] Jin, L. W.; Ninomiya, H.; Roch, J. M.; Schubert, D.; Masliah, E.; Otero, D. A.; Saitoh, T. Peptides containing the RERMS sequence of amyloid beta/A4 protein precursor bind cell surface and promote neurite extension. *J. Neurosci.* **1994**, *14*, 5461–5470.

[96] Araki, W.; Kitaguchi, N.; Tokushima, Y.; Ishii, K.; Aratake, H.; Shimohama, S.; Nakamura, S.; Kimura, J. Trophic effect of beta-amyloid precursor protein on cerebral cortical neurons in culture. *Biochem. Biophys. Res. Commun.* **1991**, *181*, 265–271.

[97] Ohsawa, I.; Takamura, C.; Kohsaka, S. The amino-terminal region of amyloid precursor protein is responsible for neurite outgrowth in rat neocortical explant culture. *Biochem. Biophys. Res. Commun.* **1997**, *236*, 59–65.

[98] Gakhar-Koppole, N.; Hundeshagen, P.; Mandl, C.; Weyer, S. W.; Allinquant, B.; Müller, U.; Ciccolini, F. Activity requires soluble amyloid precursor protein alpha to promote neurite outgrowth in neural stem cell-derived neurons via activation of the MAPK pathway. *Eur. J. Neurosci.* **2008**, *28*, 871–882.

[99] Young-Pearse, T. L.; Chen, A. C.; Chang, R.; Marquez, C.; Selkoe, D. J. Secreted APP regulates the function of full-length APP in neurite outgrowth through interaction with integrin beta1. *Neural Dev* **2008**, *3*, 15.

[100] Ohsawa, I.; Hirose, Y.; Ishiguro, M.; Imai, Y.; Ishiura, S.; Kohsaka, S. Expression, purification, and neurotrophic activity of amyloid precursor protein-secreted forms produced by yeast. *Biochem. Biophys. Res. Commun.* **1995**, *213*, 52–58.

[101] Ohsawa, I.; Takamura, C.; Morimoto, T.; Ishiguro, M.; Kohsaka, S. Amino-terminal region of secreted form of amyloid precursor protein stimulates proliferation of neural stem cells. *Eur. J. Neurosci.* **1999**, *11*, 1907–1913.

[102] Hayashi, Y.; Kashiwagi, K.; Ohta, J.; Nakajima, M.; Kawashima, T.; Yoshikawa, K. Alzheimer amyloid protein precursor enhances proliferation of neural stem cells from fetal rat brain. *Biochem. Biophys. Res. Commun.* **1994**, *205*, 936–943.

[103] Caillé, I.; Allinquant, B.; Dupont, E.; Bouillot, C.; Langer, A.; Müller, U.; Prochiantz, A. Soluble form of amyloid precursor protein regulates proliferation of progenitors in the adult subventricular zone. *Development* **2004**, *131*, 2173–2181.

[104] Kwak, Y.-D.; Brannen, C. L.; Qu, T.; Kim, H. M.; Dong, X.; Soba, P.; Majumdar, A.; Kaplan, A.; Beyreuther, K.; Sugaya, K. Amyloid precursor protein regulates differentiation of human neural stem cells. *Stem Cells Dev.* **2006**, *15*, 381–389.

[105] Bell, K. F. S.; Zheng, L.; Fahrenholz, F.; Cuello, A. C. ADAM-10 over-expression increases cortical synaptogenesis. *Neurobiol. Aging* **2008**, *29*, 554–565.

[106] Roch, J. M.; Masliah, E.; Roch-Levecq, A. C.; Sundsmo, M. P.; Otero, D. A.; Veinbergs, I.; Saitoh, T. Increase of synaptic density and memory retention by a peptide representing the trophic domain of the amyloid beta/A4 protein precursor. *Proc. Natl. Acad. Sci. U.S.A.* **1994**, *91*, 7450–7454.

[107] Morimoto, T.; Ohsawa, I.; Takamura, C.; Ishiguro, M.; Kohsaka, S. Involvement of amyloid precursor protein in functional synapse formation in cultured hippocampal neurons. *J. Neurosci. Res.* **1998**, *51*, 185–195.

[108] Taylor, C. J.; Ireland, D. R.; Ballagh, I.; Bourne, K.; Marechal, N. M.; Turner, P. R.; Bilkey, D. K.; Tate, W. P.; Abraham, W. C. Endogenous secreted amyloid precursor protein-alpha regulates hippocampal NMDA receptor function, long-term potentiation and spatial memory. *Neurobiol. Dis.* **2008**, *31*, 250–260.

[109] Ishida, A.; Furukawa, K.; Keller, J. N.; Mattson, M. P. Secreted form of beta-amyloid precursor protein shifts the frequency dependency for induction of LTD, and enhances LTP in hippocampal slices. *Neuroreport* **1997**, *8*, 2133–2137.

[110] Smith-Swintosky, V. L.; Pettigrew, L. C.; Craddock, S. D.; Culwell, A. R.; Rydel, R. E.; Mattson, M. P. Secreted forms of beta-amyloid precursor protein protect against ischemic brain injury. *J. Neurochem.* **1994**, *63*, 781–784.

[111] Goodman, Y.; Mattson, M. P. Secreted forms of beta-amyloid precursor protein protect hippocampal neurons against amyloid beta-peptide-induced oxidative injury. *Exp. Neurol.* **1994**, *128*, 1–12.

[112] Mattson, M. P.; Cheng, B.; Culwell, A. R.; Esch, F. S.; Lieberburg, I.; Rydel, R. E. Evidence for excitoprotective and intraneuronal calcium-regulating roles for secreted forms of the beta-amyloid precursor protein. *Neuron* **1993**, *10*, 243–254.

[113] Furukawa, K.; Sopher, B. L.; Rydel, R. E.; Begley, J. G.; Pham, D. G.; Martin, G. M.; Fox, M.; Mattson, M. P. Increased activity-regulating and neuroprotective efficacy of alpha-secretase-derived secreted amyloid precursor protein conferred by a C-terminal heparin-binding domain. *J. Neurochem.* **1996**, *67*, 1882–1896.

[114] Sokol, D. K.; Chen, D.; Farlow, M. R.; Dunn, D. W.; Maloney, B.; Zimmer, J. A.; Lahiri, D. K. High levels of Alzheimer beta-amyloid precursor protein (APP) in children with severely autistic behavior and aggression. *J. Child Neurol.* **2006**, *21*, 444–449.

[115] Ray, B.; Long, J. M.; Sokol, D. K.; Lahiri, D. K. Increased secreted amyloid precursor protein-α (sAPPα) in severe autism: proposal of a specific, anabolic pathway and putative biomarker. *PLoS ONE* **2011**, *6*, e20405.

[116] Sokol, D. K.; Maloney, B.; Long, J. M.; Ray, B.; Lahiri, D. K. Autism, Alzheimer disease, and fragile X: APP, FMRP, and mGluR5 are molecular links. *Neurology* **2011**, *76*, 1344–1352.

[117] Nikolaev, A.; McLaughlin, T.; O'Leary, D. D. M.; Tessier-Lavigne, M. APP binds DR6 to trigger axon pruning and neuron death via distinct caspases. *Nature* **2009**, *457*, 981–989.

[118] Cao, X.; Südhof, T. C. A transcriptionally [correction of transcriptively] active complex of APP with Fe65 and histone acetyltransferase Tip60. *Science* **2001**, *293*, 115–120.

[119] Cao, X.; Südhof, T. C. Dissection of amyloid-beta precursor protein-dependent transcriptional transactivation. *J. Biol. Chem.* **2004**, *279*, 24601–24611.

[120] Ma, Q.-H.; Futagawa, T.; Yang, W.-L.; Jiang, X.-D.; Zeng, L.; Takeda, Y.; Xu, R.-X.; Bagnard, D.; Schachner, M.; Furley, A. J.; Karagogeos, D.; Watanabe, K.; Dawe, G. S.; Xiao, Z.-C. A TAG1-APP signalling pathway through Fe65 negatively modulates neurogenesis. *Nat. Cell Biol.* **2008**, *10*, 283–294.

[121] Ge, Y.-W.; Lahiri, D. K. Regulation of promoter activity of the APP gene by cytokines and growth factors: implications in Alzheimer's disease. *Ann. N. Y. Acad. Sci.* **2002**, *973*, 463–467.

[122] Song, W.; Lahiri, D. K. Functional identification of the promoter of the gene encoding the Rhesus monkey beta-amyloid precursor protein. *Gene* **1998**, *217*, 165–176.

[123] Lahiri, D. K.; Nall, C. Promoter activity of the gene encoding the beta-amyloid precursor protein is up-regulated by growth factors, phorbol ester, retinoic acid and interleukin-1. *Brain Res. Mol. Brain Res.* **1995**, *32*, 233–240.

[124] Ruiz-León, Y.; Pascual, A. Brain-derived neurotrophic factor stimulates beta-amyloid gene promoter activity by a Ras-dependent/AP-1-independent mechanism in SH-SY5Y neuroblastoma cells. *J. Neurochem.* **2001**, *79*, 278–285.

[125] Villa, A.; Latasa, M. J.; Pascual, A. Nerve growth factor modulates the expression and secretion of beta-amyloid precursor protein through different mechanisms in PC12 cells. *J. Neurochem.* **2001**, *77*, 1077–1084.

[126] Pollwein, P.; Masters, C. L.; Beyreuther, K. The expression of the amyloid precursor protein (APP) is regulated by two GC-elements in the promoter. *Nucleic Acids Res.* **1992**, *20*, 63–68.

[127] Bourbonnière, M.; Nalbantoglu, J. Expression of amyloid precursor protein in a neuronal cell line: functional activity of proximal regulatory elements. *Brain Res. Mol. Brain Res.* **1993**, *19*, 246–250.

[128] Lahiri, D. K.; Robakis, N. K. The promoter activity of the gene encoding Alzheimer beta-amyloid precursor protein (APP) is regulated by two blocks of upstream sequences. *Brain Res. Mol. Brain Res.* **1991**, *9*, 253–257.

[129] Quitschke, W. W.; Goldgaber, D. The amyloid beta-protein precursor promoter. A region essential for transcriptional activity contains a nuclear factor binding domain. *J. Biol. Chem.* **1992**, *267*, 17362–17368.

[130] Quitschke, W. W. Two nuclear factor binding domains activate expression from the human amyloid beta-protein precursor promoter. *J. Biol. Chem.* **1994**, *269*, 21229–21233.

[131] Pollwein, P. Overlapping binding sites of two different transcription factors in the promoter of the human gene for the Alzheimer amyloid precursor protein. *Biochem. Biophys. Res. Commun.* **1993**, *190*, 637–647.

[132] Vostrov, A. A.; Quitschke, W. W.; Vidal, F.; Schwarzman, A. L.; Goldgaber, D. USF binds to the APB alpha sequence in the promoter of the amyloid beta-protein precursor gene. *Nucleic Acids Res.* **1995**, *23*, 2734–2741.

[133] Bourbonnière, M.; Nalbantoglu, J. The helix-loop-helix transcription factor USF interacts with the basal promoter of human amyloid precursor protein. *Brain Res. Mol. Brain Res.* **1996**, *35*, 304–308.

[134] Yang, Y.; Quitschke, W. W.; Vostrov, A. A.; Brewer, G. J. CTCF is essential for up-regulating expression from the amyloid precursor protein promoter during differentiation of primary hippocampal neurons. *J. Neurochem.* **1999**, *73*, 2286–2298.

[135] Vostrov, A. A.; Quitschke, W. W. The zinc finger protein CTCF binds to the APBbeta domain of the amyloid beta-protein precursor promoter. Evidence for a role in transcriptional activation. *J. Biol. Chem.* **1997**, *272*, 33353–33359.

[136] Ge, Y.-W.; Ghosh, C.; Song, W.; Maloney, B.; Lahiri, D. K. Mechanism of promoter activity of the beta-amyloid precursor protein gene in different cell lines: identification of a specific 30 bp fragment in the proximal promoter region. *J. Neurochem.* **2004**, *90*, 1432–1444.

[137] Lahiri, D. K. An region upstream of the gene promoter for the beta-amyloid precursor protein interacts with proteins from nuclear extracts of the human brain and PC12 cells. *Brain Res. Mol. Brain Res.* **1998**, *58*, 112–122.

[138] Lahiri, D. K.; Nall, C.; Ge, Y. W. Promoter activity of the beta-amyloid precursor protein gene is negatively modulated by an upstream regulatory element. *Brain Res. Mol. Brain Res.* **1999**, *71*, 32–41.

[139] Querfurth, H. W.; Jiang, J.; Xia, W.; Selkoe, D. J. Enhancer function and novel DNA binding protein activity in the near upstream betaAPP gene promoter. *Gene* **1999**, *232*, 125–141.

[140] Maloney, B.; Ge, Y.-W.; Greig, N.; Lahiri, D. K. Presence of a “CAGA box” in the APP gene unique to amyloid plaque-forming species and absent in all APLP-1/2 genes: implications in Alzheimer’s disease. *FASEB J.* **2004**, *18*, 1288–1290.

[141] Villa, A.; Santiago, J.; Belandia, B.; Pascual, A. A response unit in the first exon of the beta-amyloid precursor protein gene containing thyroid hormone receptor and Sp1 binding sites mediates negative regulation by 3,5,3’-triiodothyronine. *Mol. Endocrinol.* **2004**, *18*, 863–873.

[142] Vostrov, A. A.; Taheny, M. J.; Izkhakov, N.; Quitschke, W. W. A nuclear factor-binding domain in the 5’-untranslated region of the amyloid precursor protein promoter: implications for the regulation of gene expression. *BMC Res Notes* **2010**, *3*, 4.

[143] Rogers, J. T.; Randall, J. D.; Cahill, C. M.; Eder, P. S.; Huang, X.; Gunshin, H.; Leiter, L.; McPhee, J.; Sarang, S. S.; Utsuki, T.; Greig, N. H.; Lahiri, D. K.; Tanzi, R. E.; Bush, A. I.; Giordano, T.; Gullans, S. R. An iron-responsive element type II in the 5’-untranslated region of the Alzheimer’s amyloid precursor protein transcript. *J. Biol. Chem.* **2002**, *277*, 45518–45528.

[144] Cho, H.-H.; Cahill, C. M.; Vanderburg, C. R.; Scherzer, C. R.; Wang, B.; Huang, X.; Rogers, J. T. Selective translational control of the Alzheimer amyloid precursor protein transcript by iron regulatory protein-1. *J. Biol. Chem.* **2010**, *285*, 31217–31232.

[145] Rogers, J. T.; Leiter, L. M.; McPhee, J.; Cahill, C. M.; Zhan, S. S.; Potter, H.; Nilsson, L. N. Translation of the alzheimer amyloid precursor protein mRNA is up-regulated by interleukin-1 through 5'-untranslated region sequences. *J. Biol. Chem.* **1999**, *274*, 6421–6431.

[146] Beaudoin, M. E.; Poirel, V.-J.; Krushel, L. A. Regulating amyloid precursor protein synthesis through an internal ribosomal entry site. *Nucleic Acids Res.* **2008**, *36*, 6835–6847.

[147] Zaidi, S. H.; Malter, J. S. Amyloid precursor protein mRNA stability is controlled by a 29-base element in the 3'-untranslated region. *J. Biol. Chem.* **1994**, *269*, 24007–24013.

[148] Zaidi, S. H.; Denman, R.; Malter, J. S. Multiple proteins interact at a unique cis-element in the 3'-untranslated region of amyloid precursor protein mRNA. *J. Biol. Chem.* **1994**, *269*, 24000–24006.

[149] Westmark, P. R.; Shin, H. C.; Westmark, C. J.; Soltaninassab, S. R.; Reinke, E. K.; Malter, J. S. Decoy mRNAs reduce beta-amyloid precursor protein mRNA in neuronal cells. *Neurobiol. Aging* **2006**, *27*, 787–796.

[150] Rajagopalan, L. E.; Westmark, C. J.; Jarzembowski, J. A.; Malter, J. S. hnRNP C increases amyloid precursor protein (APP) production by stabilizing APP mRNA. *Nucleic Acids Res.* **1998**, *26*, 3418–3423.

[151] Broytman, O.; Westmark, P. R.; Gurel, Z.; Malter, J. S. Rck/p54 interacts with APP mRNA as part of a multi-protein complex and enhances APP mRNA and protein expression in neuronal cell lines. *Neurobiol. Aging* **2009**, *30*, 1962–1974.

[152] Westmark, C. J.; Malter, J. S. Up-regulation of nucleolin mRNA and protein in peripheral blood mononuclear cells by extracellular-regulated kinase. *J. Biol. Chem.* **2001**, *276*, 1119–1126.

[153] Zaidi, S. H.; Malter, J. S. Nucleolin and heterogeneous nuclear ribonucleoprotein C proteins specifically interact with the 3'-untranslated region of amyloid protein precursor mRNA. *J. Biol. Chem.* **1995**, *270*, 17292–17298.

[154] de Sauvage, F.; Kruys, V.; Marinx, O.; Huez, G.; Octave, J. N. Alternative polyadenylation of the amyloid protein precursor mRNA regulates translation. *EMBO J.* **1992**, *11*, 3099–3103.

[155] Mbella, E. G.; Bertrand, S.; Huez, G.; Octave, J. N. A GG nucleotide sequence of the 3' untranslated region of amyloid precursor protein mRNA plays a key role in the regulation of translation and the binding of proteins. *Mol. Cell. Biol.* **2000**, *20*, 4572–4579.

[156] Westmark, C. J.; Malter, J. S. FMRP mediates mGluR5-dependent translation of amyloid precursor protein. *PLoS Biol.* **2007**, *5*, e52.

[157] Lee, E. K.; Kim, H. H.; Kuwano, Y.; Abdelmohsen, K.; Srikantan, S.; Subaran, S. S.; Gleichmann, M.; Mughal, M. R.; Martindale, J. L.; Yang, X.; Worley, P. F.; Mattson, M. P.; Gorospe, M. hnRNP C promotes APP translation by competing with FMRP for APP mRNA recruitment to P bodies. *Nat. Struct. Mol. Biol.* **2010**, *17*, 732–739.

[158] Vassar, R.; Bennett, B. D.; Babu-Khan, S.; Kahn, S.; Mendiaz, E. A.; Denis, P.; Teplow, D. B.; Ross, S.; Amarante, P.; Loeloff, R.; Luo, Y.; Fisher, S.; Fuller, J.; Edenson, S.; Lile, J.; Jarosinski, M. A.; Biere, A. L.; Curran, E.; Burgess, T.; Louis, J. C.; Collins, F.; Treanor, J.; Rogers, G.; Citron, M. Beta-secretase cleavage of Alzheimer's amyloid precursor protein by the transmembrane aspartic protease BACE. *Science* **1999**, *286*, 735–41.

[159] Sinha, S.; Anderson, J. P.; Barbour, R.; Basi, G. S.; Caccavello, R.; Davis, D.; Doan, M.; Dovey, H. F.; Frigon, N.; Hong, J.; Jacobson-Croak, K.; Jewett, N.; Keim, P.; Knops, J.; Lieberburg, I.; Power, M.; Tan, H.; Tatsuno, G.; Tung, J.; Schenk, D.; Seubert, P.; Suomensaari, S. M.; Wang, S.; Walker, D.; Zhao, J.; McConlogue, L.; John, V. Purification and cloning of amyloid precursor protein beta-secretase from human brain. *Nature* **1999**, *402*, 537–540.

[160] Hussain, I.; Powell, D.; Howlett, D. R.; Tew, D. G.; Meek, T. D.; Chapman, C.; Gloger, I. S.; Murphy, K. E.; Southan, C. D.; Ryan, D. M.; Smith, T. S.; Simmons, D. L.; Walsh, F. S.; Dingwall, C.; Christie, G. Identification of a novel aspartic protease (Asp 2) as beta-secretase. *Mol. Cell. Neurosci.* **1999**, *14*, 419–427.

[161] Lin, X.; Koelsch, G.; Wu, S.; Downs, D.; Dashti, A.; Tang, J. Human aspartic protease memapsin 2 cleaves the beta-secretase site of beta-amyloid precursor protein. *Proc. Natl. Acad. Sci. U.S.A.* **2000**, *97*, 1456–1460.

[162] Vassar, R.; Kovacs, D. M.; Yan, R.; Wong, P. C. The beta-secretase enzyme BACE in health and Alzheimer's disease: regulation, cell biology, function, and therapeutic potential. *J. Neurosci.* **2009**, *29*, 12787–12794.

[163] Puzzo, D.; Privitera, L.; Leznik, E.; Fà, M.; Staniszewski, A.; Palmeri, A.; Arancio, O. Picomolar amyloid-beta positively modulates synaptic plasticity and memory in hippocampus. *J. Neurosci.* **2008**, *28*, 14537–14545.

[164] Giuffrida, M. L.; Caraci, F.; De Bona, P.; Pappalardo, G.; Nicoletti, F.; Rizzarelli, E.; Copani, A. The monomer state of beta-amyloid: where the Alzheimer's disease protein meets physiology. *Rev Neurosci* **2010**, *21*, 83–93.

[165] Puzzo, D.; Privitera, L.; Palmeri, A. Hormetic effect of amyloid-beta peptide in synaptic plasticity and memory. *Neurobiol. Aging* **2012**, *33*, 1484.e15–24.

[166] Eggert, S.; Paliga, K.; Soba, P.; Evin, G.; Masters, C. L.; Weidemann, A.; Beyreuther, K. The proteolytic processing of the amyloid precursor protein gene family members APLP-1 and APLP-2 involves alpha-, beta-, gamma-, and epsilon-like cleavages: modulation of APLP-1 processing by n-glycosylation. *J. Biol. Chem.* **2004**, *279*, 18146–18156.

[167] Li, Q.; Südhof, T. C. Cleavage of amyloid-beta precursor protein and amyloid-beta precursor-like protein by BACE 1. *J. Biol. Chem.* **2004**, *279*, 10542–10550.

[168] Wong, H.-K.; Sakurai, T.; Oyama, F.; Kaneko, K.; Wada, K.; Miyazaki, H.; Kurosawa, M.; De Strooper, B.; Saftig, P.; Nukina, N. beta Subunits of voltage-gated sodium channels are novel substrates of beta-site amyloid precursor protein-cleaving enzyme (BACE1) and gamma-secretase. *J. Biol. Chem.* **2005**, *280*, 23009–23017.

[169] Hu, X.; Hicks, C. W.; He, W.; Wong, P.; Macklin, W. B.; Trapp, B. D.; Yan, R. Bace1 modulates myelination in the central and peripheral nervous system. *Nat. Neurosci.* **2006**, *9*, 1520–1525.

[170] Hu, X.; He, W.; Diaconu, C.; Tang, X.; Kidd, G. J.; Macklin, W. B.; Trapp, B. D.; Yan, R. Genetic deletion of BACE1 in mice affects remyelination of sciatic nerves. *FASEB J.* **2008**, *22*, 2970–2980.

[171] Kim, D. Y.; Carey, B. W.; Wang, H.; Ingano, L. A. M.; Binshtok, A. M.; Wertz, M. H.; Pettingell, W. H.; He, P.; Lee, V. M.-Y.; Woolf, C. J.; Kovacs, D. M. BACE1 regulates voltage-gated sodium channels and neuronal activity. *Nat. Cell Biol.* **2007**, *9*, 755–764.

[172] Ge, Y.-W.; Maloney, B.; Sambamurti, K.; Lahiri, D. K. Functional characterization of the 5' flanking region of the BACE gene: identification of a 91 bp fragment involved in basal level of BACE promoter expression. *FASEB J.* **2004**, *18*, 1037–1039.

[173] Christensen, M. A.; Zhou, W.; Qing, H.; Lehman, A.; Philipsen, S.; Song, W. Transcriptional regulation of BACE1, the beta-amyloid precursor protein beta-secretase, by Sp1. *Mol. Cell. Biol.* **2004**, *24*, 865–874.

[174] Li, Y.; Zhou, W.; Tong, Y.; He, G.; Song, W. Control of APP processing and Abeta generation level by BACE1 enzymatic activity and transcription. *FASEB J.* **2006**, *20*, 285–292.

[175] Chu, J.; Zhuo, J.-M.; Praticò, D. Transcriptional regulation of β-secretase-1 by 12/15-lipoxygenase results in enhanced amyloidogenesis and cognitive impairments. *Ann. Neurol.* **2012**, *71*, 57–67.

[176] Nowak, K.; Lange-Dohna, C.; Zeitschel, U.; Günther, A.; Lüscher, B.; Robitzki, A.; Perez-Polo, R.; Rossner, S. The transcription factor Yin Yang 1 is an activator of BACE1 expression. *J. Neurochem.* **2006**, *96*, 1696–1707.

[177] Bourne, K. Z.; Ferrari, D. C.; Lange-Dohna, C.; Rossner, S.; Wood, T. G.; Perez-Polo, J. R. Differential regulation of BACE1 promoter activity by nuclear factor-kappaB in neurons and glia upon exposure to beta-amyloid peptides. *J. Neurosci. Res.* **2007**, *85*, 1194–1204.

[178] Byun, C. J.; Seo, J.; Jo, S. A.; Park, Y. J.; Klug, M.; Rehli, M.; Park, M.-H.; Jo, I. DNA methylation of the 5'-untranslated region at +298 and +351 represses BACE1 expression in mouse BV-2 microglial cells. *Biochem. Biophys. Res. Commun.* **2012**, *417*, 387–392.

[179] Lammich, S.; Schöbel, S.; Zimmer, A.-K.; Lichtenthaler, S. F.; Haass, C. Expression of the Alzheimer protease BACE1 is suppressed via its 5'-untranslated region. *EMBO Rep.* **2004**, *5*, 620–625.

[180] Kozak, M. Regulation of translation via mRNA structure in prokaryotes and eukaryotes. *Gene* **2005**, *361*, 13–37.

[181] De Pietri Tonelli, D.; Mihailovich, M.; Di Cesare, A.; Codazzi, F.; Grohovaz, F.; Zacchetti, D. Translational regulation of BACE-1 expression in neuronal and non-neuronal cells. *Nucleic Acids Res.* **2004**, *32*, 1808–1817.

[182] Zhou, W.; Song, W. Leaky scanning and reinitiation regulate BACE1 gene expression. *Mol. Cell. Biol.* **2006**, *26*, 3353–3364.

[183] Mihailovich, M.; Thermann, R.; Grohovaz, F.; Hentze, M. W.; Zacchetti, D. Complex translational regulation of BACE1 involves upstream AUGs and stimulatory elements within the 5' untranslated region. *Nucleic Acids Res.* **2007**, *35*, 2975–2985.

[184] O'Connor, T.; Sadleir, K. R.; Maus, E.; Velliquette, R. A.; Zhao, J.; Cole, S. L.; Eimer, W. A.; Hitt, B.; Bembinster, L. A.; Lammich, S.; Lichtenthaler, S. F.; Hébert, S. S.; De Strooper, B.; Haass, C.; Bennett, D. A.; Vassar, R. Phosphorylation of the translation initiation factor eIF2alpha increases BACE1 levels and promotes amyloidogenesis. *Neuron* **2008**, *60*, 988–1009.

[185] Faghihi, M. A.; Modarresi, F.; Khalil, A. M.; Wood, D. E.; Sahagan, B. G.; Morgan, T. E.; Finch, C. E.; St Laurent, G., 3rd; Kenny, P. J.; Wahlestedt, C. Expression of a noncoding RNA is elevated in Alzheimer's disease and drives rapid feed-forward regulation of beta-secretase. *Nat. Med.* **2008**, *14*, 723–730.

[186] Faghihi, M. A.; Zhang, M.; Huang, J.; Modarresi, F.; Van der Brug, M. P.; Nalls, M. A.; Cookson, M. R.; St-Laurent, G., 3rd; Wahlestedt, C. Evidence for natural antisense transcript-mediated inhibition of microRNA function. *Genome Biol.* **2010**, *11*, R56.

[187] Selkoe, D. J. Resolving controversies on the path to Alzheimer's therapeutics. *Nat. Med.* **2011**, *17*, 1060–1065.

[188] Karran, E.; Mercken, M.; De Strooper, B. The amyloid cascade hypothesis for Alzheimer's disease: an appraisal for the development of therapeutics. *Nat Rev Drug Discov* **2011**, *10*, 698–712.

[189] Hébert, S. S.; Horré, K.; Nicolaï, L.; Papadopoulou, A. S.; Mandemakers, W.; Silahtaroglu, A. N.; Kauppinen, S.; Delacourte, A.; De Strooper, B. Loss of microRNA cluster miR-29a/b-1 in sporadic Alzheimer's disease correlates with increased BACE1/beta-secretase expression. *Proc. Natl. Acad. Sci. U.S.A.* **2008**, *105*, 6415–6420.

[190] Poon, H. F.; Joshi, G.; Sultana, R.; Farr, S. A.; Banks, W. A.; Morley, J. E.; Calabrese, V.; Butterfield, D. A. Antisense directed at the Abeta region of APP decreases brain oxidative markers in aged senescence accelerated mice. *Brain Res.* **2004**, *1018*, 86–96.

[191] Kumar, V. B.; Farr, S. A.; Flood, J. F.; Kamlesh, V.; Franko, M.; Banks, W. A.; Morley, J. E. Site-directed antisense oligonucleotide decreases the expression of amyloid precursor protein and reverses deficits in learning and memory in aged SAMP8 mice. *Peptides* **2000**, *21*, 1769–1775.

[192] Payton, S.; Cahill, C. M.; Randall, J. D.; Gullans, S. R.; Rogers, J. T. Drug discovery targeted to the Alzheimer's APP mRNA 5'-untranslated region: the action of paroxetine and dimercaptopropanol. *J. Mol. Neurosci.* **2003**, *20*, 267–275.

[193] Ohno, M.; Sametsky, E. A.; Younkin, L. H.; Oakley, H.; Younkin, S. G.; Citron, M.; Vassar, R.; Disterhoft, J. F. BACE1 deficiency rescues memory deficits and cholinergic dysfunction in a mouse model of Alzheimer's disease. *Neuron* **2004**, *41*, 27–33.

[194] Alvarez-Erviti, L.; Seow, Y.; Yin, H.; Betts, C.; Lakhal, S.; Wood, M. J. A. Delivery of siRNA to the mouse brain by systemic injection of targeted exosomes. *Nat. Biotechnol.* **2011**, *29*, 341–345.

[195] Zheng, H.; Jiang, M.; Trumbauer, M. E.; Sirinathsinghji, D. J.; Hopkins, R.; Smith, D. W.; Heavens, R. P.; Dawson, G. R.; Boyce, S.; Conner, M. W.; Stevens, K. A.; Slunt, H. H.; Sisoda, S. S.; Chen, H. Y.; Van der Ploeg, L. H. beta-Amyloid precursor protein-deficient mice show reactive gliosis and decreased locomotor activity. *Cell* **1995**, *81*, 525–531.

[196] Lee, R. C.; Feinbaum, R. L.; Ambros, V. The C. elegans heterochronic gene lin-4 encodes small RNAs with antisense complementarity to lin-14. *Cell* **1993**, *75*, 843–854.

[197] Wightman, B.; Ha, I.; Ruvkun, G. Posttranscriptional regulation of the heterochronic gene lin-14 by lin-4 mediates temporal pattern formation in C. elegans. *Cell* **1993**, *75*, 855–62.

[198] Reinhart, B. J.; Slack, F. J.; Basson, M.; Pasquinelli, A. E.; Bettinger, J. C.; Rougvie, A. E.; Horvitz, H. R.; Ruvkun, G. The 21-nucleotide let-7 RNA regulates developmental timing in Caenorhabditis elegans. *Nature* **2000**, *403*, 901–906.

[199] Pasquinelli, A. E.; Reinhart, B. J.; Slack, F.; Martindale, M. Q.; Kuroda, M. I.; Maller, B.; Hayward, D. C.; Ball, E. E.; Degnan, B.; Muller, P.; Spring, J.; Srinivasan, A.; Fishman, M.; Finnerty, J.; Corbo, J.; Levine, M.; Leahy, P.; Davidson, E.; Ruvkun, G. Conservation of the sequence and temporal expression of let-7 heterochronic regulatory RNA. *Nature* **2000**, *408*, 86–9.

[200] Lagos-Quintana, M.; Rauhut, R.; Lendeckel, W.; Tuschl, T. Identification of novel genes coding for small expressed RNAs. *Science* **2001**, *294*, 853–858.

[201] Lau, N. C.; Lim, L. P.; Weinstein, E. G.; Bartel, D. P. An abundant class of tiny RNAs with probable regulatory roles in Caenorhabditis elegans. *Science* **2001**, *294*, 858–862.

[202] Lee, R. C.; Ambros, V. An extensive class of small RNAs in Caenorhabditis elegans. *Science* **2001**, *294*, 862–864.

[203] Lai, E. C. Micro RNAs are complementary to 3' UTR sequence motifs that mediate negative post-transcriptional regulation. *Nat. Genet.* **2002**, *30*, 363–364.

[204] Lewis, B. P.; Shih, I.; Jones-Rhoades, M. W.; Bartel, D. P.; Burge, C. B. Prediction of mammalian microRNA targets. *Cell* **2003**, *115*, 787–798.

[205] Griffiths-Jones, S.; Grocock, R. J.; van Dongen, S.; Bateman, A.; Enright, A. J. miRBase: microRNA sequences, targets and gene nomenclature. *Nucleic Acids Res.* **2006**, *34*, D140–144.

[206] Lee, Y.; Kim, M.; Han, J.; Yeom, K.-H.; Lee, S.; Baek, S. H.; Kim, V. N. MicroRNA genes are transcribed by RNA polymerase II. *EMBO J.* **2004**, *23*, 4051–4060.

[207] Kim, V. N.; Han, J.; Siomi, M. C. Biogenesis of small RNAs in animals. *Nat Rev Mol Cell Biol* **2009**, *10*, 126–39.

[208] Han, J.; Lee, Y.; Yeom, K.-H.; Kim, Y.-K.; Jin, H.; Kim, V. N. The Drosha-DGCR8 complex in primary microRNA processing. *Genes Dev.* **2004**, *18*, 3016–3027.

[209] Lee, Y.; Ahn, C.; Han, J.; Choi, H.; Kim, J.; Yim, J.; Lee, J.; Provost, P.; Radmark, O.; Kim, S.; Kim, V. N. The nuclear RNase III Drosha initiates microRNA processing. *Nature* **2003**, *425*, 415–9.

[210] Han, J.; Lee, Y.; Yeom, K.-H.; Nam, J.-W.; Heo, I.; Rhee, J.-K.; Sohn, S. Y.; Cho, Y.; Zhang, B.-T.; Kim, V. N. Molecular basis for the recognition of primary microRNAs by the Drosha-DGCR8 complex. *Cell* **2006**, *125*, 887–901.

[211] Lund, E.; Güttinger, S.; Calado, A.; Dahlberg, J. E.; Kutay, U. Nuclear export of microRNA precursors. *Science* **2004**, *303*, 95–98.

[212] Chendrimada, T. P.; Gregory, R. I.; Kumaraswamy, E.; Norman, J.; Cooch, N.; Nishikura, K.; Shiekhattar, R. TRBP recruits the Dicer complex to Ago2 for microRNA processing and gene silencing. *Nature* **2005**, *436*, 740–744.

[213] Hutvágner, G.; McLachlan, J.; Pasquinelli, A. E.; Bálint, E.; Tuschl, T.; Zamore, P. D. A cellular function for the RNA-interference enzyme Dicer in the maturation of the let-7 small temporal RNA. *Science* **2001**, *293*, 834–838.

[214] Mourelatos, Z.; Dostie, J.; Paushkin, S.; Sharma, A.; Charroux, B.; Abel, L.; Rappsilber, J.; Mann, M.; Dreyfuss, G. miRNPs: a novel class of ribonucleoproteins containing numerous microRNAs. *Genes Dev.* **2002**, *16*, 720–728.

[215] Pratt, A. J.; MacRae, I. J. The RNA-induced silencing complex: a versatile gene-silencing machine. *J. Biol. Chem.* **2009**, *284*, 17897–17901.

[216] Kwak, P. B.; Tomari, Y. The N domain of Argonaute drives duplex unwinding during RISC assembly. *Nat. Struct. Mol. Biol.* **2012**, *19*, 145–151.

[217] MacRae, I. J.; Ma, E.; Zhou, M.; Robinson, C. V.; Doudna, J. A. In vitro reconstitution of the human RISC-loading complex. *Proc. Natl. Acad. Sci. U.S.A.* **2008**, *105*, 512–517.

[218] Ye, X.; Huang, N.; Liu, Y.; Paroo, Z.; Huerta, C.; Li, P.; Chen, S.; Liu, Q.; Zhang, H. Structure of C3PO and mechanism of human RISC activation. *Nat. Struct. Mol. Biol.* **2011**, *18*, 650–657.

[219] Johnston, M.; Geoffroy, M.-C.; Sobala, A.; Hay, R.; Hutvagner, G. HSP90 protein stabilizes unloaded argonaute complexes and microscopic P-bodies in human cells. *Mol. Biol. Cell* **2010**, *21*, 1462–1469.

[220] Miyoshi, T.; Takeuchi, A.; Siomi, H.; Siomi, M. C. A direct role for Hsp90 in pre-RISC formation in Drosophila. *Nat. Struct. Mol. Biol.* **2010**, *17*, 1024–1026.

[221] Kawamata, T.; Yoda, M.; Tomari, Y. Multilayer checkpoints for microRNA authenticity during RISC assembly. *EMBO Rep.* **2011**, *12*, 944–949.

[222] Schwarz, D. S.; Hutvágner, G.; Du, T.; Xu, Z.; Aronin, N.; Zamore, P. D. Asymmetry in the assembly of the RNAi enzyme complex. *Cell* **2003**, *115*, 199–208.

[223] Long, J. M.; Lahiri, D. K. Advances in microRNA experimental approaches to study physiological regulation of gene products implicated in CNS disorders. *Exp. Neurol.* **2012**, *235*, 402–418.

[224] Gu, S.; Jin, L.; Zhang, F.; Sarnow, P.; Kay, M. A. Biological basis for restriction of microRNA targets to the 3' untranslated region in mammalian mRNAs. *Nat. Struct. Mol. Biol.* **2009**, *16*, 144–150.

[225] Chi, S. W.; Zang, J. B.; Mele, A.; Darnell, R. B. Argonaute HITS-CLIP decodes microRNA-mRNA interaction maps. *Nature* **2009**, *460*, 479–486.

[226] Vasudevan, S. Posttranscriptional Upregulation by MicroRNAs. *Wiley Interdiscip Rev RNA* **2012**, *3*, 311–330.

[227] Guo, H.; Ingolia, N. T.; Weissman, J. S.; Bartel, D. P. Mammalian microRNAs predominantly act to decrease target mRNA levels. *Nature* **2010**, *466*, 835–840.

[228] Hendrickson, D. G.; Hogan, D. J.; McCullough, H. L.; Myers, J. W.; Herschlag, D.; Ferrell, J. E.; Brown, P. O. Concordant regulation of translation and mRNA abundance for hundreds of targets of a human microRNA. *PLoS Biol.* **2009**, *7*, e1000238.

[229] Djuranovic, S.; Nahvi, A.; Green, R. miRNA-mediated gene silencing by translational repression followed by mRNA deadenylation and decay. *Science* **2012**, *336*, 237–240.

[230] Djuranovic, S.; Nahvi, A.; Green, R. A Parsimonious Model for Gene Regulation by miRNAs. *Science* **2011**, *331*, 550–553.

[231] Bazzini, A. A.; Lee, M. T.; Giraldez, A. J. Ribosome Profiling Shows That miR-430 Reduces Translation Before Causing mRNA Decay in Zebrafish. *Science (New York, N.Y.)* **2012**.

[232] Takimoto, K.; Wakiyama, M.; Yokoyama, S. Mammalian GW182 contains multiple Argonaute-binding sites and functions in microRNA-mediated translational repression. *RNA* **2009**, *15*, 1078–1089.

[233] Eulalio, A.; Huntzinger, E.; Izaurralde, E. GW182 interaction with Argonaute is essential for miRNA-mediated translational repression and mRNA decay. *Nat. Struct. Mol. Biol.* **2008**, *15*, 346–353.

[234] Behm-Ansmant, I.; Rehwinkel, J.; Doerks, T.; Stark, A.; Bork, P.; Izaurralde, E. mRNA degradation by miRNAs and GW182 requires both CCR4:NOT deadenylase and DCP1:DCP2 decapping complexes. *Genes Dev.* **2006**, *20*, 1885–1898.

[235] Eulalio, A.; Rehwinkel, J.; Stricker, M.; Huntzinger, E.; Yang, S.-F.; Doerks, T.; Dorner, S.; Bork, P.; Boutros, M.; Izaurralde, E. Target-specific requirements for enhancers of decapping in miRNA-mediated gene silencing. *Genes Dev.* **2007**, *21*, 2558–2570.

[236] Chen, C.-Y. A.; Zheng, D.; Xia, Z.; Shyu, A.-B. Ago-TNRC6 triggers microRNA-mediated decay by promoting two deadenylation steps. *Nat. Struct. Mol. Biol.* **2009**, *16*, 1160–1166.

[237] Braun, J. E.; Huntzinger, E.; Fauser, M.; Izaurralde, E. GW182 proteins directly recruit cytoplasmic deadenylase complexes to miRNA targets. *Mol. Cell* **2011**, *44*, 120–133.

[238] Chekulaeva, M.; Mathys, H.; Zipprich, J. T.; Attig, J.; Colic, M.; Parker, R.; Filipowicz, W. miRNA repression involves GW182-mediated recruitment of CCR4-NOT through conserved W-containing motifs. *Nat. Struct. Mol. Biol.* **2011**, *18*, 1218–1226.

[239] Humphreys, D. T.; Westman, B. J.; Martin, D. I. K.; Preiss, T. MicroRNAs control translation initiation by inhibiting eukaryotic initiation factor 4E/cap and poly(A) tail function. *Proc. Natl. Acad. Sci. U.S.A.* **2005**, *102*, 16961–16966.

[240] Friend, K.; Campbell, Z. T.; Cooke, A.; Kroll-Conner, P.; Wickens, M. P.; Kimble, J. A conserved PUF-Ago-eEF1A complex attenuates translation elongation. *Nat. Struct. Mol. Biol.* **2012**, *19*, 176–183.

[241] Mukherji, S.; Ebert, M. S.; Zheng, G. X. Y.; Tsang, J. S.; Sharp, P. A.; van Oudenaarden, A. MicroRNAs can generate thresholds in target gene expression. *Nat. Genet.* **2011**, *43*, 854–859.

[242] Brown, B. D.; Gentner, B.; Cantore, A.; Colleoni, S.; Amendola, M.; Zingale, A.; Baccarini, A.; Lazzari, G.; Galli, C.; Naldini, L. Endogenous microRNA can be broadly exploited to regulate transgene expression according to tissue, lineage and differentiation state. *Nat. Biotechnol.* **2007**, *25*, 1457–1467.

[243] Friedman, R. C.; Farh, K. K.-H.; Burge, C. B.; Bartel, D. P. Most mammalian mRNAs are conserved targets of microRNAs. *Genome Res.* **2009**, *19*, 92–105.

[244] Selbach, M.; Schwanhäusser, B.; Thierfelder, N.; Fang, Z.; Khanin, R.; Rajewsky, N. Widespread changes in protein synthesis induced by microRNAs. *Nature* **2008**, *455*, 58–63.

[245] Baek, D.; Villén, J.; Shin, C.; Camargo, F. D.; Gygi, S. P.; Bartel, D. P. The impact of microRNAs on protein output. *Nature* **2008**, *455*, 64–71.

[246] Seitz, H. Redefining microRNA targets. *Curr. Biol.* **2009**, *19*, 870–873.

[247] Salmena, L.; Poliseno, L.; Tay, Y.; Kats, L.; Pandolfi, P. P. A ceRNA hypothesis: the Rosetta Stone of a hidden RNA language? *Cell* **2011**, *146*, 353–358.

[248] Karreth, F. A.; Tay, Y.; Perna, D.; Ala, U.; Tan, S. M.; Rust, A. G.; Denicola, G.; Webster, K. A.; Weiss, D.; Perez-Mancera, P. A.; Krauthammer, M.; Halaban, R.; Provero, P.; Adams, D. J.; Tuveson, D. A.; Pandolfi, P. P. In Vivo Identification of Tumor- Suppressive PTEN ceRNAs in an Oncogenic BRAF-Induced Mouse Model of Melanoma. *Cell* **2011**, *147*, 382–95.

[249] Tay, Y.; Kats, L.; Salmena, L.; Weiss, D.; Tan, S. M.; Ala, U.; Karreth, F.; Poliseno, L.; Provero, P.; Di Cunto, F.; Lieberman, J.; Rigoutsos, I.; Pandolfi, P. P. Coding-Independent Regulation of the Tumor Suppressor PTEN by Competing Endogenous mRNAs. *Cell* **2011**, *147*, 344–357.

[250] Cesana, M.; Cacchiarelli, D.; Legnini, I.; Santini, T.; Sthandier, O.; Chinappi, M.; Tramontano, A.; Bozzoni, I. A long noncoding RNA controls muscle differentiation by functioning as a competing endogenous RNA. *Cell* **2011**, *147*, 358–369.

[251] Larsson, E.; Sander, C.; Marks, D. mRNA turnover rate limits siRNA and microRNA efficacy. *Mol. Syst. Biol.* **2010**, *6*, 433.

[252] Wang, Y.; Sheng, G.; Juranek, S.; Tuschl, T.; Patel, D. J. Structure of the guide-strand-containing argonaute silencing complex. *Nature* **2008**, *456*, 209–213.

[253] Winter, J.; Diederichs, S. Argonaute proteins regulate microRNA stability: Increased microRNA abundance by Argonaute proteins is due to microRNA stabilization. *RNA Biol.* **2011**, *8*.

[254] Gantier, M. P.; McCoy, C. E.; Rusinova, I.; Saulep, D.; Wang, D.; Xu, D.; Irving, A. T.; Behlke, M. A.; Hertzog, P. J.; Mackay, F.; Williams, B. R. G. Analysis of microRNA turnover in mammalian cells following Dicer1 ablation. *Nucleic Acids Res.* **2011**, *39*, 5692–5703.

[255] Sethi, P.; Lukiw, W. J. Micro-RNA abundance and stability in human brain: specific alterations in Alzheimer's disease temporal lobe neocortex. *Neurosci. Lett.* **2009**, *459*, 100–104.

[256] Krol, J.; Busskamp, V.; Markiewicz, I.; Stadler, M. B.; Ribi, S.; Richter, J.; Duebel, J.; Bicker, S.; Fehling, H. J.; Schübeler, D.; Oertner, T. G.; Schratt, G.; Bibel, M.; Roska, B.; Filipowicz, W. Characterizing light-regulated retinal microRNAs reveals rapid turnover as a common property of neuronal microRNAs. *Cell* **2010**, *141*, 618–631.

[257] Kai, Z. S.; Pasquinelli, A. E. MicroRNA assassins: factors that regulate the disappearance of miRNAs. *Nat. Struct. Mol. Biol.* **2010**, *17*, 5–10.

[258] Siomi, H.; Siomi, M. C. Posttranscriptional regulation of microRNA biogenesis in animals. *Mol. Cell* **2010**, *38*, 323–332.

[259] Katoh, T.; Sakaguchi, Y.; Miyauchi, K.; Suzuki, T.; Kashiwabara, S.-I.; Baba, T.; Suzuki, T. Selective stabilization of mammalian microRNAs by 3' adenylation mediated by the cytoplasmic poly(A) polymerase GLD-2. *Genes Dev.* **2009**, *23*, 433–438.

[260] Heo, I.; Joo, C.; Cho, J.; Ha, M.; Han, J.; Kim, V. N. Lin28 mediates the terminal uridylation of let-7 precursor MicroRNA. *Mol. Cell* **2008**, *32*, 276–284.

[261] Heo, I.; Joo, C.; Kim, Y.-K.; Ha, M.; Yoon, M.-J.; Cho, J.; Yeom, K.-H.; Han, J.; Kim, V. N. TUT4 in concert with Lin28 suppresses microRNA biogenesis through pre-microRNA uridylation. *Cell* **2009**, *138*, 696–708.

[262] Yeom, K.-H.; Heo, I.; Lee, J.; Hohng, S.; Kim, V. N.; Joo, C. Single-molecule approach to immunoprecipitated protein complexes: insights into miRNA uridylation. *EMBO Rep.* **2011**, *12*, 690–696.

[263] Burroughs, A. M.; Kawano, M.; Ando, Y.; Daub, C. O.; Hayashizaki, Y. pre-miRNA profiles obtained through application of locked nucleic acids and deep sequencing reveals complex 5'/3' arm variation including concomitant cleavage and polyuridylation patterns. *Nucleic Acids Res.* **2011**.

[264] Newman, M. A.; Mani, V.; Hammond, S. M. Deep sequencing of microRNA precursors reveals extensive 3' end modification. *RNA* **2011**, *17*, 1795–1803.

[265] Lukiw, W. J. Micro-RNA speciation in fetal, adult and Alzheimer's disease hippocampus. *Neuroreport* **2007**, *18*, 297–300.

[266] Wang, W.-X.; Rajeev, B. W.; Stromberg, A. J.; Ren, N.; Tang, G.; Huang, Q.; Rigoutsos, I.; Nelson, P. T. The expression of microRNA miR-107 decreases early in Alzheimer's disease and may accelerate disease progression through regulation of beta-site amyloid precursor protein-cleaving enzyme 1. *J. Neurosci.* **2008**, *28*, 1213–1223.

[267] Cogswell, J. P.; Ward, J.; Taylor, I. A.; Waters, M.; Shi, Y.; Cannon, B.; Kelnar, K.; Kemppainen, J.; Brown, D.; Chen, C.; Prinjha, R. K.; Richardson, J. C.; Saunders, A. M.; Roses, A. D.; Richards, C. A. Identification of miRNA changes in Alzheimer's disease brain and CSF yields putative biomarkers and insights into disease pathways. *J. Alzheimers Dis.* **2008**, *14*, 27–41.

[268] Nunez-Iglesias, J.; Liu, C.-C.; Morgan, T. E.; Finch, C. E.; Zhou, X. J. Joint genome-wide profiling of miRNA and mRNA expression in Alzheimer's disease cortex reveals altered miRNA regulation. *PLoS ONE* **2010**, *5*, e8898.

[269] Schipper, H. M.; Maes, O. C.; Chertkow, H. M.; Wang, E. MicroRNA expression in Alzheimer blood mononuclear cells. *Gene Regul. Syst. Bio.* **2007**, *1*, 263–274.

[270] Delay, C.; Mandemakers, W.; Hébert, S. S. MicroRNAs in Alzheimer's disease. *Neurobiol. Dis.* **2012**, *46*, 285–290.

[271] Geekiyanage, H.; Chan, C. MicroRNA-137/181c Regulates Serine Palmitoyltransferase and In Turn Amyloid {beta}, Novel Targets in Sporadic Alzheimer's Disease. *J Neurosci* **2011**, *31*, 14820–30.

[272] Shioya, M.; Obayashi, S.; Tabunoki, H.; Arima, K.; Saito, Y.; Ishida, T.; Satoh, J. Aberrant microRNA expression in the brains of neurodegenerative diseases: miR-29a decreased in Alzheimer disease brains targets neurone navigator 3. *Neuropathol Appl Neurobiol* **2010**, *36*, 320–30.

[273] Nelson, P. T.; Wang, W.-X. MiR-107 is reduced in Alzheimer's disease brain neocortex: validation study. *J. Alzheimers Dis.* **2010**, *21*, 75–79.

[274] Smith, P.; Al Hashimi, A.; Girard, J.; Delay, C.; Hébert, S. S. In vivo regulation of amyloid precursor protein neuronal splicing by microRNAs. *J. Neurochem.* **2011**, *116*, 240–247.

[275] Cimmino, A.; Calin, G. A.; Fabbri, M.; Iorio, M. V.; Ferracin, M.; Shimizu, M.; Wojcik, S. E.; Aqeilan, R. I.; Zupo, S.; Dono, M.; Rassenti, L.; Alder, H.; Volinia, S.; Liu, C.-G.; Kipps, T. J.; Negrini, M.; Croce, C. M. miR-15 and miR-16 induce apoptosis by targeting BCL2. *Proc. Natl. Acad. Sci. U.S.A.* **2005**, *102*, 13944–13949.

[276] Hébert, S. S.; Horré, K.; Nicolaï, L.; Bergmans, B.; Papadopoulou, A. S.; Delacourte, A.; De Strooper, B. MicroRNA regulation of Alzheimer's Amyloid precursor protein expression. *Neurobiol. Dis.* **2009**, *33*, 422–428.

[277] Wang, H.; Liu, J.; Zong, Y.; Xu, Y.; Deng, W.; Zhu, H.; Liu, Y.; Ma, C.; Huang, L.; Zhang, L.; Qin, C. miR-106b aberrantly expressed in a double transgenic mouse model for Alzheimer's disease targets TGF-beta type II receptor. *Brain Res* **2010**, *1357*, 166–74.

[278] Lukiw, W. J.; Zhao, Y.; Cui, J. G. An NF-kappaB-sensitive micro RNA-146a-mediated inflammatory circuit in Alzheimer disease and in stressed human brain cells. *J Biol Chem* **2008**, *283*, 31315–22.

[279] Li, Y. Y.; Cui, J. G.; Hill, J. M.; Bhattacharjee, S.; Zhao, Y.; Lukiw, W. J. Increased expression of miRNA-146a in Alzheimer's disease transgenic mouse models. *Neurosci. Lett.* **2011**, *487*, 94–98.

[280] de Lencastre, A.; Pincus, Z.; Zhou, K.; Kato, M.; Lee, S. S.; Slack, F. J. MicroRNAs both promote and antagonize longevity in C. elegans. *Curr. Biol.* **2010**, *20*, 2159–2168.

[281] Inukai, S.; de Lencastre, A.; Turner, M.; Slack, F. Novel microRNAs differentially expressed during aging in the mouse brain. *PLoS ONE* **2012**, *7*, e40028.

[282] Liu, N.; Landreh, M.; Cao, K.; Abe, M.; Hendriks, G.-J.; Kennerdell, J. R.; Zhu, Y.; Wang, L.-S.; Bonini, N. M. The microRNA miR-34 modulates ageing and neurodegeneration in Drosophila. *Nature* **2012**, *482*, 519–523.

[283] Noren Hooten, N.; Abdelmohsen, K.; Gorospe, M.; Ejiogu, N.; Zonderman, A. B.; Evans, M. K. microRNA expression patterns reveal differential expression of target genes with age. *PLoS ONE* **2010**, *5*, e10724.

[284] Yankner, B. A.; Lu, T.; Loerch, P. The aging brain. *Annu Rev Pathol* **2008**, *3*, 41–66.

[285] Morrison, J. H.; Hof, P. R. Life and death of neurons in the aging brain. *Science* **1997**, *278*, 412–419.

[286] Lee, C. K.; Weindruch, R.; Prolla, T. A. Gene-expression profile of the ageing brain in mice. *Nat. Genet.* **2000**, *25*, 294–297.

[287] Lu, T.; Pan, Y.; Kao, S.-Y.; Li, C.; Kohane, I.; Chan, J.; Yankner, B. A. Gene regulation and DNA damage in the ageing human brain. *Nature* **2004**, *429*, 883–891.

[288] Fraser, H. B.; Khaitovich, P.; Plotkin, J. B.; Pääbo, S.; Eisen, M. B. Aging and gene expression in the primate brain. *PLoS Biol.* **2005**, *3*, e274.

[289] Jiang, C. H.; Tsien, J. Z.; Schultz, P. G.; Hu, Y. The effects of aging on gene expression in the hypothalamus and cortex of mice. *Proc. Natl. Acad. Sci. U.S.A.* **2001**, *98*, 1930–1934.

[290] Blalock, E. M.; Chen, K.-C.; Sharrow, K.; Herman, J. P.; Porter, N. M.; Foster, T. C.; Landfield, P. W. Gene microarrays in hippocampal aging: statistical profiling identifies novel processes correlated with cognitive impairment. *J. Neurosci.* **2003**, *23*, 3807–3819.

[291] Persengiev, S.; Kondova, I.; Otting, N.; Koeppen, A. H.; Bontrop, R. E. Genome-wide analysis of miRNA expression reveals a potential role for miR-144 in brain aging and spinocerebellar ataxia pathogenesis. *Neurobiol. Aging* **2011**, *32*, 2316.e17–27.

[292] Pleasure, S. J.; Page, C.; Lee, V. M. Pure, postmitotic, polarized human neurons derived from NTera 2 cells provide a system for expressing exogenous proteins in terminally differentiated neurons. *J. Neurosci.* **1992**, *12*, 1802–1815.

[293] Pleasure, S. J.; Lee, V. M. NTera 2 cells: a human cell line which displays characteristics expected of a human committed neuronal progenitor cell. *J. Neurosci. Res.* **1993**, *35*, 585–602.

[294] Ray, B.; Bailey, J. A.; Sarkar, S.; Lahiri, D. K. Molecular and immunocytochemical characterization of primary neuronal cultures from adult rat brain: Differential expression of neuronal and glial protein markers. *J. Neurosci. Methods* **2009**, *184*, 294–302.

[295] Schroeder, A.; Mueller, O.; Stocker, S.; Salowsky, R.; Leiber, M.; Gassmann, M.; Lightfoot, S.; Menzel, W.; Granzow, M.; Ragg, T. The RIN: an RNA integrity number for assigning integrity values to RNA measurements. *BMC Mol. Biol.* **2006**, *7*, 3.

[296] Smith, P. K.; Krohn, R. I.; Hermanson, G. T.; Mallia, A. K.; Gartner, F. H.; Provenzano, M. D.; Fujimoto, E. K.; Goeke, N. M.; Olson, B. J.; Klenk, D. C. Measurement of protein using bicinchoninic acid. *Anal. Biochem.* **1985**, *150*, 76–85.

[297] Laemmli, U. K. Cleavage of structural proteins during the assembly of the head of bacteriophage T4. *Nature* **1970**, *227*, 680–685.

[298] Chen, C.; Ridzon, D. A.; Broomer, A. J.; Zhou, Z.; Lee, D. H.; Nguyen, J. T.; Barbisin, M.; Xu, N. L.; Mahuvakar, V. R.; Andersen, M. R.; Lao, K. Q.; Livak, K. J.; Guegler, K. J. Real-time quantification of microRNAs by stem-loop RT-PCR. *Nucleic Acids Res.* **2005**, *33*, e179.

[299] Livak, K. J.; Schmittgen, T. D. Analysis of relative gene expression data using real-time quantitative PCR and the 2(-Delta Delta C(T)) Method. *Methods* **2001**, *25*, 402–408.

[300] Pfaffl, M. W. A new mathematical model for relative quantification in real-time RT-PCR. *Nucleic Acids Res.* **2001**, *29*, e45.

[301] Vandesompele, J.; De Preter, K.; Pattyn, F.; Poppe, B.; Van Roy, N.; De Paepe, A.; Speleman, F. Accurate normalization of real-time quantitative RT-PCR data by geometric averaging of multiple internal control genes. *Genome Biol.* **2002**, *3*, research0034.1–0034.11.

[302] Hellemans, J.; Mortier, G.; De Paepe, A.; Speleman, F.; Vandesompele, J. qBase relative quantification framework and software for management and automated analysis of real-time quantitative PCR data. *Genome Biol* **2007**, *8*, R19.

[303] Lewis, B. P.; Burge, C. B.; Bartel, D. P. Conserved seed pairing, often flanked by adenosines, indicates that thousands of human genes are microRNA targets. *Cell* **2005**, *120*, 15–20.

[304] Grimson, A.; Farh, K. K.-H.; Johnston, W. K.; Garrett-Engele, P.; Lim, L. P.; Bartel, D. P. MicroRNA targeting specificity in mammals: determinants beyond seed pairing. *Mol. Cell* **2007**, *27*, 91–105.

[305] Garcia, D. M.; Baek, D.; Shin, C.; Bell, G. W.; Grimson, A.; Bartel, D. P. Weak seed-pairing stability and high target-site abundance decrease the proficiency of lsy-6 and other microRNAs. *Nat. Struct. Mol. Biol.* **2011**, *18*, 1139–1146.

[306] Krek, A.; Grün, D.; Poy, M. N.; Wolf, R.; Rosenberg, L.; Epstein, E. J.; MacMenamin, P.; da Piedade, I.; Gunsalus, K. C.; Stoffel, M.; Rajewsky, N. Combinatorial microRNA target predictions. *Nat. Genet.* **2005**, *37*, 495–500.

[307] Kiriakidou, M.; Nelson, P. T.; Kouranov, A.; Fitziev, P.; Bouyioukos, C.; Mourelatos, Z.; Hatzigeorgiou, A. A combined computational-experimental approach predicts human microRNA targets. *Genes Dev.* **2004**, *18*, 1165–1178.

[308] Maragkakis, M.; Alexiou, P.; Papadopoulos, G. L.; Reczko, M.; Dalamagas, T.; Giannopoulos, G.; Goumas, G.; Koukis, E.; Kourtis, K.; Simossis, V. A.; Sethupathy, P.; Vergoulis, T.; Koziris, N.; Sellis, T.; Tsanakas, P.; Hatzigeorgiou, A. G. Accurate microRNA target prediction correlates with protein repression levels. *BMC Bioinformatics* **2009**, *10*, 295.

[309] Maragkakis, M.; Reczko, M.; Simossis, V. A.; Alexiou, P.; Papadopoulos, G. L.; Dalamagas, T.; Giannopoulos, G.; Goumas, G.; Koukis, E.; Kourtis, K.; Vergoulis, T.; Koziris, N.; Sellis, T.; Tsanakas, P.; Hatzigeorgiou, A. G. DIANA-microT web server: elucidating microRNA functions through target prediction. *Nucleic Acids Res.* **2009**, *37*, W273–276.

[310] Maragkakis, M.; Vergoulis, T.; Alexiou, P.; Reczko, M.; Plomaritou, K.; Gousis, M.; Kourtis, K.; Koziris, N.; Dalamagas, T.; Hatzigeorgiou, A. G. DIANA-microT Web server upgrade supports Fly and Worm miRNA target prediction and bibliographic miRNA to disease association. *Nucleic Acids Res.* **2011**, *39*, W145–148.

[311] Enright, A. J.; John, B.; Gaul, U.; Tuschl, T.; Sander, C.; Marks, D. S. MicroRNA targets in Drosophila. *Genome Biol.* **2003**, *5*, R1.

[312] John, B.; Enright, A. J.; Aravin, A.; Tuschl, T.; Sander, C.; Marks, D. S. Human MicroRNA targets. *PLoS Biol.* **2004**, *2*, e363.

[313] Betel, D.; Wilson, M.; Gabow, A.; Marks, D. S.; Sander, C. The microRNA.org resource: targets and expression. *Nucleic Acids Res.* **2008**, *36*, D149–153.

[314] Betel, D.; Koppal, A.; Agius, P.; Sander, C.; Leslie, C. Comprehensive modeling of microRNA targets predicts functional non-conserved and non-canonical sites. *Genome Biol.* **2010**, *11*, R90.

[315] Kertesz, M.; Iovino, N.; Unnerstall, U.; Gaul, U.; Segal, E. The role of site accessibility in microRNA target recognition. *Nat. Genet.* **2007**, *39*, 1278–1284.

[316] Miranda, K. C.; Huynh, T.; Tay, Y.; Ang, Y.-S.; Tam, W.-L.; Thomson, A. M.; Lim, B.; Rigoutsos, I. A pattern-based method for the identification of MicroRNA binding sites and their corresponding heteroduplexes. *Cell* **2006**, *126*, 1203–1217.

[317] Meister, G.; Landthaler, M.; Patkaniowska, A.; Dorsett, Y.; Teng, G.; Tuschl, T. Human Argonaute2 mediates RNA cleavage targeted by miRNAs and siRNAs. *Mol. Cell* **2004**, *15*, 185–197.

[318] Patel, N.; Hoang, D.; Miller, N.; Ansaloni, S.; Huang, Q.; Rogers, J. T.; Lee, J. C.; Saunders, A. J. MicroRNAs can regulate human APP levels. *Mol. Neurodegener.* **2008**, *3*, 10.

[319] Buechner, J.; Tømte, E.; Haug, B. H.; Henriksen, J. R.; Løkke, C.; Flægstad, T.; Einvik, C. Tumour-suppressor microRNAs let-7 and mir-101 target the proto-oncogene MYCN and inhibit cell proliferation in MYCN-amplified neuroblastoma. *Br. J. Cancer* **2011**, *105*, 296–303.

[320] Cao, P.; Deng, Z.; Wan, M.; Huang, W.; Cramer, S. D.; Xu, J.; Lei, M.; Sui, G. MicroRNA-101 negatively regulates Ezh2 and its expression is modulated by androgen receptor and HIF-1alpha/HIF-1beta. *Mol. Cancer* **2010**, *9*, 108.

[321] Varambally, S.; Cao, Q.; Mani, R.-S.; Shankar, S.; Wang, X.; Ateeq, B.; Laxman, B.; Cao, X.; Jing, X.; Ramnarayanan, K.; Brenner, J. C.; Yu, J.; Kim, J. H.; Han, B.; Tan, P.; Kumar-Sinha, C.; Lonigro, R. J.; Palanisamy, N.; Maher, C. A.; Chinnaiyan, A. M. Genomic loss of microRNA-101 leads to overexpression of histone methyltransferase EZH2 in cancer. *Science* **2008**, *322*, 1695–1699.

[322] Frankel, L. B.; Wen, J.; Lees, M.; Høyer-Hansen, M.; Farkas, T.; Krogh, A.; Jäättelä, M.; Lund, A. H. microRNA-101 is a potent inhibitor of autophagy. *EMBO J.* **2011**, *30*, 4628–4641.

[323] Lee, Y.; Samaco, R. C.; Gatchel, J. R.; Thaller, C.; Orr, H. T.; Zoghbi, H. Y. miR-19, miR-101 and miR-130 co-regulate ATXN1 levels to potentially modulate SCA1 pathogenesis. *Nat. Neurosci.* **2008**, *11*, 1137–1139.

[324] Ørom, U. A.; Nielsen, F. C.; Lund, A. H. MicroRNA-10a binds the 5'UTR of ribosomal protein mRNAs and enhances their translation. *Mol. Cell* **2008**, *30*, 460–471.

[325] Wang, W.-X.; Wilfred, B. R.; Madathil, S. K.; Tang, G.; Hu, Y.; Dimayuga, J.; Stromberg, A. J.; Huang, Q.; Saatman, K. E.; Nelson, P. T. miR-107 regulates granulin/progranulin with implications for traumatic brain injury and neurodegenerative disease. *Am. J. Pathol.* **2010**, *177*, 334–345.

[326] Huang, H.-Y.; Chien, C.-H.; Jen, K. H.; Huang, H. D. RegRNA: an integrated web server for identifying regulatory RNA motifs and elements. *Nucleic Acids Res* **2006**, *34*, W429–434.

[327] Filipowicz, W.; Bhattacharyya, S. N.; Sonenberg, N. Mechanisms of post-transcriptional regulation by microRNAs: are the answers in sight? *Nat. Rev. Genet.* **2008**, *9*, 102–114.

[328] Mirra, S. S.; Heyman, A.; McKeel, D.; Sumi, S. M.; Crain, B. J.; Brownlee, L. M.; Vogel, F. S.; Hughes, J. P.; van Belle, G.; Berg, L. The Consortium to Establish a Registry for Alzheimer's Disease (CERAD). Part II. Standardization of the neuropathologic assessment of Alzheimer's disease. *Neurology* **1991**, *41*, 479–486.

[329] Manczak, M.; Calkins, M. J.; Reddy, P. H. Impaired mitochondrial dynamics and abnormal interaction of amyloid beta with mitochondrial protein Drp1 in neurons from patients with Alzheimer's disease: implications for neuronal damage. *Hum. Mol. Genet.* **2011**, *20*, 2495–2509.

[330] Consensus recommendations for the postmortem diagnosis of Alzheimer's disease. The National Institute on Aging, and Reagan Institute Working Group on Diagnostic Criteria for the Neuropathological Assessment of Alzheimer's Disease. *Neurobiol. Aging* **1997**, *18*, S1–2.

[331] Mishima, T.; Mizuguchi, Y.; Kawahigashi, Y.; Takizawa, T.; Takizawa, T. RT-PCR-based analysis of microRNA (miR-1 and -124) expression in mouse CNS. *Brain Res.* **2007**, *1131*, 37–43.

[332] Deo, M.; Yu, J.-Y.; Chung, K.-H.; Tippens, M.; Turner, D. L. Detection of mammalian microRNA expression by in situ hybridization with RNA oligonucleotides. *Dev. Dyn.* **2006**, *235*, 2538–2548.

[333] Fang, M.; Wang, J.; Zhang, X.; Geng, Y.; Hu, Z.; Rudd, J. A.; Ling, S.; Chen, W.; Han, S. The miR-124 regulates the expression of BACE1/β-secretase correlated with cell death in Alzheimer's disease. *Toxicol. Lett.* **2012**, *209*, 94–105.

[334] Nelson, P. T.; Jicha, G. A.; Schmitt, F. A.; Liu, H.; Davis, D. G.; Mendiondo, M. S.; Abner, E. L.; Markesbery, W. R. Clinicopathologic correlations in a large Alzheimer disease center autopsy cohort: neuritic plaques and neurofibrillary tangles "do count" when staging disease severity. *J. Neuropathol. Exp. Neurol.* **2007**, *66*, 1136–1146.

[335] Fukumoto, H.; Cheung, B. S.; Hyman, B. T.; Irizarry, M. C. Beta-secretase protein and activity are increased in the neocortex in Alzheimer disease. *Arch. Neurol.* **2002**, *59*, 1381–1389.

[336] De Sauvage, F.; Kruis, V.; Maloteaux, J. M.; Huez, G.; Octave, J. N. The 3' untranslated region of the A4 amyloid mRNA stimulates the translation. *Acta Neurol Belg* **1989**, *89*, 313.

[337] Amara, F. M.; Junaid, A.; Clough, R. R.; Liang, B. TGF-beta(1), regulation of alzheimer amyloid precursor protein mRNA expression in a normal human astrocyte cell line: mRNA stabilization. *Brain Res. Mol. Brain Res.* **1999**, *71*, 42–49.

[338] Fan, X.; Liu, Y.; Jiang, J.; Ma, Z.; Wu, H.; Liu, T.; Liu, M.; Li, X.; Tang, H. miR-20a promotes proliferation and invasion by targeting APP in human ovarian cancer cells. *Acta Biochim. Biophys. Sin. (Shanghai)* **2010**, *42*, 318–324.

[339] Hafner, M.; Landthaler, M.; Burger, L.; Khorshid, M.; Hausser, J.; Berninger, P.; Rothballer, A.; Ascano, M., Jr; Jungkamp, A.-C.; Munschauer, M.; Ulrich, A.; Wardle, G. S.; Dewell, S.; Zavolan, M.; Tuschl, T. Transcriptome-wide identification of RNA-binding protein and microRNA target sites by PAR-CLIP. *Cell* **2010**, *141*, 129–141.

[340] Wang, W.-X.; Wilfred, B. R.; Hu, Y.; Stromberg, A. J.; Nelson, P. T. Anti-Argonaute RIP-Chip shows that miRNA transfections alter global patterns of mRNA recruitment to microribonucleoprotein complexes. *RNA* **2010**, *16*, 394–404.

[341] Nonne, N.; Ameyar-Zazoua, M.; Souidi, M.; Harel-Bellan, A. Tandem affinity purification of miRNA target mRNAs (TAP-Tar). *Nucleic Acids Res.* **2010**, *38*, e20.

[342] Doxakis, E. Post-transcriptional regulation of alpha-synuclein expression by mir-7 and mir-153. *J Biol Chem* **2010**, *285*, 12726–34.

[343] Baba, M.; Nakajo, S.; Tu, P. H.; Tomita, T.; Nakaya, K.; Lee, V. M.; Trojanowski, J. Q.; Iwatsubo, T. Aggregation of alpha-synuclein in Lewy bodies of sporadic Parkinson's disease and dementia with Lewy bodies. *Am. J. Pathol.* **1998**, *152*, 879–884.

[344] Förstl, H.; Burns, A.; Luthert, P.; Cairns, N.; Levy, R. The Lewy-body variant of Alzheimer's disease. Clinical and pathological findings. *Br. J. Psychiatry* **1993**, *162*, 385–392.

[345] Heyman, A.; Fillenbaum, G. G.; Gearing, M.; Mirra, S. S.; Welsh-Bohmer, K. A.; Peterson, B.; Pieper, C. Comparison of Lewy body variant of Alzheimer's disease with pure Alzheimer's disease: Consortium to Establish a Registry for Alzheimer's Disease, Part XIX. *Neurology* **1999**, *52*, 1839–1844.

[346] Hansen, L.; Salmon, D.; Galasko, D.; Masliah, E.; Katzman, R.; DeTeresa, R.; Thal, L.; Pay, M. M.; Hofstetter, R.; Klauber, M. The Lewy body variant of Alzheimer's disease: a clinical and pathologic entity. *Neurology* **1990**, *40*, 1–8.

[347] Hamilton, R. L. Lewy bodies in Alzheimer's disease: a neuropathological review of 145 cases using alpha-synuclein immunohistochemistry. *Brain Pathol.* **2000**, *10*, 378–384.

[348] Kraybill, M. L.; Larson, E. B.; Tsuang, D. W.; Teri, L.; McCormick, W. C.; Bowen, J. D.; Kukull, W. A.; Leverenz, J. B.; Cherrier, M. M. Cognitive differences in dementia patients with autopsy-verified AD, Lewy body pathology, or both. *Neurology* **2005**, *64*, 2069–2073.

[349] Olichney, J. M.; Galasko, D.; Salmon, D. P.; Hofstetter, C. R.; Hansen, L. A.; Katzman, R.; Thal, L. J. Cognitive decline is faster in Lewy body variant than in Alzheimer's disease. *Neurology* **1998**, *51*, 351–357.

[350] Mukaetova-Ladinska, E. B.; Xuereb, J. H.; Garcia-Sierra, F.; Hurt, J.; Gertz, H.-J.; Hills, R.; Brayne, C.; Huppert, F. A.; Paykel, E. S.; McGee, M. A.; Jakes, R.; Honer, W. G.; Harrington, C. R.; Wischik, C. M. Lewy body variant of Alzheimer's disease: selective neocortical loss of t-SNARE proteins and loss of MAP2 and alpha-synuclein in medial temporal lobe. *ScientificWorldJournal* **2009**, *9*, 1463–1475.

[351] Clinton, L. K.; Blurton-Jones, M.; Myczek, K.; Trojanowski, J. Q.; LaFerla, F. M. Synergistic Interactions between Abeta, tau, and alpha-synuclein: acceleration of neuropathology and cognitive decline. *J. Neurosci.* **2010**, *30*, 7281–7289.

[352] Nixon, R. A.; Wegiel, J.; Kumar, A.; Yu, W. H.; Peterhoff, C.; Cataldo, A.; Cuervo, A. M. Extensive involvement of autophagy in Alzheimer disease: an immuno-electron microscopy study. *J. Neuropathol. Exp. Neurol.* **2005**, *64*, 113–122.

[353] Yu, W. H.; Cuervo, A. M.; Kumar, A.; Peterhoff, C. M.; Schmidt, S. D.; Lee, J.-H.; Mohan, P. S.; Mercken, M.; Farmery, M. R.; Tjernberg, L. O.; Jiang, Y.; Duff, K.; Uchiyama, Y.; Näslund, J.; Mathews, P. M.; Cataldo, A. M.; Nixon, R. A. Macroautophagy--a novel Beta-amyloid peptide-generating pathway activated in Alzheimer's disease. *J. Cell Biol.* **2005**, *171*, 87–98.

[354] Cheung, Z. H.; Ip, N. Y. Autophagy deregulation in neurodegenerative diseases - recent advances and future perspectives. *J. Neurochem.* **2011**, *118*, 317–325.

[355] Hung, S.-Y.; Huang, W.-P.; Liou, H.-C.; Fu, W.-M. Autophagy protects neuron from Abeta-induced cytotoxicity. *Autophagy* **2009**, *5*, 502–510.

[356] Jaeger, P. A.; Pickford, F.; Sun, C.-H.; Lucin, K. M.; Masliah, E.; Wyss-Coray, T. Regulation of amyloid precursor protein processing by the Beclin 1 complex. *PLoS ONE* **2010**, *5*, e11102.

[357] Banfi, S.; Servadio, A.; Chung, M. Y.; Kwiatkowski, T. J., Jr; McCall, A. E.; Duvick, L. A.; Shen, Y.; Roth, E. J.; Orr, H. T.; Zoghbi, H. Y. Identification and characterization of the gene causing type 1 spinocerebellar ataxia. *Nat. Genet.* **1994**, *7*, 513–520.

[358] Bertram, L.; Lange, C.; Mullin, K.; Parkinson, M.; Hsiao, M.; Hogan, M. F.; Schjeide, B. M. M.; Hooli, B.; Divito, J.; Ionita, I.; Jiang, H.; Laird, N.; Moscarillo, T.; Ohlsen, K. L.; Elliott, K.; Wang, X.; Hu-Lince, D.; Ryder, M.; Murphy, A.; Wagner, S. L.; Blacker, D.; Becker, K. D.; Tanzi, R. E. Genome-wide association analysis reveals putative Alzheimer's disease susceptibility loci in addition to APOE. *Am. J. Hum. Genet.* **2008**, *83*, 623–632.

[359] Zhang, C.; Browne, A.; Child, D.; Divito, J. R.; Stevenson, J. A.; Tanzi, R. E. Loss of function of ATXN1 increases amyloid beta-protein levels by potentiating beta-secretase processing of beta-amyloid precursor protein. *J. Biol. Chem.* **2010**, *285*, 8515–8526.

[360] Heber, S.; Herms, J.; Gajic, V.; Hainfellner, J.; Aguzzi, A.; Rülicke, T.; von Kretzschmar, H.; von Koch, C.; Sisodia, S.; Tremml, P.; Lipp, H. P.; Wolfer, D. P.; Müller, U. Mice with combined gene knock-outs reveal essential and partially redundant functions of amyloid precursor protein family members. *J. Neurosci.* **2000**, *20*, 7951–7963.

[361] Liang, C.; Zhu, H.; Xu, Y.; Huang, L.; Ma, C.; Deng, W.; Liu, Y.; Qin, C. MicroRNA-153 negatively regulates the expression of amyloid precursor protein and amyloid precursor-like protein 2. *Brain Res.* **2012**, *1455*, 103–113.

[362] Strillacci, A.; Griffoni, C.; Sansone, P.; Paterini, P.; Piazzi, G.; Lazzarini, G.; Spisni, E.; Pantaleo, M. A.; Biasco, G.; Tomasi, V. MiR-101 downregulation is involved in cyclooxygenase-2 overexpression in human colon cancer cells. *Exp. Cell Res.* **2009**, *315*, 1439–1447.

[363] Su, H.; Yang, J.-R.; Xu, T.; Huang, J.; Xu, L.; Yuan, Y.; Zhuang, S.-M. MicroRNA-101, down-regulated in hepatocellular carcinoma, promotes apoptosis and suppresses tumorigenicity. *Cancer Res.* **2009**, *69*, 1135–1142.

[364] Wang, H.-J.; Ruan, H.-J.; He, X.-J.; Ma, Y.-Y.; Jiang, X.-T.; Xia, Y.-J.; Ye, Z.-Y.; Tao, H.-Q. MicroRNA-101 is down-regulated in gastric cancer and involved in cell migration and invasion. *Eur. J. Cancer* **2010**, *46*, 2295–2303.

[365] Merkel, O.; Hamacher, F.; Laimer, D.; Sifft, E.; Trajanoski, Z.; Scheideler, M.; Egger, G.; Hassler, M. R.; Thallinger, C.; Schmatz, A.; Turner, S. D.; Greil, R.; Kenner, L. Identification of differential and functionally active miRNAs in both anaplastic lymphoma kinase (ALK)+ and ALK- anaplastic large-cell lymphoma. *Proc. Natl. Acad. Sci. U.S.A.* **2010**, *107*, 16228–16233.

[366] Gao, W.; Shen, H.; Liu, L.; Xu, J.; Xu, J.; Shu, Y. MiR-21 overexpression in human primary squamous cell lung carcinoma is associated with poor patient prognosis. *J. Cancer Res. Clin. Oncol.* **2011**, *137*, 557–566.

[367] Yang, Y.; Li, X.; Yang, Q.; Wang, X.; Zhou, Y.; Jiang, T.; Ma, Q.; Wang, Y.-J. The role of microRNA in human lung squamous cell carcinoma. *Cancer Genet. Cytogenet.* **2010**, *200*, 127–133.

[368] Friedman, J. M.; Liang, G.; Liu, C.-C.; Wolff, E. M.; Tsai, Y. C.; Ye, W.; Zhou, X.; Jones, P. A. The putative tumor suppressor microRNA-101 modulates the cancer epigenome by repressing the polycomb group protein EZH2. *Cancer Res.* **2009**, *69*, 2623–2629.

[369] Li, S.; Fu, H.; Wang, Y.; Tie, Y.; Xing, R.; Zhu, J.; Sun, Z.; Wei, L.; Zheng, X. MicroRNA-101 regulates expression of the v-fos FBJ murine osteosarcoma viral oncogene homolog (FOS) oncogene in human hepatocellular carcinoma. *Hepatology* **2009**, *49*, 1194–1202.

[370] Gaur, A.; Jewell, D. A.; Liang, Y.; Ridzon, D.; Moore, J. H.; Chen, C.; Ambros, V. R.; Israel, M. A. Characterization of microRNA expression levels and their biological correlates in human cancer cell lines. *Cancer Res.* **2007**, *67*, 2456–2468.

[371] Kim, T. H.; Kim, Y. K.; Kwon, Y.; Heo, J. H.; Kang, H.; Kim, G.; An, H. J. Deregulation of miR-519a, 153, and 485-5p and its clinicopathological relevance in ovarian epithelial tumours. *Histopathology* **2010**, *57*, 734–43.

[372] Xu, J.; Liao, X.; Wong, C. Downregulations of B-cell lymphoma 2 and myeloid cell leukemia sequence 1 by microRNA 153 induce apoptosis in a glioblastoma cell line DBTRG-05MG. *Int. J. Cancer* **2010**, *126*, 1029–1035.

[373] Xu, J.; Liao, X.; Lu, N.; Liu, W.; Wong, C.-W. Chromatin-modifying drugs induce miRNA-153 expression to suppress Irs-2 in glioblastoma cell lines. *Int. J. Cancer* **2011**, *129*, 2527–2531.

[374] Liu, L.; Chen, R.; Huang, S.; Wu, Y.; Li, G.; Zhang, B.; Liu, Q.; Yin, D.; Liang, Y. miR-153 sensitized the K562 cells to As2O3-induced apoptosis. *Med. Oncol.* **2011**.

[375] Xie, T.; Liang, J.; Guo, R.; Liu, N.; Noble, P. W.; Jiang, D. Comprehensive microRNA analysis in bleomycin-induced pulmonary fibrosis identifies multiple sites of molecular regulation. *Physiol. Genomics* **2011**, *43*, 479–487.

[376] Stark, A.; Brennecke, J.; Bushati, N.; Russell, R. B.; Cohen, S. M. Animal MicroRNAs confer robustness to gene expression and have a significant impact on 3'UTR evolution. *Cell* **2005**, *123*, 1133–1146.

[377] Lee, I.; Ajay, S. S.; Yook, J. I.; Kim, H. S.; Hong, S. H.; Kim, N. H.; Dhanasekaran, S. M.; Chinnaiyan, A. M.; Athey, B. D. New class of microRNA targets containing simultaneous 5'-UTR and 3'-UTR interaction sites. *Genome Res* **2009**, *19*, 1175–83.

[378] Lytle, J. R.; Yario, T. A.; Steitz, J. A. Target mRNAs are repressed as efficiently by microRNA-binding sites in the 5' UTR as in the 3' UTR. *Proc Natl Acad Sci U S A* **2007**, *104*, 9667–72.

[379] Lin, H.-R.; Ganem, D. Viral microRNA target allows insight into the role of translation in governing microRNA target accessibility. *Proc. Natl. Acad. Sci. U.S.A.* **2011**, *108*, 5148–5153.

[380] Tsai, N. P.; Lin, Y. L.; Wei, L. N. MicroRNA mir-346 targets the 5'-untranslated region of receptor-interacting protein 140 (RIP140) mRNA and up-regulates its protein expression. *Biochem J* **2009**, *424*, 411–8.

[381] Vasudevan, S.; Tong, Y.; Steitz, J. A. Switching from repression to activation: microRNAs can up-regulate translation. *Science* **2007**, *318*, 1931–1934.

[382] Mortensen, R. D.; Serra, M.; Steitz, J. A.; Vasudevan, S. Posttranscriptional activation of gene expression in Xenopus laevis oocytes by microRNA-protein complexes (microRNPs). *Proc. Natl. Acad. Sci. U.S.A.* **2011**, *108*, 8281–8286.

[383] Ma, F.; Liu, X.; Li, D.; Wang, P.; Li, N.; Lu, L.; Cao, X. MicroRNA-466l upregulates IL-10 expression in TLR-triggered macrophages by antagonizing RNA-binding protein tristetraprolin-mediated IL-10 mRNA degradation. *J. Immunol.* **2010**, *184*, 6053–6059.

[384] Ghosh, T.; Soni, K.; Scaria, V.; Halimani, M.; Bhattacharjee, C.; Pillai, B. MicroRNA-mediated up-regulation of an alternatively polyadenylated variant of the mouse cytoplasmic {beta}-actin gene. *Nucleic Acids Res.* **2008**, *36*, 6318–6332.

[385] Semaan, N.; Frenzel, L.; Alsaleh, G.; Suffert, G.; Gottenberg, J. E.; Sibilia, J.; Pfeffer, S.; Wachsmann, D. miR-346 controls release of TNF-alpha protein and stability of its mRNA in rheumatoid arthritis via tristetraprolin stabilization. *PLoS One* **2011**, *6*, e19827.

[386] Bartoszewski, R.; Brewer, J. W.; Rab, A.; Crossman, D. K.; Bartoszewska, S.; Kapoor, N.; Fuller, C.; Collawn, J. F.; Bebok, Z. The unfolded protein response (UPR)-activated transcription factor X-box-binding protein 1 (XBP1) induces microRNA-346 expression that targets the human antigen peptide transporter 1 (TAP1) mRNA and governs immune regulatory genes. *J. Biol. Chem.* **2011**, *286*, 41862–41870.

[387] Weber, F.; Teresi, R. E.; Broelsch, C. E.; Frilling, A.; Eng, C. A limited set of human MicroRNA is deregulated in follicular thyroid carcinoma. *J. Clin. Endocrinol. Metab.* **2006**, *91*, 3584–3591.

[388] Zhu, Y.; Kalbfleisch, T.; Brennan, M. D.; Li, Y. A MicroRNA gene is hosted in an intron of a schizophrenia-susceptibility gene. *Schizophr Res* **2009**, *109*, 86–9.

[389] Fallin, M. D.; Lasseter, V. K.; Avramopoulos, D.; Nicodemus, K. K.; Wolyniec, P. S.; McGrath, J. A.; Steel, G.; Nestadt, G.; Liang, K.-Y.; Huganir, R. L.; Valle, D.; Pulver, A. E. Bipolar I disorder and schizophrenia: a 440-single-nucleotide polymorphism screen of 64 candidate genes among Ashkenazi Jewish case-parent trios. *Am. J. Hum. Genet.* **2005**, *77*, 918–936.

[390] Schröder, M.; Kaufman, R. J. The mammalian unfolded protein response. *Annu. Rev. Biochem.* **2005**, *74*, 739–789.

[391] Hoozemans, J. J. M.; van Haastert, E. S.; Nijholt, D. A. T.; Rozemuller, A. J. M.; Eikelenboom, P.; Scheper, W. The unfolded protein response is activated in pretangle neurons in Alzheimer's disease hippocampus. *Am. J. Pathol.* **2009**, *174*, 1241–1251.

[392] Scheper, W.; Nijholt, D. A. T.; Hoozemans, J. J. M. The unfolded protein response and proteostasis in Alzheimer disease: preferential activation of autophagy by endoplasmic reticulum stress. *Autophagy* **2011**, *7*, 910–911.

[393] Takahashi, K.; Niidome, T.; Akaike, A.; Kihara, T.; Sugimoto, H. Amyloid precursor protein promotes endoplasmic reticulum stress-induced cell death via C/EBP homologous protein-mediated pathway. *J. Neurochem.* **2009**, *109*, 1324–1337.

[394] Zou, C.; Zhang, Z.; Wu, S.; Osterman, J. C. Molecular cloning and characterization of a rabbit eIF2C protein. *Gene* **1998**, *211*, 187–194.

[395] Wang, H. W.; Noland, C.; Siridechadilok, B.; Taylor, D. W.; Ma, E.; Felderer, K.; Doudna, J. A.; Nogales, E. Structural insights into RNA processing by the human RISC-loading complex. *Nat Struct Mol Biol* **2009**, *16*, 1148–53.

[396] Betancur, J. G.; Tomari, Y. Dicer is dispensable for asymmetric RISC loading in mammals. *RNA* **2012**, *18*, 24–30.

[397] Duce, J. A.; Tsatsanis, A.; Cater, M. A.; James, S. A.; Robb, E.; Wikhe, K.; Leong, S. L.; Perez, K.; Johanssen, T.; Greenough, M. A.; Cho, H.-H.; Galatis, D.; Moir, R. D.; Masters, C. L.; McLean, C.; Tanzi, R. E.; Cappai, R.; Barnham, K. J.; Ciccotosto, G. D.; Rogers, J. T.; Bush, A. I. Iron-export ferroxidase activity of β-amyloid precursor protein is inhibited by zinc in Alzheimer's disease. *Cell* **2010**, *142*, 857–867.

[398] Lovell, M. A.; Robertson, J. D.; Teesdale, W. J.; Campbell, J. L.; Markesbery, W. R. Copper, iron and zinc in Alzheimer's disease senile plaques. *J. Neurol. Sci.* **1998**, *158*, 47–52.

[399] Connor, J. R.; Menzies, S. L.; St Martin, S. M.; Mufson, E. J. A histochemical study of iron, transferrin, and ferritin in Alzheimer's diseased brains. *J. Neurosci. Res.* **1992**, *31*, 75–83.

[400] Liu, B.; Moloney, A.; Meehan, S.; Morris, K.; Thomas, S. E.; Serpell, L. C.; Hider, R.; Marciniak, S. J.; Lomas, D. A.; Crowther, D. C. Iron promotes the toxicity of amyloid beta peptide by impeding its ordered aggregation. *J. Biol. Chem.* **2011**, *286*, 4248–4256.

[401] Rottkamp, C. A.; Raina, A. K.; Zhu, X.; Gaier, E.; Bush, A. I.; Atwood, C. S.; Chevion, M.; Perry, G.; Smith, M. A. Redox-active iron mediates amyloid-beta toxicity. *Free Radic. Biol. Med.* **2001**, *30*, 447–450.

[402] Roberts, B. R.; Ryan, T. M.; Bush, A. I.; Masters, C. L.; Duce, J. A. The role of metallobiology and amyloid-β peptides in Alzheimer's disease. *J. Neurochem.* **2012**, *120 Suppl 1*, 149–166.

[403] Khan, A.; Dobson, J. P.; Exley, C. Redox cycling of iron by Abeta42. *Free Radic. Biol. Med.* **2006**, *40*, 557–569.

[404] Duce, J. A.; Bush, A. I. Biological metals and Alzheimer's disease: implications for therapeutics and diagnostics. *Prog. Neurobiol.* **2010**, *92*, 1–18.

[405] Hider, R. C.; Ma, Y.; Molina-Holgado, F.; Gaeta, A.; Roy, S. Iron chelation as a potential therapy for neurodegenerative disease. *Biochem. Soc. Trans.* **2008**, *36*, 1304–1308.

[406] Scott, L. E.; Orvig, C. Medicinal inorganic chemistry approaches to passivation and removal of aberrant metal ions in disease. *Chem. Rev.* **2009**, *109*, 4885–4910.

[407] Dedeoglu, A.; Cormier, K.; Payton, S.; Tseitlin, K. A.; Kremsky, J. N.; Lai, L.; Li, X.; Moir, R. D.; Tanzi, R. E.; Bush, A. I.; Kowall, N. W.; Rogers, J. T.; Huang, X. Preliminary studies of a novel bifunctional metal chelator targeting Alzheimer's amyloidogenesis. *Exp. Gerontol.* **2004**, *39*, 1641–1649.

[408] Long, J. M.; Lahiri, D. K. Current drug targets for modulating Alzheimer's amyloid precursor protein: role of specific micro-RNA species. *Curr. Med. Chem.* **2011**, *18*, 3314–3321.

[409] Schonrock, N.; Matamales, M.; Ittner, L. M.; Götz, J. MicroRNA networks surrounding APP and amyloid-β metabolism - Implications for Alzheimer's disease. *Exp. Neurol.* **2011**.

[410] Long, J. M.; Lahiri, D. K. MicroRNA-101 downregulates Alzheimer's amyloid-β precursor protein levels in human cell cultures and is differentially expressed. *Biochem. Biophys. Res. Commun.* **2011**, *404*, 889–895.

[411] Long J. M., Ray B., Lahiri D. K. MicroRNA-153 physiologically inhibits expression of amyloid-β precursor protein in cultured human fetal brain cells and is dysregulated in a subset of Alzheimer disease patients. *J. Biol. Chem.* **2012,** 287, 31298–31310.

[412] Vilardo, E.; Barbato, C.; Ciotti, M.; Cogoni, C.; Ruberti, F. MicroRNA-101 regulates amyloid precursor protein expression in hippocampal neurons. *J. Biol. Chem.* **2010**, *285*, 18344–18351.

[413] Delay, C.; Calon, F.; Mathews, P.; Hébert, S. S. Alzheimer-specific variants in the 3'UTR of Amyloid precursor protein affect microRNA function. *Mol. Neurodegener.* **2011**, *6*, 70.

[414] Liu, W.; Liu, C.; Zhu, J.; Shu, P.; Yin, B.; Gong, Y.; Qiang, B.; Yuan, J.; Peng, X. MicroRNA-16 targets amyloid precursor protein to potentially modulate Alzheimer's-associated pathogenesis in SAMP8 mice. *Neurobiol. Aging* **2012**, *33*, 522–534.

[415] Boissonneault, V.; Plante, I.; Rivest, S.; Provost, P. MicroRNA-298 and microRNA-328 regulate expression of mouse beta-amyloid precursor protein-converting enzyme 1. *J. Biol. Chem.* **2009**, *284*, 1971–1981.

[416] Bruchova, H.; Yoon, D.; Agarwal, A. M.; Mendell, J.; Prchal, J. T. Regulated expression of microRNAs in normal and polycythemia vera erythropoiesis. *Exp. Hematol.* **2007**, *35*, 1657–1667.

[417] Ju, X.; Li, D.; Shi, Q.; Hou, H.; Sun, N.; Shen, B. Differential microRNA expression in childhood B-cell precursor acute lymphoblastic leukemia. *Pediatr Hematol Oncol* **2009**, *26*, 1–10.

[418] Wu, Z.-S.; Wu, Q.; Wang, C.-Q.; Wang, X.-N.; Wang, Y.; Zhao, J.-J.; Mao, S.-S.; Zhang, G.-H.; Zhang, N.; Xu, X.-C. MiR-339-5p inhibits breast cancer cell migration and invasion in vitro and may be a potential biomarker for breast cancer prognosis. *BMC Cancer* **2010**, *10*, 542.

[419] Ueda, R.; Kohanbash, G.; Sasaki, K.; Fujita, M.; Zhu, X.; Kastenhuber, E. R.; McDonald, H. A.; Potter, D. M.; Hamilton, R. L.; Lotze, M. T.; Khan, S. A.; Sobol, R. W.; Okada, H. Dicer-regulated microRNAs 222 and 339 promote resistance of cancer cells to cytotoxic T-lymphocytes by down-regulation of ICAM-1. *Proc. Natl. Acad. Sci. U.S.A.* **2009**, *106*, 10746–10751.

[420] Okada, H.; Kohanbash, G.; Lotze, M. T. MicroRNAs in immune regulation--opportunities for cancer immunotherapy. *Int. J. Biochem. Cell Biol.* **2010**, *42*, 1256–1261.

[421] Ichi, S.; Costa, F. F.; Bischof, J. M.; Nakazaki, H.; Shen, Y.-W.; Boshnjaku, V.; Sharma, S.; Mania-Farnell, B.; McLone, D. G.; Tomita, T.; Soares, M. B.; Mayanil, C. S. K. Folic acid remodels chromatin on Hes1 and Neurog2 promoters during caudal neural tube development. *J. Biol. Chem.* **2010**, *285*, 36922–36932.

[422] Baker, M.; Mackenzie, I. R.; Pickering-Brown, S. M.; Gass, J.; Rademakers, R.; Lindholm, C.; Snowden, J.; Adamson, J.; Sadovnick, A. D.; Rollinson, S.; Cannon, A.; Dwosh, E.; Neary, D.; Melquist, S.; Richardson, A.; Dickson, D.; Berger, Z.; Eriksen, J.; Robinson, T.; Zehr, C.; Dickey, C. A.; Crook, R.; McGowan, E.; Mann, D.; Boeve, B.; Feldman, H.; Hutton, M. Mutations in progranulin cause tau-negative frontotemporal dementia linked to chromosome 17. *Nature* **2006**, *442*, 916–919.

[423] Cruts, M.; Gijselinck, I.; van der Zee, J.; Engelborghs, S.; Wils, H.; Pirici, D.; Rademakers, R.; Vandenberghe, R.; Dermaut, B.; Martin, J.-J.; van Duijn, C.; Peeters, K.; Sciot, R.; Santens, P.; De Pooter, T.; Mattheijssens, M.; Van den Broeck, M.; Cuijt, I.; Vennekens, K.; De Deyn, P. P.; Kumar-Singh, S.; Van Broeckhoven, C. Null mutations in progranulin cause ubiquitin-positive frontotemporal dementia linked to chromosome 17q21. *Nature* **2006**, *442*, 920–924.

[424] Jiao, J.; Herl, L. D.; Farese, R. V.; Gao, F.-B. MicroRNA-29b regulates the expression level of human progranulin, a secreted glycoprotein implicated in frontotemporal dementia. *PLoS ONE* **2010**, *5*, e10551.

[425] Zong, Y.; Wang, H.; Dong, W.; Quan, X.; Zhu, H.; Xu, Y.; Huang, L.; Ma, C.; Qin, C. miR-29c regulates BACE1 protein expression. *Brain Res* **2011**.

[426] Landgraf, P.; Rusu, M.; Sheridan, R.; Sewer, A.; Iovino, N.; Aravin, A.; Pfeffer, S.; Rice, A.; Kamphorst, A. O.; Landthaler, M.; Lin, C.; Socci, N. D.; Hermida, L.; Fulci, V.; Chiaretti, S.; Foà, R.; Schliwka, J.; Fuchs, U.; Novosel, A.; Müller, R.-U.; Schermer, B.; Bissels, U.; Inman, J.; Phan, Q.; Chien, M.; Weir, D. B.; Choksi, R.; De Vita, G.; Frezzetti, D.; Trompeter, H.-I.; Hornung, V.; Teng, G.; Hartmann, G.; Palkovits, M.; Di Lauro, R.; Wernet, P.; Macino, G.; Rogler, C. E.; Nagle, J. W.; Ju, J.; Papavasiliou, F. N.; Benzing, T.; Lichter, P.; Tam, W.; Brownstein, M. J.; Bosio, A.; Borkhardt, A.; Russo, J. J.; Sander, C.; Zavolan, M.; Tuschl, T. A mammalian microRNA expression atlas based on small RNA library sequencing. *Cell* **2007**, *129*, 1401–1414.

[427] Shao, N.-Y.; Hu, H. Y.; Yan, Z.; Xu, Y.; Hu, H.; Menzel, C.; Li, N.; Chen, W.; Khaitovich, P. Comprehensive survey of human brain microRNA by deep sequencing. *BMC Genomics* **2010**, *11*, 409.

[428] Ling, K.-H.; Brautigan, P. J.; Hahn, C. N.; Daish, T.; Rayner, J. R.; Cheah, P.-S.; Raison, J. M.; Piltz, S.; Mann, J. R.; Mattiske, D. M.; Thomas, P. Q.; Adelson, D. L.; Scott, H. S. Deep sequencing analysis of the developing mouse brain reveals a novel microRNA. *BMC Genomics* **2011**, *12*, 176.

[429] Ach, R. A.; Wang, H.; Curry, B. Measuring microRNAs: comparisons of microarray and quantitative PCR measurements, and of different total RNA prep methods. *BMC Biotechnol.* **2008**, *8*, 69.

[430] Wang, W. X.; Huang, Q.; Hu, Y.; Stromberg, A. J.; Nelson, P. T. Patterns of microRNA expression in normal and early Alzheimer's disease human temporal cortex: white matter versus gray matter. *Acta Neuropathol* **2011**, *121*, 193–205.

[431] Zhao, J.; Fu, Y.; Yasvoina, M.; Shao, P.; Hitt, B.; O'Connor, T.; Logan, S.; Maus, E.; Citron, M.; Berry, R.; Binder, L.; Vassar, R. Beta-site amyloid precursor protein cleaving enzyme 1 levels become elevated in neurons around amyloid plaques: implications for Alzheimer's disease pathogenesis. *J. Neurosci.* **2007**, *27*, 3639–3649.

[432] Rodríguez, J. J.; Olabarria, M.; Chvatal, A.; Verkhratsky, A. Astroglia in dementia and Alzheimer's disease. *Cell Death Differ.* **2009**, *16*, 378–385.

[433] Guo, Q.; Li, H.; Gaddam, S. S. K.; Justice, N. J.; Robertson, C. S.; Zheng, H. Amyloid Precursor Protein Revisited: NEURON-SPECIFIC EXPRESSION AND HIGHLY STABLE NATURE OF SOLUBLE DERIVATIVES. *J. Biol. Chem.* **2012**, *287*, 2437–2445.

[434] Small, S. A.; Perera, G. M.; DeLaPaz, R.; Mayeux, R.; Stern, Y. Differential regional dysfunction of the hippocampal formation among elderly with memory decline and Alzheimer's disease. *Ann Neurol* **1999**, *45*, 466–72.

[435] Small, S. A.; Tsai, W. Y.; DeLaPaz, R.; Mayeux, R.; Stern, Y. Imaging hippocampal function across the human life span: is memory decline normal or not? *Ann Neurol* **2002**, *51*, 290–5.

[436] Lewandowski, N. M.; Small, S. A. Brain microarray: finding needles in molecular haystacks. *J. Neurosci.* **2005**, *25*, 10341–10346.

[437] Small, S. A.; Kent, K.; Pierce, A.; Leung, C.; Kang, M. S.; Okada, H.; Honig, L.; Vonsattel, J. P.; Kim, T. W. Model-guided microarray implicates the retromer complex in Alzheimer's disease. *Ann Neurol* **2005**, *58*, 909–19.

[438] Arvey, A.; Larsson, E.; Sander, C.; Leslie, C. S.; Marks, D. S. Target mRNA abundance dilutes microRNA and siRNA activity. *Mol. Syst. Biol.* **2010**, *6*, 363.

[439] Krützfeldt, J.; Kuwajima, S.; Braich, R.; Rajeev, K. G.; Pena, J.; Tuschl, T.; Manoharan, M.; Stoffel, M. Specificity, duplex degradation and subcellular localization of antagomirs. *Nucleic Acids Res.* **2007**, *35*, 2885–2892.

[440] Carè, A.; Catalucci, D.; Felicetti, F.; Bonci, D.; Addario, A.; Gallo, P.; Bang, M.-L.; Segnalini, P.; Gu, Y.; Dalton, N. D.; Elia, L.; Latronico, M. V. G.; Høydal, M.; Autore, C.; Russo, M. A.; Dorn, G. W., 2nd; Ellingsen, O.; Ruiz-Lozano, P.; Peterson, K. L.; Croce, C. M.; Peschle, C.; Condorelli, G. MicroRNA-133 controls cardiac hypertrophy. *Nat. Med.* **2007**, *13*, 613–618.

[441] Trang, P.; Wiggins, J. F.; Daige, C. L.; Cho, C.; Omotola, M.; Brown, D.; Weidhaas, J. B.; Bader, A. G.; Slack, F. J. Systemic delivery of tumor suppressor microRNA mimics using a neutral lipid emulsion inhibits lung tumors in mice. *Mol. Ther.* **2011**, *19*, 1116–1122.

[442] Elmen, J.; Lindow, M.; Schutz, S.; Lawrence, M.; Petri, A.; Obad, S.; Lindholm, M.; Hedtjarn, M.; Hansen, H. F.; Berger, U.; Gullans, S.; Kearney, P.; Sarnow, P.; Straarup, E. M.; Kauppinen, S. LNA-mediated microRNA silencing in non-human primates. *Nature* **2008**, *452*, 896–9.

[443] Elmén, J.; Lindow, M.; Silahtaroglu, A.; Bak, M.; Christensen, M.; Lind-Thomsen, A.; Hedtjärn, M.; Hansen, J. B.; Hansen, H. F.; Straarup, E. M.; McCullagh, K.; Kearney, P.; Kauppinen, S. Antagonism of microRNA-122 in mice by systemically administered LNA-antimiR leads to up-regulation of a large set of predicted target mRNAs in the liver. *Nucleic Acids Res.* **2008**, *36*, 1153–1162.

[444] Jopling, C. L.; Yi, M.; Lancaster, A. M.; Lemon, S. M.; Sarnow, P. Modulation of hepatitis C virus RNA abundance by a liver-specific MicroRNA. *Science* **2005**, *309*, 1577–1581.

[445] Lanford, R. E.; Hildebrandt-Eriksen, E. S.; Petri, A.; Persson, R.; Lindow, M.; Munk, M. E.; Kauppinen, S.; Ørum, H. Therapeutic silencing of microRNA-122 in primates with chronic hepatitis C virus infection. *Science* **2010**, *327*, 198–201.

[446] Hildebrandt-Eriksen, E. S.; Aarup, V.; Persson, R.; Hansen, H. F.; Munk, M. E.; Orum, H. A Locked Nucleic Acid Oligonucleotide Targeting MicroRNA 122 Is Well-Tolerated in Cynomolgus Monkeys. *Nucleic acid therapeutics* **2012**.

[447] Su, J.; Baigude, H.; McCarroll, J.; Rana, T. M. Silencing microRNA by interfering nanoparticles in mice. *Nucleic Acids Res.* **2011**, *39*, e38.

[448] Cheng, C. J.; Saltzman, W. M. Polymer Nanoparticle-Mediated Delivery of MicroRNA Inhibition and Alternative Splicing. *Mol. Pharm.* **2012**, *9*, 1481–1488.

[449] Scherr, M.; Venturini, L.; Battmer, K.; Schaller-Schoenitz, M.; Schaefer, D.; Dallmann, I.; Ganser, A.; Eder, M. Lentivirus-mediated antagomir expression for specific inhibition of miRNA function. *Nucleic Acids Res.* **2007**, *35*, e149.

[450] Langlois, R. A.; Shapiro, J. S.; Pham, A. M.; tenOever, B. R. In vivo delivery of cytoplasmic RNA virus-derived miRNAs. *Mol. Ther.* **2012**, *20*, 367–375.

[451] Rahim, A. A.; Wong, A. M. S.; Howe, S. J.; Buckley, S. M. K.; Acosta-Saltos, A. D.; Elston, K. E.; Ward, N. J.; Philpott, N. J.; Cooper, J. D.; Anderson, P. N.; Waddington, S. N.; Thrasher, A. J.; Raivich, G. Efficient gene delivery to the adult and fetal CNS using pseudotyped non-integrating lentiviral vectors. *Gene Ther.* **2009**, *16*, 509–520.

[452] Gumireddy, K.; Young, D. D.; Xiong, X.; Hogenesch, J. B.; Huang, Q.; Deiters, A. Small-molecule inhibitors of microrna miR-21 function. *Angew. Chem. Int. Ed. Engl.* **2008**, *47*, 7482–7484.

[453] Young, D. D.; Connelly, C. M.; Grohmann, C.; Deiters, A. Small molecule modifiers of microRNA miR-122 function for the treatment of hepatitis C virus infection and hepatocellular carcinoma. *J. Am. Chem. Soc.* **2010**, *132*, 7976–7981.

[454] Bao, B.; Rodriguez-Melendez, R.; Zempleni, J. Cytosine methylation in miR-153 gene promoters increases the expression of holocarboxylase synthetase, thereby increasing the abundance of histone H4 biotinylation marks in HEK-293 human kidney cells. *J. Nutr. Biochem.* **2011**.

[455] Morrissette, D. A.; Parachikova, A.; Green, K. N.; LaFerla, F. M. Relevance of transgenic mouse models to human Alzheimer disease. *J. Biol. Chem.* **2009**, *284*, 6033–6037.

[456] Götz, J.; Ittner, L. M. Animal models of Alzheimer's disease and frontotemporal dementia. *Nat. Rev. Neurosci.* **2008**, *9*, 532–544.

[457] Lamb, B. T.; Call, L. M.; Slunt, H. H.; Bardel, K. A.; Lawler, A. M.; Eckman, C. B.; Younkin, S. G.; Holtz, G.; Wagner, S. L.; Price, D. L.; Sisodia, S. S.; Gearhart, J. D. Altered metabolism of familial Alzheimer's disease-linked amyloid precursor protein variants in yeast artificial chromosome transgenic mice. *Hum. Mol. Genet.* **1997**, *6*, 1535–1541.

[458] Kulnane, L. S.; Lamb, B. T. Neuropathological characterization of mutant amyloid precursor protein yeast artificial chromosome transgenic mice. *Neurobiol. Dis.* **2001**, *8*, 982–992.

[459] Hock, B. J.; Lattal, K. M.; Kulnane, L. S.; Abel, T.; Lamb, B. T. Pathology associated memory deficits in Swedish mutant genome-based amyloid precursor protein transgenic mice. *Curr Aging Sci* **2009**, *2*, 205–213.

[460] Chiocco, M. J.; Kulnane, L. S.; Younkin, L.; Younkin, S.; Evin, G.; Lamb, B. T. Altered amyloid-beta metabolism and deposition in genomic-based beta-secretase transgenic mice. *J. Biol. Chem.* **2004**, *279*, 52535–52542.

[461] Kriegstein, A.; Alvarez-Buylla, A. The glial nature of embryonic and adult neural stem cells. *Annu. Rev. Neurosci.* **2009**, *32*, 149–184.

[462] Lendahl, U.; Zimmerman, L. B.; McKay, R. D. CNS stem cells express a new class of intermediate filament protein. *Cell* **1990**, *60*, 585–595.

[463] Rieske, P.; Azizi, S. A.; Augelli, B.; Gaughan, J.; Krynska, B. A population of human brain parenchymal cells express markers of glial, neuronal and early neural cells and differentiate into cells of neuronal and glial lineages. *Eur. J. Neurosci.* **2007**, *25*, 31–37.

CURRICULUM VITAE

Justin M. Long

EDUCATION:

2001 – 2004 Indiana University, Biology BS and Chemistry BS (Highest Academic Distinction & Honors Notation)

2005 – 2014 Indiana University School of Medicine, MD, Medical Scientist Training Program

2007 – 2013 Indiana University, PhD, Medical Neuroscience Graduate Program, Advisor: Debomoy Lahiri

HONORS/AWARDS/AFFILIATIONS:

2004 – present	Associate Member, Sigma Xi, The Scientific Research Society
2004 – present	Phi Beta Kappa Society Member
2009	IU School of Medicine & Department of Psychiatry Joseph Hingtgen Travel Award
2009 – present	Student Member, Society for Neuroscience
2010	IU Medical Scientist Training Program Keystone National MD/PhD Student Conference Travel Award
2011 – present	Student Member, Alzheimer's Association ISTAART
2011	Alzheimer's Association Travel Fellowship Award to attend ICAD in Paris, France
2011	Larry Kays Fellowship Award

ABSTRACTS:

1. **Long, JM**, Kaefer, M and Packer, CS. In search of non-adrenergic non-cholinergic (NANC) neurotransmitters in rat bladder. EB 2003 Late-Breaking Abstracts p28, 2003; Awarded a Ribbon for Excellence at the National Sigma Xi Student Conference, 2003; Accepted for presentation at the 2004 National Conference on Undergraduate Research.

2. **Long, JM**, Kaefer, M and Packer, CS. Agonists of protease-activated receptors (PAR 1, PAR 2 and PAR 4) do not appear to be mediators of NANC contractions in rat bladder. Selected as one of 12 Finalists for the 2004 David S Bruce Excellence in Undergraduate Research Award, The FASEB J 18: A1083, 2004.
3. Packer, CS, **Long, JM** and Kaefer, M. Possible role of hydrogen peroxide (H_2O_2) in bladder dysfunction. The FASEB J 18: A1083, 2004.
4. **Long, JM**, Kaefer, M and Packer, CS. Non-adrenergic, non-cholinergic (NANC) contractions in rat and human urinary bladder. Northwest Urological Society meetings, Vancouver, Canada, 2004, and The FASEB J 19: A122, 2005.
5. Sokol D, **Long JM**, Maloney BR, Chen D, and Lahiri DK. Potential Alzheimer's Disease Markers for Autism? Beta-Amyloid Precursor Protein and Acetylcholinesterase Correlate with Aggression in Autism. P02.010. Abstracts2View. Seattle, WA: Annual Meeting of the American Association of Neurology, 2009. Online.
6. Ray B, Gaskins DL, **Long JM**, and Lahiri DK. Acute restraint stress decreases neurotrophic factors (BDNF & GDNF) and presynaptic protein syntaxin in rat cortex and its relevance in neurodegeneration. Program No. 739.21. 2008 Neuroscience Meeting Planner. Washington, DC: Society for Neuroscience, 2008. Online.
7. **Long JM** and Lahiri DK. Testing microRNA as a novel target for Alzheimer disease – miR-101 regulates levels of amyloid precursor protein (APP). Program No. 427.13. 2009 Neuroscience Meeting Planner. Chicago, IL: Society for Neuroscience, 2009. Online.
8. **Long JM** and Lahiri DK. Novel Specific MicroRNAs in Regulating Neuronal Genes Implicated In Alzheimer's Disease. Alzheimers Dement 6(4 Supplement 1): e13, 2010.

9. Lahiri DK, Bailey JA, Ray B, Tanila H, Banerjee P, and **Long, JM**. The effect of memantine and rivastigmine on synaptic markers and amyloid processing in cell culture and animal models of Alzheimer's disease. Alzheimers Dement 6(4 Supplement 1): S581–S582, 2010.
10. **Long JM** and Lahiri DK. A novel target for Alzheimer disease: miR-101 regulates levels of Amyloid Precursor Protein. Session II, Abstract 41. 25th Annual National MD/PhD Student Conference Abstract Book. Keystone, CO: National MD/PhD Student Conference, 2010.
11. Ray B, Bailey JA, **Long JM**, Pathak Y, Sambamurti K, Rogers JT, Greig NH, Maitra A, and Lahiri DK. Historical journey of the application and use of curcumin from culinary purposes to therapeutics in neurodegenerative disorders. Program No 27.21. 2010 Neuroscience Meeting Planner. San Diego, CA: Society for Neuroscience, 2010. Online
12. **Long JM** and Lahiri DK. Role of specific microRNAs in regulating neuronal genes implicated in Alzheimer disease. Program No. 424.1. 2010 Neuroscience Meeting Planner. San Diego, CA: Society for Neuroscience, 2010. Online
13. Lahiri DK, and **Long JM**. Discovery of a novel drug target for Alzheimer's disease: miR-101 regulates levels of the amyloid precursor protein. Session IL-90. Dubai, UAE: 3rd International Conference on Drug Discovery and Therapy. Curr Med Chem (Special Abstract Issue): 32, 2011.
14. Lahiri DK, Ray B, Chauhan N, Bailey JA, and **Long JM**. SAC (S-allyl-cysteine) as a novel therapeutic agent for Alzheimer's disease (AD) based on studies from neuronal cultures and APP-transgenic model for AD. Session PO-164. Dubai, UAE: 3rd International Conference on Drug Discovery and Therapy. Curr Med Chem (Special Abstract Issue): 174, 2011.

15. Ray B, and **Long JM**, Sokol DK, Lahiri DK. Biochemical evidence for the dysregulation of Alzheimer's amyloid precursor protein (APP) expression and metabolism in fragile X syndrome (FXS) and severe autism. To be presented at the 66th Annual meeting of the Society of Biological Psychiatry, San Francisco, CA, 2011.
16. Lahiri DK, Ray B, Bailey JA, and **Long JM**. Early-life environment and epigenetics in Alzheimer's disease: A new paradigm represented by the LEARn model. Presented at the 66th Annual meeting of the Society of Biological Psychiatry, San Francisco, CA, 2011.
17. **Long JM** and Lahiri DK. A novel microRNA interaction relevant to Alzheimer's disease pathogenesis and drug target discovery: miR-346 induces expression of amyloid precursor protein. Alzheimers Dement 7 (4 Supplement 1): S566–S567, 2011.

MANUSCRIPTS:

1. **Long JM** and Lahiri DK. MicroRNA-101 downregulates Alzheimer's amyloid-β precursor protein levels in human cell cultures and is differentially expressed. Biochem Biophys Res Commun (404): 889–895, 2011.
2. Sokol DK, Maloney BR, **Long JM**, Ray B, and Lahiri DK. Autism, Alzheimer's Disease and Fragile X: APP, FMRP and mGluR5 are molecular links. Neurology 76(15):1344–1352, 2011.
3. Ray B*, **Long JM***, Sokol DK, and Lahiri DK. Increased secreted amyloid precursor protein-α (sAPPα) in severe autism: Proposal of a specific anabolic pathway and biomarker. PLoS ONE 6(6): e20405, 2011.

4. **Long JM** and Lahiri DK. Current drug targets for modulating Alzheimer's amyloid precursor protein: role of specific microRNA species. Curr Med Chem 18(22): 3314–3321, 2011.
5. **Long JM** and Lahiri DK. Advances in MicroRNA experimental approaches to study physiological regulation of gene products implicated in CNS disorders. Exp Neurol 235(2): 402–418, 2012
6. **Long JM**, Ray B and Lahiri DK. MicroRNA-153 Physiologically Inhibits Expression of Amyloid-β Precursor Protein in Cultured Human Fetal Brain Cells and is Dysregulated in a Subset of Alzheimer Disease Patients. J Biol Chem 287(37):31298–31310, 2012.

*Co-first author